

300 MHz ARRAY USING PHYSICALLY SMALL
SLOT ANTENNA ELEMENTS

M. A. H. Ibrahim

and

J. A. M. Lyon

This document is subject to special export controls and each transmittal to foreign governments or foreign nationals may be made only with the prior approval of AFAL (AVWE), Wright-Patterson Air Force Base, Ohio 45433

FOREWORD

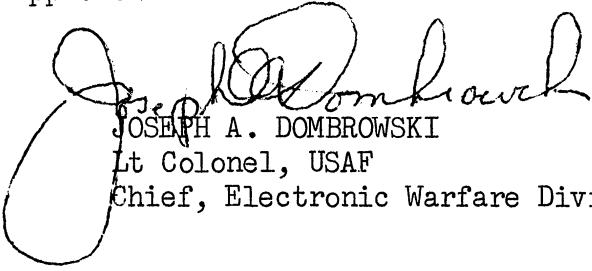
This report, 1770-2-T, was prepared by the Radiation Laboratory of The University of Michigan, Department of Electrical Engineering, 201 Catherine Street, Ann Arbor, Michigan 48108, under the direction of Professor Ralph E. Hiatt and Professor John A. M. Lyon on Air Force Contract F33615-68-C-1381, Task 627801 of Project 6278, "Study and Investigation of UHF-VHF Antennas." The work was administered under the direction of the Air Force Avionics Laboratory, Wright-Patterson Air Force Base, Ohio 45433. The Task Engineer was Mr. Olin E. Horton and the Project Engineer, Mr. Edwin M. Turner, AVWE. This report was submitted by the authors in October 1969.

The prefatory material to this report, Sections 01, 02, and 03, covers the general aspects of the utilization of miniaturized slot elements in antenna arrays. The remainder of the report, Chapters I through V and the Appendices, presents detailed background information and an analysis of the coupling of loaded slot elements. Chapters I through V and the Appendices have been written entirely by Dr. M.A.H. Ibrahim and constitute his recent doctoral dissertation.

ACKNOWLEDGEMENT

The following individuals contributed either analytical or experimental effort for some parts of this report: Dr. C.J. Digenis, Y-P Liu, D.G. Berry and B. Whitney.

This report has been reviewed and is approved.


JOSEPH A. DOMBROWSKI
Lt Colonel, USAF
Chief, Electronic Warfare Division

ABSTRACT

The coupling between two loaded rectangular waveguides opening in an infinite conducting ground plane has been investigated. The slots are equal in size and placed so as to have the broadsides parallel. The analysis is made in two steps:

- i) the coupling between the apertures is derived;
- ii) the effect of the backing cavities on the coupling is determined.

The reaction concept, a form of the "variational technique", was used in the analysis. This method helped to simplify the mathematical work and provided very reasonable results.

Substantial experimental work on the behavior of coupling versus frequency and coupling versus slot separation was performed. In order to simplify the experimental investigation the standard empty X-band waveguide (0.9"x0.4") was filled with dielectric loading of Emerson and Cuming Stycast Hi-K dielectric material. Materials having dielectric constants of 5, 7, 11 and 15 were used. Most of the measurements for the loaded case were in the S-band range of frequency (2.6 - 3.95 GHz). The choices of the S-band frequency range and the dielectric constant were made to permit use of the anechoic chamber in the first instance with reasonable accuracy and small waveguide in the second instance.

An extensive comparison of coupling for the case of standard waveguides with and without loading has been made and explanations are given for the observed differences. An iteration procedure has been used to determine the effect of the electromagnetic interaction between the slots.

Detailed computer programs were developed for the analytical expressions. Numerical results for many important cases were then obtained. Methods and results can readily be extended to other frequencies and other slot sizes.

TABLE OF CONTENTS

	PREFATORY MATERIAL	1
	Section 01: Introduction	1
	Section 02: Arrays and Interaction	2
	Section 03: Conclusions	23
I	INTRODUCTION	25
	1.1 Approach to the Problem	26
II	THEORETICAL ANALYSIS	28
	2.1 Assumptions	28
	2.2 Formulation of the Fields in the Different Regions	28
	2.3 Evaluation of U	36
	2.4 Iteration Procedure	50
	2.5 Consideration of the Short-circuited Waveguide Backing the Slots	53
III	NUMERICAL ANALYSIS	66
	3.1 General	66
	3.2 Calculation of Reflection Coefficients at the Aperture	66
	3.3 Calculations of the Aperture-to-Aperture Coupling Between Slots versus Frequency	70
	3.4 Coupling Aperture to Aperture versus Spacing	86
	3.5 Evaluation of the Cavity Effect	96
	3.6 Evaluation of Coupling	120
IV	EXPERIMENTAL INVESTIGATION	121
	4.1 General Discussion	121
	4.2 Coupling Measurements	126
	4.3 The Far-field Patterns	148
V	SUMMARY AND CONCLUSIONS	152
	5.1 Areas for Future Investigation	155
	REFERENCES	157
	APPENDIX A: The Reduction of Quadruple Integrals to Double Integrals.	159
	APPENDIX B: Examples of Computer Output Data on Coupling	162

LIST OF TABLES

3.1	Relation between FN and f for $\mu_r=1$, $\epsilon_r=15$, $a=0.02286m$, $b=0.01016m$.	78
3.2	Relation between FN and f for $\mu_r=1$, $\epsilon_r=11$, $a=0.02286m$, $b=0.01016m$.	78
3.3	Relation between FN and f for $\mu_r=1$, $\epsilon_r=7$, $a=0.02286m$, $b=0.01016m$.	78
3.4	Relation between FN and f for $\mu_r=1$, $\epsilon_r=1$, $a=0.07136m$, $b=0.034036m$ (S-band).	79
3.5a	Relation between FN and f for $\mu_r=1$, $\epsilon_r=1$, $a=0.02286m$, $b=0.01016m$ (X-band).	79
3.5b	Relation between FN and f for $\mu_r=1$, $\epsilon_r=1$, $a=0.0157988$, $b=0.0078994$ (Ku-band)	79
3.6	Cutoff Frequency vs Dielectric Constant of the Loading Material; $a=0.02286m$, $b=0.01016m$.	80

LIST OF ILLUSTRATIONS

0.2-1	Experimental Power Pattern (linear) of Ferrite Slot in Ground Plane, H-plane Cut.	7
0.2-2	Calculated Power Pattern (linear) for 3-element Ferrite Slot Array (H-plane).	7
0.2-3	Experimental Power Pattern (linear) for 3-element Ferrite Slot Array (H-plane).	7
0.2-4	Broadside to Broadside Coupling of Closely Spaced Rectangular Slots Showing a $1/r^2$ Trend.	9
0.2-5	Far-field Coupling for Representative Angles.	10
0.2-6	End to End Coupling of Closely Spaced Rectangular Slots Showing a $1/r^4$ Trend.	11
0.2-7	Comparison between Experimental and Theoretical Results.	12
0.2-8	Coupling of Air-filled S-band Waveguide Slots in Common Ground Plane, 0.5λ spacing, Broadside to Broadside Arrangement .	13
0.2-9	Coupling of Ferrite Loaded Slots in Conducting Plane, 0.5λ Spacing, Broadside to Broadside Arrangement.	15
0.2-10	Coupling of Ferrite Loaded Slots in Conducting Plane, 0.5λ Spacing, End to End Arrangement.	15
0.2-11	Interaction of Certain Chosen Groups of Slots Corresponding to Three Radii; A, B and C. Polarization Aligned Left to Right.	18
0.2-12	Returned Power Level to Feed Generator for Many Element Array as Function of Number of Slots Used in Computing Interaction.	21
2-1	Arrangement and Slot Configuration.	29
2-2	Method of Images .	32
2-3	Source and Scatterer .	36
2-4	Coordinate Transformation.	47
2-5	Coordinate Transformation for Reduction of Quadruple Integral to Double Integral.	48
2-6	Multiple Reflection between Transmitter and Receiver to Represent Interaction between them.	52
2-7	Short-circuited Cavity.	55
2-8	Standing Electric and Magnetic Fields in Cavity.	56
2-9	Input Impedance to the Cavity at $z=0$.	57
2-10	Configuration of Waveguide when it is Closed at Both Ends.	58
2-11	Equivalent Circuit for Cavity Slot Antenna.	59
2-12	Resonance and Half-power Bandwidth.	64
3-1	Aperture Normalized Conductance and Susceptance, $\epsilon_r=5$.	71
3-2	Aperture Normalized Conductance and Susceptance, $\epsilon_r=6$.	72
3-3	Aperture Normalized Conductance and Susceptance, $\epsilon_r=10$.	73
3-4	Aperture Normalized Conductance and Susceptance, $\epsilon_r=11$.	74
3-5	Aperture Normalized Conductance and Susceptance, $\epsilon_r=15$.	75
3-6	Variation of Cutoff Frequency vs Permittivity of Loaded X-band Waveguide.	81

3-7	Standard S-band Coupling vs Normalized Frequency.	84
3-8	Standard X-band Coupling vs Normalized Frequency.	85
3-9	Standard Ku-band Coupling vs Frequency.	87
3-10a	Aperture to Aperture E-Plane Coupling of Loaded Slots, $\epsilon_r=2$.	88
3-10b	Aperture to Aperture E-Plane Coupling of Loaded Slots, $\epsilon_r=3$.	89
3-10c	Aperture to Aperture E-Plane Coupling of Loaded Slots, $\epsilon_r=4$.	90
3-10d	Aperture to Aperture E-Plane Coupling of Loaded Slots, $\epsilon_r=5$.	91
3-10e	Aperture to Aperture E-Plane Coupling of Loaded Slots, $\epsilon_r=7$.	92
3-10f	Aperture to Aperture E-Plane Coupling of Loaded Slots, $\epsilon_r=11$.	93
3-10g	Aperture to Aperture E-Plane Coupling of Loaded Slots, $\epsilon_r=15$.	94
3-10h	Aperture to Aperture E-Plane Coupling of Loaded Slots, $\epsilon_r=20$.	95
3-11	Broadside Coupling between Empty Slots (Separation Center to Center).	97
3-12	Aperture to Aperture Coupling vs Distance in Wavelength.	98
3-13a	Resonance of the Cavity (Digital Plot), $d=0.031$, $\epsilon_r=7$.	105
3-13b	Resonance of the Cavity (Digital Plot), $d=0.031$, $\epsilon_r=11$.	106
3-13c	Resonance of the Cavity (Digital Plot), $d=0.031$, $\epsilon_r=15$.	107
3-14a	Resonance of the Cavity (Digital Plot), $d=0.1015$, $\epsilon_r=7$.	108
3-14b	Resonance of the Cavity (Digital Plot), $d=0.1015$, $\epsilon_r=11$.	109
3-14c	Resonance of the Cavity (Digital Plot), $d=0.1015$, $\epsilon_r=15$.	110
3-15a	An Expanded Digital Plot for the Resonance Peaks, $n=1$.	111
3-15b	An Expanded Digital Plot for the Resonance Peaks, $n=2$.	112
3-16a	An Expanded Digital Plot for the Resonance Peaks, $n=3$.	113
3-16b	An Expanded Digital Plot for the Resonance Peaks, $n=4$.	114
3-16c	An Expanded Digital Plot for the Resonance Peaks, $n=5$.	115
3-16d	An Expanded Digital Plot for the Resonance Peaks, $n=6$.	116
3-16e	An Expanded Digital Plot for the Resonance Peaks, $n=7$.	117
3-16f	An Expanded Digital Plot for the Resonance Peaks, $n=8$.	118
3-16g	An Expanded Digital Plot for the Resonance Peaks, $n=9$.	119
4-1	Anechoic Chamber Ground Plane.	122
4-2a	Test Antenna Mount.	123
4-2b	Arrangements for Loaded X-band Waveguides.	124
4-2c	Arrangements for Standard S-band Waveguides.	125
4-3a	Resonance Cavity and Dielectric Filling plus Coaxial to Waveguide Feed.	127
4-3b	The 0.031m and the 0.1015m Dielectric Loaded Cavities.	128
4-3c	Comparison between Loaded and Unloaded Cavity.	129

4-4	Standard S-band Waveguide Coupling vs Frequency	131
4-5	E-plane Coupling vs Frequency for Two Slots Spaced 11.4 cm	132
4-6	Coupling vs Frequency for Loaded X-band Waveguides, $\epsilon_r=11$, d=0.031	133
4-7	Coupling vs Frequency for Loaded X-band Waveguides, $\epsilon_r=15$, d=0.1015	134
4-8	Gain vs Frequency of Dielectric Loaded Cavity	135
4-9	Anechoic Chamber Set-up for Far-field Pattern Measurements	136
4-10	Coupling vs Frequency for Loaded Cavity	138
4-11	Gain vs Frequency for Loaded Cavity	139
4-12	Coupling vs Frequency for Loaded Waveguides	140
4-13	Gain vs Frequency for Loaded Cavity	141
4-14	Experimental Set-up for Coupling with Point by Point Tuning	142
4-15	Coupling vs Frequency with Tuning both Transmitter and Receiver at Each point	143
4-16a	Coupling vs Frequency Point by Point, $\epsilon_r=15$	144
4-16b	Coupling vs Frequency Point by Point, $\epsilon_r=11$	145
4-16c	Coupling vs Frequency Point by Point, $\epsilon_r=7$	146
4-17	Coupling vs Frequency Point by Point, $x_1=0.03$, $\epsilon_r=7$	147
4-18a	E-plane Radiation Pattern of a Loaded X-band Waveguide	149
4-18b	H-plane Radiation Pattern of a Loaded X-band Waveguide	150
5-1	Explanation of Non-Uniformity of Separation of the Resonance Peaks	156

LIST OF SYMBOLS

a	Slot dimension in H-plane
b	Slot dimension in E-plane
d	Cavity length
d_1	Aperture to feeding probe dimension in the cavity
d_2	Probe to short side dimension of the cavity
E	Electric field intensity
f	Frequency
\bar{F}	Electric vector potential
F_x, F_y, F_z	Cartesian coordinates of \bar{F}
FN	Normalized frequency (FN = ka / π)
J	Surface current in amp/meter
H	Magnetic field intensity
k	Wave number
k_0	Free space wave number
l	Cavity length
M	Magnetic moment
n	An integer
\bar{n}	Unit vector perpendicular to the aperture
U	Amplitude of the received illumination
v	Velocity of waves in material medium
x	Cartesian coordinate
x_1	Center to center separation of slots
\hat{x}	Unit vector in the x-direction
y	Cartesian coordinate
Y	Admittance
\hat{y}	Unit vector in the y-direction
z	Cartesian coordinate
Z	Impedance
\hat{z}	Unit vector in z-direction

α	Attenuation constant
β	Phase constant
γ	Propagation constant, or a variable of integration
ϵ	Dielectric permittivity
ϵ_0	Free-space permittivity
ϵ_r	Relative dielectric constant or permittivity
η	Second cartesian coordinate (source point)
ξ	First cartesian coordinate (source point)
λ	Wavelength
λ_0	Free-space wavelength
λ_c	Cutoff wavelength
λ_g	Waveguide wavelength
μ	Permeability
μ_0	Free-space permeability
μ_r	Relative permeability
$\bar{\pi}$	Hertzian electric vector potential
$\bar{\pi}^*$	Hertzian magnetic vector potential
ρ	First cylindrical coordinate
ω	Angular frequency

PREFATORY MATERIAL

Section 0.1 : Introduction

This report covers the work to date on a task devoted to the utilization of loaded slot antenna elements in arrays. The objective of the task has been to develop the advantages and criteria for the use of physically small slot antenna elements in a 300 MHz array. It was recognized early that one of the chief advantages of such an array would be the possibility of reduced interaction between elements. A large part of this report is devoted to an analysis of loaded slot elements and an evaluation of the coupling between such elements. The reduced level of coupling can easily be ascertained from these analytical methods for specific instances through the use of an appropriate computer program. The detailed studies, including the essentials for programming on a computer, are found in later chapters.

This report includes the study of simple three-element linear arrays. The data obtained clearly show that with miniaturized slots the coupling involved from one element to another is sufficiently small so that the interaction can frequently be considered negligible. This fact has been deduced by comparing the array patterns obtained analytically based on assumed element illumination with experimentally determined patterns. It has been found that the experimentally derived patterns are extremely close to the theoretically calculated patterns. This means that the illumination of each element has been very close to the assumed illumination neglecting interaction and as used in the calculations. No modifications in the feed network were made in order to compensate for the driving point impedance level of each element. For instance in the case of the broadside three-element array, the feed network was arranged to give three in-phase values of illumination of equal magnitude. Equal lengths of lines were used so that the phasing and feed current magnitude were all the same before each of the feeds was connected to a loaded slot element. After the feeds were connected to the individual slots and the array pattern tests made, it was found that the patterns so derived were very close to those

predicted by calculation. The spacing of the elements was very nearly the usual half wavelength for a broadside beam.

Section 0.2 of this chapter describes the nature of the interaction problem among various elements of an array. This section also gives the experimental results on simple three-element linear arrays.

Section 0.3 indicates the conclusions obtained through the use of the information contained in this report. The remaining chapters contain the detailed analytical work on the interaction of elements. Chapters I through V and the Appendices comprise in their entirety the doctoral dissertation of M. A. H. Ibrahim of which he is the sole author.

Section 0.2 : Arrays and Interaction

0.2a: General Discussion

The interaction of elements in an array of elements can be expressed in at least two ways. One is by means of the mesh equations for coupled antennas. These mesh equations contain impedance parameters which theoretically can be evaluated by means of appropriate line integrals. The most important impedance for each element is the driving point of impedance. The driving point of impedance itself is a function of the self impedance as well as each of the mutual impedances which come into being through the interaction of each element on every other element.

In the analytical work which has been done and is contained in Chapters II and III, the analysis of the interaction of one loaded slot upon another has been on the basis of a consideration of the electromagnetic field boundary value problem. Results have frequently been given in terms of the power level in dB received at one antenna referred to the power level input at the other antenna. The coupling then gives the power level of the receiving antenna as so many dB below the power level of the transmitting antenna. The dB coupling level data can be directly interpreted in terms of mutual impedance. However, this is not always necessary. The main objective of the analytical work has been to show that

miniaturized slots are accompanied by much lower interaction than air-filled slots at the same frequency and of standard size. On this basis, the work in Chapters I through V is back-up or supporting information for the proposition that miniaturized slots used in phased array antennas are accompanied by the very considerable benefit of decreased interaction. In fact, the interaction level is now sufficiently low to allow the frequently used compensation schemes for the driving network to be eliminated or greatly simplified.

In the consideration of phased arrays the problem of driving point impedance becomes strikingly evident especially in the case of using the array for transmitting. In general, power from each element may be coupled back into every other element. If there is a relatively high level of interaction of one element upon another, then it is necessary to have appropriate matching techniques at every frequency and for every beam position. Obviously, it is extremely difficult to obtain a good impedance match over a wide bandwidth. It is even more difficult when matching must be good for wide ranges of scan and for various scanning modes. A convenient measure of the need for matching is obtained by considering an array of elements with respect to the total returned power from all the elements normalized to the total power fed to the array. This return of power to all elements will be a function of frequency and position of scan for the array beam. The advantages of miniaturized slots would then be associated with a major reduction of the returned power summed over all elements over a useful range of frequency and over the desired range of scan.

There is some restriction on the bandwidth associated with a need to keep the interaction low. This is brought out in the analysis given in the later chapters. A possible bandwidth goal for phased arrays might be 15 percent. It is less easy to generalize on a desirable scan angle. The requirements for scan are very closely associated with the system requirements of the antenna. Certainly for many anticipated uses it is desired that the scanning angle from the normal to the array approach 90° . The indications given in this report are that interaction may be so considerably reduced that the influence of scanning angle on the interaction, although present, is relatively

insignificant since the overall level of interaction is always small. This fact will be explored in some detail in succeeding paragraphs.

The use of loading material in a slot in order to reduce the size of the slot for a given operating frequency points to the possibility of an additional advantage not mentioned heretofore. There are available high quality dielectric materials, some of which are of ceramic nature. Such materials can be utilized to improve the hardening aspect of the antenna array, where hardening is used to denote capability of withstanding the effects of nuclear detonations. On the other hand, there are also useful materials for loading such as the ferrites. Ferrite material also may be useful for hardening purposes. However, there is a temperature limitation on ferrite which should be taken into full consideration.

0.2b: Reduction of Coupling with Dielectric Loading

For miniaturized slots the nature of the reduction in coupling from one element to another is due to the reduced area of aperture of each element and to the impedance mismatch at the aperture associated with the loading material. The reduced aperture means that a receiving element, or more properly an element receiving energy from another element, is capturing less energy. This advantage would be true for either linear polarization of each element or for circular polarization for each element. However, in this discussion, major attention is being placed upon linearly polarized elements. Each element investigated in this study was a dielectrically loaded element. The size of the element was so reduced that a slot formed by the open end of an X-band waveguide when loaded with dielectric material within the waveguide constituted a dipole slot suitable for S-band operation. This means that slots $2 \frac{13}{16}$ " x $1 \frac{11}{32}$ " formed by the use of WR-284 S-band waveguide, will be supplanted by loaded slots $2 \frac{9}{32}$ " x $\frac{3}{8}$ " formed by WR-90 standard X-band waveguide filled with Emerson and Cuming stycast high-K solid dielectric. Various values of relative dielectric permeability were used; 5, 7, 11 and 15.

The relative sizes of these slots are illustrated in Chapter IV (Fig. 4-2a) .

The miniature slots as just described and as used in the experimental arrangement utilized a short length of waveguide behind each slot. Each slot was, of course, mounted in a common large conducting plane. In actual array use, it is very likely that the many elements would also be mounted in a common conducting plane. The use of the common conducting plane provides a 3 dB increase in the directivity of each slot element. Furthermore, the plane defines the physical field situation much more precisely than if the slot elements are merely an arrangement of cut off waveguides without a common boundary metal plane surface. Without such a plane surface, considerable uncertainty is introduced into the effective radiative structure of each element. Currents will tend to run back down the outside of the waveguide walls. For this reason it is believed that the use of the common ground plane has been justified in the experimental effort which is to be described.

It was convenient in undertaking the experimental work on the interaction of elements to have the experiments performed at S-band. The analysis of the interaction between two slots based upon an iterative procedure as described in Chapter II is applicable to slots at any frequency and with any size as well as any type of loading material.

0.2c: Experimental Ferrite Loaded Slot Arrays

The experimental work done on simple three-element linear arrays utilized slots having ferrite loading and the size of each slot element was different from that described in the comparison of loaded and air-filled slots. For these experiments on the three-element arrays the slot was 5" x 2" . The depth of the cavity backing of each slot was 1 1/2" . The center frequency of each slot was 350 MHz. The loading of filling material of these slots was ferrite EAF-2 ; the relative permeability of this ferrite was 6.6, the relative permittivity, 12.6 and the magnetic quality factor, 30.

As a preliminary in the experimental work it was appropriate to take the radiation pattern of a typical ferrite loaded slot. For this purpose Slot No. 108

was mounted in a $5 \times 1\frac{1}{2}$ ' aluminum ground plane . A radiation pattern taken at 345 MHz is shown in Fig. 0.2-1.

Use of standard procedures for the calculation of a broadside array of three slots similar to No. 108 and fed equally both in magnitude and phase resulted in the pattern shown in Fig. 0.2-2. An array of three slots was then fabricated with the slots having the magnetic fields collinear (slots arranged end to end in a line). The experimentally determined radiation pattern is shown in Fig. 0.2-3. Since the patterns of these three figures are so similar it was concluded that there was comparatively little interaction between slots. This means that the illumination of the slots was not appreciably modified by mutual coupling. The feed network to the three slots was made with three identical branches, one being connected to each slot. Further work on the same three-element array with uniform progression of phasing of the elements also showed agreement between calculated and experimental patterns. Thus it appeared that for ferrite loaded slots the interaction of coupling of slots was relatively low. This indicates that the driving point impedance of each slot in an array is relatively independent of scan angle.

0.2d : Observed Coupling Effects of Dielectric Loading

Utilizing the information shown in Chapter III, it is possible to make some simple comparisons which are helpful in evaluating the return power. For example, in the consideration of a phased array of elements assume a requirement of 15 percent bandwidth. If two slot elements are made using the usual air-filled S-band waveguide, it can be found from Fig. 3-11 (Ch. III) that the coupling for a spacing of 0.5λ will be approximately -15 dB . On the other hand, the same frequency band can be used with X-band waveguide if it is filled with appropriate loading material such as with a permittivity of 7.0. In Fig. 4-17 (Ch. IV), it can be seen that X-band waveguide so loaded as to be used for S-band frequencies can provide for a 15 percent bandwidth with a coupling of the order of -30 dB. It is observed that the use of dielectric loading material has made the waveguide feed components somewhat frequency sensitive whereas the air-filled waveguide slots did not exhibit this degree of sensitivity. However,

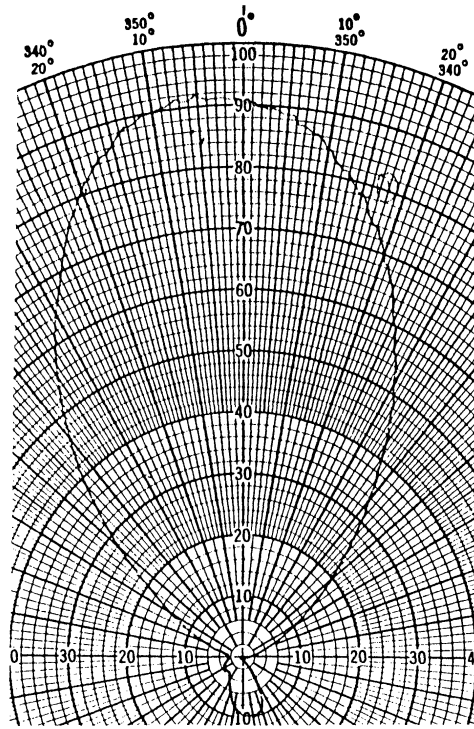


FIG. 0.2-1; EXPERIMENTAL POWER PATTERN (LINEAR) OF FERRITE SLOT IN GROUND PLANE, H-PLANE CUT.

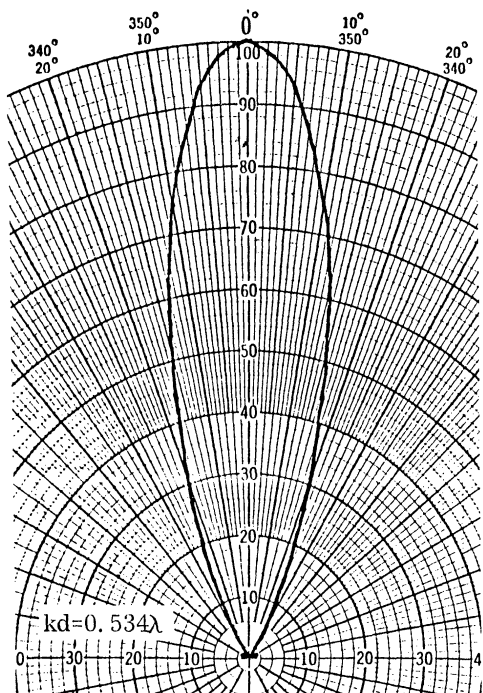


FIG. 0.2-2; CALCULATED POWER PATTERN (LINEAR) FOR 3-ELEMENT FERRITE SLOT ARRAY (H-PLANE)

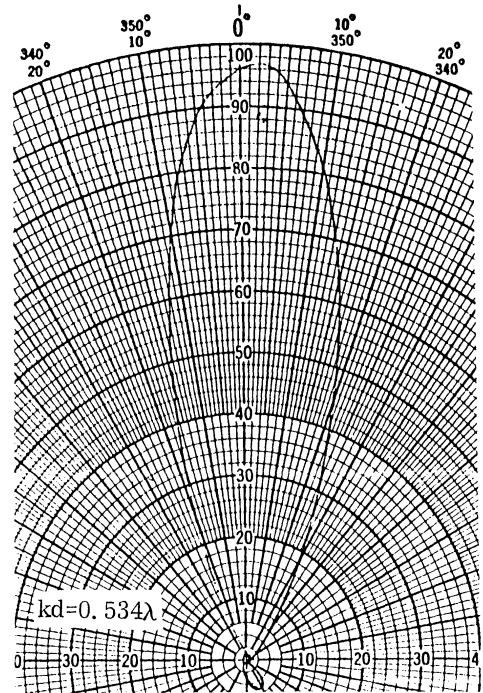


FIG. 0.2-3; EXPERIMENTAL POWER PATTERN (LINEAR) FOR 3-ELEMENT FERRITE SLOT ARRAY (H-PLANE).

increased isolation can be obtained using the smaller slots and the loading material over a useful frequency bandwidth. In order to make this comparison still more apparent, attention is called to Fig. 4-4 (Ch. IV) which shows the experimentally determined coupling for S-band air-filled slots. From this curve it is observed that for a frequency of 3.0 GHz, the coupling is approximately -17 dB.

It is interesting to note that the coupling between the air-loaded slots can also be determined from previously published reports (Lyon et al, 1963; 1966). A number of graphs from these earlier reports are introduced here as Figures 0.2-4, -5, -6 and -7. Figure 0.2-4 shows that for a spacing of 0.5λ , two broadside slots would have a coupling level of -14 dB. This figure was based on X-band but is valid at other frequencies, if the slots scale exactly with frequency. Figure 0.2-5, when applied to the same physical situation, would yield about the same result. For this case, $\theta=0^\circ$. Read along the vertical axis for a separation of 2λ , the value of -26 dB. Then for a separation of 1λ , add 6 dB. Then for a separation of 0.5λ add still another 6 dB. The total is: $026\text{ dB} + 6\text{ dB} + 6\text{ dB} = -14\text{ dB}$. The graphs in Fig. 0.2-5 were also obtained for X-band but are applicable to other frequencies, upon scaling. This presupposes the size of the slot has been changed proportionally to wavelength. This of course is the case for standard size waveguides, and it is true in comparing S-band waveguide in size with X-band waveguide. Figure 0.2-8 shows coupling for S-band slots at various frequencies but at a spacing of 0.5λ .

The frequency bandwidth associated with dielectrically loaded waveguide slots is quite different from that with ferrite material loading in a waveguide. This presupposes that the ferrite material has approximately equal values of relative permittivity and permeability. This being the case, the addition of such material does not change the susceptance at given points of discontinuity in the waveguide and the waveguide fittings as much as a dielectric material. A dielectric material tends to increase the capacitive susceptance at points of discontinuity whereas the ferrite material involves increases of both kinds of susceptance and thus there is compensation.

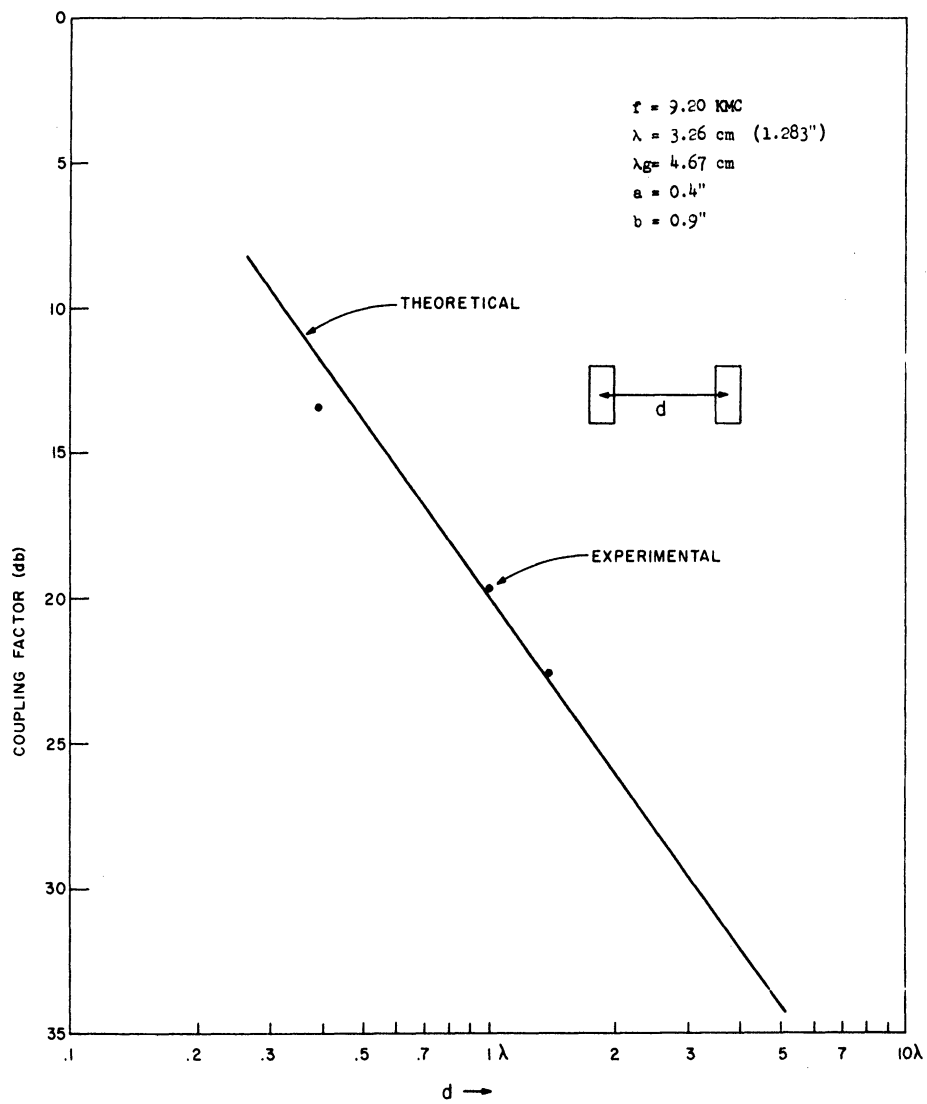


FIG. 0.2-4; BROADSIDE TO BROADSIDE COUPLING OF CLOSELY SPACED RECTANGULAR SLOTS SHOWING A $1/r^2$ TREND.

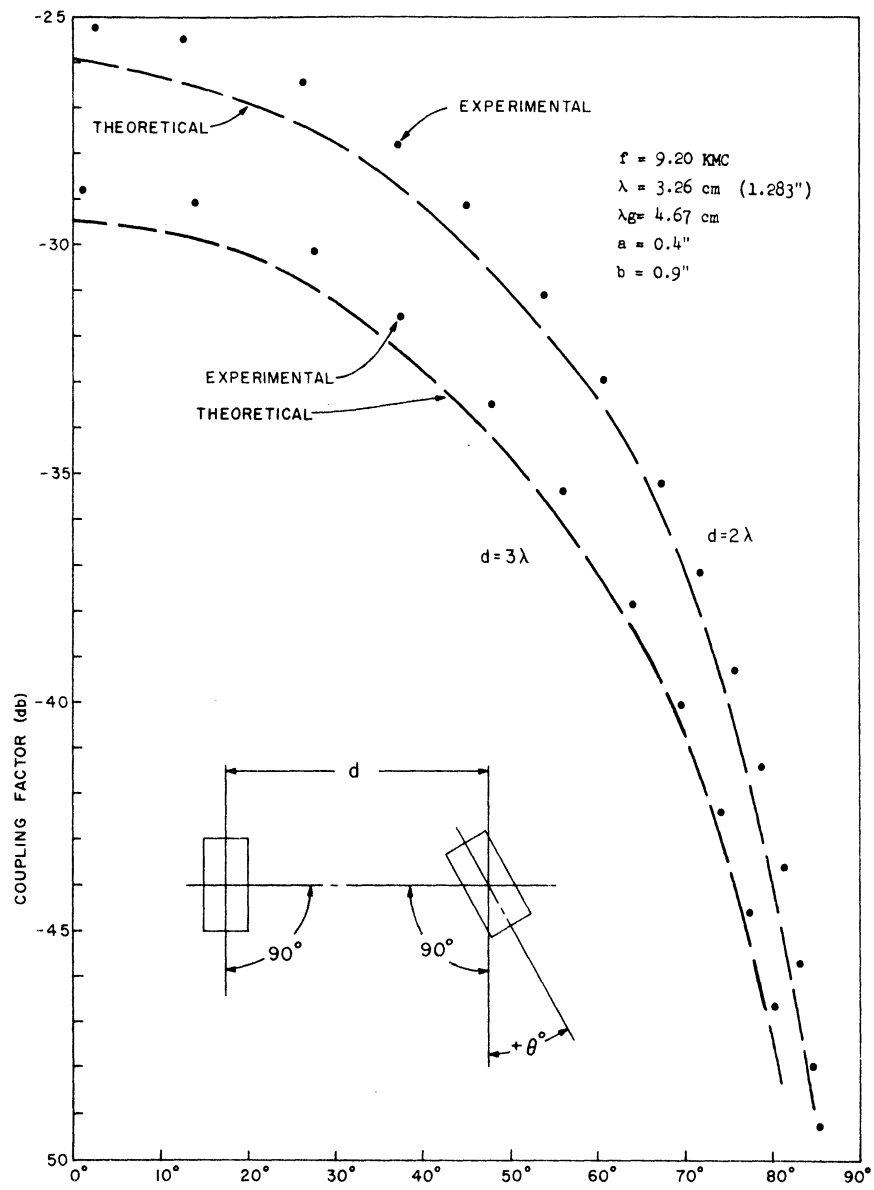


FIG. 0.2-5: FAR-FIELD COUPLING FOR REPRESENTATIVE ANGLES.

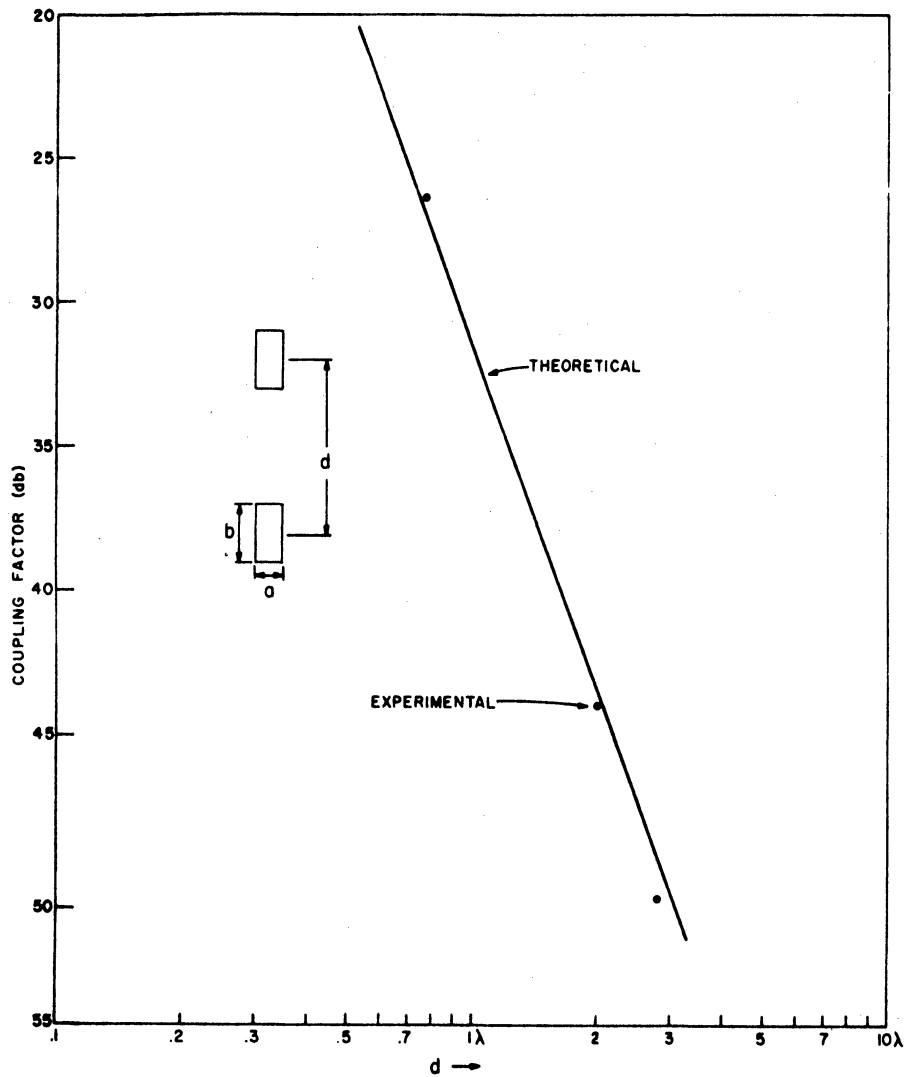


FIG. 0. 2-6: END TO END COUPLING OF CLOSELY SPACED RECTANGULAR SLOTS SHOWING A $1/r^4$ TREND. $f = 9.20$ GHz, $\lambda = 3.26$ cm (1.283"), $\lambda_g = 4.67$ cm, $a = 0.4$ ", and $b = 0.9$ ".

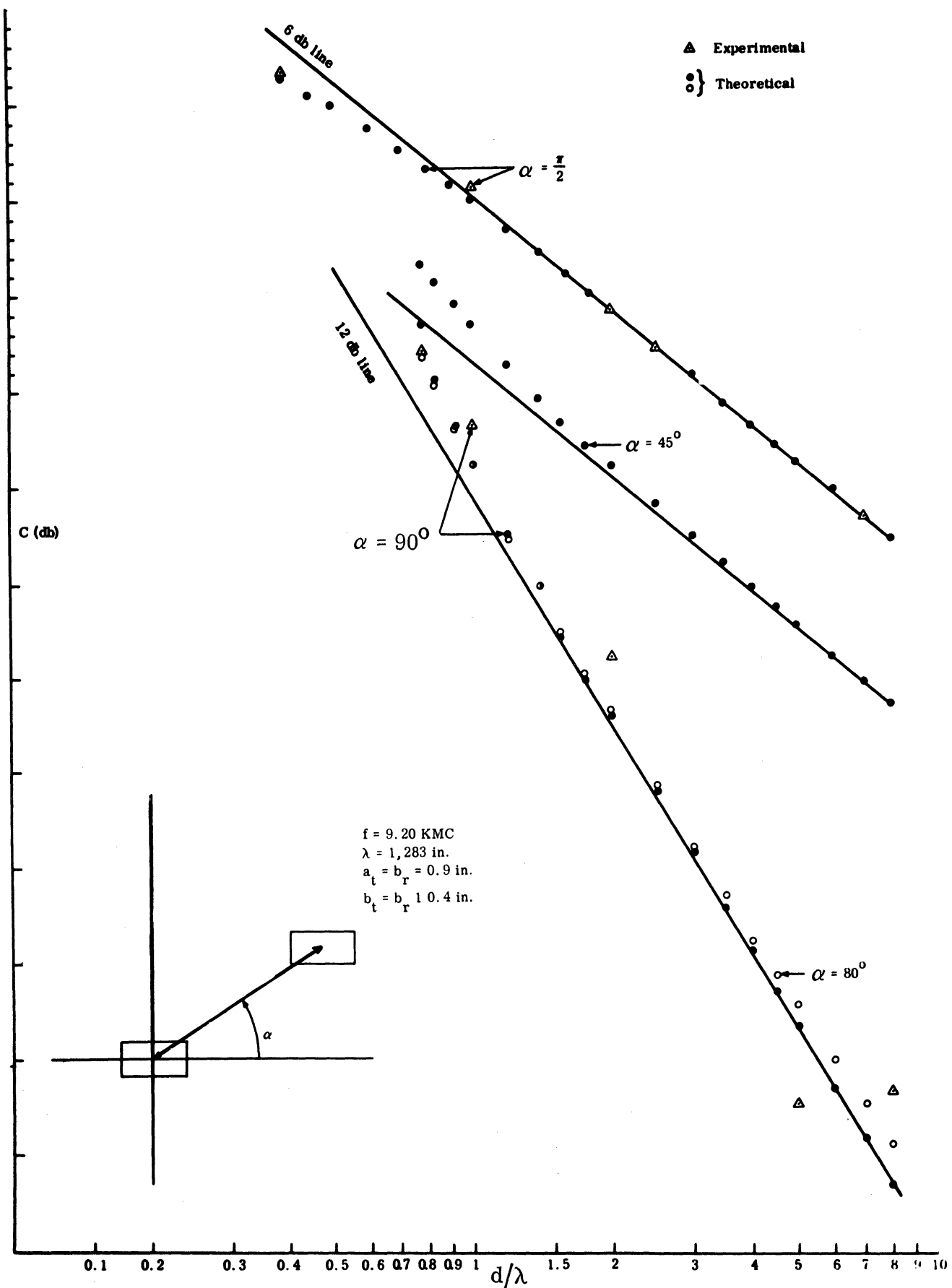


FIG. 0.2-7: COMPARISON BETWEEN EXPERIMENTAL AND THEORETICAL RESULTS .

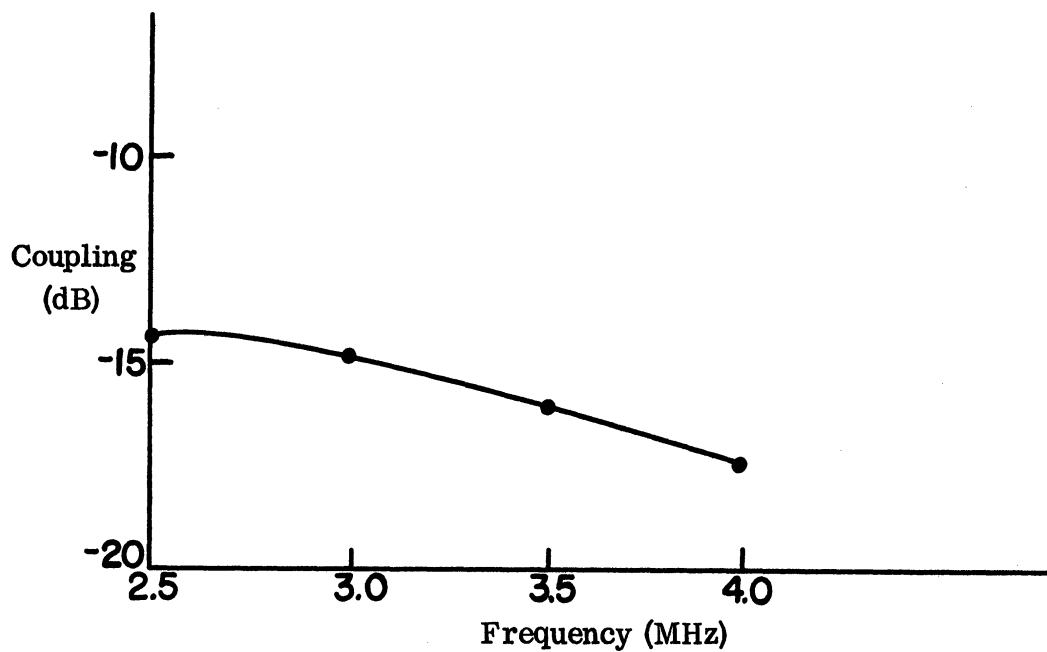


FIG. 0. 2-8: COUPLING OF AIR-FILLED S-BAND WAVEGUIDE SLOTS IN COMMON GROUND PLANE, 0.5λ SPACING, BROADSIDE TO BROADSIDE ARRANGEMENT.

0.2e : Observed Coupling Effects of Ferrite Loading

In the consideration of the advantages of miniaturized elements in arrays, some of the experimental work was done with dielectric loading material merely for convenience. Other parts of the experimental work used ferrite material. The type of ferrite used was EAF-2 characterized by a relative permittivity of 12.6 and a relative permeability of 6.63.

The contention that a ferrite loaded slot is less frequency sensitive than a dielectric loaded slot has been borne out by experimental evidence of other studies (Adams, 1964). One of the slots used in this current study (5"x2"x1 1/2"), has a bandwidth of 19 MHz based on a VSWR of 3. A comparable dielectrically filled slot of the size 12" x 3" x 5" has a bandwidth of 10 MHz on the same VSWR basis .

Additional experimental measurements have been made for the coupling from one ferrite loaded slot to another. These coupling values have been obtained for spacings of approximately 0.5λ and are values for the slots being end to end and also for the slots broadside to broadside. The data are plotted in Figs. 0.2-9 and 0.2-10. It is observed, as expected, that the broadside to broadside level of coupling is somewhat higher than the end to end coupling. However, both levels of coupling are very much reduced from what they would be if air-filled slots were used. Again, in this case the comparable values for air-filled slots would be -14 dB (Fig. 0.2-4) for broadside to broadside coupling and -20 dB (Fig. 0.2-6) for end to end coupling for this spacing. Note that the experimental data on S-band slots as shown in Fig. 0.2-8 shows -15 dB for broadside to broadside coupling. In an array of slots, the end to end coupling is relatively insignificant.

0.2f : Array Returned Power

One of the important measures for an array of many elements is the total returned power from all active elements. For instance an array of many elements may be fed with illumination to give a desired steer angle. Then for a given position of the beam a measure of the returned power coming from all

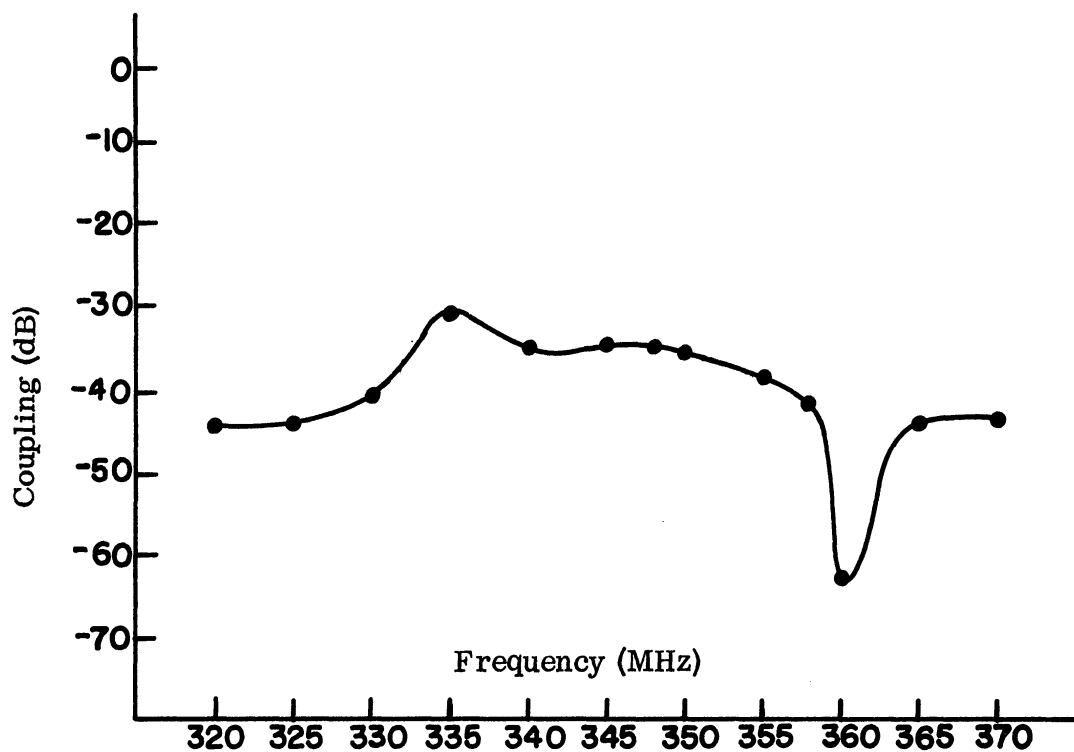


FIG. 0.2-9: COUPLING OF FERRITE LOADED SLOTS IN CONDUCTING PLANE, 0.5λ SPACING, BROADSIDE TO BROADSIDE ARRANGEMENT.

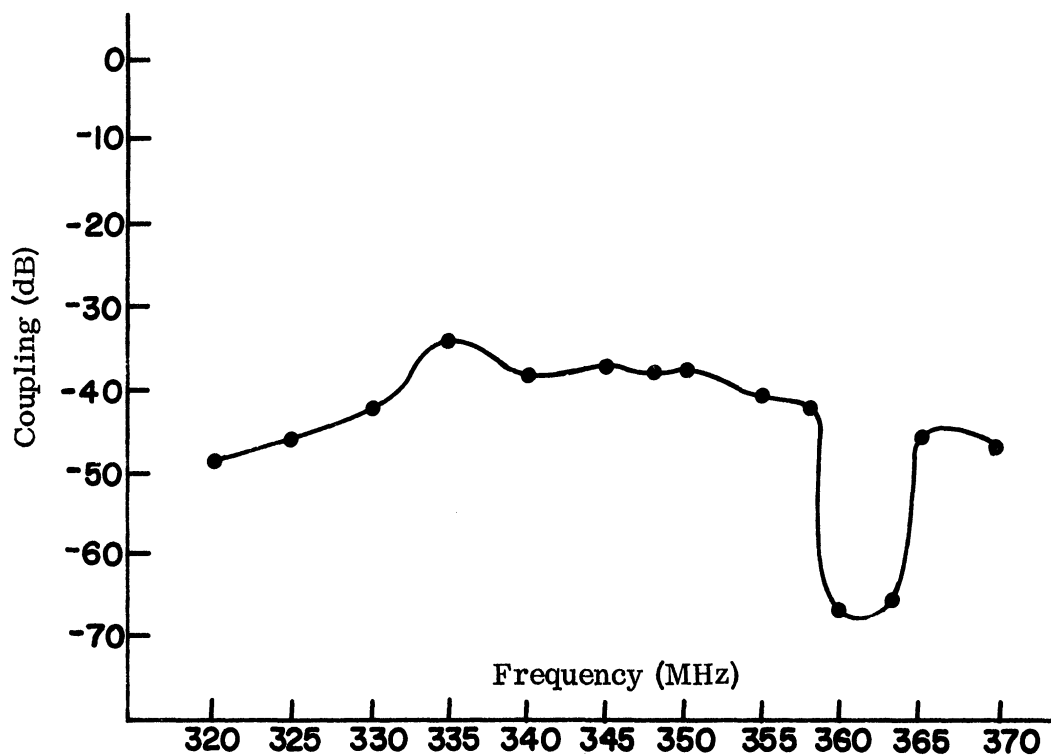


FIG. 0.2-10: COUPLING OF FERRITE LOADED SLOTS IN CONDUCTING PLANE, 0.5λ SPACING, END TO END ARRANGEMENT.

of the elements can be made. A total returned power of 10 percent or less would be considered reasonably good. A returned power of 10 percent would mean the returned power is 10 dB below the incident total feed power. If there were 100 elements in an array, each of them coupling at the level of -30 dB to each of the others, and then all of the returned powers in each of the elements added together in going back to the feed network, the returned power level in the feed network would be 10 dB above the incident feed power to one element. However, this would be -10 dB below the total incident feed power to all elements. Obviously, it is assumed that each element is fed the same power as every other element, and also the phase of each element is the same. This would correspond to the beaming being broadside. Such crude calculations tend to be conservative. Fields are assumed to be in phase and, therefore, additive.

0.2 g: Interaction of Elements in an Array

Consideration of the interaction of every element of an array on every other element can assume somewhat sophisticated levels. At the time of writing this interim report, the ultimate in detailed analysis of this interaction has not been accomplished. However, methods are available for this. If, in the future, additional effort is required on this project, it is expected that it will assume the form of detailed machine calculation of this interaction problem. Two significant sources of information on this general analytical approach are Lechtreck (1968) and Amitay et al (1968)

Approaching the problem of interaction in a relatively simple manner corresponds to the method which is outlined in the following paragraphs. For this purpose, interaction is considered on the basis of an array with all elements equally illuminated and in phase. This corresponds to having a broadside beam for the array. Of course, as the beam scans, the interaction will change. However, having evaluated the interaction in terms of returned power for the broadside beam, it is possible by comparing with results of others (Butzien, 1968) to get a reasonable assessment of interaction and to predict the change in

the interaction level due to having miniaturized slots. Miniaturized slots using dielectric loading will give a somewhat different level of interaction from miniaturized slots using ferrite loading, as will be discussed in succeeding paragraphs.

0.2 h: Examples of Returned Power for Full-Sized Air-Filled Slots

The returned power compared to the input power per single slot is considered. Figure 0.2-11 indicates a two-dimensional array of rectangular slots with uniform separation of 0.5λ . Assume that all of the slots are fed with the same power level. Also, assume that each slot is in phase with every other slot.

The returned power to slot No. 0 is considered. Referring again to Fig. 0.2-11, the contribution due to the slots inside circle "A" is as follows:

- (1) Slots 2 and 4: The coupling between 0 and 2 or 0 and 4 is of the order -14 dB. This can be obtained by looking at Fig. 0.2-4. Therefore, the coupling to slot 0 is of the order $-14 + 10 \log 2 = -11$ dB.
- (2) Slots 1 and 3: The coupling between either 0 and 1 or 0 and 3 is of the order -20 dB (see Fig. 0.2-6). Therefore, the power received by slot 0 from elements 1 and 3 is of the order: $-20 + 10 \log 2 = -17$ dB. Then the power received by element 0 from all four slots in circle "A" can be computed.

$$\begin{aligned} \text{antilog } -1.7 &= 0.01995 \\ \text{antilog } -1.1 &= \underline{0.07943} \\ \text{sum} &= 0.09938 \end{aligned}$$

$10 \log 0.09938 = -10.03$ dB power received
from all four slots.

The contributions due to the slots in a larger circle "B" can be found as follows:

- (3) To calculate the power received by slot 0, take all the slots enclosed by circle "B". The contributions due to 5, 6, 7 and 8 must now be added to the contributions found for slots inside "A". The separations of these slots from slot 0 is:

$$\sqrt{2} \times 0.5\lambda = 0.707 \lambda .$$

From Fig. 0.2-7, the coupling level between each of these slots (5, 6, 7 and 8) and slot 0 can be obtained for $\alpha = 45^\circ$;

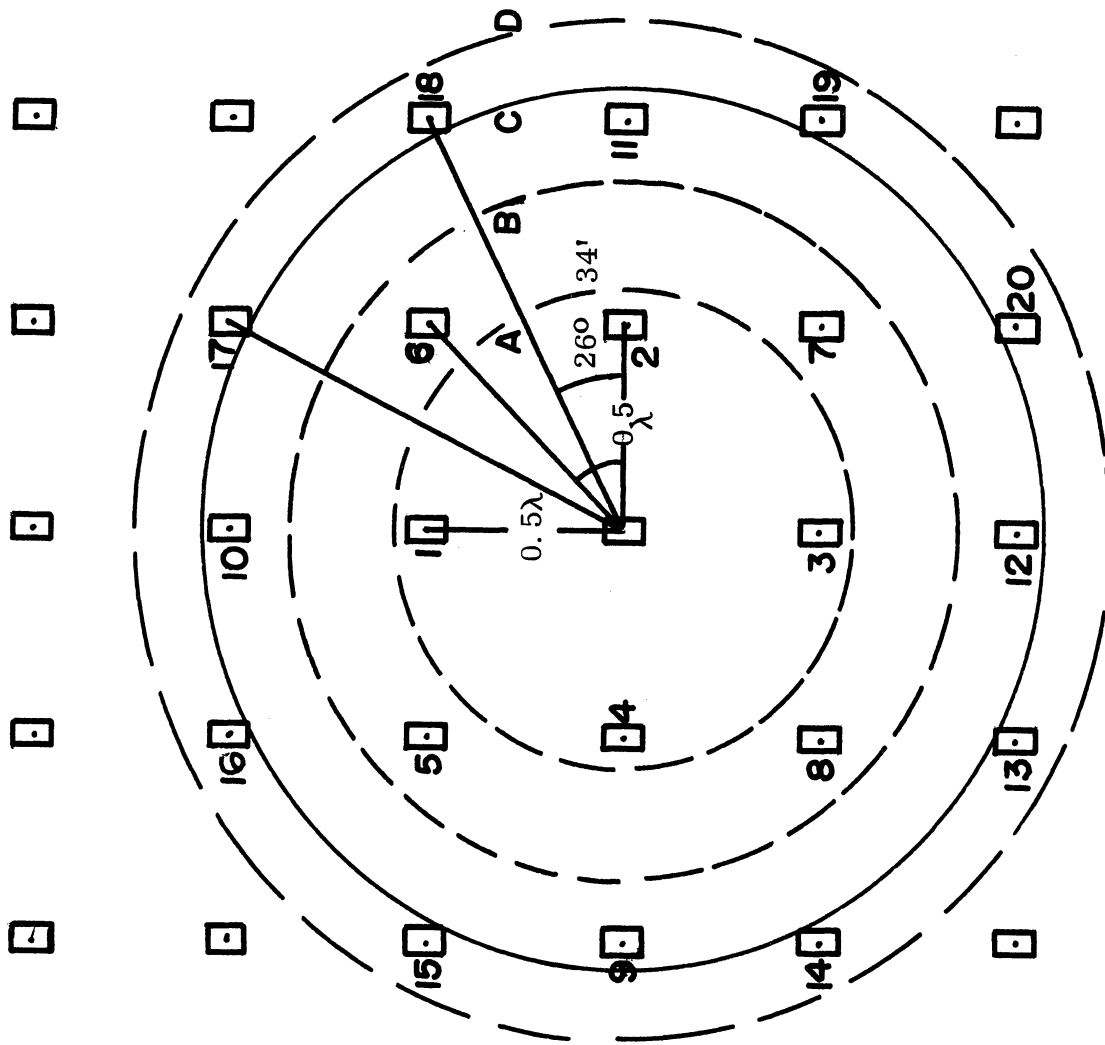


FIG. 0.2-11: INTERACTION OF CERTAIN CHOSEN GROUPS OF SLOTS
CORRESPONDING TO FOUR RADII A, B, C AND D.
POLARIZATION ALIGNED LEFT TO RIGHT.

the value of this coupling is -25 dB. Therefore, the total of the contributions from the four elements is:

$$\begin{aligned}
 10 \log 4 - 25 &\cong -19 \text{ dB} \\
 \text{antilog } -1.9 &= .0127 \\
 \text{antilog } -1.003 &= .0998 \\
 .0127 + .0998 &= .1125 \\
 10 \log 0.1125 &= -9.5 \text{ dB}
 \end{aligned}$$

The -9.5 dB indicates 11.25 percent of the incident power per slot is returned to slot 0 considering all slots in circle "B".

The contributions due to the slots in the still larger circle "C" can be found:

- (4) For the enclosed elements in circle "C", the additional elements will be 9, 10, 11 and 12. The received power from elements 9 and 11 is obtained from Fig. 0.2-4. Each of these has a coupling to slot 0 of -20 dB.

$$10 \log 2 - 20 = -17 \text{ dB contribution from 9 and 11.}$$

The coupling from slot 10 or 12 to slot 0 can be found from Fig. 0.2-6 to be -32 dB.

$$\begin{aligned}
 10 \log 2 - 32 &= -29 \text{ dB contribution from 10 and 12} \\
 \text{antilog } -2.9 &= 0.00125.
 \end{aligned}$$

Then the total power level from all elements enclosed in circle "C" can be found:

$$\begin{aligned}
 10 \log (0.07943 + 0.01995 + 0.0127 + 0.01995 + \\
 0.00125) &= 10 \log 0.13328 = \\
 -8.75 \text{ dB} &\text{ power received from all} \\
 &\text{elements in circle "C" .}
 \end{aligned}$$

The contributions of all elements within circle "D" may be obtained now by including elements 13, 14, 15, 16, 17, 18, 19 and 20:

- (5) Slots 14, 15, 18 and 19 are spaced 2.23λ from slot 0 and the angle $\alpha = 63^\circ 20'$ using Figs. 0.2-11 and 0.2-7. Interpolation on Fig. 0.2-7 will yield -31 dB of coupling each slot to slot 0.

$$10 \log 4 - 31 = -25 \text{ dB.}$$

For elements 13, 16, 17 and 20 the spacing is still 2.23λ but the angle α is $26^\circ 30'$. Again, using Fig. 0.2-7 the coupling of each slot to slot 0 is -44 dB.

$$\begin{aligned}
10 \log 4 - 44 &= -38\text{dB} \\
\text{antilog} - 2.5 &= .003145 \\
\text{antilog} - 3.8 &= .000137 \\
10 \log (0.13328 + 0.003145 + 0.000137) \\
&= 10 \log 0.136562 = -8.65 \text{ dB power received from} \\
&\text{all elements in circle "D" .}
\end{aligned}$$

The results of the interaction for various numbers of nearby elements considered are shown in the graph of Fig. 0.2-12. As shown, the returned power of an array of many elements (say, 1000) will be on the order of -8.65 dB as judged by consideration of the first 20 elements surrounding any one element.

0.2 i : Returned Power for Dielectrically Loaded Slots

As examples of returned power for air-filled slots it is to be noted that the two great contributions are from the two nearest slots which couple broadside to broadside with the slot under consideration. For air-filled slots this coupling level is -14 dB. For dielectrically loaded slots the corresponding level is -30 dB, (see Fig. 4-17, Ch. IV). Although complete information is not yet available it appears with good certainty that for bandwidths of approximately 15 percent or less, the returned power for an array of dielectrically filled slots will be substantially less than for air-filled slots.

0.2 j : Returned Power for Ferrite Loaded Slots

Recent experimental data on the coupling of ferrite filled slots are shown in Figs. 0.2-9 and -10. The lower levels of coupling would then result in a substantially lower returned power level. Reading from the figures for a frequency of 350 MHz and spacing of 0.5λ the broadside to broadside coupling is -35 dB; the end to end coupling is -37 dB. It is interesting to observe that these two coupling values are very close. This contrasts with the unloaded slot case with corresponding values of -14 dB and -20 dB.

Again, making use of Fig. 0.2-11, the returned power to slot number 0 is considered, assuming all slots are ferrite loaded and have the above coupling behavior. The contributions due to the slots inside the circle "A" are as follows:

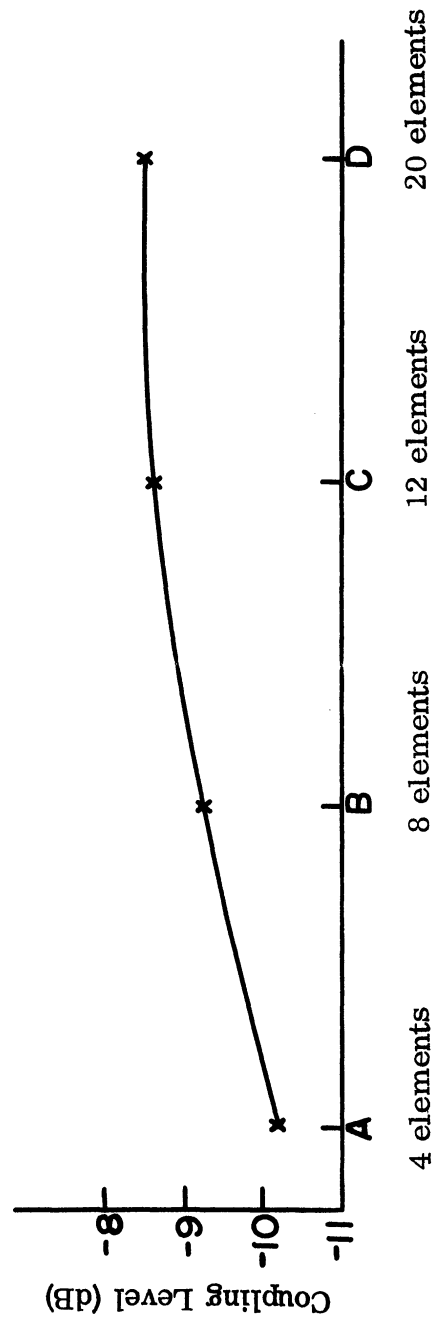


FIG. 0. 2-12: RETURNED POWER LEVEL TO FEED GENERATOR FOR MANY ELEMENT ARRAY AS A FUNCTION OF THE NUMBER OF SLOTS USED IN COMPUTING INTERACTION. Array has all elements illuminated with same phase and magnitude. Spacing of elements is 0.5λ and the coupling level is in terms of input power level to any one slot.

- (1) Slots 2 and 4: the coupling between 0 and 2 or 0 and 4 is of the order -35 dB. This can be obtained from Fig. 0.2-9 for ferrite loaded slots. Therefore the coupling to slot 0 is of the order

$$-35 \text{ dB} + 10 \log 2 = -32 \text{ dB.}$$

- (2) Slots 1 and 3: the coupling between either 0 and 1 or 0 and 3 is of the order -37 dB as can be obtained from Fig. 0.2-10. Therefore, the power received by the slot 0 from elements 1 and 3 is of the order

$$-37 \text{ dB} + 10 \log 2 = -34 \text{ dB.}$$

Then the power received by element 0 from all four slots in the circle "A" can be computed:

$$\text{antilog } -3.2 = 0.00063$$

$$\text{antilog } -3.4 = \underline{0.00040}$$

$$\text{sum} = 0.00103$$

$$10 \log 0.00103 = -29.9 \text{ dB}$$

This last value is the power received in terms of the incident power level to one slot. The contributions due to the slots in a larger circle "B" can be found:

- (3) To calculate the power received by slot 0 take all the slots enclosed by circle "B". The contributions due to 5, 6, 7 and 8 must now be added to the contributions found for slots inside "A". The separation of these slots from slot 0 is:

$$\sqrt{2} \times 0.5\lambda = 0.707\lambda$$

Since tests have not been made for the dependence of coupling of ferrite loaded slots on separation in echelon, assume the most conservative dependence of 6 dB per octave of distance as for broadside to broadside alignment (this is well established). This is conservative since 12 dB is the value for end to end alignment.

$$20 \log \frac{0.707\lambda}{0.5\lambda} = 20 \log 1.414 = 3 \text{ dB}$$

The coupling level between each of these slots, 5, 6, 7 and 8, and slot 0 can be obtained as:

$$-35 - 3 = -38 \text{ dB.}$$

Note that -35 dB has been chosen arbitrarily rather than -37 dB, again being conservative. Therefore the total of the contributions from the four elements is:

$$\begin{aligned}
10 \log 4^{-38} &= -32 \text{ dB} \\
\text{antilog} - 3.2 &= 0.000629 \\
\text{antilog} - 2.99 &= \underline{0.00102} \\
\text{sum} &= 0.001649 \\
10 \log 0.001649 &= -27.9 \text{ dB}.
\end{aligned}$$

This -27.9 dB is for all slots 1 through 8. It indicates that 0.16 percent of the incident power in a slot is returned considering all slots in circle "B". This contrasts with 10.99 percent for air-filled slots.

The contributions of slots in the still larger circles "C" and "D" can readily be included by similar calculations. In this way it is found that the returned power level using contributions from all slots in the "D" circle is -26.9 dB. This value -26.9 dB means the returned power per element from 20 elements surrounding this element is 0.2 percent of the incident power fed to each slot.

Section 0.3 : Conclusions

The work covered in this report has considered a simple linear array of three elements. The experimental radiation patterns of this array indicated a low level of interaction of elements. This low level of interaction is attributed to the use of miniaturized slot elements. The miniaturization has been accomplished by either ferrite or dielectric loading. Such loading imposes some bandwidth restriction on the elements but this constitutes no real limitation for the usual application of phased arrays. Of course, the loading material in slots creates an additional material interface which is of importance both as to the interaction of the elements, and the bandwidth. The following chapters give considerable analysis of the slot-to-slot interaction with loaded slots. The net result of the work reported here is that the use of smaller loaded slots reduces element interaction; the driving point impedance of each slot in an array of other active elements remains more nearly constant than for unloaded slots. It has been shown that the use of ferrite loaded slots rather than air-loaded slots at a given frequency can result in a returned power level of 0.2 percent instead of 13.6

percent. This example was based on conservative calculations for an array of 21 elements. This great reduction in returned power or level of interaction would carry over to much larger arrays using ferrite loaded slots.

References

- Adams, A. T. (1964), "The Rectangular Slot Antenna with Homogeneous Isotropic Loading," The University of Michigan Cooley Electronics Laboratory Technical Report No. 147 (5549-7-T).
- Amitay, N., P. E. Butzien and R. C. Heidt (January 1968), "Match Optimization of a Two-Port Phased Array Antenna Element," IEEE Trans., AP-16, No. 1, 47-57.
- Butzien, P. E. (1968), "Antenna Element Match Design for Planar Phased Array Antennas," Proceedings of the 18th Annual USAF Symposium on Antenna Research and Development, 22 pp.
- Lechtreck, L. W. (1968), "Effects of Coupling Accumulation in Antenna Arrays," IEEE Trans., AP-16, No. 1, 31-36.
- Lyon, J. A. M. and R. M. Kalafus (March 1963), "Aerospace Antenna Coupling Factor Interference Prediction Techniques as Related to the Electromagnetic Compatibility of Different Systems," presented at the Contractor's Conference on Electromagnetic Compatibility Research, Wright-Patterson Air Force Base, 3 pp.
- Lyon, J. A. M., R. M. Kalafus, Y-K Kwon, C. J. Digenis, M. A. H. Ibrahim and C-C Chen (1966), "Derivation of Aerospace Coupling-Factor Interference Prediction Techniques - Final Report," The University of Michigan Radiation Laboratory Report 6633-1-F, AFAL-TR-66-57, AD 483051, UNCLASSIFIED, 334 pp.

Chapter I

INTRODUCTION

The interest in the problem of coupling between two loaded slots backed by loaded waveguide cavities arose when a study was initiated on the use of arrays of miniaturized slot antenna elements. The interest was based upon prior work of the writer on the coupling between unloaded slots and also by the writer's early association with the design problems of antennas of reduced size. The problem of electromagnetic coupling between loaded slots is considerably more complicated than the coupling between unloaded slots. The problem can be considered from a physical viewpoint as a microwave network of considerable complexity due in part to material interfaces. Such a picture is helpful in the consideration of incident and reflected waves at various locations in the physical arrangement.

A thorough search of prior literature was made in three directions:

i) A survey of the literature was made for information on loaded rectangular cavities including the characteristics of these antennas as individual elements: aperture admittance data were sought. There were several papers on this subject such as Adams¹ and Swift and Hatcher¹⁸. There were some reports on the properties of rectangular waveguides covered by dielectric or plasma slabs as in Cockrell¹⁹ and Galejs¹³. The report by Adams¹ was studied very carefully. He used the variational technique to obtain the normalized conductance and susceptance. Some slight changes in his formulas were made and then used as indicated in Section 3.2 of Chapter III. It was possible to obtain the aperture reflection coefficient using simple relations involving normalized conductance and normalized susceptance.

ii) Information was sought on the radiation from empty rectangular waveguide openings in a ground plane and also coupling between such guides. There were several papers and reports in this area in addition to work in which the writer

had participated at an earlier date. Some of these are; the final report by Archer and Hardie¹⁷, Galejs¹³ and Mikenas and Mayes¹⁴. Both Galejs and Mayes have used the reaction concept in their formulations. Some reports from The Ohio State University such as Jennetti¹⁰, Svoboda¹¹, OSU^{20, 21}, have some discussions on an empty or unloaded cavity-backed rectangular slot antenna.

Finally, the report of Lyon, et al², where integral equation formulations were used to predict the coupling of empty slots flush mounted in a ground plane proved helpful.

iii) A search in the literature for information on coupling between loaded slots proved fruitless. There were no papers which have treated the coupling between loaded slots except one recent paper by Wu¹⁶ which appeared in the March 1969 issue of Radio Science. The paper describes a theoretical investigation whereby an integral equation method is used for an analysis of coupling between parallel plate waveguides loaded with dielectric plugs. This present investigation is different in several ways. The analysis is completely different from Wu's since in the present investigation there is a short-circuit at the bottom of each cavity. Also in this investigation, using rectangular waveguide, both theoretical and experimental results have been achieved. The resonance phenomena in this investigation has been explained very carefully; Wu¹⁶ did not do this but indicated more information was needed.

This literature search was continued at the same time the experimental work was being conducted on the coupling of loaded slots with cavity backing. In the meantime several papers on the reaction concept such as Rumsey¹⁵ and Richmond¹² were read carefully and the reaction concept was applied in the theoretical analysis.

1.1 Approach to the Problem

The coupling was sought by first obtaining the coupling between loaded slots on an aperture-to-aperture basis and then to ascertain the effect of the

backing cavity later. From these two analytical steps the total coupling can be obtained. An iterative procedure has been used to compensate for the interaction between the two slots especially when they are very close to each other in spacing.

Some of the graphs in the text will show that the effect of interaction is more pronounced in the case of near field spacing. Interaction is of much less significance for large spacings of slot elements. The situation closely parallels the inductive coupling of two wire circuits.

Chapter II

THEORETICAL ANALYSIS

2.1 Assumptions

In order to formulate the problem there are several assumptions which are appropriate. The exact solution of this problem is very complex. Some of these assumptions are going to be listed at the beginning and the rest will be mentioned at the point where the assumption is made. To simplify the analysis, it will be assumed that only the dominant TE₁₀ mode is propagated at both transmitting and receiving waveguides. The assumption is justified by the experimental work, as we shall see later. Of course, for operation above the cutoff frequency there may be more than one mode propagating. It will be assumed at the start that the scattered field from the receiving slot is not going to affect the excitation at the transmitting slot but compensation for this will be made later in the analysis, by means of an iterative technique. Also it will be assumed that the apertures are equal in size with the broad sides parallel as shown in Fig. 2-1(a).

2.2 Formulation of the Fields in the Different Regions

The proposed method of solving the problem is to assume an aperture illumination at the transmitting slot and then solve to obtain the scattered field inside the receiving aperture. The analysis is that of a three region boundary value problem with Regions I, II and III as shown in Fig. 2-1(b).

Region I

The fields are formulated in general as shown in the equations:

$$\bar{E} = \nabla(\nabla \cdot \bar{\pi}) + \omega^2 \mu \epsilon \bar{\pi} - j\omega\mu \nabla \times \bar{\pi}^* \quad (2.1)$$

$$\bar{H} = \nabla(\nabla \cdot \bar{\pi}^*) + k^2 \bar{\pi}^* + j\omega\epsilon \nabla \times \bar{\pi} \quad (2.2)$$

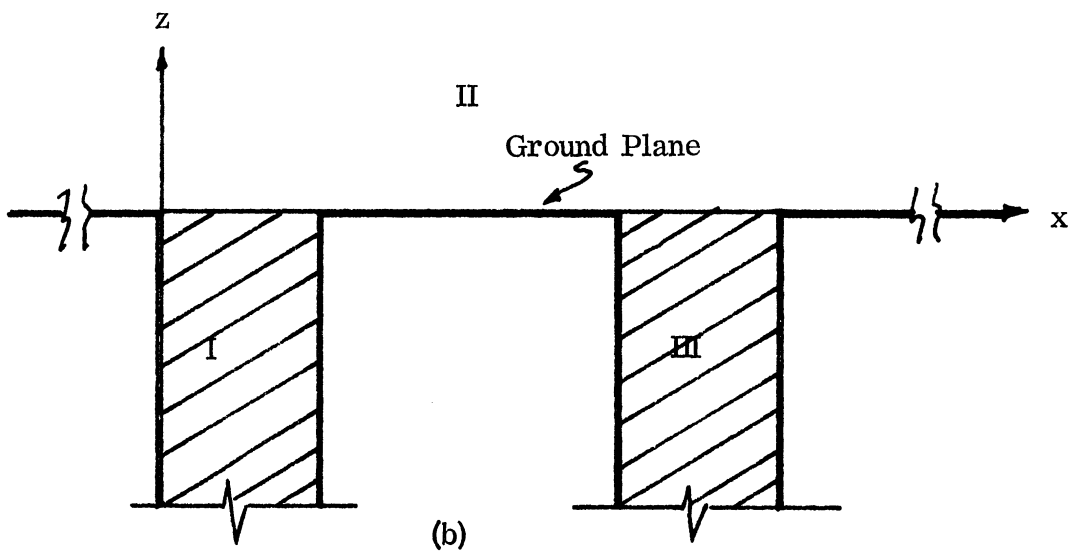
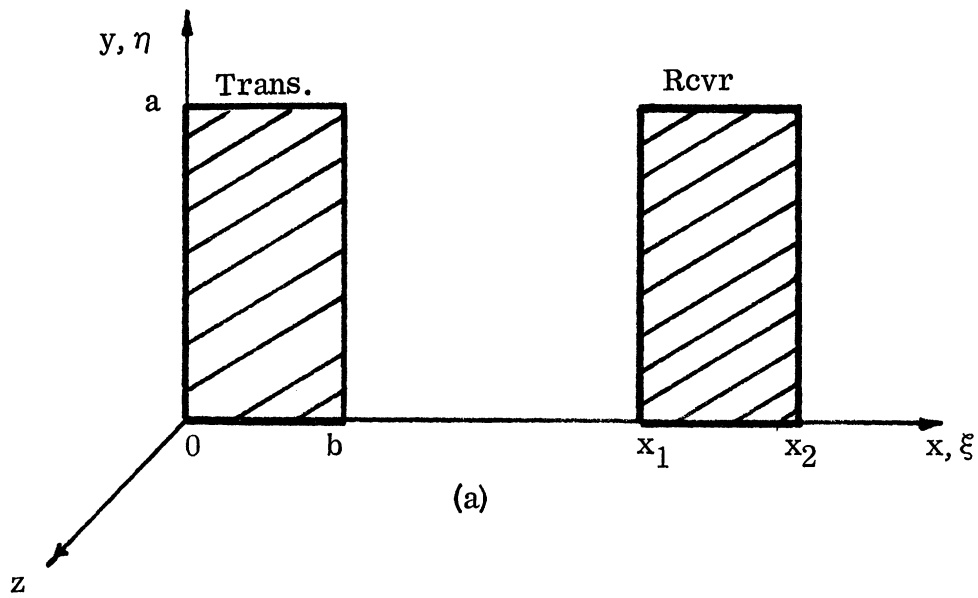


FIG. 2-1: ARRANGEMENT AND SLOT CONFIGURATION

where

$$k^2 = \omega^2 \mu \epsilon \quad (2.3)$$

$\bar{\pi}$ is the Hertzian electric vector potential

and

$\bar{\pi}^*$ is the Hertzian magnetic vector potential.

From the vector identity,

$$\nabla_{\mathbf{x}} \nabla_{\mathbf{x}} \bar{\mathbf{L}} = \nabla(\nabla \cdot \bar{\mathbf{L}}) - \nabla^2 \bar{\mathbf{L}} \quad (2.4)$$

and knowing

$$\nabla^2 \bar{\mathbf{L}} + k^2 \bar{\mathbf{L}} = 0, \quad (2.5)$$

then $\bar{\mathbf{E}}$ and $\bar{\mathbf{H}}$ equations can be rewritten in the form

$$\bar{\mathbf{E}} = \nabla_{\mathbf{x}} \nabla_{\mathbf{x}} \bar{\pi} - j\omega\mu \nabla_{\mathbf{x}} \bar{\pi}^*; \quad (2.6)$$

$$\bar{\mathbf{H}} = \nabla_{\mathbf{x}} \nabla_{\mathbf{x}} \bar{\pi}^* + j\omega\epsilon \nabla_{\mathbf{x}} \bar{\pi}. \quad (2.7)$$

For $E_y = 0$, then set $\pi = \pi_x^* = \pi_z^* = 0$ and substitute in (2.6) and (2.7) obtaining $\bar{\mathbf{E}}_I$ and $\bar{\mathbf{H}}_I$ in the waveguide which are:

$$\bar{\mathbf{E}}_I = -j\omega\mu \nabla_{\mathbf{x}} (\pi_y^* \hat{\mathbf{y}}) \quad (2.8)$$

and

$$\bar{\mathbf{H}}_I = \nabla_{\mathbf{x}} \nabla_{\mathbf{x}} (\pi_y^* \hat{\mathbf{y}}) \quad (2.9)$$

where the subscript I is taken to denote the fields in Region I. Therefore, there results

$$E_{I_x} = (e^{-j\beta z} + Re^{j\beta z}) \sin \frac{\pi y}{a} \sum_{m=1}^{\infty} \sum_{n=0}' A_{mn} \sin \frac{m\pi y}{a} \cos \frac{n\pi x}{b} e^{j\beta_{mn} z}, \quad (2.10)$$

where the prime on the double summation indicates that (1, 0) term has already been removed and where the subscript x is used to denote the x-component of the field,

$$\beta = \frac{\omega}{v} \sqrt{1 - \left(\frac{f_c}{f}\right)^2}, \quad \text{where } f > f_c \quad (2.11)$$

f_c is the cutoff frequency,

$$v = \frac{1}{\sqrt{\mu \epsilon}} , \quad (2.12)$$

and

R is the reflection coefficient of the dominant mode at the aperture.

Region II

Region II is the free space upper hemisphere over the ground plane (see Fig. 2-1(b)). The method of images is going to be used to derive the fields. To formulate the equations of the fields in Region II take

$$\bar{F} = \frac{1}{4\pi} \int_0^a \int_0^b \bar{M} \frac{e^{-jk\rho}}{\rho} ds . \quad (2.13)$$

From Fig. 2-2 an application of the equivalence principle yields (b) from (a) and according to Huygen's principle the result as (c) is obtained and this is going to be used in (2.13). Therefore

$$\bar{F} = \frac{1}{4\pi} \int_0^a \int_0^b 2\bar{E} \times \bar{n} \frac{e^{-jk_0\rho}}{\rho} dx dy,$$

where \bar{M} is the magnetic moment vector

$$\rho = \sqrt{(x-\xi)^2 + (y-\eta)^2 + z^2} , \quad (2.14)$$

and \bar{F} is the electric vector potential.

Since for the problem at hand

$$\bar{E} \times \bar{n} = \bar{E} \times \hat{z} = -E_x \hat{y} \quad (2.15)$$

then

$$\bar{F} = \bar{F}_y = - \left(\frac{1}{2\pi} \int_0^a \int_0^b E_x \frac{e^{-jk_0\rho}}{\rho} dx dy \right) \cdot \hat{y} \quad (2.16)$$

and

$$F_x = F_z = 0 , \quad (2.17)$$

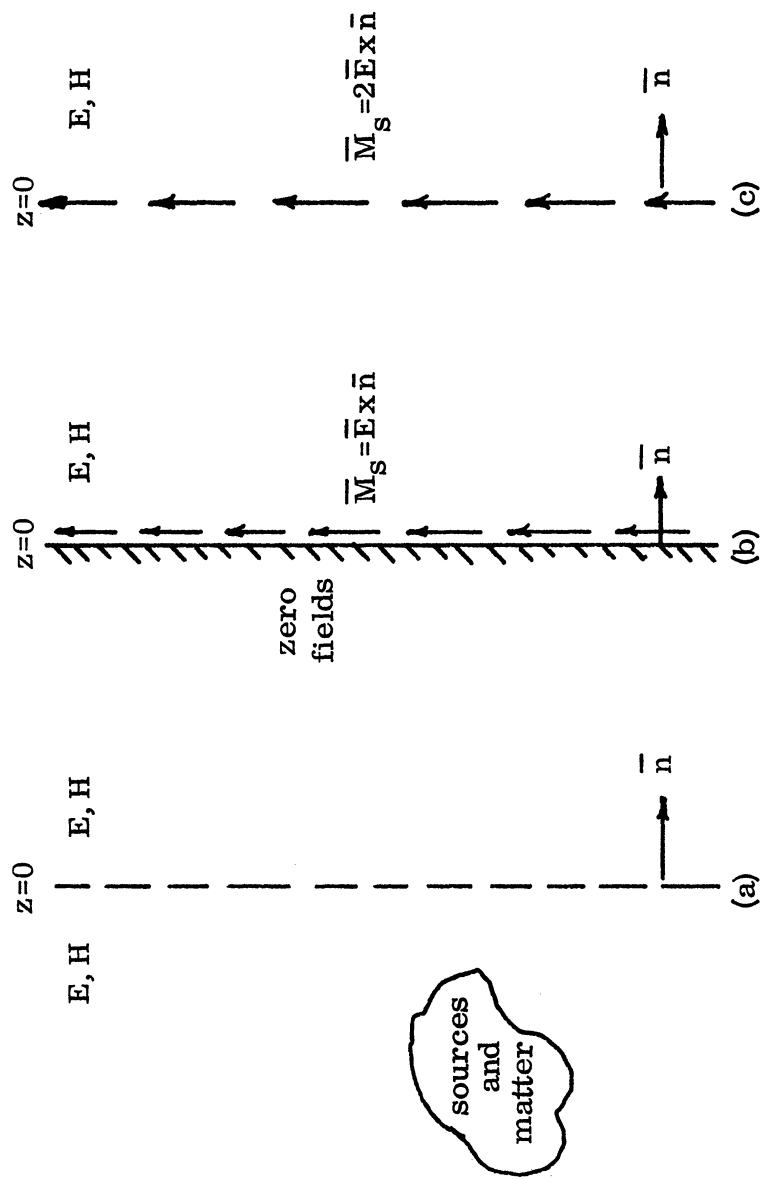


FIG. 2-2: METHOD OF IMAGES

where E_x is the x-component of the field at the transmitting aperture or, in this case, the aperture illumination.

The fields in Region II could be represented, in general, by these equations:

$$\bar{E} = -\nabla \times \bar{F} - j\omega \mu_0 \bar{A} + \frac{1}{j\omega \epsilon_0} \nabla (\nabla \cdot \bar{A}) \quad (2.18)$$

and

$$\bar{H} = \nabla \times \bar{A} - j\omega \epsilon_0 \bar{F} + \frac{1}{j\omega \mu_0} \nabla (\nabla \cdot \bar{F}) \quad (2.19)$$

The radiating source in this case is the rectangular slot denoted by TR and located in an infinite ground plane (see Fig. 2-1). Since only a dominant mode is going to be assumed then the aperture illumination can be given as:

$$\bar{E}_T(\xi, \eta, 0) = (1+R) \sin \frac{\pi \eta}{a} \hat{x} \quad (2.20)$$

where R is the reflection coefficient of the dominant mode at the aperture and ξ, η are the source coordinates as shown in Fig. 2-1(b). Therefore from (2.20) and (2.16)

$$\bar{F} = -\frac{\hat{y}}{4\pi} \int_0^a \int_0^b 2(1+R) \sin \frac{\pi \eta}{a} \frac{e^{-jk_0 \sqrt{(x-\xi)^2 + (y-\eta)^2 + z^2}}}{\sqrt{(x-\xi)^2 + (y-\eta)^2 + z^2}} d\xi d\eta \quad (2.21)$$

where x, y, z are the field points of the coordinate system and

$$k_0 = \omega \sqrt{\mu_0 \epsilon_0} \quad (2.22)$$

From eqs. (2.18) and (2.19) by setting $\bar{A} = 0$, then

$$\bar{E} = -\nabla \times \bar{F} \quad (2.23)$$

and

$$\bar{H} = -j\omega \epsilon_0 \bar{F} + \frac{1}{j\omega \mu_0} \nabla (\nabla \cdot \bar{F}) \quad (2.24)$$

Therefore

$$\bar{E}_{II} = - \left[-\hat{x} \frac{\partial F}{\partial z} + \hat{z} \frac{\partial F}{\partial x} \right] = \hat{x} \frac{\partial F}{\partial z} - \hat{z} \frac{\partial F}{\partial x}$$

and

$$E_{II_x} = \frac{1}{4\pi} \int_0^a \int_0^b 2(1+R) \sin\left(\frac{\pi\eta}{a}\right) \frac{e^{-jk_0\rho}}{\rho^3} \cdot z (-jk_0\rho - 1) d\xi d\eta \quad (2.25)$$

which is the x component of the field in Region II. Notice that $E_{II_x} = 0$ at $z=0$ or the tangential component of the electric field is zero over the ground plane (perfectly conducting) . Also the other components can be obtained in the same manner .

For the \bar{H} field we can write

$$H_{II_x} = - \frac{1}{4\pi j \omega \mu_0} \frac{\partial^2}{\partial x \partial y} \left(\int_0^a \int_0^b 2(1+R) \sin\left(\frac{\pi\eta}{a}\right) \frac{e^{-jk_0\rho}}{\rho} d\xi d\eta \right) \quad (2.26)$$

$$H_{II_y} = - \frac{1}{4\pi j \omega \mu_0} \frac{\partial^2}{\partial y^2} \left(\int_0^a \int_0^b 2(1+R) \sin\left(\frac{\pi\eta}{a}\right) \frac{e^{-jk_0\rho}}{\rho} d\xi d\eta \right) + \frac{j\omega\epsilon_0}{4\pi} \left(\int_0^a \int_0^b 2(1+R) \sin\left(\frac{\pi\eta}{a}\right) \frac{e^{-jk_0\rho}}{\rho} d\xi d\eta \right), \quad (2.27)$$

and

$$H_{II_z} = - \frac{1}{4\pi j \omega \mu_0} \frac{\partial^2}{\partial z \partial y} \left(\int_0^a \int_0^b 2(1+R) \sin\left(\frac{\pi\eta}{a}\right) \frac{e^{-jk_0\rho}}{\rho} d\xi d\eta \right). \quad (2.28)$$

Region III

In Region III again it is to be assumed that the only mode existing is the dominant mode. Therefore as in Region I:

$$\bar{E}_{III_x}(x, y, z) = U \sin \frac{\pi y}{a} e^{j\beta z} \hat{x}, \quad (2.29)$$

where U is the complex amplitude of the electric field at the receiving aperture

and from Maxwell's equations,

$$\frac{\partial E_x}{\partial z} = -\mu j \omega H_y \quad (2.30)$$

Therefore:

$$H_{III_y} = -\frac{1}{j\omega\mu} \frac{\partial}{\partial z} (U \sin \frac{\pi y}{a} e^{j\beta z})$$

and

$$H_{III_y} = -\frac{\beta}{\omega\mu} U \sin \frac{\pi y}{a} e^{j\beta z} \quad (2.31)$$

At the surface of the ground plane or at $z = 0$,

$$\bar{H}_{III_y} = -\frac{\beta}{\omega\mu} U \sin \left(\frac{\pi y}{a} \right) \hat{y} \quad (2.32)$$

where as before

$$\beta = \frac{\omega}{v} \sqrt{1 - \left(\frac{f_c}{f} \right)^2} \quad (2.33)$$

or

$$\beta = \frac{2\pi f}{\lambda x f} \sqrt{1 - \left(\frac{f_c}{f} \right)^2} = 2\pi \sqrt{\left(\frac{1}{\lambda} \right)^2 - \left(\frac{1}{\lambda} \right)^2 \left(\frac{v/\lambda_c}{v/\lambda} \right)^2}$$

or

$$\beta = 2\pi \sqrt{\left(\frac{1}{\lambda} \right)^2 - \left(\frac{1}{2a} \right)^2} \quad (2.34)$$

where λ is the wavelength in the material medium. Therefore, from (2.33)

and (2.32),

$$\bar{H}_{III_y} = -U \sqrt{\frac{\epsilon}{\mu}} \sqrt{1 - \left(\frac{\lambda}{2a} \right)^2} \sin \frac{\pi y}{a} \hat{y} \quad (2.35)$$

where

μ is the permeability of the material

ϵ is the permittivity of the material used

$$\epsilon = \epsilon_0 \epsilon_r$$

$$\mu = \mu_0 \mu_r \quad ,$$

ϵ_0, ϵ_r are the free space and relative permittivity of the material respectively, and

μ_0, μ_r are the free space and relative permeability respectively.

The objective now is to use the formulations of the fields in Regions I, II and III to obtain an expression for U the complex amplitude of the electric field at the receiving apertures corresponding to a given excitation of the transmitting aperture.

2.3 Evaluation of U

To obtain an expression for U there are several ways, including an integral equation formulation or variational technique. For this analysis the reaction concept of Rumsey¹⁵ is going to be used since it simplifies the formulations. As stated by Rumsey, J(c) generates the same field as "g" on the source free side of S as shown in Fig. 2-3, where g is the source, J(c) represents the surface distribution of the electric current which is induced on the scatterer by g, and S is the scattering body.

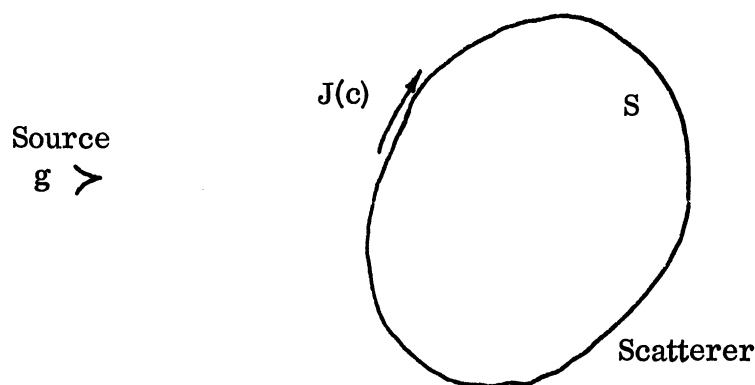


FIG. 2-3: SOURCE AND SCATTERER.

For the specific problem at hand g is the same as the transmitting aperture with a given illumination and the scatterer is the receiving slot.

The boundary conditions with the tangential magnetic fields at the receiving aperture states:

$$\hat{Z} \times \bar{H}_{in} = \hat{Z} \times \bar{H}_s + \hat{Z} \times \bar{H}_{II}, \quad (2.36)$$

where

\bar{H}_{in} is the scattered field inside the waveguide,

\bar{H}_s is the scattered field in the half-space over the ground plane,

and \bar{H}_{II} is the field due to the illumination of the transmitting aperture.

Also

$$\hat{Z} \times \bar{H}_s = -C \hat{Z} \times \bar{H}_{in}, \quad (2.37)$$

$$\text{and } \hat{Z} \times \bar{H}_{in} = \frac{1}{1+C} \hat{Z} \times \bar{H}_{II} \quad (2.38)$$

For the free space case C is taken to be unity as in Lyon². Therefore,

$$\hat{Z} \times \bar{H}_{in} = \frac{1}{2} \hat{Z} \times \bar{H}_{II}. \quad (2.39)$$

Also from the reaction concept which states

$$\langle a, b \rangle = \iiint_V [\bar{E}(b) \cdot d\bar{J}(a) - \bar{H}(b) \cdot d\bar{K}(a)] , \quad (2.40)$$

where

V is the volume which contains the sources,

$\bar{J}(a), \bar{K}(a)$ are the electric and magnetic current densities of source "a",

and $\bar{J}(b), \bar{K}(b)$ are the electric and magnetic current densities of source "b".

It is also helpful to note that the reaction formula has the properties of a scalar product.

The reciprocity theorem of all the sources that can be contained in a finite volume is expressed by

$$\langle a, b \rangle = \langle b, a \rangle . \quad (2.41)$$

The linearity of the fields is implied by the identities ,

$$\langle a, b+C \rangle = \langle a, b \rangle + \langle a, C \rangle , \quad (2.42)$$

and

$$\langle A a, b \rangle = A \langle a, b \rangle = \langle a, A b \rangle , \quad (2.43)$$

where the notation "A a" means the "a" field and source are multiplied by the number A. Also

$$\langle x, a \rangle = \langle x, C \rangle , \quad (2.44)$$

where

x is the test source.

Equation (2.44) expresses the condition that "a" and "C" should "look" the same to an arbitrary test source "x" . Choosing the test source to be "a" itself, then (2.44) contains "a" as the assumed value of sources and C is the correct value of it.

$$\langle a, a \rangle = \langle a, C \rangle \quad (2.45)$$

from (2.40), (2.41) and

$$\langle a, C \rangle = \langle C, a \rangle = \iint_S -\bar{J}(c) \cdot \bar{E}_{III_t} dS . \quad (2.46)$$

From the boundary conditions it is known that

$$\bar{J} = \hat{z} \times \bar{H} . \quad (2.47)$$

Therefore

$$\bar{J}(c) = -H_{II_t} \hat{x} , \quad (2.48)$$

where the subscript t is to denote the tangential component at the aperture.

From Eqs. (2.46) and (2.48) there results

$$\langle a, C \rangle = \iint_S H_{II_t} E_{III_t} dS , \quad (2.49)$$

and

$$\langle a, a \rangle = \iint_S \bar{J}(a) \cdot \bar{E}_{III_t} dS \quad (2.50)$$

in which $\bar{J}(a)$ is the current assumed when the scatterer is removed or

$$J(a) = -H_{II_t} + H_{III_t} , \quad (2.51)$$

where H_{III_t} is the tangential component of the magnetic field in the Region III at $z = 0$. Following the same procedure as given by Rumsey¹⁵, let

$$a = U u . \quad (2.52)$$

Then apply (2.50) and (2.52),

$$\langle a, a \rangle = \iint_S (-H_{II_t} + H_{III_t}) (U E_{III u_t}) dS \quad (2.53)$$

where

$$\bar{E}_{III u_t} = \sin \frac{\pi y}{a} \hat{x} . \quad (2.54)$$

From Eqs. (2.45), (2.49), (2.52) and (2.53),

$$U \iint_S H_{II_t} E_{III u_t} dS = U^2 \iint_S \left(-\frac{H_{II_t}}{U} + H_{III u_t} \right) E_{III u_t} dS .$$

Simplifying the above to get an expression in U,

$$2U \iint_S H_{II_t} E_{III u_t} dS = U^2 \iint_S H_{III u_t} E_{III u_t} dS ,$$

or

$$U = \frac{2 \iint_S H_{II_t} E_{III u_t} dS}{\iint_S H_{III u_t} E_{III u_t} dS} , \quad (2.55)$$

where

$$E_{III u_t} = \sin \frac{\pi y}{a} , \text{ at } z = 0 ,$$

$$H_{III u_t} = -\frac{\beta}{\omega \mu} \sin \frac{\pi y}{a} , \text{ at } z = 0 ,$$

S is the area over the aperture of the receiving slot, and

β is defined as before in Eq. (2.34).

A special case of the above would be that of free space slots and it can be analyzed as follows.

Again

$$\langle a, a \rangle = \iint_S (-H_{II_t} + H_{III_t}) U E_{III_t} u_t dS, \quad (2.53)$$

where

$$E_{III_t} = \sin \frac{\pi y}{a} \hat{x}.$$

From (2.39), which is

$$\hat{z} \times \bar{H}_{in} = \frac{1}{2} \hat{z} \times \bar{H}_{II}$$

and using $C = 1$ as in Lyon² then in this case

$$\bar{H}_{in} = \bar{H}_{III}$$

or

$$H_{II_t} = 2H_{III_t}. \quad (2.56)$$

Substituting in Eq. (2.53):

$$\langle a, a \rangle = \iint_S (-2H_{III_t} + H_{III_t}) U E_{III_t} u_t dS,$$

or

$$\langle a, a \rangle = -U \iint_S H_{III_t} E_{III_t} u_t dS.$$

However

$$H_{III_t} = U H_{III_t} u_t.$$

Therefore

$$\langle a, a \rangle = -U^2 \iint_S H_{III_t} u_t E_{III_t} u_t dS, \quad (2.57)$$

from Eqs. (2.45) and (2.46).

Therefore

$$-U \iint_S J(c) E_{III u_t} dS = -U^2 \iint_S H_{III u_t} E_{III u_t} dS$$

or

$$U = \frac{\iint_S H_{II_t} E_{III u_t} dS}{\iint_S H_{III u_t} E_{III u_t} dS} . \quad (2.58)$$

This is for the free space case where $\mu = \mu_0$ and $\epsilon = \epsilon_0$, where S is the receiving aperture area, and

$$E_{III u_t} = \sin \frac{\pi y}{a}, \quad z = 0, \\ H_{III u_t} = -\frac{\beta}{\omega \mu} \sin \frac{\pi y}{a}, \quad z = 0.$$

To obtain the value of U it is necessary first to obtain H_{II_t} . From (2.27), again write

$$H_{II_y} = \frac{j\omega\epsilon_0}{4\pi} \left(\int_0^a \int_0^b 2(1+R) \sin \frac{\pi \eta}{a} \frac{e^{-jk_0 \rho}}{\rho} d\xi d\eta \right) \\ - \frac{1}{4\pi j\omega\mu_0} \frac{\partial^2}{\partial y^2} \left(\int_0^a \int_0^b 2(1+R) \sin \frac{\pi \eta}{a} \frac{e^{-jk_0 \rho}}{\rho} d\xi d\eta \right), \quad (2.27)$$

where

$$\rho = \sqrt{(x-\xi)^2 + (y-\eta)^2 + z^2}.$$

To simplify (2.27), consider the second term on the right hand side,

$$L = \frac{\partial^2}{\partial y^2} \left(\int_0^a \int_0^b 2(1+R) \sin \frac{\pi \eta}{a} \frac{e^{-jk_0 \rho}}{\rho} d\xi d\eta \right).$$

Interchanging the order of differentiation and integration and substituting

$$\frac{\partial^2}{\partial y^2} = \frac{\partial^2}{\partial y \partial \eta}$$

yields

$$L = - \int_0^a \int_0^b 2(1+R) \sin \frac{\pi \eta}{a} \frac{\partial^2}{\partial y \partial \eta} \left(\frac{e^{-jk_0 \rho}}{\rho} \right) d\xi d\eta . \quad (2.59)$$

Integrating once by parts with respect to η in the manner

$$\int u(x)v'(x)dx = u(x)v(x) - \int v(x)u'(x)dx .$$

Let $u = \sin \frac{\pi \eta}{a}$, $u' = \frac{\pi}{a} \cos \frac{\pi \eta}{a}$,
 $v = \frac{\partial}{\partial y} \left(\frac{e^{-jk_0 \rho}}{\rho} \right)$, and $v' = \frac{\partial}{\partial \eta} \left(\frac{\partial}{\partial y} \frac{e^{-jk_0 \rho}}{\rho} \right)$.

Hence

$$L = - \int_0^b 2(1+R) \sin \frac{\pi \eta}{a} \frac{\partial}{\partial y} \frac{e^{-jk_0 \rho}}{\rho} \Big|_0^a d\xi + \frac{\pi}{a} \int_0^a \int_0^b 2(1+R) \cos \frac{\pi \eta}{a} \frac{\partial}{\partial y} \left(\frac{e^{-jk_0 \rho}}{\rho} \right) d\xi d\eta,$$

or

$$L = \frac{\pi}{a} \int_0^a \int_0^b 2(1+R) \cos \frac{\pi \eta}{a} \frac{\partial}{\partial y} \left(\frac{e^{-jk_0 \rho}}{\rho} \right) d\xi d\eta . \quad (2.60)$$

Therefore, Eq. (2.27) reduces to

$$H_{\Pi_y} = \frac{j\omega \epsilon_0}{4\pi} \left(\int_0^a \int_0^b 2(1+R) \sin \frac{\pi \eta}{a} \frac{e^{-jk_0 \rho}}{\rho} d\xi d\eta \right) - \frac{1}{4\pi j\omega \mu_0} \frac{\pi}{a} \int_0^a \int_0^b 2(1+R) \cos \frac{\pi \eta}{a} \frac{\partial}{\partial y} \left(\frac{e^{-jk_0 \rho}}{\rho} \right) d\xi d\eta . \quad (2.61)$$

Next, return to evaluate U using (2.61). At $z = 0$,

$$\rho = \rho' = \sqrt{(x-\xi)^2 + (y-\eta)^2} \quad . \quad (2.62)$$

Then the numerator of Eq. (2.55) can be written in the form

$$\begin{aligned} \text{Numerator} = & 2 \left\{ \int_{x_1}^{x_2} \int_0^a \sin \frac{\pi y}{a} \left[\frac{j\omega\epsilon_0}{4\pi} \left(\int_0^a \int_0^b 2(1+R) \sin \frac{\pi \eta}{a} \frac{e^{-jk_0 \rho'}}{\rho'} \right) \right. \right. \\ & \left. \left. - \frac{1}{4\pi j\omega\mu_0} \frac{\pi}{a} \int_0^a \int_0^b 2(1+R) \cos \frac{\pi \eta}{a} \frac{\partial}{\partial y} \left(\frac{e^{-jk_0 \rho'}}{\rho'} \right) d\xi d\eta \right] dy dx \right\}, \end{aligned}$$

or

Numerator =

$$\begin{aligned} & 2 \left\{ \frac{j\omega\epsilon_0}{4\pi} \int_{x_1}^{x_2} \int_0^a \int_0^a \int_0^b 2(1+R) \sin \frac{\pi \eta}{a} \sin \frac{\pi y}{a} \frac{e^{-jk_0 \rho'}}{\rho'} d\xi d\eta dy dx \right. \\ & \left. - \frac{1}{4\pi j\omega\mu_0} \frac{\pi}{a} \int_{x_1}^{x_2} \int_0^a \int_0^a \int_0^b 2(1+R) \cos \frac{\pi \eta}{a} \sin \frac{\pi y}{a} \frac{\partial}{\partial y} \left(\frac{e^{-jk_0 \rho'}}{\rho'} \right) d\xi d\eta dy dx \right\}. \quad (2.63) \end{aligned}$$

Then simplify the second part on the right hand side of (2.63) by means of integration by parts as before.

$$\begin{aligned} \text{Take} \quad u &= \sin \frac{\pi y}{a}, & u' &= \frac{\pi}{a} \cos \frac{\pi y}{a}, \\ v &= \frac{e^{-jk_0 \rho'}}{\rho'}, \quad \text{and} & v' &= \frac{\partial}{\partial y} \frac{e^{-jk_0 \rho'}}{\rho'}. \end{aligned}$$

Let

$$I = \int_{x_1}^{x_2} \int_0^a \int_0^a \int_0^b 2(1+R) \cos\left(\frac{\pi\eta}{a}\right) \sin\left(\frac{\pi y}{a}\right) \frac{\partial}{\partial y} \frac{e^{-jk_0\rho'}}{\rho'} d\xi d\eta dy dx .$$

Then integrate by parts

$$I = \int_{x_1}^{x_2} \int_0^a \int_0^a \int_0^b 2(1+R) \cos\frac{\pi\eta}{a} \sin\frac{\pi y}{a} \frac{e^{-jk_0\rho'}}{\rho'} \Bigg|_0^a d\xi d\eta dx \\ - \frac{\pi}{a} \int_{x_1}^{x_2} \int_0^a \int_0^a \int_0^b 2(1+R) \cos\frac{\pi\eta}{a} \cos\frac{\pi y}{a} \frac{e^{-jk_0\rho'}}{\rho'} d\xi d\eta dy dx .$$

Again the numerator can be written as follows

Numerator =

$$2 \left\{ \frac{j\omega\epsilon_0}{4\pi} \int_{x_1}^{x_2} \int_0^a \int_0^a \int_0^b 2(1+R) \sin\frac{\pi\eta}{a} \sin\frac{\pi y}{a} \frac{e^{-jk_0\rho'}}{\rho'} d\xi d\eta dy dx \right. \\ \left. + \frac{1}{4\pi j\omega\mu_0} \frac{\pi}{a} \int_{x_1}^{x_2} \int_0^a \int_0^a \int_0^b 2(1+R) \cos\frac{\pi\eta}{a} \cos\frac{\pi y}{a} \frac{e^{-jk_0\rho'}}{\rho'} d\xi d\eta dy dx \right\} .$$

Some simplification yields:

Numerator =

$$\int_{x_1}^{x_2} \int_0^a \int_0^a \int_0^b \left[\frac{j\omega\epsilon_0(1+R)}{\pi} \sin\frac{\pi\eta}{a} \sin\frac{\pi y}{a} + \frac{(1+R)}{\omega\mu_0 a^2 j} \cos\frac{\pi\eta}{a} \cos\frac{\pi y}{a} \right] \frac{e^{-jk_0\rho'}}{\rho'} d\xi d\eta dy dx .$$

(2.64)

Use the trigonometric identity below:

$$C_1 \cos \frac{\pi \eta}{a} \cos \frac{\pi y}{a} - C_2 \sin \frac{\pi \eta}{a} \sin \frac{\pi y}{a} = \frac{1}{2} \left[(C_1 - C_2) \cos \frac{\pi}{a} (y - \eta) + (C_1 + C_2) \cos \frac{\pi}{a} (y + \eta) \right]$$

C_1 and C_2 would be defined as:

$$C_1 = \frac{\pi(1+R)}{j\omega\mu_0 a^2}, \quad (2.65)$$

and

$$C_2 = \frac{\omega\epsilon_0(1+R)}{j\pi}. \quad (2.66)$$

Finally U can be rewritten in the somewhat simpler form:

$$U = \frac{1}{2C_3} \int_{x_1}^{x_2} \int_0^a \int_0^a \int_0^b \left[(C_1 - C_2) \cos \frac{\pi}{a} (y - \eta) + (C_1 + C_2) \cos \frac{\pi}{a} (y + \eta) \right] \frac{e^{-jk_0 \rho'}}{\rho'} d\xi d\eta dy dx, \quad (2.67)$$

where

$$\begin{aligned} C_3 &= \int_S \int H_{III} u_t E_{III} u_t dS \\ &= - \int_{x_1}^{x_2} \int_0^a \sqrt{\frac{\epsilon}{\mu}} \sqrt{1 - \left(\frac{\lambda}{2a}\right)^2} \sin^2 \frac{\pi y}{a} dy dx \\ &= - \frac{a}{2} \sqrt{\frac{\epsilon}{\mu}} \sqrt{1 - \left(\frac{\lambda}{2a}\right)^2} (x_2 - x_1). \end{aligned}$$

In Eq. (2.67)

$$C_3 = - \frac{ab}{2} \sqrt{\frac{\epsilon}{\mu}} \sqrt{1 - \left(\frac{\lambda}{2a}\right)^2} \quad (2.68)$$

since from Fig. 2-1(a), $x_2 - x_1 = b$. λ in this case is the wavelength in material medium corresponding to a certain operating frequency.

Since this integration of (2.67) could not be obtained in a closed form, computational techniques are needed.

From the point of view of computational techniques a quadruple integral is impractical to use. Therefore, the aim here is to reduce Eq. (2.67) to a simpler form. The simplification is going to be achieved by means of transformation of coordinates. First change the limits of integration for x from $x_1 \rightarrow x_2$, to the new limits $0 \rightarrow b$ using a new variable x' . This corresponds to a shift of axis as in Fig. 2-4.

The new variable x' is defined by:

$$x' = x - x_1 .$$

Thus

$$dx' = dx .$$

Also, take

$$\rho' = \sqrt{(x-\xi)^2 + (y-\eta)^2} = \sqrt{(x'+x_1-\xi)^2 + (y-\eta)^2} .$$

To reduce (2.67) to a double integral which is practical in numerical calculation, another coordinate transformation is now performed.

$$\begin{aligned} y - \eta = \gamma \quad , \quad & x' - \xi = \sigma \quad , \\ y + \eta = a + \mu \quad , \quad & \text{and} \quad x' + \xi = b + \nu \quad . \end{aligned}$$

The above are equivalent to a rotation by 45° , translation and magnification by $\sqrt{2}$ (see Appendix A and Fig. 2-5). Notice that

$$f(\gamma, \mu, \sigma, \nu) = \left\{ (C_1 - C_2) \cos \frac{\pi}{a} \gamma + (C_1 + C_2) \cos \frac{\pi}{a} (a + \mu) \right\} \frac{e^{-jk_0 \sqrt{(\sigma+x_1)^2 + \gamma^2}}}{\sqrt{(\sigma+x_1)^2 + \gamma^2}} .$$

This simplifies to

$$f(\gamma, \mu, \sigma, \nu) = \left\{ (C_1 - C_2) \cos \frac{\pi}{a} \gamma - (C_1 + C_2) \cos \frac{\pi}{a} \mu \right\} \frac{e^{-jk_0 \sqrt{(\sigma+x_1)^2 + \gamma^2}}}{\sqrt{(\sigma+x_1)^2 + \gamma^2}} , \quad (2.69)$$

where f is an even function in γ , μ and ν .

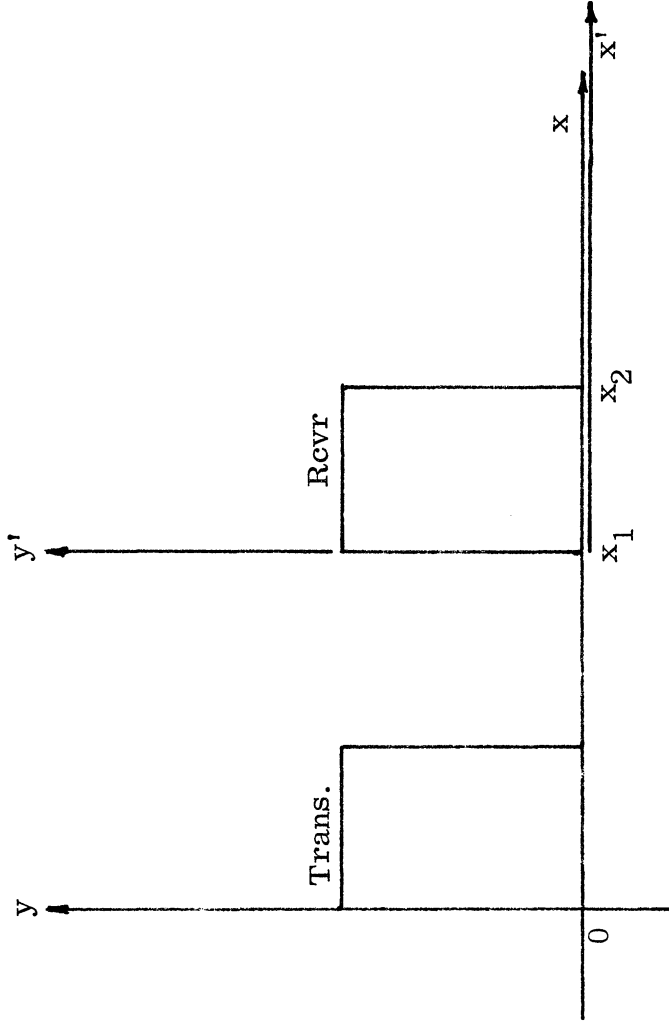


FIG. 2-4: COORDINATE TRANSFORMATION

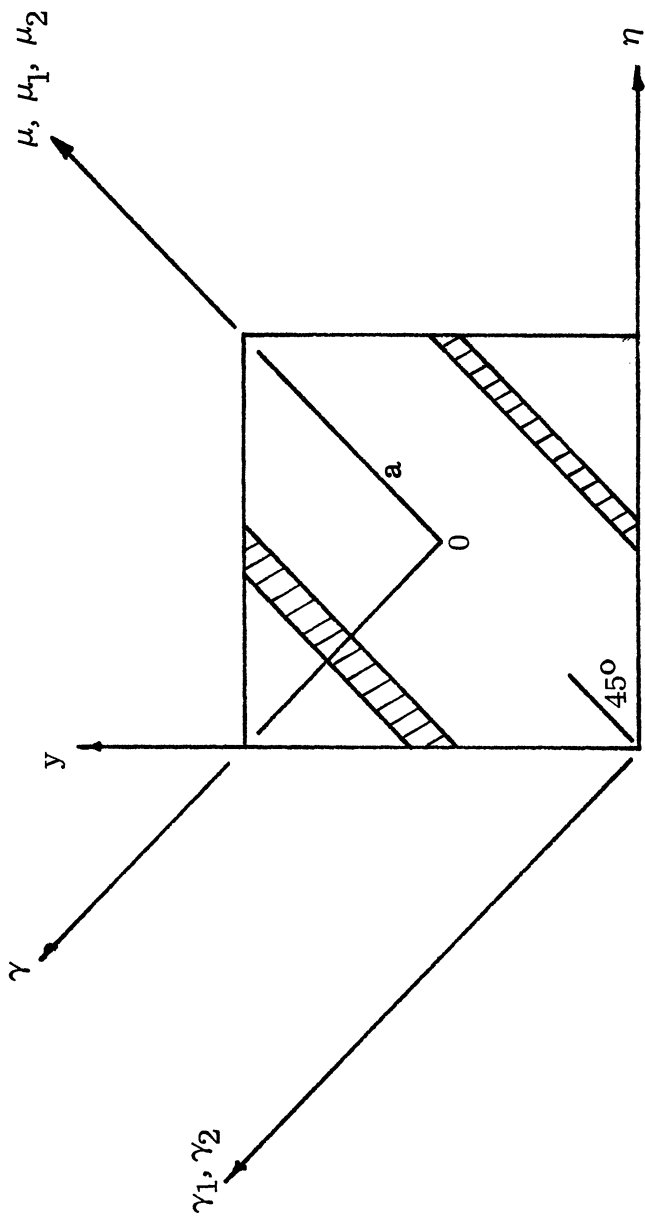


FIG. 2-5: COORDINATE TRANSFORMATION FOR REDUCTION OF QUADRUPLE INTEGRAL TO DOUBLE INTEGRAL.

Then:

$$U = \frac{1}{2C_3} \left\{ \int_0^a \int_0^b \int_0^{a-\gamma} \int_{-(b-\sigma)}^{(b-\sigma)} \left[(C_1 - C_2) \cos \frac{\pi}{a} \gamma - (C_1 + C_2) \cos \frac{\pi}{a} \mu \right] e^{\frac{-jk_0 \sqrt{(\sigma+x_1)^2 + \gamma^2}}{\sqrt{(\sigma+x_1)^2 + \gamma^2}}} d\nu d\mu d\sigma d\gamma \right. \\ \left. + \int_0^a \int_{-b}^0 \int_0^{a-\gamma} \int_{-(b+\sigma)}^{(b+\sigma)} \left[(C_1 - C_2) \cos \frac{\pi}{a} \gamma - (C_1 + C_2) \cos \frac{\pi}{a} \mu \right] e^{\frac{-jk_0 \sqrt{(\sigma+x_1)^2 + \gamma^2}}{\sqrt{(\sigma+x_1)^2 + \gamma^2}}} d\nu d\mu d\sigma d\gamma \right\} \quad (2.70)$$

Performing integration in both ν and μ the expression for U can be reduced to

$$U = \frac{1}{2C_3} \left\{ \int_0^a \int_0^b 2(b-\sigma) \left[(C_1 - C_2)(a-\gamma) \cos \frac{\pi}{a} \gamma - \frac{a}{\pi} (C_1 + C_2) \sin \frac{\pi \gamma}{a} \right] \frac{e^{-jk_0 \rho'}}{\rho'} d\sigma d\gamma \right. \\ \left. + \int_0^a \int_{-b}^0 2(b+\sigma) \left[(C_1 - C_2)(a-\gamma) \cos \frac{\pi}{a} \gamma - \frac{a}{\pi} (C_1 + C_2) \sin \frac{\pi \gamma}{a} \right] \frac{e^{-jk_0 \rho'}}{\rho'} d\sigma d\gamma \right\}. \quad (2.71)$$

This is for $\lambda < 2a$,

$$\rho' = \sqrt{(\sigma+x_1)^2 + \gamma^2}, \\ C_1 = \frac{\pi(1+R)}{jk_0 a^2} \sqrt{\frac{\epsilon_0}{\mu_0}}, \\ C_2 = \frac{k_0(1+R)}{j\pi} \sqrt{\frac{\epsilon_0}{\mu_0}},$$

and

$$C_3 = -\frac{ab}{2} \sqrt{\frac{\epsilon'}{\mu}} \sqrt{1 - \left(\frac{\lambda}{2a}\right)^2} = -\frac{ab}{2} \sqrt{\frac{\epsilon'}{\mu}} \sqrt{1 - \left(\frac{\pi}{ka}\right)^2}.$$

R is the aperture reflection coefficient.

A further simplification can be made:

Consider:

$$\begin{aligned}
 I_1 &= \int_0^a \int_{-b}^0 2(b+\sigma) \left[(C_1 - C_2)(a-\gamma) \cos \frac{\pi}{a} \gamma - \frac{a}{\pi} (C_1 + C_2) \sin \frac{\pi \gamma}{a} \right] \frac{e^{-jk_0 \rho'}}{\rho'} d\sigma d\gamma \\
 &= \int_0^a \int_0^b 2(b-\sigma) \left[(C_1 - C_2)(a-\gamma) \cos \frac{\pi}{a} \gamma - \frac{a}{\pi} (C_1 + C_2) \sin \frac{\pi \gamma}{a} \right] \frac{e^{-jk_0 \rho''}}{\rho''} d\sigma d\gamma, \quad (2.72)
 \end{aligned}$$

where

$$\rho'' = \sqrt{(x_1 - \sigma)^2 + \gamma^2}.$$

Therefore, Eq. (2.71) reduces to:

$$U = \frac{1}{C_3} \int_0^a \int_0^b \left[(C_1 - C_2)(a-\gamma) \cos \frac{\pi}{a} \gamma - \frac{a}{\pi} (C_1 + C_2) \sin \frac{\pi \gamma}{a} \right] (b-\sigma) \left\{ \frac{e^{-jk_0 \rho'}}{\rho'} + \frac{e^{-jk_0 \rho''}}{\rho''} \right\} d\sigma d\gamma. \quad (2.73)$$

2.4 Iteration Procedure

It was assumed at the beginning of the analysis that the illumination of the transmitting aperture is not affected by the scattered field from the receiving aperture. This is a very good assumption if the two apertures are sufficiently far apart. The assumption is not justified for very close spacings of the aperture.

The interaction between a transmitting and receiving antenna as a result of scattering can be described as follows. If a transmitting antenna is considered completely isolated and matched to its line, then when a receiving antenna is introduced into the field of this antenna there will be a scattered field as can be seen from Eq. (2.36). This scattered field from the receiving aperture when intercepted by the transmitting slot, in turn gives rise to a wave transmitted down the feed line causing a mismatch. Also the transmitting slot gives rise to scattered fields that again will be partly intercepted and partly scattered at the

receiving aperture. Thus the interaction is due to a multiple scattering and absorption process as can be represented by Fig. 2-6.

An analysis corresponding to the above explanation can be made. From Eqs. (2.73), (2.65) and (2.66) then:

$$C_1 - C_2 = \frac{\pi(1+R)}{j\omega\mu_0 a^2} - \frac{\omega\epsilon_0(1+R)}{j\pi} = (1+R) \left[\frac{\pi}{j\omega\mu_0 a^2} - \frac{\omega\epsilon_0}{j\pi} \right],$$

$$C_1 - C_2 = (1+R)C_4,$$

and

$$C_1 + C_2 = (1+R)C_5,$$

where

$$C_4 = \frac{\pi}{j\omega\mu_0 a^2} - \frac{\omega\epsilon_0}{j\pi}, \quad (2.74)$$

and

$$C_5 = \frac{\pi}{j\omega\mu_0 a^2} + \frac{\omega\epsilon_0}{j\pi}. \quad (2.75)$$

$$U = (1+R) \frac{1}{C_3} \left\{ \int_0^a \int_0^b \left[C_4 (a-\gamma) \cos \frac{\pi}{a} \gamma - \frac{a}{\pi} C_5 \sin \frac{\pi}{a} \gamma \right] (b-\sigma) \left[\frac{e^{-jk_0 \rho'}}{\rho'} + \frac{e^{-jk_0 \rho''}}{\rho''} \right] d\sigma d\gamma = (1+R)F \right\} \quad (2.76)$$

where

$$F = \frac{1}{C_3} \int_0^a \int_0^b \left[C_4 (a-\gamma) \cos \frac{\pi}{a} \gamma - \frac{a}{\pi} C_5 \sin \frac{\pi}{a} \gamma \right] (b-\sigma) \left\{ \frac{e^{-jk_0 \rho'}}{\rho'} + \frac{e^{-jk_0 \rho''}}{\rho''} \right\} d\sigma d\gamma. \quad (2.77)$$

Now assume that the magnitude of the aperture illumination is $(1+R)$. Then the received aperture illumination will be $(1+R)F$ for the first iteration. For the second iteration there will be $(1+R)F^3$ added to the results for the first iteration and so on. Therefore the received aperture illumination is:

$$UI = (1+R)F \left[1 + F^2 + F^4 + F^6 + F^8 + \dots \right],$$

or

$$UI = (1+R) \frac{F}{1-F^2}. \quad (2.78)$$

This is the upper hemisphere in the problem

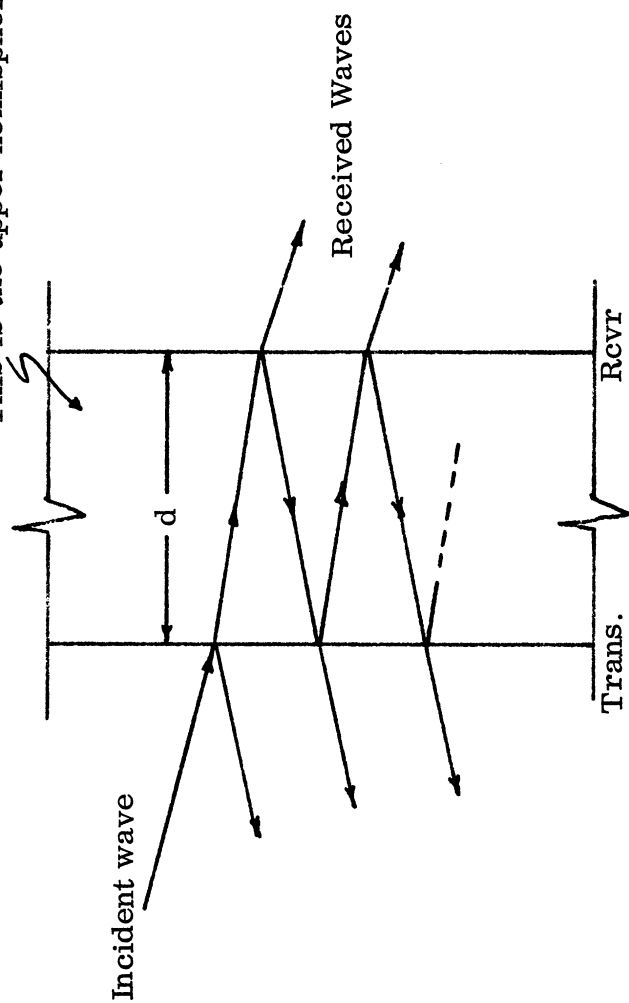


FIG 2-6: MULTIPLE REFLECTION BETWEEN TRANSMITTER AND RECEIVER TO REPRESENT INTERACTION BETWEEN THEM.

where U_I stands for the modified U . This iterative process has been described rather simply due to the fact that the reciprocity property has been used. The factor F of coupling is the same from transmitter to the receiver as from the receiver to transmitter. The absorbed power or energy in the transmitter due to scattering from receiver has been ignored since it is small compared to the original excitation.

2.5 Consideration of the Short-Circuited Waveguide Backing the Slots

2.5.1 General Discussion

The problem under study uses a short-circuited waveguide section at both transmitter and receiver. The shorted waveguide section is fed by means of a coaxial-to-waveguide probe. Consider first the effect of the cavity alone as shown in Fig. 2-7.

The arrangement of the axis for formulation is taken as in Fig. 2-1 except for taking z to be positive in the reverse direction. Note that the input impedance seen at $z=0$ or at the aperture of the homogeneously filled waveguide with material described by μ_1 and ϵ_1 and shorted at " l " is:

$$Z_{g1}(0) = Z_{g1} \tanh \gamma_{g1} l, \quad (2.79)$$

with the subscript " g " referring to the field in the guide and the subscript " 1 " referring to waveguide Number 1. Also,

$$\gamma_{g1} = \alpha_{g1} + j \beta_{g1}, \quad (2.80)$$

and

$$\beta_{g1} = 2\pi / \lambda_{g1} \quad (2.81)$$

where λ_{g1} is the guide wavelength in the filled guide. If the attenuation could be neglected, Eq. (2.79) could be rewritten

$$Z_{g1}(0) = Z_{g1} j \tan \frac{2\pi}{\lambda_{g1}} l, \quad (2.82)$$

where

$$Z_{g1} = \frac{\eta}{\sqrt{1-(f_c/f)^2}} = \frac{\sqrt{\mu_1/\epsilon_1}}{\sqrt{1-(f_c/f)^2}}. \quad (2.83)$$

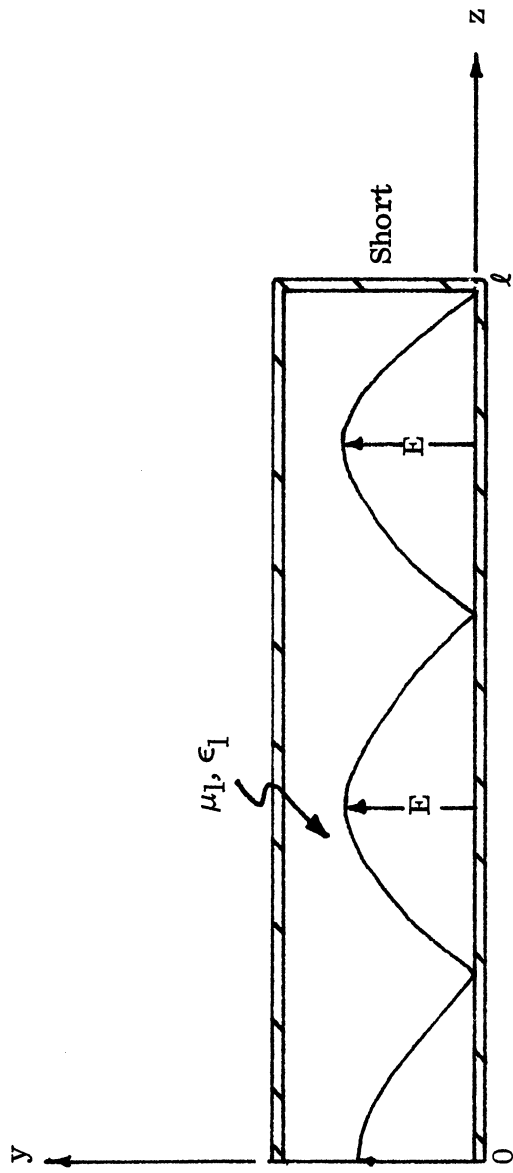


FIG. 2-7: SHORT-CIRCUITED CAVITY.

The real parts of the fields in the waveguide are:

$$\operatorname{Re}(E_y) = U \sin \omega t \sin \left[\frac{2\pi}{\lambda_{g1}} (z - \ell) \right] \quad (2.84)$$

and

$$\operatorname{Re}(H_x) = \frac{U}{z_{g1}} \cos \omega t \cos \left[\frac{2\pi}{\lambda_{g1}} (z - \ell) \right] . \quad (2.85)$$

The standing electric and magnetic waves in front of the short-circuit are displayed in Fig. 2-8 in terms of λ_{g1} the guide wavelength for Section 1.

The impedance $z_g(0)$ which is the input impedance at $z=0$ varies as shown in Fig. 2-9. It is noticed from Fig. 2-9 that the impedance is zero at $z=\ell$ which is at the shorted end of the waveguide. It varies from $-\infty$ to $+\infty$ at $\ell - \lambda_{g1}/4$ and then returns to zero again at $\ell - \lambda_{g1}/2$ and so on. The pattern shows resonance points at $n \lambda_{g1}/2$ where $n = 1, 2, 3, \dots$, from the shorted end and antiresonance at points $n \lambda_{g1}/4$ where $n=1, 2, 3, \dots$, from the shorted end.

It is to be remembered that these resonances and anti-resonances do not take into consideration perturbations due to the material or the perturbation due to the feed probe into the waveguide. These effects can be included as was done by Adams¹ and will be mentioned later.

For more physical insight, it is to be noted that if the waveguide is tuned to a multiple of a half wavelength, then in this case if a short is placed on the open end of the guide, as in Fig. 2-10, at $z=0$, nothing will be changed inside the guide. The wave pattern in this special case can satisfy the boundary conditions at both ends. On the other hand for the case of any arbitrary length ℓ , a phase mismatch results between the standing wave building up in front of the shorted end at $z=\ell$ and that required by the boundary at $z=0$. Destructive interference takes place between the incident waves and the reflected waves at the aperture ($z=0$) and therefore the amplitude of the standing wave decreases. Note that the impedance expression (2.79) remains the same since the only requirement is that a wave entering from the aperture at $z=0$ is totally reflected at

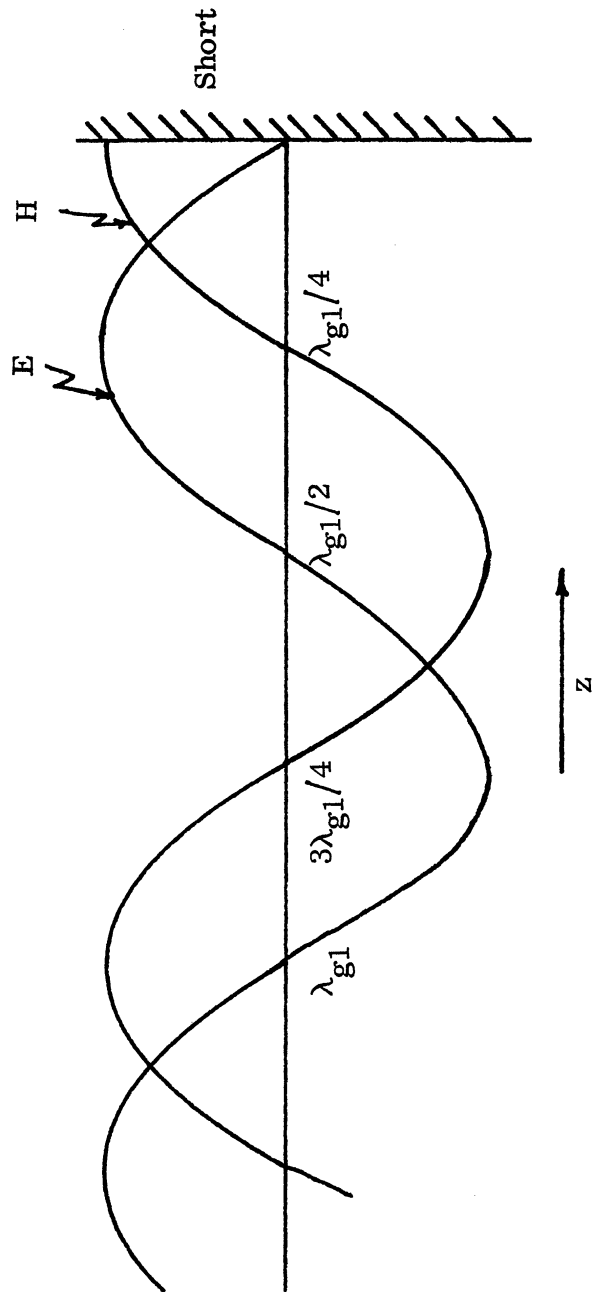


FIG. 2-8: STANDING ELECTRIC AND MAGNETIC FIELDS IN CAVITY.

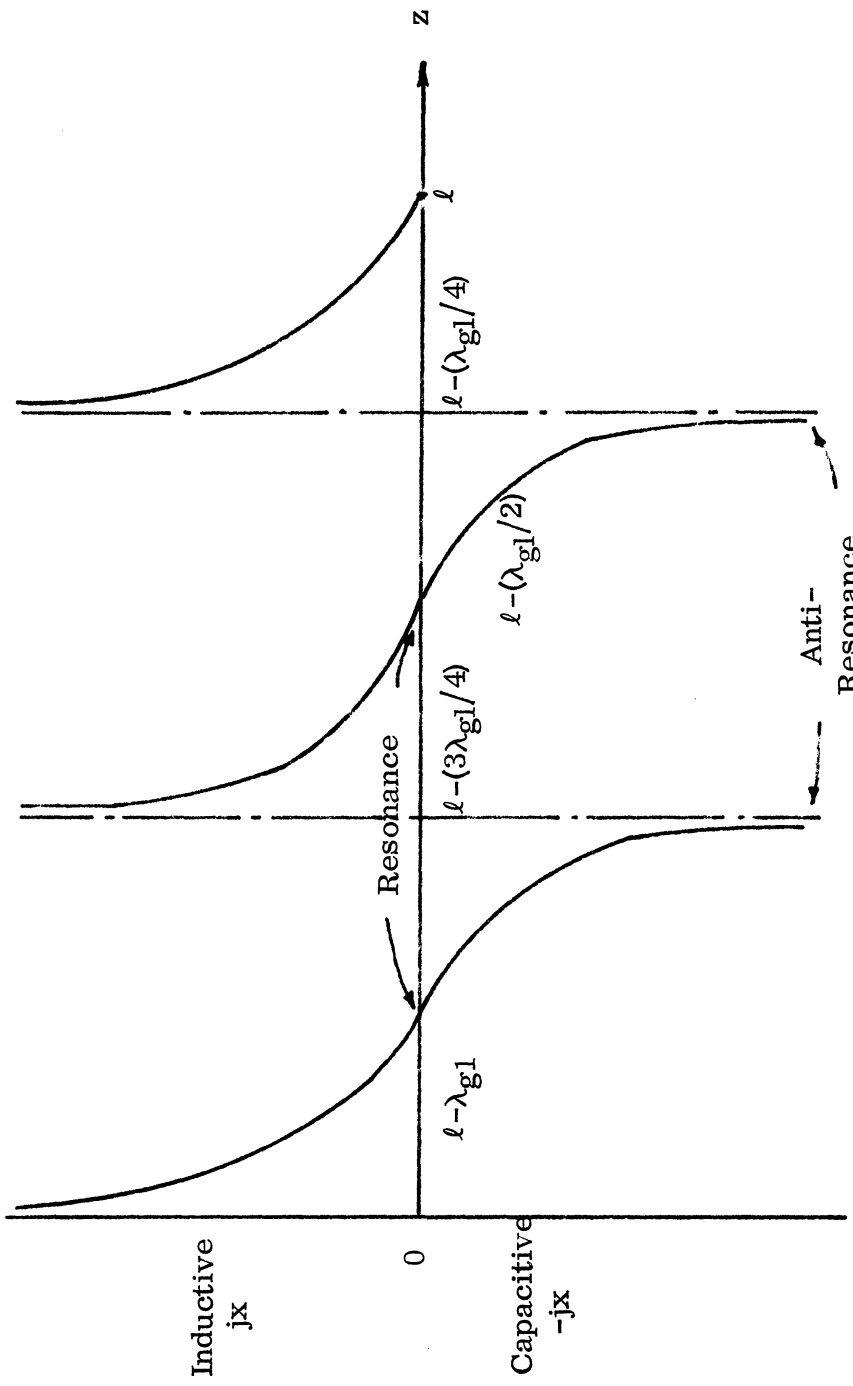


FIG. 2-9: INPUT IMPEDANCE OF THE CAVITY AT $z=0$.

short end or $z=l$ and thus superposes with the returning wave to form a standing wave pattern.

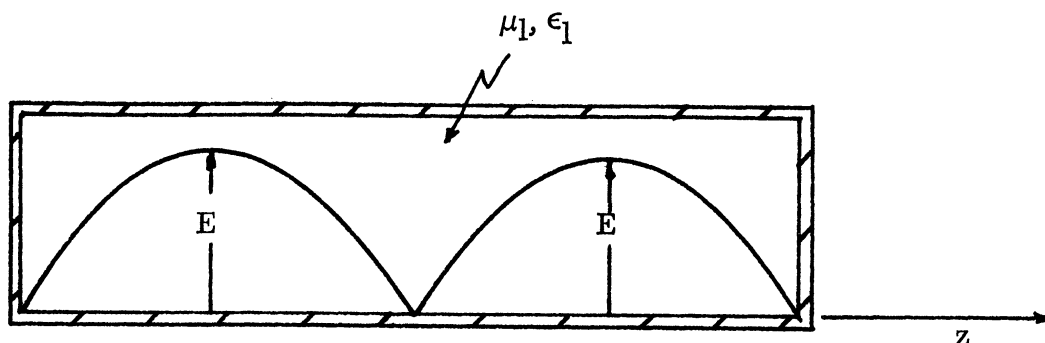


FIG. 2-10: CONFIGURATION OF WAVEGUIDE WHEN IT IS CLOSED AT BOTH ENDS.

2.5.2 Feed Perturbations

Perturbation of Metal Probe : The equation for the correction of the frequency of resonance is

$$\frac{\omega - \omega_0}{\omega_0} = \frac{2V}{abd} \left[\cos^2 \frac{2\pi d_1}{d} - \frac{\pi^2}{k_a^2} \cos^2 \frac{\pi d_1}{d} \right], \quad (2.86)$$

where

ω_0 is the resonance frequency obtained without perturbation

V is the volume of the probe

and

d_1, d are as shown in the simplified equivalent circuit of a cavity slot antenna (Fig. 2-11) .

a and b are the dimensions of the cross section perpendicular to the z -axis as shown in Fig. 2-1 at the beginning of the analysis.

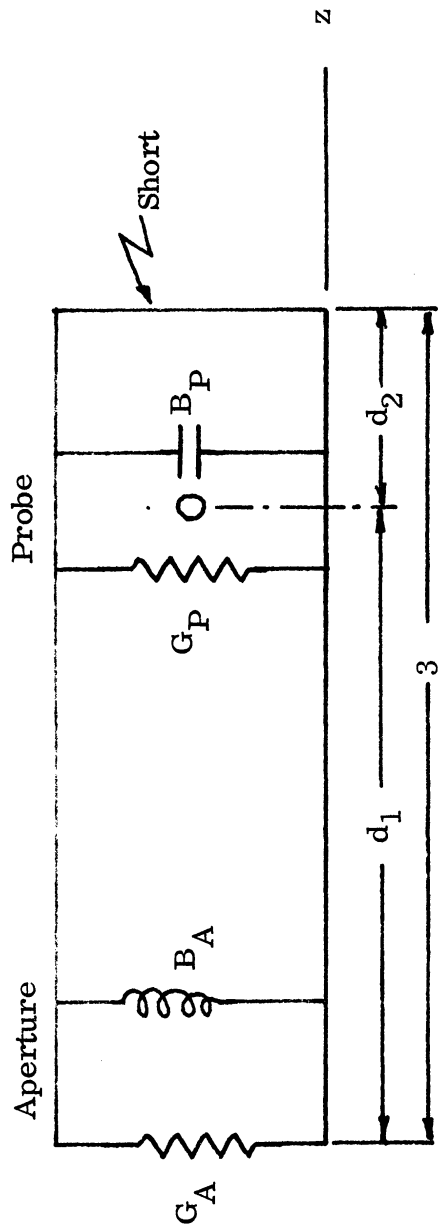


FIG. 2-11: EQUIVALENT CIRCUIT FOR CAVITY SLOT ANTENNA.

Material Perturbation: The equation of material perturbation compensation is given by:

$$\frac{\omega - \omega_0}{\omega_0} = \frac{2V_1}{abd} \left[\frac{k_a^2 - \pi^2}{k_a^2} \frac{\Delta\mu}{\mu} \cos^2 \frac{\pi d_1}{d} + \frac{\Delta\epsilon}{\epsilon} \sin^2 \frac{\pi d_1}{d} \right], \quad (2.87)$$

and for dielectric material, $\mu_r = 1$ degenerates into

$$\frac{\omega - \omega_0}{\omega_0} = \frac{2V_1}{abd} \frac{\Delta\epsilon}{\epsilon} \sin^2 \frac{\pi d_1}{d}, \quad (2.88)$$

where

V_1 is the volume of a cylindrical hole in the material,

and

ω_0 is the resonance frequency without perturbation.

It is to be noted that the resonance frequency of the cavity corresponds to the resonance frequency for the coupling. This fact will be shown in a subsequent chapter on experimental work. The Smith chart can also be used to obtain frequencies as was done by Adams¹.

2.5.3 Resonance Frequencies and Bandwidth

As can be seen in Section 2.5.2 where are several ways to obtain the unperturbed resonance frequencies. The resonance frequencies could be obtained from the equation

$$l = n \frac{\lambda_g}{2} \quad (n=1, 2, 3, \dots) \quad (2.89)$$

Another way to do this is by consideration of Eq. (2.79) which is:

$$Z_{g1}(0) = Z_{g1} \tanh \gamma_{g1} l.$$

Then

$$Y_{g1}(0) = \frac{1}{Z_{g1}(0)} = \frac{1}{Z_{g1}} \coth (\alpha_{g1} + j\beta_{g1}) l, \quad (2.90)$$

where

$Y_{g1}(0)$ is the input admittance to the cavity,

$$Z_{g1} = \sqrt{\frac{\mu_1}{\epsilon_1}} / \sqrt{1 - \left(\frac{f_c}{f}\right)^2} \quad \text{as defined before,}$$

$$\alpha_{g1} = \omega \sqrt{\frac{1}{2} \mu \epsilon'} \left\{ \sqrt{1 + \tan^2 \delta} - 1 \right\} \left[1 - \left(\frac{f_c}{f}\right)^2 \right] \quad , \quad (2.91)$$

and

$$\beta_{g1} = \omega \sqrt{\frac{\mu \epsilon'}{2}} \left\{ \sqrt{1 + \tan^2 \delta} - 1 \right\} \left[1 - \left(\frac{f_c}{f}\right)^2 \right] \quad . \quad (2.92)$$

Then

$$\frac{\alpha_{g1}}{\beta_{g1}} = \frac{\left[\sqrt{1 + \tan^2 \delta} - 1 \right]}{\left[\sqrt{1 + \tan^2 \delta} + 1 \right]} \quad (2.93)$$

where $\tan \delta$ is the loss tangent of the material and

$$\epsilon^* = \epsilon' - j\epsilon'' \quad . \quad (2.94)$$

From (2.91), since

$$k_0 = \omega \sqrt{\mu_0 \epsilon_0} \quad ,$$

then

$$\alpha_{g1} = k_0 \sqrt{\frac{1}{2} \mu_r \epsilon_r} \left\{ \sqrt{1 + \tan^2 \delta} - 1 \right\} \left[1 - \left(\frac{f_c}{f}\right)^2 \right] \quad , \quad (2.95)$$

where

μ_r and ϵ_r are the relative permeability and permittivity of the material.

For the case of dielectric material with a low loss tangent, Eq. (2.95) can be rewritten as:

$$\alpha_{g1} = k_0 \sqrt{\mu_r \epsilon_r} \sqrt{\frac{\tan^2 \delta}{4}} \left[1 - \left(\frac{f_c}{f}\right)^2 \right] \quad ,$$

since

$$\frac{k}{k_0} = \frac{\omega \sqrt{\mu \epsilon'}}{\omega \sqrt{\mu_0 \epsilon_0}} = \sqrt{\mu_r \epsilon_r} \quad . \quad (2.96)$$

Therefore

$$\alpha_{g1} = (k \tan \delta / 2) \sqrt{1 - \left(\frac{f_c}{f}\right)^2} \quad (2.97)$$

Now Eq. (2.90) becomes

$$Y(0) = \frac{1}{Z_{g1}} \frac{\cos(\alpha_{g1} + j\beta_{g1})\ell}{\sin(\alpha_{g1} + j\beta_{g1})\ell},$$

but

$$|\coth(\alpha + j\beta)\ell| = \sqrt{\frac{\cosh^2 \alpha_{g1} \ell \cos^2 \beta_{g1} \ell + \sinh^2 \alpha_{g1} \ell \sin^2 \beta_{g1} \ell}{\sinh^2 \alpha_{g1} \ell \cos^2 \beta_{g1} \ell + \cosh^2 \alpha_{g1} \ell \sin^2 \beta_{g1} \ell}} \quad (2.98)$$

Therefore

$$|Y^2(0)| = \frac{\epsilon_o \epsilon_r}{\mu_o \mu_r} \left\{ 1 - \left(\frac{f_c}{f}\right)^2 \right\} \left[\frac{\cosh^2 \alpha_{g1} \ell \cos^2 \beta_{g1} \ell + \sinh^2 \alpha_{g1} \ell \sin^2 \beta_{g1} \ell}{\sinh^2 \alpha_{g1} \ell \cos^2 \beta_{g1} \ell + \cosh^2 \alpha_{g1} \ell \sin^2 \beta_{g1} \ell} \right] \quad (2.99)$$

Since the energy delivered to the waveguide varies with $|Y^2(0)|$ then by computing Eq. (2.99) for various frequencies it is possible to obtain the unperturbed resonance frequencies and also the bandwidth as will be shown in Chapter III.

To approximate, roughly, for the bandwidth of a cavity with low loss material in it and for small phase deviation Δ from resonance, insert in Eq. (2.99) the approximate forms;

$$\begin{aligned} \sinh^2 \alpha_{g1} \ell &\rightarrow (\alpha_{g1} \ell)^2, & \cosh^2 \alpha_{g1} \ell &\rightarrow 1, \\ \sin^2 \beta_{b1} \ell &\rightarrow \Delta^2, & \text{and } \cos^2 \beta_{g1} \ell &\rightarrow 1. \end{aligned}$$

Then

$$|Y(0)|^2 = \frac{\epsilon_o \epsilon_r}{\mu_o \mu_r} \left\{ 1 - \left(\frac{f_c}{f}\right)^2 \right\} \left[\frac{1}{\Delta^2 + (\alpha_{g1} \ell)^2} \right] \quad (2.100)$$

But for resonance, the approximation condition is that ℓ should be an integral multiple of the half wavelength or,

$$\alpha_{g1} \ell - \frac{\alpha_{g1} n \lambda_{g1}}{2} = \frac{\alpha_{g1}}{\beta_{g1}} n \pi . \quad (2.101)$$

Consider that $|Y(0)|^2$ falls to its half value, when the section is detuned from resonance by a change in phase .

$$\Delta = \frac{\Delta_h}{2} = \pm \frac{\alpha_{g1}}{\beta_{g1}} n \pi . \quad (2.102)$$

This is equivalent to a change in the resonant length by $\pm \Delta Z_h/2$. But

$$\frac{\Delta Z_h}{2} = \frac{\lambda_{g1}}{2\pi} \frac{\Delta_h}{2} = \pm \frac{\alpha_{g1}}{\beta_{g1}} \ell . \quad (2.103)$$

Alternatively, the phase shift can be produced by changing the input frequency from its resonance point f_o to $f_o \pm \frac{\Delta f_h}{2}$. Therefore

$$\frac{\Delta Z_h}{\ell} = \frac{\Delta f}{f_o} = 2 \frac{\alpha_{g1}}{\beta_{g1}} . \quad (2.104)$$

From another viewpoint Eq. (2.104) indicates that the bandwidth for the case using low loss material is approximately equal to the loss tangent (see Fig. 2-12 for symbols defined above) .

2.5.4 Waveguide Wavelength λ_g

In general there are multiple modes in the waveguide with dielectric material filling of relative permittivity ϵ_r .

The general formula for waveguide wavelength is:

$$\lambda_{no} = \frac{\lambda_o}{\sqrt{\mu_r \epsilon_r - \left(\frac{n \lambda_o}{2a}\right)^2}} , \quad (2.105)$$

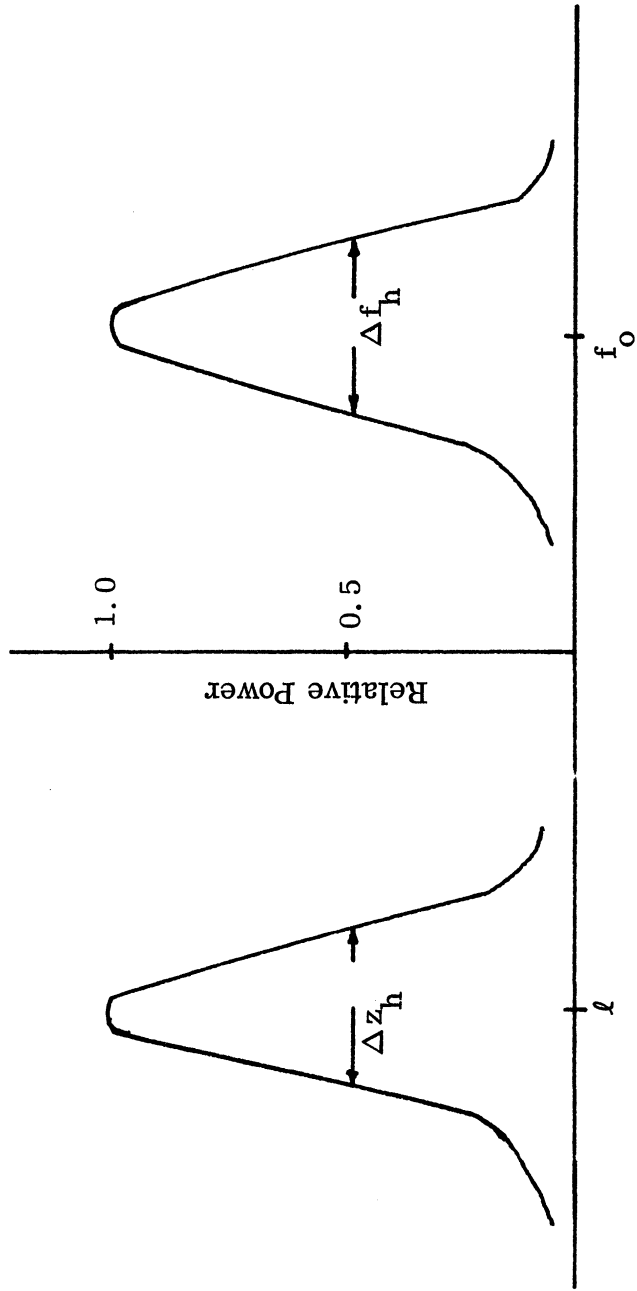


FIG. 2-12: RESONANCE AND HALF-POWER BANDWIDTH.

where

λ_{no} is the wavelength of the TE_{no} mode,

λ_o is the free-space wavelength, and

a is the dimension of the broadside of the waveguide.

For example, for the assumption of the dominant mode TE_{10} in the section filled with the dielectric material,

$$(\lambda_{10})_g = \frac{\lambda_o}{\sqrt{\epsilon_r} \sqrt{1 - \left(\frac{f_c}{f}\right)^2}}$$

where

f_c is the cutoff frequency of the filled guide and

$$f_c = \frac{1}{2a \sqrt{\mu \epsilon}} \quad (2.106)$$

Chapter III
 NUMERICAL ANALYSIS

3.1 General

Since some of the formulation was not obtainable in a closed form, extensive use was made of The University of Michigan's Computing Center for the evaluation of these integrals. The IBM 360/67 digital computer has been used in most of these calculations.

The Fortran programs for each case were written and compiled using the *Fortran compiler and both the Fortran programs and the object programs were stored in the IBM 360/67 memory. After the specific program was cleared of errors and made operational, the Fortran program was destroyed from the file leaving only the object program, thus releasing storage space. Then the object program was available for either a 'batch job' or for MTS (Michigan Terminal system through teleprinter).

3.2 Calculation of Reflection Coefficients at the Aperture

The first program was written to find the reflection coefficient, R, at the aperture. Since there was already an analysis of this in the literature, rather than duplicate that of Adams¹, a careful examination was made and some slight variations were introduced.

The formulas which have been used in computations of the normalized conductance and susceptance are:

$$\frac{G}{Y_0} = \frac{2\mu_r(k_0^2 a^2 - \pi^2)}{\pi^2 a^2 b \sqrt{k_0^2 a^2 - \pi^2}} \int_0^a \int_0^b (b-\sigma) \left[\pi(a-\gamma) \cos \frac{\pi\gamma}{a} + a \frac{C_1}{D_1} \sin \frac{\pi\gamma}{a} \right] \frac{\sin(k_0 \sqrt{\gamma^2 + \sigma^2})}{\sqrt{\gamma^2 + \sigma^2}} d\sigma d\gamma \quad (i)$$

$$\frac{B}{Y_o} = \frac{2\mu_r (k_o^2 a^2 - \pi^2)}{\pi^2 a^2 b k^2 a^2 - \pi^2} \int_0^a \int_0^b (b-\sigma) \left[\pi(a-\gamma) + a \frac{C_1}{D_1} \sin \frac{\pi\gamma}{a} \right] \frac{\cos k \sqrt{\gamma^2 + \sigma^2}}{\sqrt{\gamma^2 + \sigma^2}} d\sigma d\gamma \quad (\text{ii})$$

Since both (i) and (ii) have a singularity at the origin, a small rectangle was considered with sides of ratio Q to the original dimensions of the slot, or, namely, Qa and Qb .

An approximate formulation was then developed for that area and these were:

$$\frac{G}{Y_o} = \frac{2\mu_r (k_o^2 a^2 - \pi^2)}{\pi \sqrt{k^2 a^2 - \pi^2}} \frac{b}{a} \frac{1}{\sqrt{\mu_r \epsilon_r}} \left[Q^2 + \left(\frac{C_1}{D_1} - 2 \right) Q^3 - \left(\frac{5.57 + \frac{C_1}{D_1}}{4} \right) Q^4 + 2.06Q^5 - .616 Q^6 \right], \quad (\text{iii})$$

$$\frac{B}{Y_o} = \frac{2\mu_r (k_o^2 a^2 - \pi^2)}{\pi \sqrt{k^2 a^2 - \pi^2}} \left\{ \left[f - \frac{b}{a} g \right] Q \left[\frac{\left(\frac{C_1}{D_1} - 1 \right) f}{2} - \frac{a}{2b} (d-1) + g \frac{b}{2a} + \frac{1}{2} \frac{b^2}{a^2} \left(\frac{C_1}{D_1} - 1 \right) \left(\frac{a}{b} d - 1 \right) \right] Q^2 + \left[-\frac{f}{12} (2\pi^2 + k_o^2 a^2) + \frac{g}{12} \frac{b^3}{a^3} (k_o^2 a^2 - \pi^2) \frac{\left(\frac{C_1}{D_1} - 1 \right)}{3} \left(\frac{a}{b} (d-1) + \frac{b^2}{a^2} \left(\frac{a}{b} d - 1 \right) \right) - \frac{1}{12} \frac{bd}{a} (2k_o^2 a^2 - \pi^2) \right] Q^3 \right\}, \quad (\text{iv})$$

where $\theta_1 = \tan^{-1} \frac{b}{a}$,

$$f = \log \tan \left(\frac{\theta_1}{2} + \frac{\pi}{4} \right),$$

$$g = \log \tan \frac{\theta_1}{2},$$

$$d = \sqrt{\frac{b^2}{a^2} + 1} = \sec \theta_1$$

$$C_1 = k_o^2 a^2 + \pi^2$$

and

$$D_1 = k_o^2 a^2 - \pi^2 .$$

The change was mainly in Eq. (iii) where $1/\sqrt{\mu_r \epsilon_r}$ was used rather than $\sqrt{\mu_r/\epsilon_r}$. The contribution for the small area around the origin was calculated by (iii) and (iv) and was compared with the polar coordinate integration on the same area. A good agreement was obtained. The rest of the integration was performed by cartesian integration using Eqs. (i) and (ii). The two results were added together to give G/Y_o and B/Y_o .

The change in Eq. (iii) has helped to stabilize the integration with respect to both the parameter Q and the number of divisions to be taken in using Simpson's rule. An example from the computer calculations is shown below using Adams' formula (2.54) and the corrected one (iii). Using Eq. (2.54), Adams¹, with other equations to calculate G/Y_o , B/Y_o gave these results.

Case (a): For $b/a = 0.444$, $\mu_r = 3.0$, $\epsilon_r = 3.0$, $NS=30$, $NL= 50$ where NS and NL are the divisions for the integrations and $Q = 0.05$,

$$G_1 = 0.2542843 \qquad B_1 = -0.9999304$$

$$G'_1 = -0.1218292 \qquad B'_1 = -0.9656234$$

$$G_2 = -0.3980840D-01^* \qquad B_2 = -0.5975625$$

Then $FN = 1.100000, \quad G/Y_o = 0.9264673D-01, \quad B/Y_o = -2.563116 ,$

where G_1 and G'_1 are for the integration outside the small rectangle around the origin. Similarly, B_1 and B'_1 give the susceptance for outside the small rectangle. G_2 and B_2 are for the integration over the small rectangle around the origin, and FN is the normalized frequency.

$$FN = ka / \pi \qquad (3.1)$$

*Note: $-0.3980840D-01 \equiv -0.03980840$

Case (b): For the same parameters as in Case (a), except for the change $Q = 0.01$;

$$\begin{array}{l}
 \text{Then} \\
 G_1 = 0.1476497 \qquad B_1 = -2.064409 \\
 G'_1 = -0.2789158D-01 \qquad B'_1 = -0.3865364 \\
 G_2 = -0.1711596D-02^* \qquad B_2 = -0.1254613 \\
 \\
 FN=1.100000, \quad G/Y_0=0.1180465, \quad B/Y_0=-2.576407
 \end{array}$$

Case (c): For the same parameters as in Case (a), except for $Q=0.1$;

$$\begin{array}{l}
 \text{Then} \\
 G_1 = 0.3695354 \qquad B_1 = -0.2567721 \\
 G'_1 = -0.2024414 \qquad B'_1 = -1.190663 \\
 G_2 = -0.1437410 \qquad B_2 = -1.118208 \\
 \\
 FN=1.100000, \quad G/Y_0=0.2335299D-01, \quad B/Y_0=-2.565642
 \end{array}$$

Note that corresponding to the change in Q , there is a significant change in G/Y_0 . This should not be so distinct. However, using Eq. (iii) along with the others, the computer gave these results.

Case (1): For $b/a = 0.444$, $\mu_r = 3.0$, $\epsilon_r = 3.0$, $NS = 30$, $NL = 50$ and $Q=0.05$.

$$\begin{array}{l}
 \text{Then} \\
 G_1 = 0.2542843 \qquad B_1 = -0.9999304 \\
 G'_1 = -0.1218292 \qquad B'_1 = -0.9656234 \\
 G_2 = -0.1326947D-01 \qquad B_2 = -0.5975625 \\
 \\
 FN=1.100000, \quad G/Y_0=0.1191857, \quad B/Y_0=-2.563116
 \end{array}$$

Case (2): For the same parameters as Case (1) except $Q = 0.01$.

$$\begin{array}{l}
 \text{Then} \\
 G_1 = 0.1476497 \qquad B_1 = -2.064409 \\
 G'_1 = -0.2789158D-01 \qquad B'_1 = -0.3865364 \\
 G_2 = -0.5705321D-03 \qquad B_2 = -0.1254613 \\
 \\
 FN=1.100000, \quad G/Y_0=0.1191876, \quad B/Y_0=-2.576407
 \end{array}$$

* $-0.1711596D-02 \equiv -0.001711596$.

Case (3): For the same parameters as Case (1) except $Q = 0.1$,

$$\begin{aligned} G_1 &= 0.3695354 & B_1 &= -0.2567721 \\ G_1' &= -0.2024414 & B_1' &= -1.190663 \\ G_2 &= -0.4791366D-01 & B_2 &= -1.118208 \end{aligned}$$

Then

$$FN=1.100000, \quad G/Y_0=0.1191803, \quad B/Y_0=-2.56542.$$

Note that G/Y_0 and B/Y_0 are more stable with the change of Q . Also, in choosing Q to be very small, both results come very closely together. Also, a variation of the number of the divisions for the integration has been made according to formula (iii) rather than (2.54), Adams¹, and thus gave these results.

For $b/a=0.444$, $\epsilon_r=10.0$, $\mu_r=10.0$, $NS=30$, $NL=50$ and $Q=0.05$,

then $FN = 1.5$ gives $G/Y_0=0.1134798D-01$ and $B/Y_0=-4.186671$.

Keeping all the parameters the same as before except $NS=100$ and $NL=100$, then

$$FN = 1.5 \text{ gives } G/Y_0=0.1134785D-01 \text{ and } B/Y_0= -4.189243 .$$

These indicate that there is no error of 2.5 percent in the value of G/Y_0 which has been claimed when Eq. (2.54) of Adams¹ was used.

The reflection coefficient can be obtained from G/Y_0 and B/Y_0 :

$$\frac{1-R}{1+R} = G/Y_0 + j B/Y_0 . \quad (3.2)$$

Using the computer, several values of ϵ_r were considered as well as different values of the ratio b/a as shown in Figs. 3-1 through 3-5.

3.3 Calculations of the Aperture-to-Aperture Coupling Between Slots versus Frequency

3.3.1. General Discussion

A computer program has been written to calculate the coupling between two parallel slots in an infinite conducting ground plane. Since the formulas to predict the coupling as shown in Chapter II could not be obtained in a closed form they

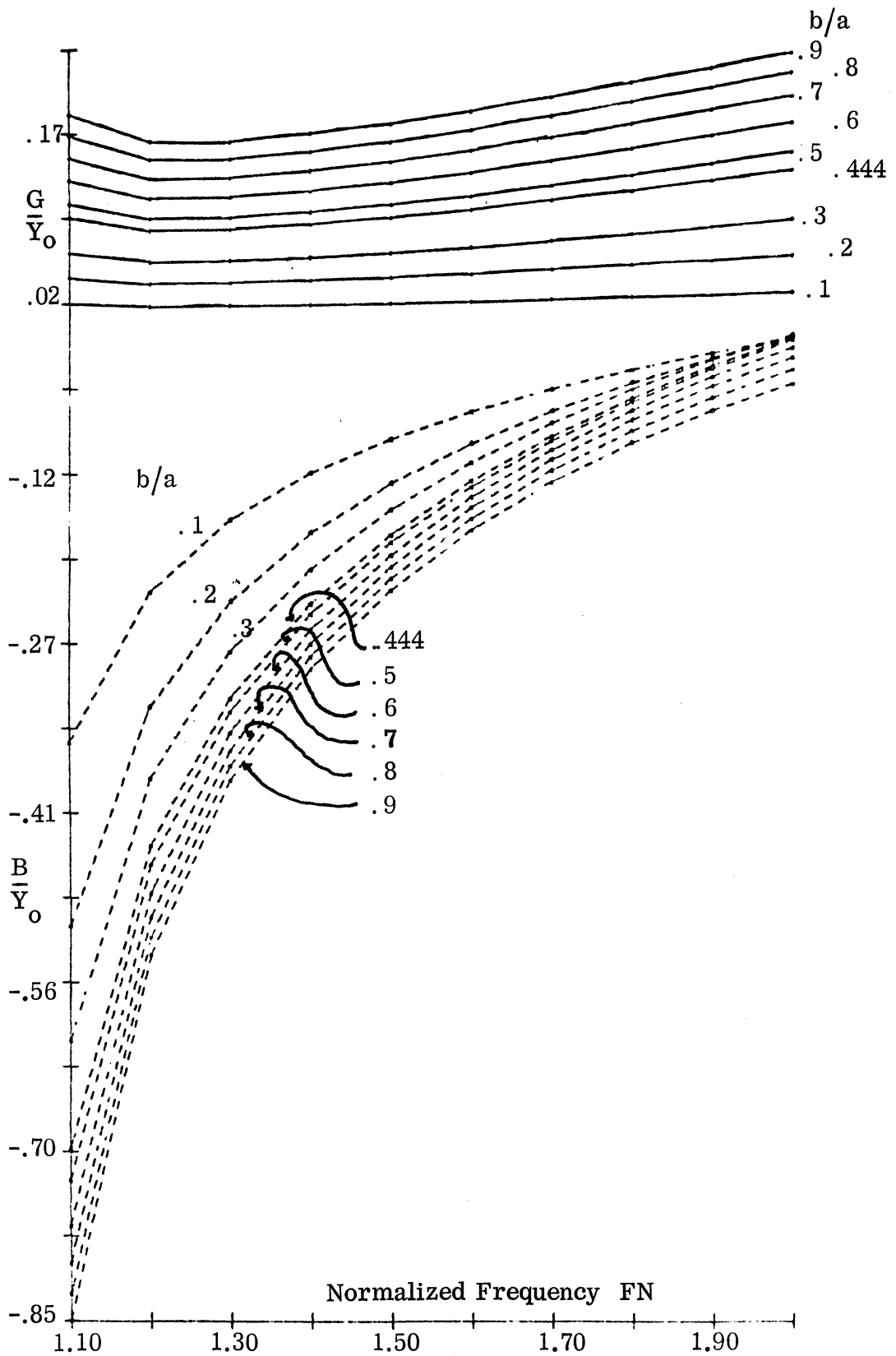


FIG. 3-1: APERTURE NORMALIZED CONDUCTANCE AND SUSCEPTANCE FOR $\mu_r=1.0$, $\epsilon_r=5.0$, --- (B/Y_0) — (G/Y_0)

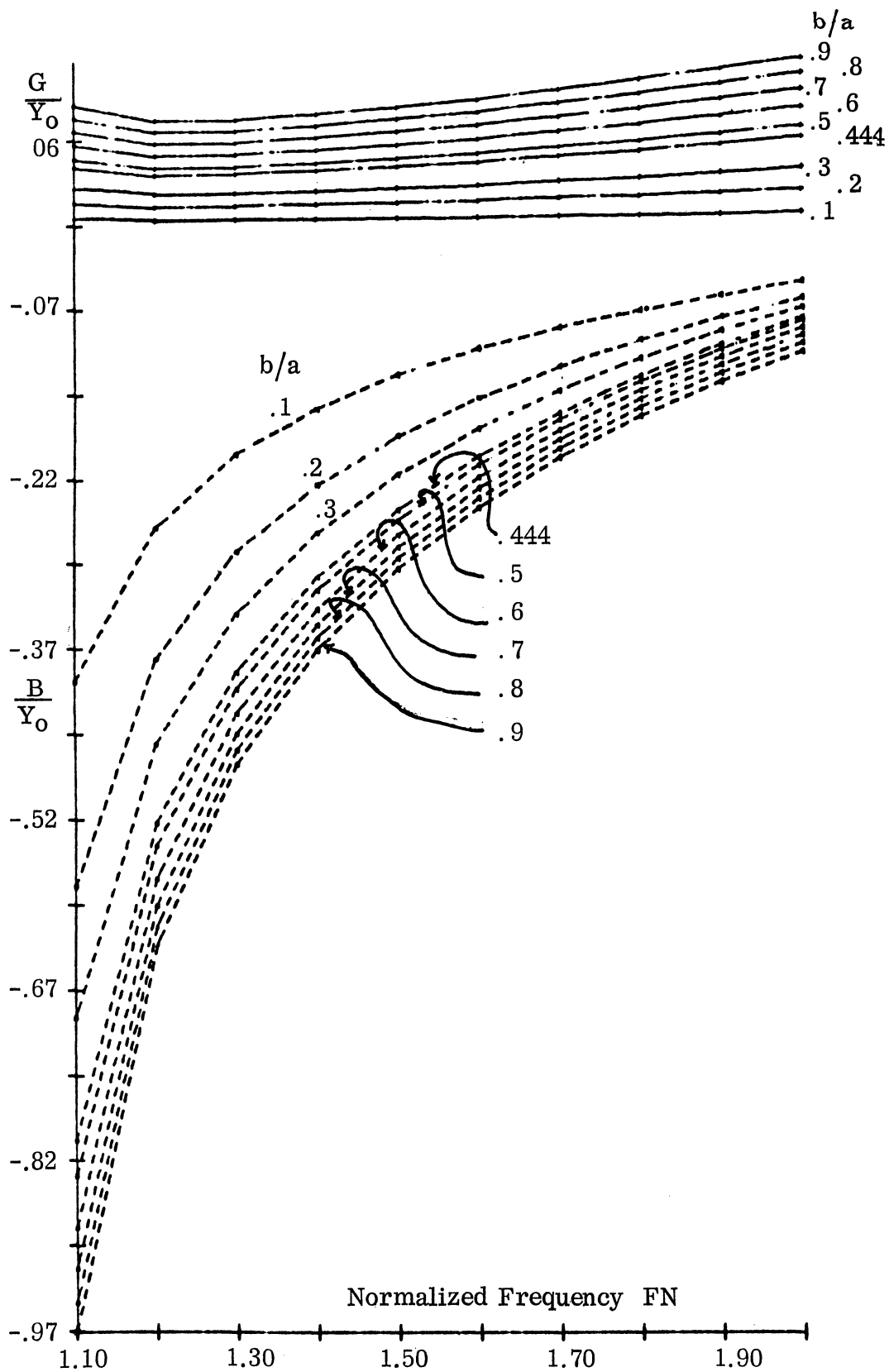


FIG. 3-2: APERTURE NORMALIZED CONDUCTANCE AND SUSCEPTANCE FOR $\mu_r=1.0$, $\epsilon_r=7.0$, - - - (B/Y_0), — (G/Y_0).

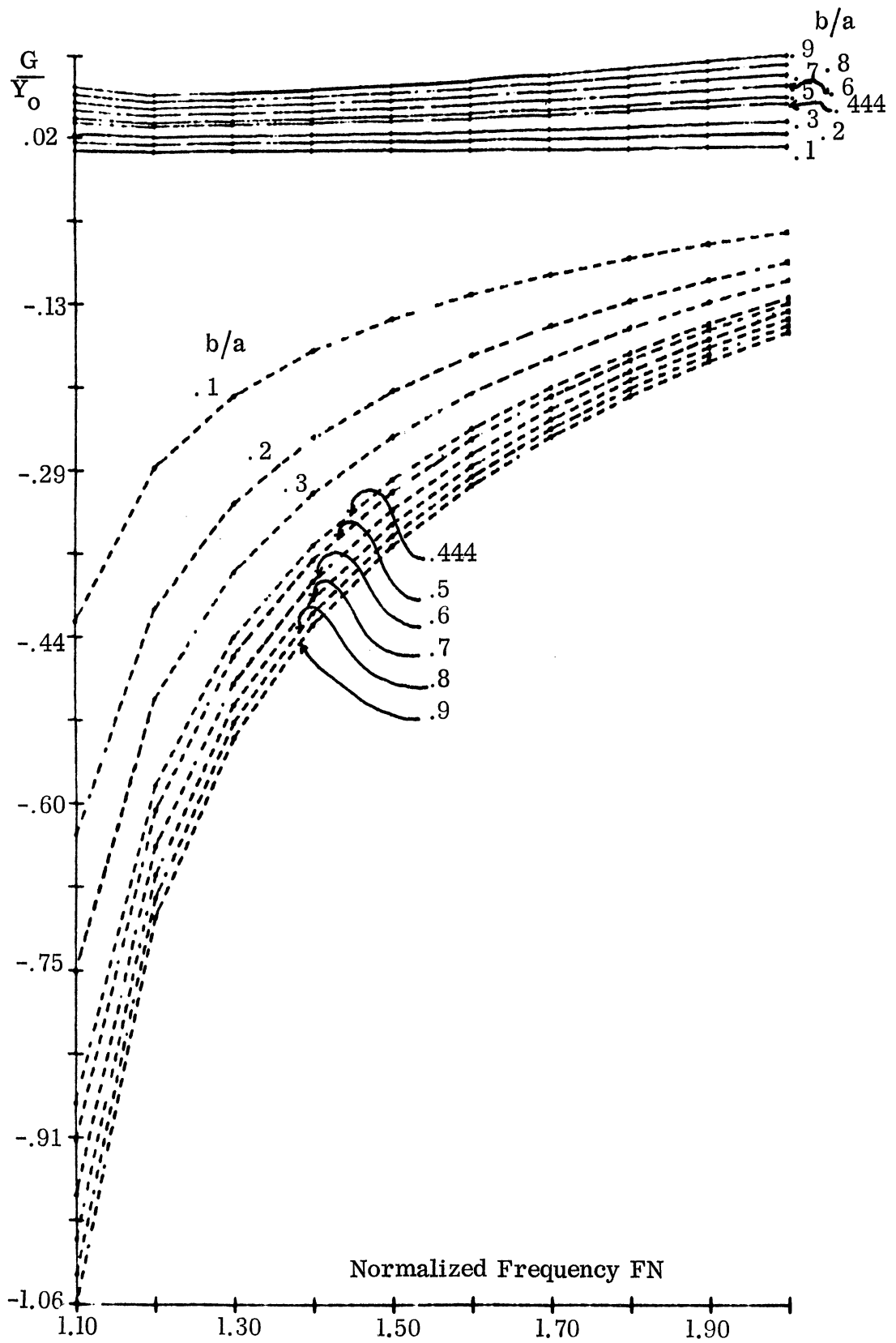


FIG. 3-3: APERTURE NORMALIZED CONDUCTANCE AND SUSCEPTANCE FOR $\mu_r=1.0$, $\epsilon_r=10.0$, - - - (B/Y_0) , — (G/Y_0) .

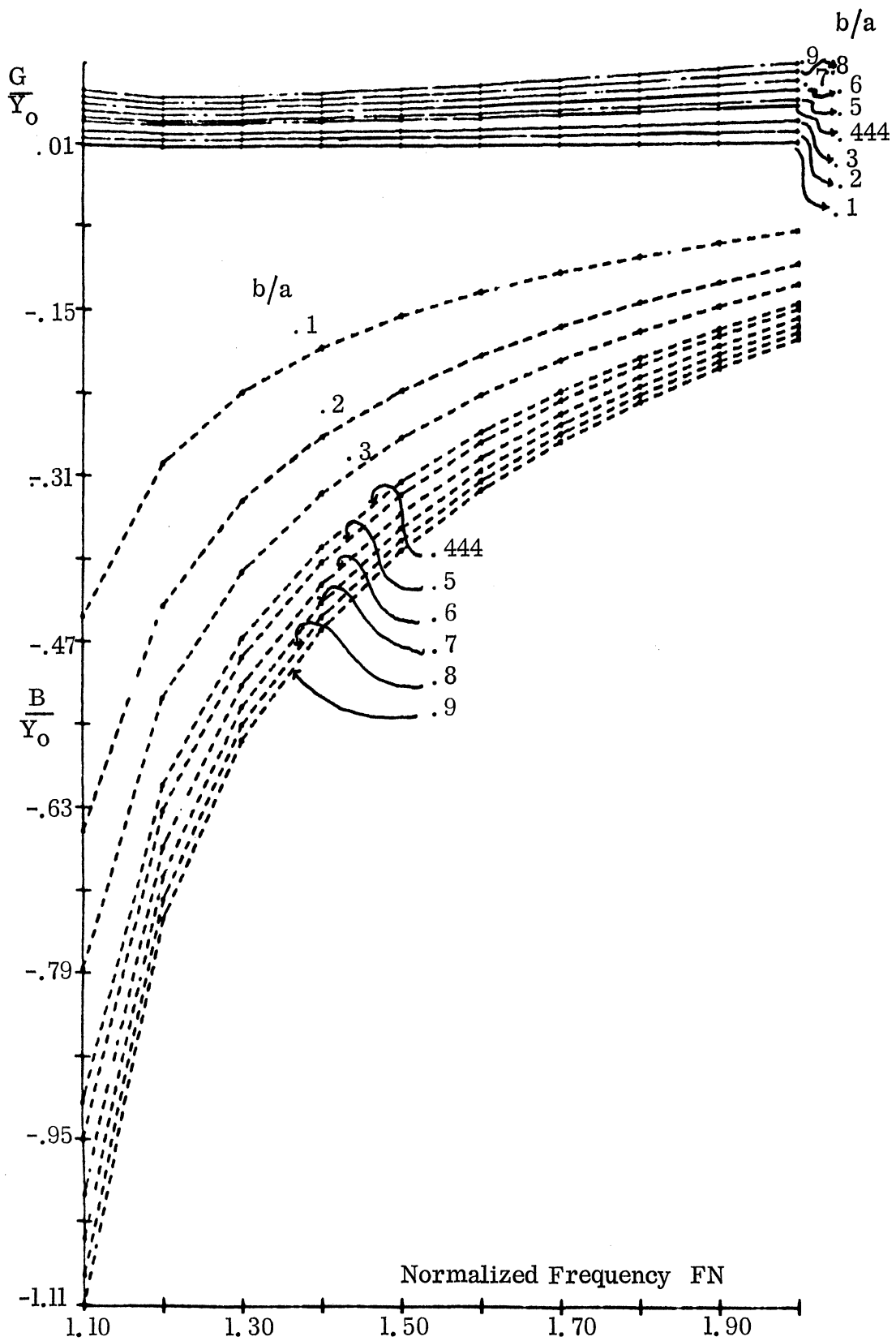


FIG. 3-4: APERTURE NORMALIZED CONDUCTANCE AND SUSCEPTANCE FOR $\mu_r=1.0$, $\epsilon_r=11.0$, - - - (B/Y_0), — (G/Y_0).

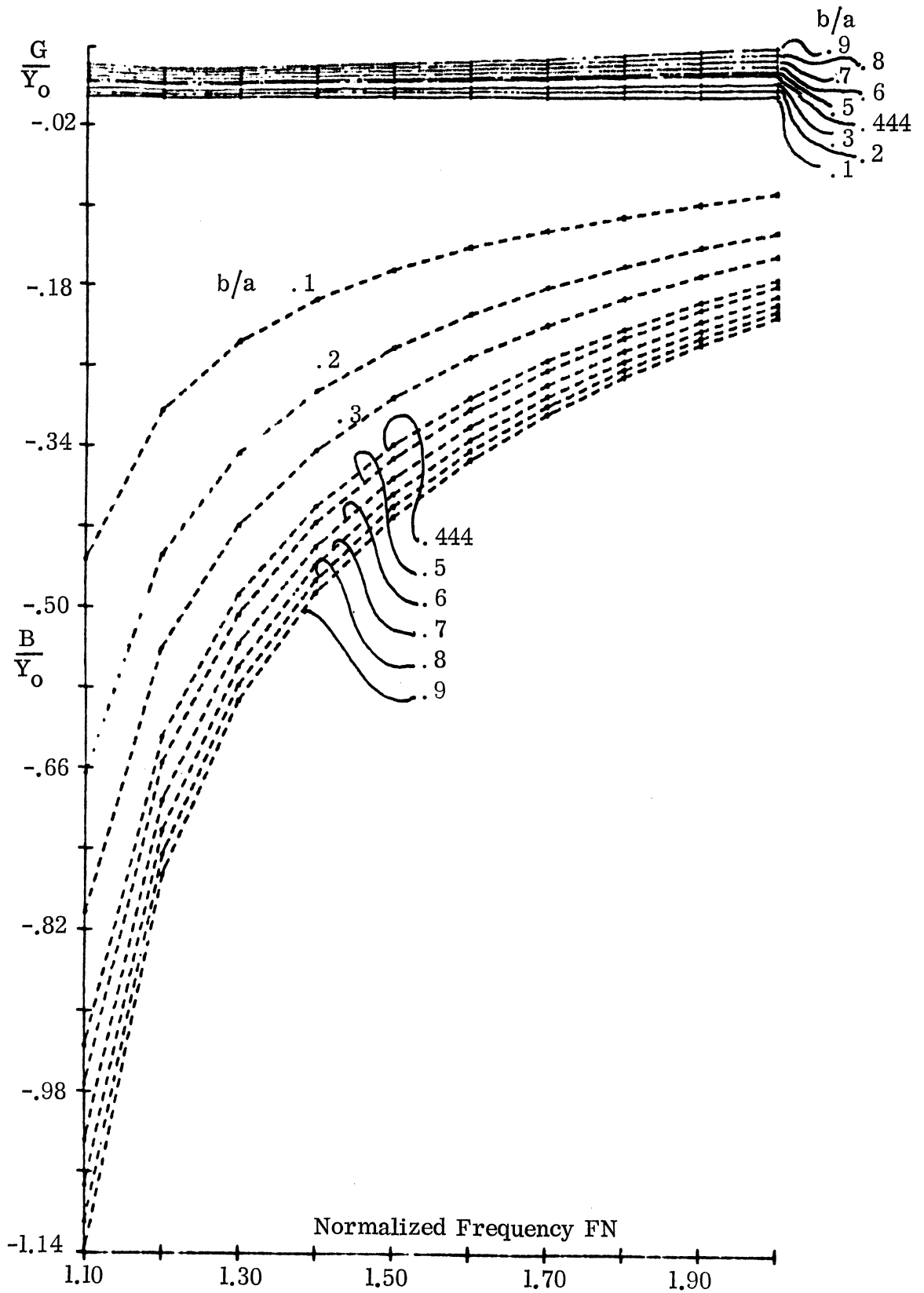


FIG. 3-5: APERTURE NORMALIZED CONDUCTANCE AND SUSCEPTANCE FOR $\mu_r=1.0$, $\epsilon_r=15.0$, - - - (B/Y_0) , — (G/Y_0) .

were evaluated by numerical calculation using Simpson's rule of integration. The program was devised at the beginning to calculate the coupling versus frequency (normalized frequency, $FN = ka/\pi$). The parameters which were considered variable in this case were the dimensions of the aperture 'a' and 'b', separation of the slots from center to center, the permeability and permittivity of the material loading. The object program was stored in the memory of the IBM 360/67 in such a way that the input data required by the program were a, b, μ_r , ϵ_r , x_1 (separation of center to center) and the range of frequencies over which the calculations are required. For example, if the frequency range is between a normalized frequency $FN1 = 1.1$ (which is just over the cutoff frequency of the guide), and $FN2 = 2.0$ (which is the upper range of the frequency), then the program would call for repetitive calculations for the desired frequencies. The desired frequencies can be chosen with a uniform separation DFN (divisions of FN). The cutoff frequency corresponds to the normalized frequency of 1.0 .

For example, if it is desirable to make calculations at intervals of 0.1, from 1.1 to 2.0 (normalized frequency), then $DFN = 0.1$. Then the number of repetitive calculations = $FN2-FN1/DFN = (2.0 - 1.1)/0.1 = 9$ and

$$NFN = \frac{FN2-FN1}{DFN} + 1.5 ,$$

where NFN is an integer,

$$FN = FN1 + (NFN-1) *DFN ,$$

where * is the Fortran multiplication symbol and NFN takes the values of 1 up to 10.

The relation between the normalized frequency and frequency depends on the size of the guide . It also depends on the parameters of the material loading.

Since

$$FN = ka/\pi \quad (3.3)$$

where

$$k = 2\pi/\lambda \quad (3.4)$$

or

$$k = k_0 \sqrt{\mu_r \epsilon_r} \quad (3.5)$$

and

$$k_0 = \frac{2\pi}{\lambda_0} = 2\pi \sqrt{\mu_0 \epsilon_0} f \quad (3.6)$$

Then

$$f = \frac{FN \times 0.3}{2a \sqrt{\mu_r \epsilon_r}} \text{ GHz} \quad (3.7)$$

The cutoff frequency

$$f_c = \frac{0.3}{2a \sqrt{\mu_r \epsilon_r}} \text{ GHz} \quad (3.8)$$

where a is taken to be in meters, and FN is the normalized frequency which is dimensionless. A scale can be obtained between FN and f for different values of waveguide parameters and material loading. Consider the case of dielectric loading where $\mu_r = 1$, $\epsilon_r = 15$, $a = 0.02286$ meter and $b = 0.01016$ meter (the dimensions of standard x-band waveguide). The cutoff frequency in this case from Eq. (3.8) is

$$f_c = \frac{0.3}{2 \times 0.02286 \times \sqrt{1 \times 15}} = 1.6942 \text{ GHz} .$$

In the following tables, correspondence between FN and f in the S-band range is shown for different parameters of material loading.

TABLE 3.1: $\mu_r=1$, $\epsilon_r=15$, $a = 0.02286\text{m.}$, $b=0.01016 \text{ m.}$

$\text{FN} = \frac{ka}{\pi}$	f (GHz)
1.0	1.694
1.1	1.864
1.2	2.033
1.3	2.202
1.4	2.374
1.5	2.541
1.6	2.711
1.7	2.880
1.8	3.050
1.9	3.219
2.0	3.388
2.1	3.558
2.2	3.727
2.3	3.897

TABLE 3.2: $\mu_r=1$, $\epsilon_r=11$, $a=0.02286\text{m.}$, $b=0.01016\text{m.}$

$\text{FN} = \frac{ka}{\pi}$	f (GHz)
1.0	1.978
1.1	2.176
1.2	2.374
1.3	2.572
1.4	2.770
1.5	2.968
1.6	3.165
1.7	3.363
1.8	3.561
1.9	3.759
2.0	3.957

TABLE 3.3: $\mu_r=1$, $\epsilon_r=7$, $a=0.02286\text{m.}$, $b=0.01016 \text{ m.}$

$\text{FN} = \frac{ka}{\pi}$	f (GHz)
1.0	2.480
1.1	2.728
1.2	2.976
1.3	3.224
1.4	3.472
1.5	3.720
1.6	3.968
1.7	4.216

TABLE 3. 4: $\mu_r=1$, $\epsilon_r=1$, $a=0.07136m.$, $b=0.034036m.$ (S-band) *

$FN = \frac{ka}{\pi}$	f (GHz)
1.0	2.102
1.1	2.312
1.2	2.522
1.3	2.733
1.4	2.943
1.5	3.153
1.6	3.363
1.7	3.573
1.8	3.784
1.9	3.994
2.0	4.204

TABLE3. 5a: $\mu_r=1$, $\epsilon_r=1$, $a=0.02286m.$, $b=0.01016m.$ (X-band) *

$FN = \frac{ka}{\pi}$	f (GHz)
1.0	6.562
1.1	7.218
1.2	7.874
1.3	8.530
1.4	9.186
1.5	9.843
1.6	10.499
1.7	11.155
1.8	11.811
1.9	12.467
2.0	13.123

TABLE 3.5b : $\mu_r=1$, $\epsilon_r=1$, $a=0.0157988$, $b=0.0078994$ (Ku-band) *

$FN = \frac{ka}{\pi}$	f (GHz)
1.1	10.444
1.2	11.393
1.3	12.343
1.4	13.292
1.5	14.242
1.6	15.191
1.7	16.140
1.8	17.090
1.9	18.039
2.0	18.989

* S-band (2.6 - 3.95 GHz); X-band (8.2 - 12.4 GHz); Ku-band (12.4 - 18.0 GHz)

Note that FN=1.0 corresponds to the cutoff frequency and the Table 3.6 indicates how the cutoff frequency depends upon the values of ϵ_r of the dielectric material for a fixed waveguide with transverse cross section of $a=0.02286$, $b=0.01016$ meters (standard X-band waveguide).

TABLE 3.6: $\mu_r = 1.0$, $a=0.02286\text{m.}$, $b=0.01016\text{m.}$ (X-band)

ϵ_r	f_c (GHz)
1.0	6.5617
2.0	4.6398
3.0	3.7884
4.0	3.2808
5.0	2.9345
6.0	2.6788
7.0	2.4801
8.0	2.3199
9.0	2.1877
10.0	2.0750
11.0	1.9784
12.0	1.8942
13.0	1.8199
14.0	1.7537
15.0	1.6942
16.0	1.6404

Therefore the cutoff frequency for standard X-band waveguide filled with dielectric material versus ϵ_r is as shown in Fig. 3-6.

The coupling was calculated without the iterative procedure of Section 2.4. To compensate for the interaction between the two slots, especially if they are very close to each other, the iteration factor was included in the evaluation. On this basis the coupling was obtained. As expected the effect of the interaction becomes more noticeable if the two slots are very close to each other in wavelengths. Of course, the separation in wavelength depends on the separation of the guides in the physical layout. For a given physical separation it also depends on the operating frequency. For example, if the physical separation were kept constant and the operating frequency were swept higher, in effect, the separation

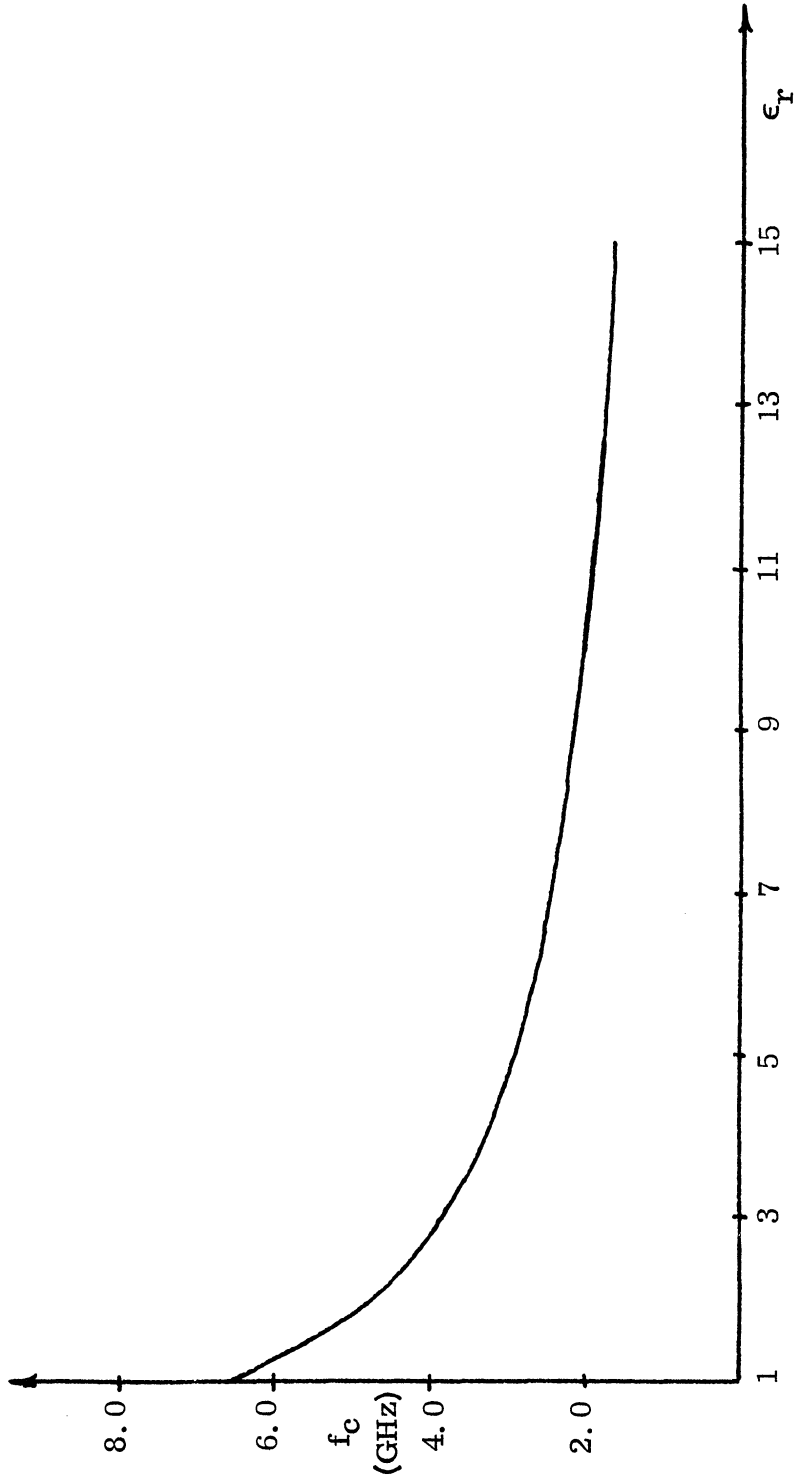


FIG. 3-6: VARIATION OF CUTOFF FREQUENCY VS PERMITTIVITY OF LOADED X-BAND WAVEGUIDE, $a=0.02286\text{m.}$, $b=0.01016\text{m.}$

in wavelengths of the two apertures increases . Also it was noticed that the value obtained with the iteration converges to the one obtained without iteration for large separation of the slot antennas in wavelengths.

To formulate the coupling from an assumed illumination of the transmitting aperture and to evaluate the corresponding illumination of the receiving aperture consider the Poynting vector \bar{P} .

$$\bar{P} = \bar{E} \times \bar{H} ,$$

$$\bar{P}_{av} = \text{Re} (\bar{E} \times \bar{H}^*) .$$

Therefore, the average received power in the receiving slot is:

$$\bar{P}_{av} = \text{Re} \left\{ \int_0^b \int_0^a \left[(U \sin \frac{\pi y}{a} \hat{x}) \times \left(- \frac{\beta}{\omega \mu} U^* \sin \frac{\pi y}{a} \hat{y} \right) \right] dy dx \right\}$$

$$= -\text{Re} \left\{ \int_0^b \int_0^a |U|^2 \frac{\beta}{\omega \mu} \sin^2 \frac{\pi y}{a} dy dx \right\} ,$$

where the negative sign indicates that the power flow is in the negative direction of the z-axis shown in Fig. 2-1.

$$P_{av} = \frac{ab}{2} \frac{\beta}{\omega \mu} |U|^2 ,$$

where

$$\beta = 2\pi \sqrt{\left(\frac{1}{\lambda}\right)^2 - \left(\frac{1}{2a}\right)^2} .$$

Similarly, the transmitted power can be obtained.

$$C \text{ (coupling in dB)} = 10 \log_{10} \frac{P_r}{P_T} = 10 \log_{10} \frac{|U|^2}{[\text{amplitude of TR aperture illum.}]^2}$$

$$= 20 \log_{10} \frac{|U|}{[\text{amplitude of TR aperture illum.}]}$$

For the calculations the amplitude of the aperture illumination was assumed to be $1+R$.

Several curves of coupling versus frequency were evaluated for both empty and loaded operation of the waveguide cavities. Of course, it should be noted here that this is the coupling from aperture to aperture; the effect of the backing cavities is not taken into consideration at this point but will be later on.

3.3.2 Empty Waveguide Case

For the case of empty waveguide the effect of the cavity is less pronounced than in the case of loaded cavity. This is because in the case of the empty cavity the bandwidth is wider than in the case of the dielectric loaded cavity.

The bandwidth for a low loss material is approximately equal to the loss tangent. The graphs obtained for empty or air-filled cases show very good agreement to the order of a fraction of dB with the theoretical counterpart as in Lyon et al ². Also it is within approximately 1 dB of the experimental results as will be seen in Chapter IV. But for the case of the loaded slot, the effect of the cavity has to be added and then the comparison can be made. The coupling versus normalized frequency for the case of empty S-band waveguide of dimensions $a=0.07136$ m., $b=0.034036$ m., is shown in Fig. 3-7. The separation of the two slots (center-to-center) is 0.075 m., and the range of variation of frequency is from 1.1 to 2.0 on a normalized scale. The relation between the normalized frequency and frequency in GHz is given in Table 3.4.

In Fig. 3-8 the coupling versus frequency is shown for the case of the empty X-band waveguide of dimensions $a=0.02286$ m., $b=0.01016$ m., for a separation of 0.114 m., and a range of frequency between 1.3 and 1.9 normalized frequency (see Table 3.5 for corresponding real frequencies). Notice in both cases that the coupling pattern drops with an increase of frequency according to a 6 dB/octave frequency characteristic. Also, the differences between curves, with and without interaction between the two slots, decreases as the separation between the two slots increases (see Appendix B).

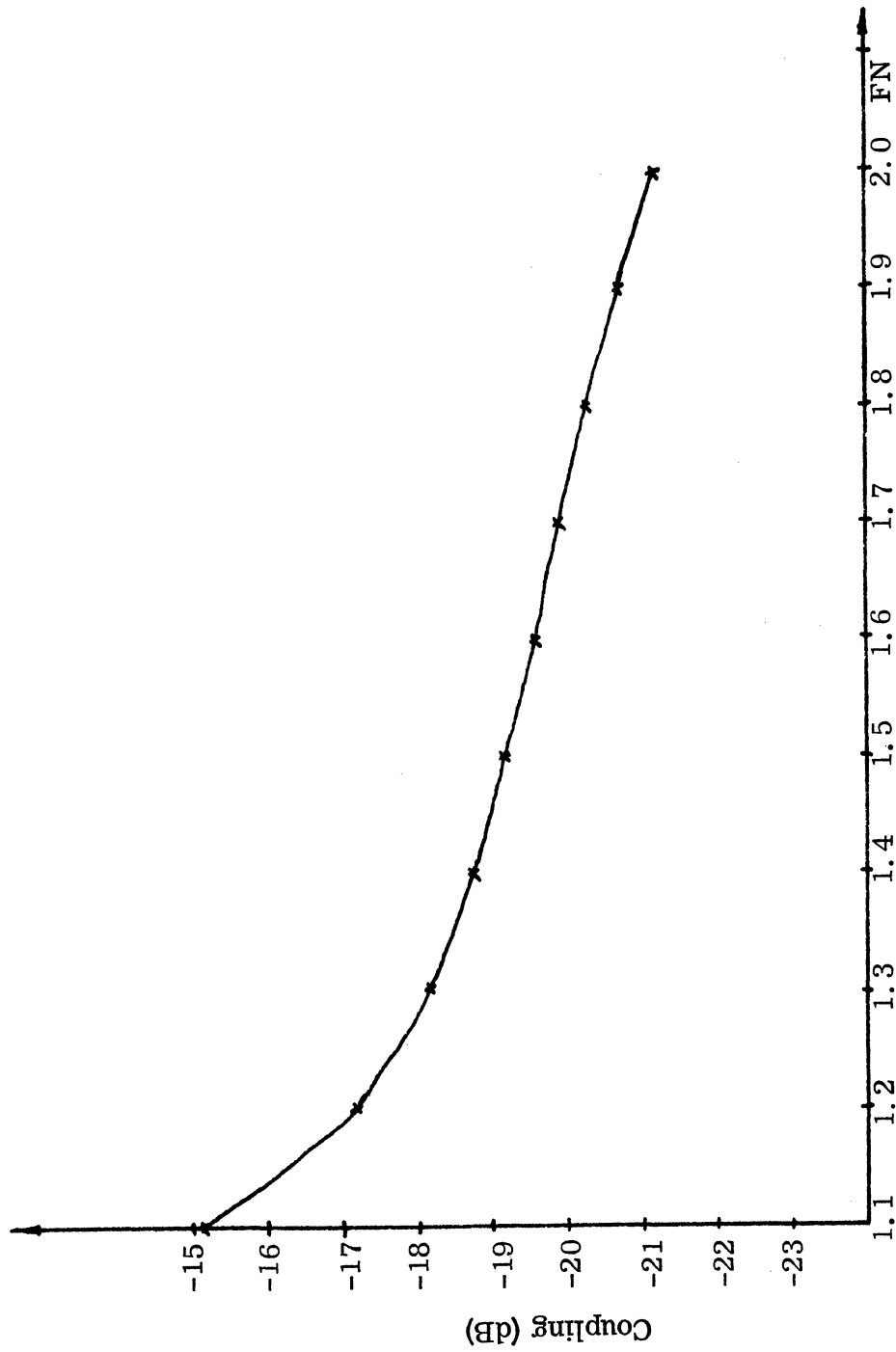


FIG. 3-7: STANDARD S-BAND COUPLING VS NORMALIZED FREQUENCY,
 $a=0.07136$ m., $b=0.034036$ m., $x_1=0.075$ m., $\mu_r=1.0$, $\epsilon_r=1.0$

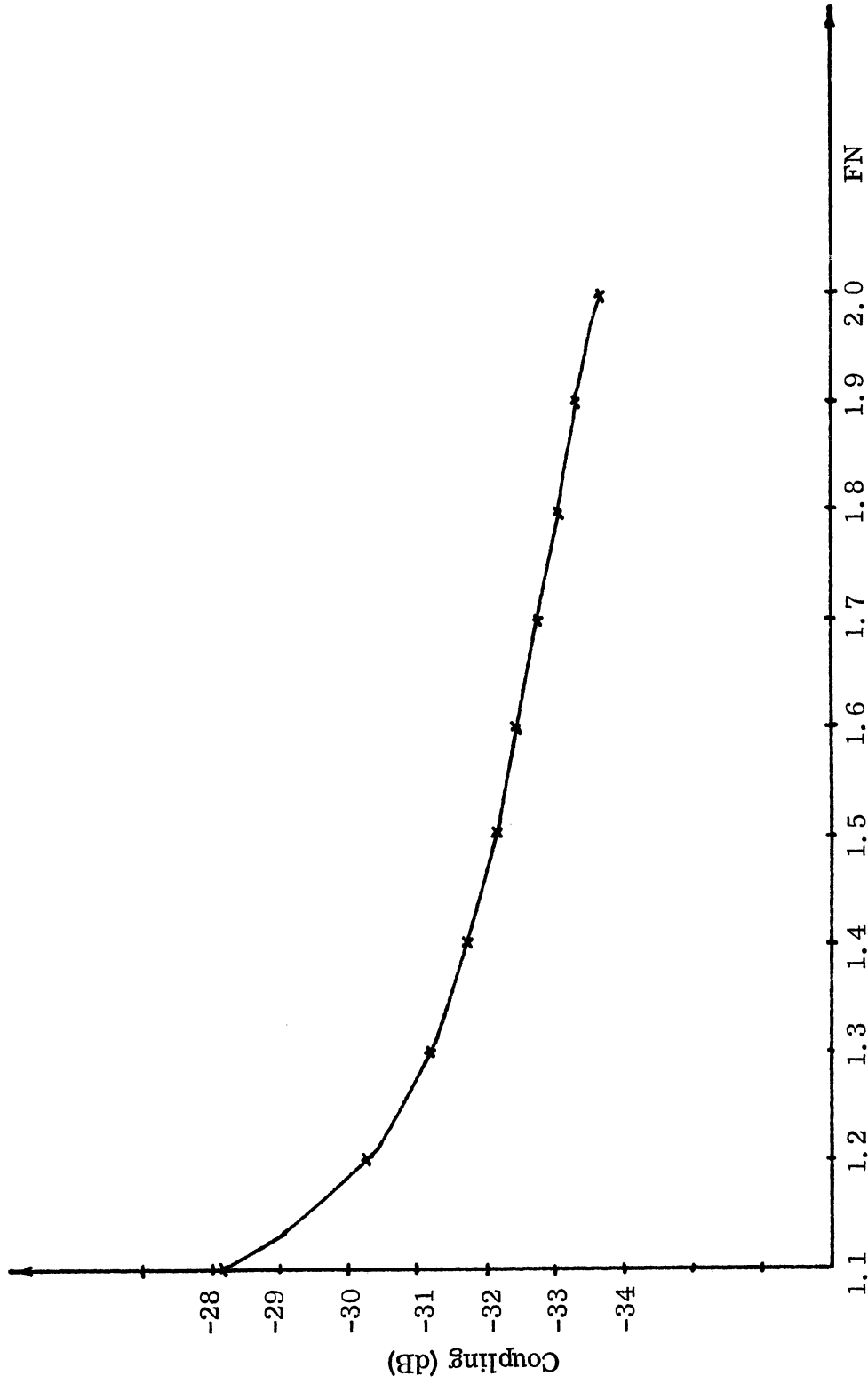


FIG. 3-8: STANDARD X-BAND COUPLING VS NORMALIZED FREQUENCY,
 $a=0.02286m$, $b=0.01016m$, $x_1=0.114m$, $\mu_r=1.0$, $\epsilon_r=1.0$.

Then the coupling for a pair of Ku-band slots spaced at 0.114 m. from each other was studied. The coupling was calculated at different normalized frequencies (see Fig. 3-9). The results agree with Fig. 4-6(b) in the chapter on experimental investigations.

3.3.3 Dielectric Loaded Case

Several graphical curves have been evaluated for standard X-band waveguide with dimensions $a=0.02286$ m., $b=0.01016$ m., filled with dielectric material of $\epsilon_r = 2, 3, 4, 5, 7, 11, 15$ and 20 (see Fig. 3-10, a \rightarrow h). Notice that $x_1 = 0.013$ m., corresponds to two slots put next to each other or metal-to-metal contact. It is very interesting to note that the coupling in this case does not follow the 6 dB/octave of frequency trend as in the case of empty slots. The variation depends on the material loading parameters. It is to be noticed that the lower the permittivity number, the more the variation is restricted; in some cases it is about constant, as in Fig. 3-9. For the higher electric permittivity the curve goes to a minimum with increasing frequency and then rises. For a large portion of the frequency band the variation is confined to about 2 dB. Also since the coupling level is low in this case the iteration process has little effect (see Appendix B). Of course, it should be remembered that this coupling is aperture-to-aperture and does not take into consideration the resonance cavity which is feeding it.

3.4 Coupling Aperture to Aperture versus Spacing

3.4.1 General Discussion

The computer program of Section 3.3.1 was next modified to permit variation in frequency for a fixed spacing and to obtain the corresponding coupling level. Also for a fixed frequency the program provides for variation in spacing between the slots and then the evaluation of the corresponding coupling level. Therefore, upon supplying the proper data, the computer will evaluate coupling versus frequency or coupling versus distance according to need.

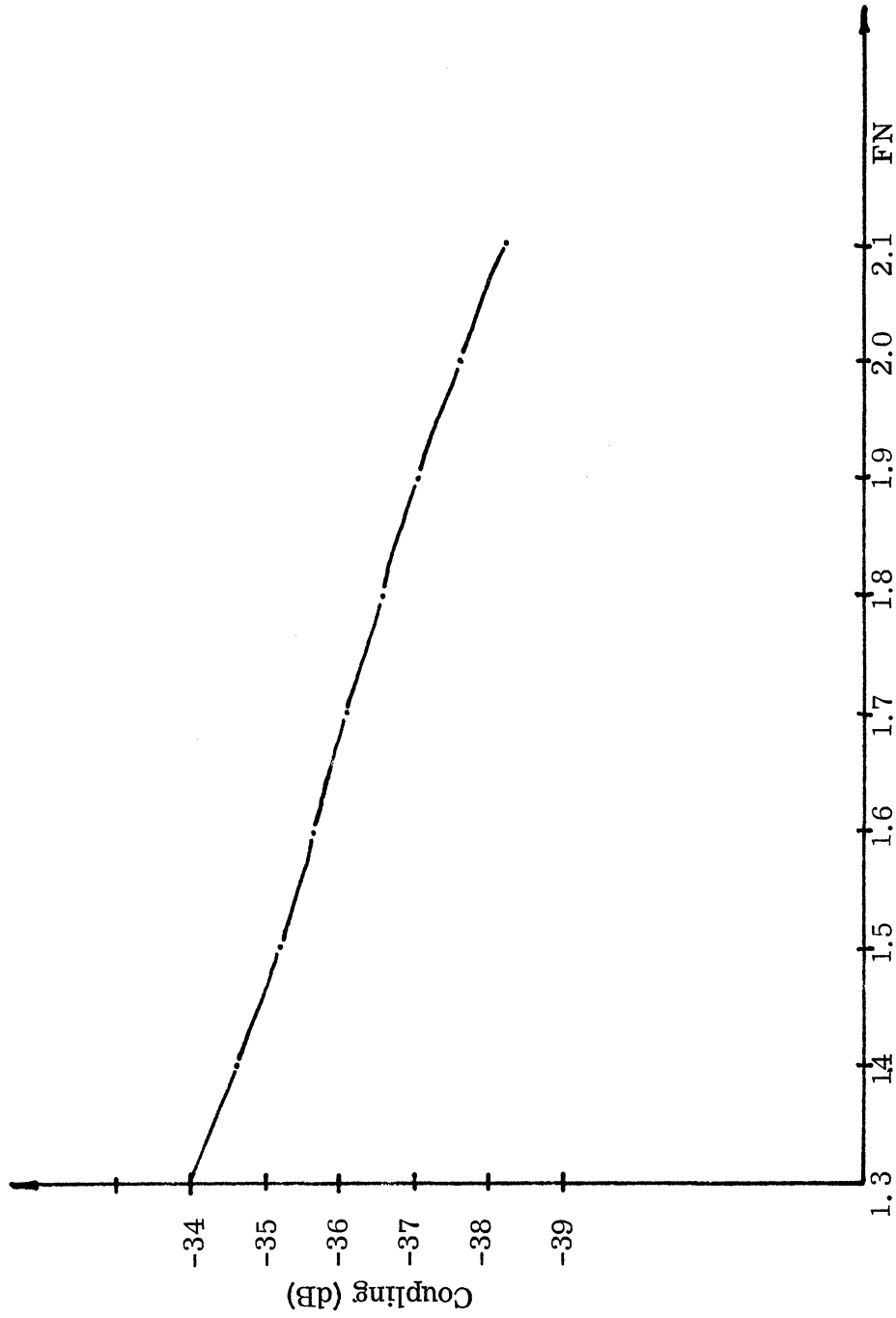


FIG. 3-9: STANDARD Ku - BAND COUPLING, $x_1=0.114m.$, VS FREQUENCY,
 $a=0.015988m.$, $b=0.0078994m.$, $\mu_r=1.0$, $\epsilon_r=1.0$.

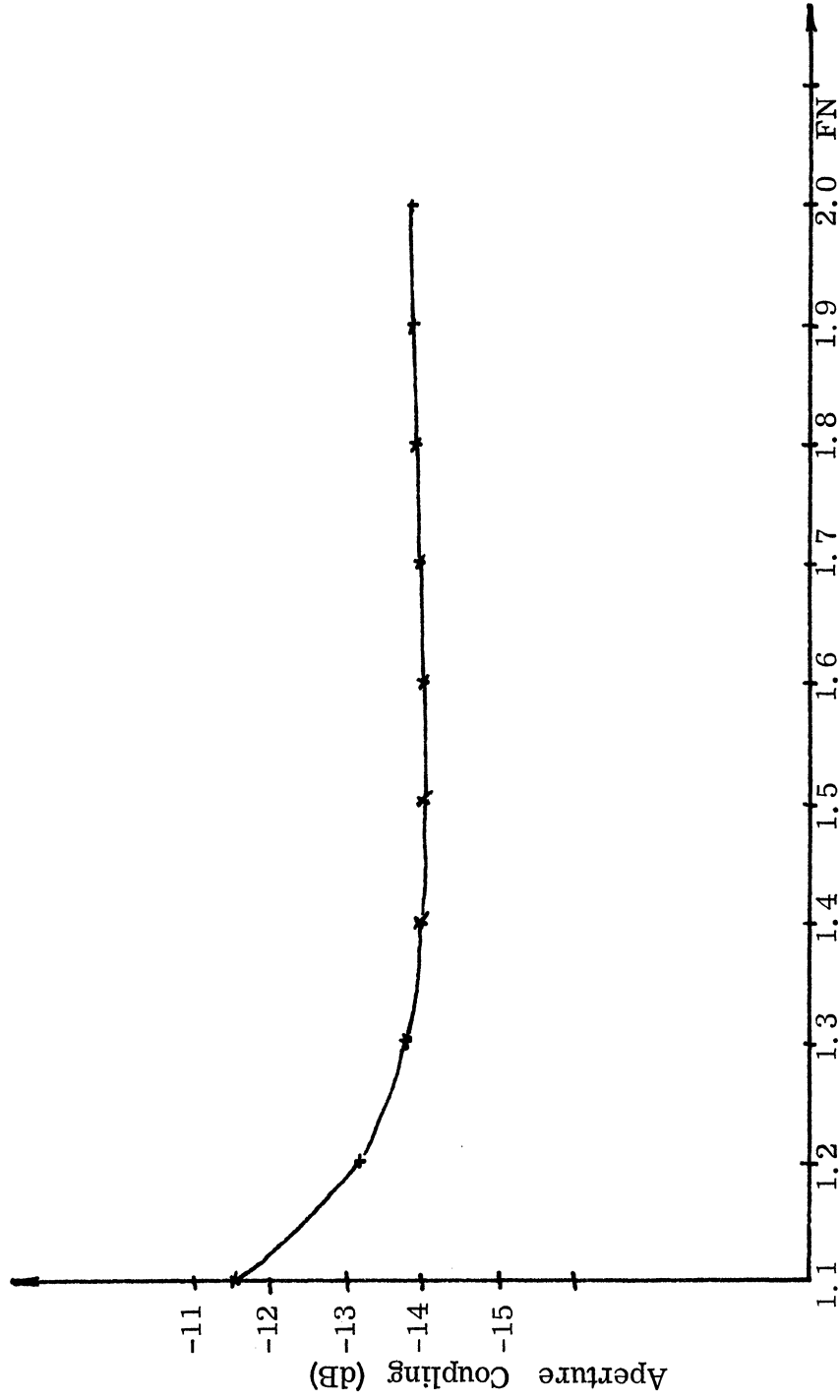


FIG. 3-10(a): APERTURE TO APERTURE E-PLANE COUPLING OF LOADED SLOTS
 $a=0.02286\text{m.}$, $b=0.01016\text{m.}$, $x_1=0.013\text{m.}$, $\mu_r=1.0$, $\epsilon_r=2.0$.

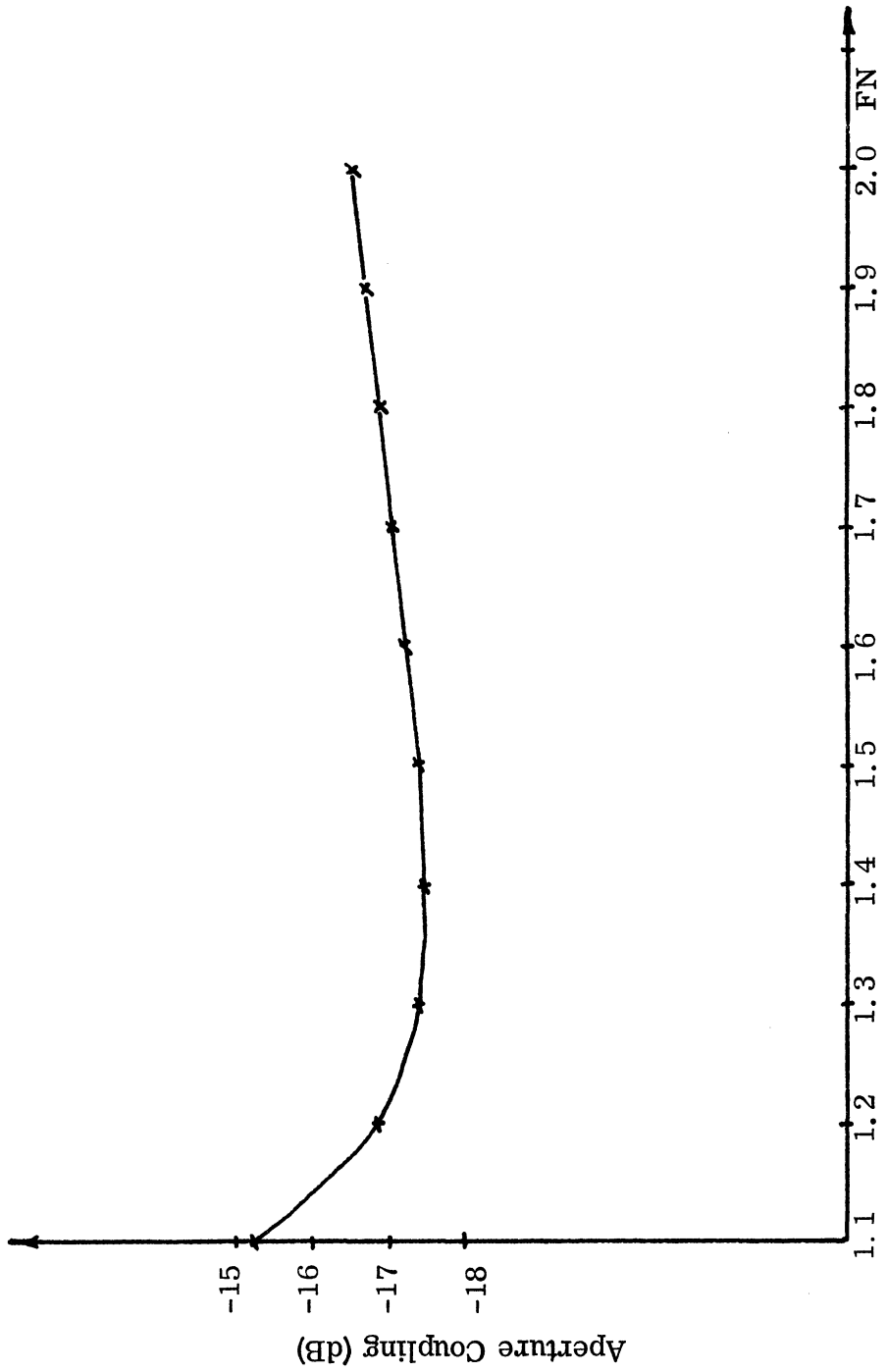


FIG. 3-10(b): APERTURE TO APERTURE E-PLANE COUPLING OF LOADED SLOTS
 $a=0.02286\text{m.}$, $b=0.01016\text{m.}$, $x_1=0.013\text{m.}$, $\mu_r=1.0$, $\epsilon_r=3.0$.

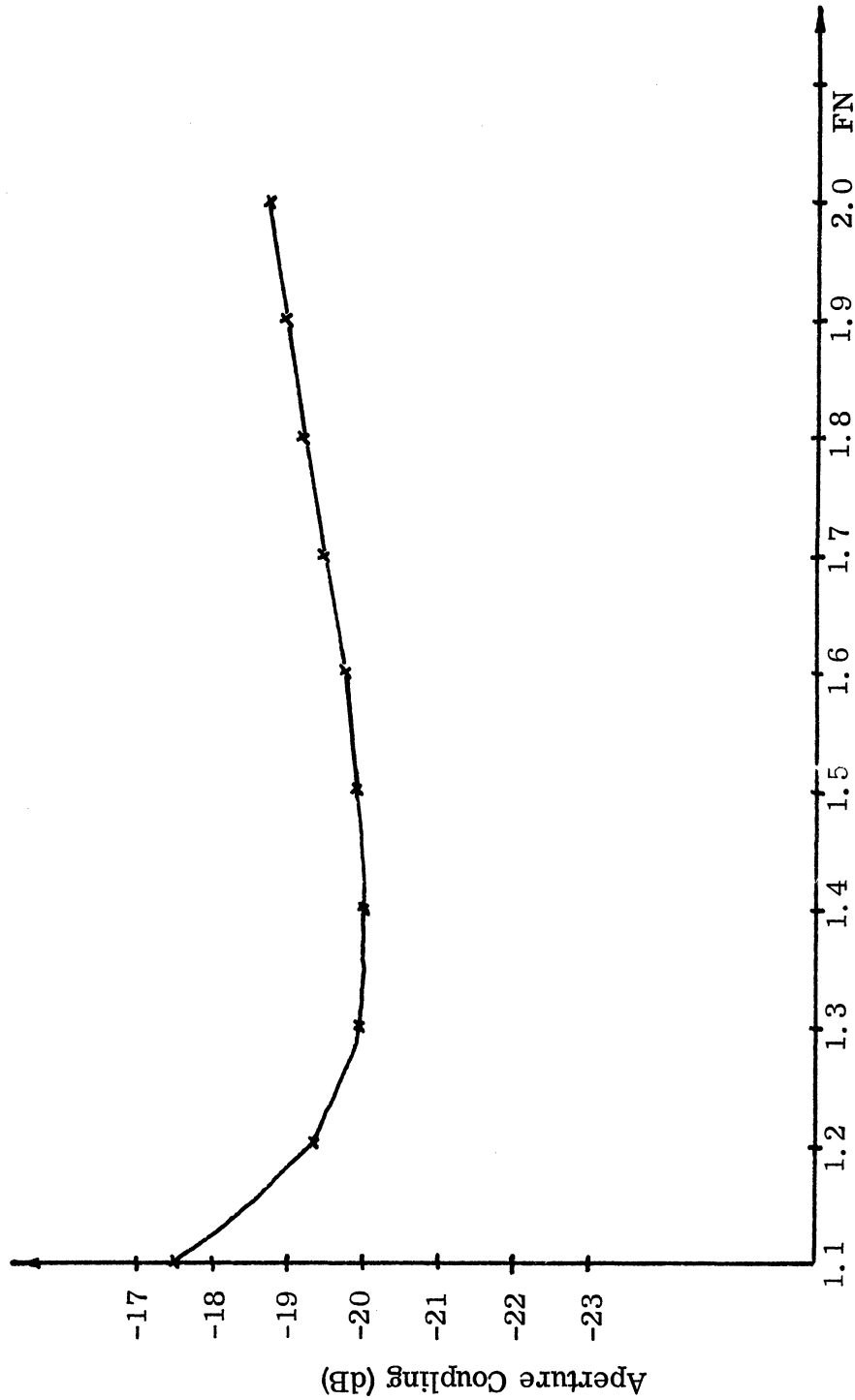


FIG. 3-10(c): APERTURE TO APERTURE E-PLANE COUPLING OF LOADED SLOTS
 $a=0.02286\text{m.}$, $b=0.016\text{m.}$, $x_1=0.013\text{m.}$, $\mu_r=1.0$, $\epsilon_r=4.0$.

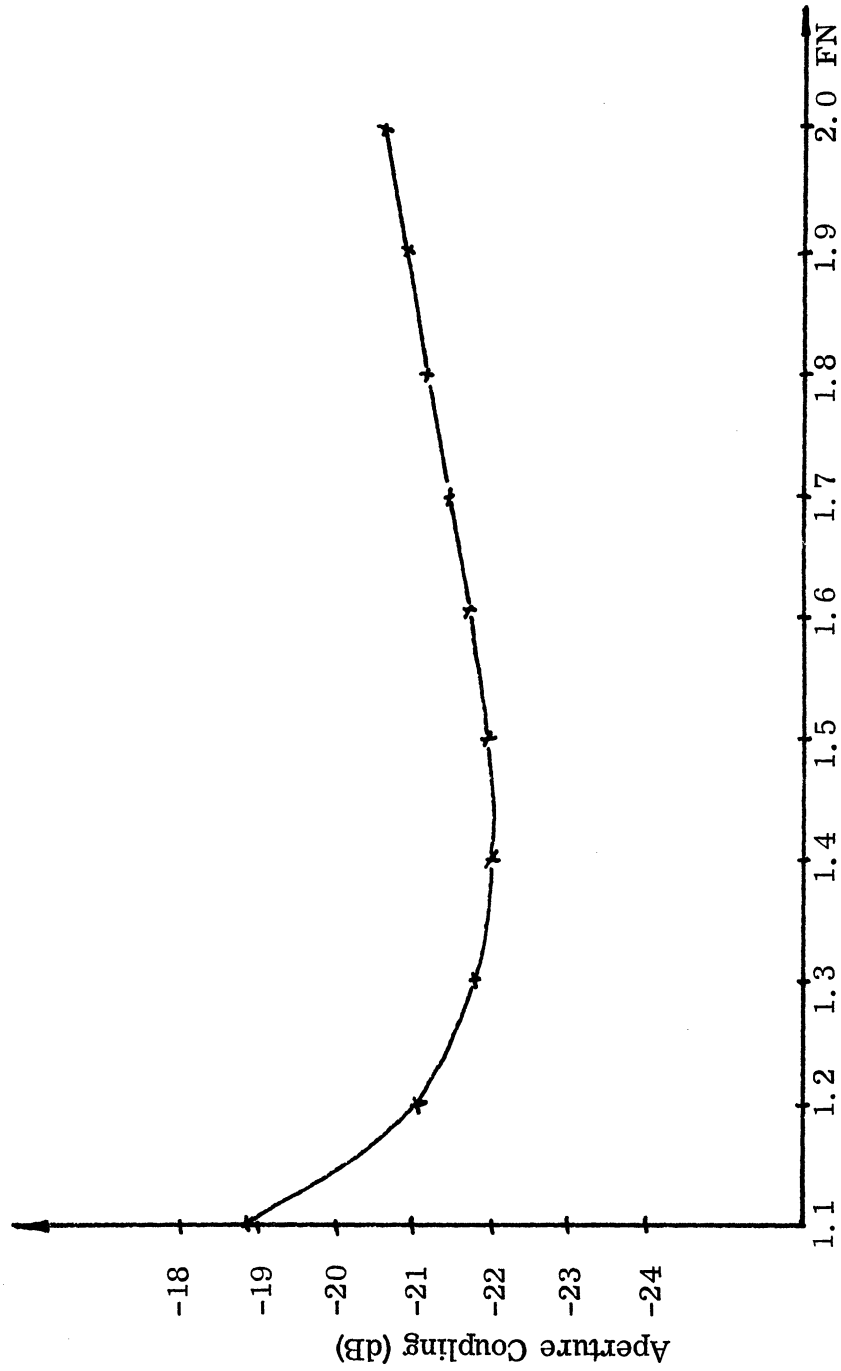


FIG. 3-10(d): APERTURE TO APERTURE E-PLANE COUPLING OF LOADED SLOTS
 $a=0.02286\text{m.}$, $b=0.01016\text{m.}$, $x_1=0.013\text{m.}$, $\mu_r=1.0$, $\epsilon_r=5.0$.

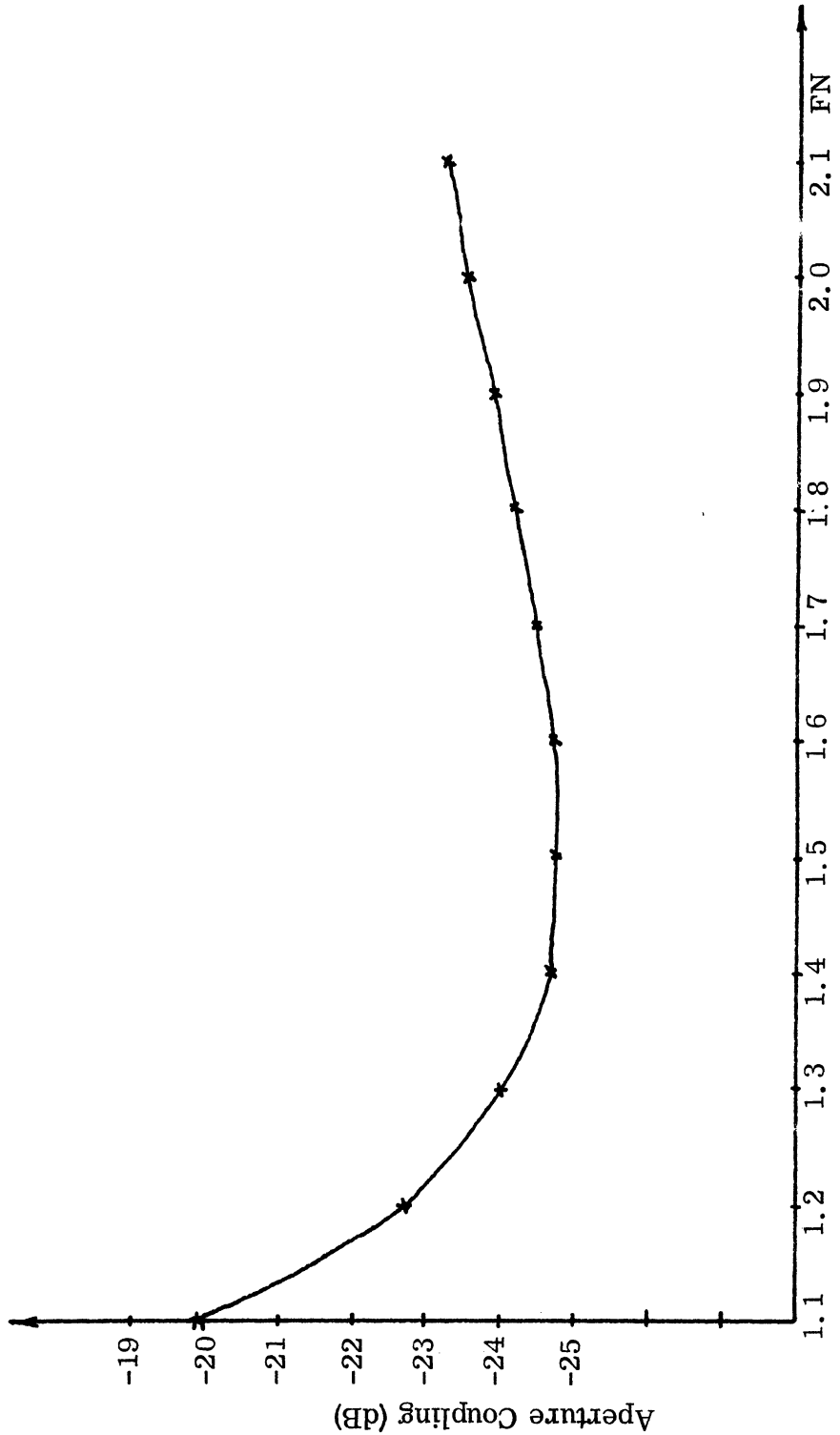


FIG. 3-10(e): APERTURE TO APERTURE E-PLANE COUPLING OF LOADED SLOTS
 $a=0.02286m.$, $b=0.01016m.$, $x_1=0.013m.$, $\mu_r=1$, $\epsilon_r=7$.

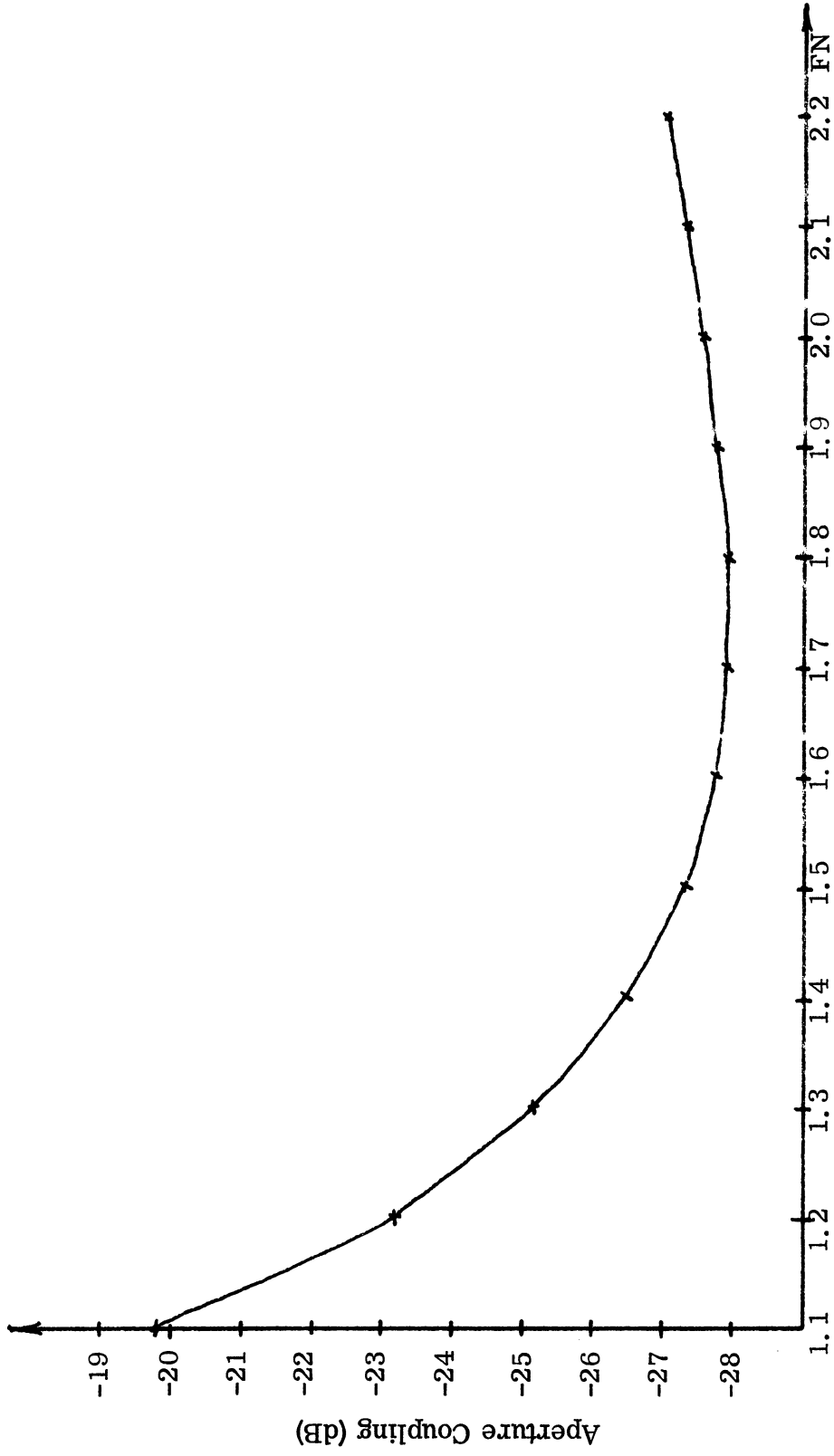


FIG. 3-10(f): APERTURE TO APERTURE E-PLANE COUPLING OF LOADED SLOTS
 $a=0.02286m.$, $b=0.01016m.$, $x_1=0.013m.$, $\mu_r=1$, $\epsilon_r=11$.

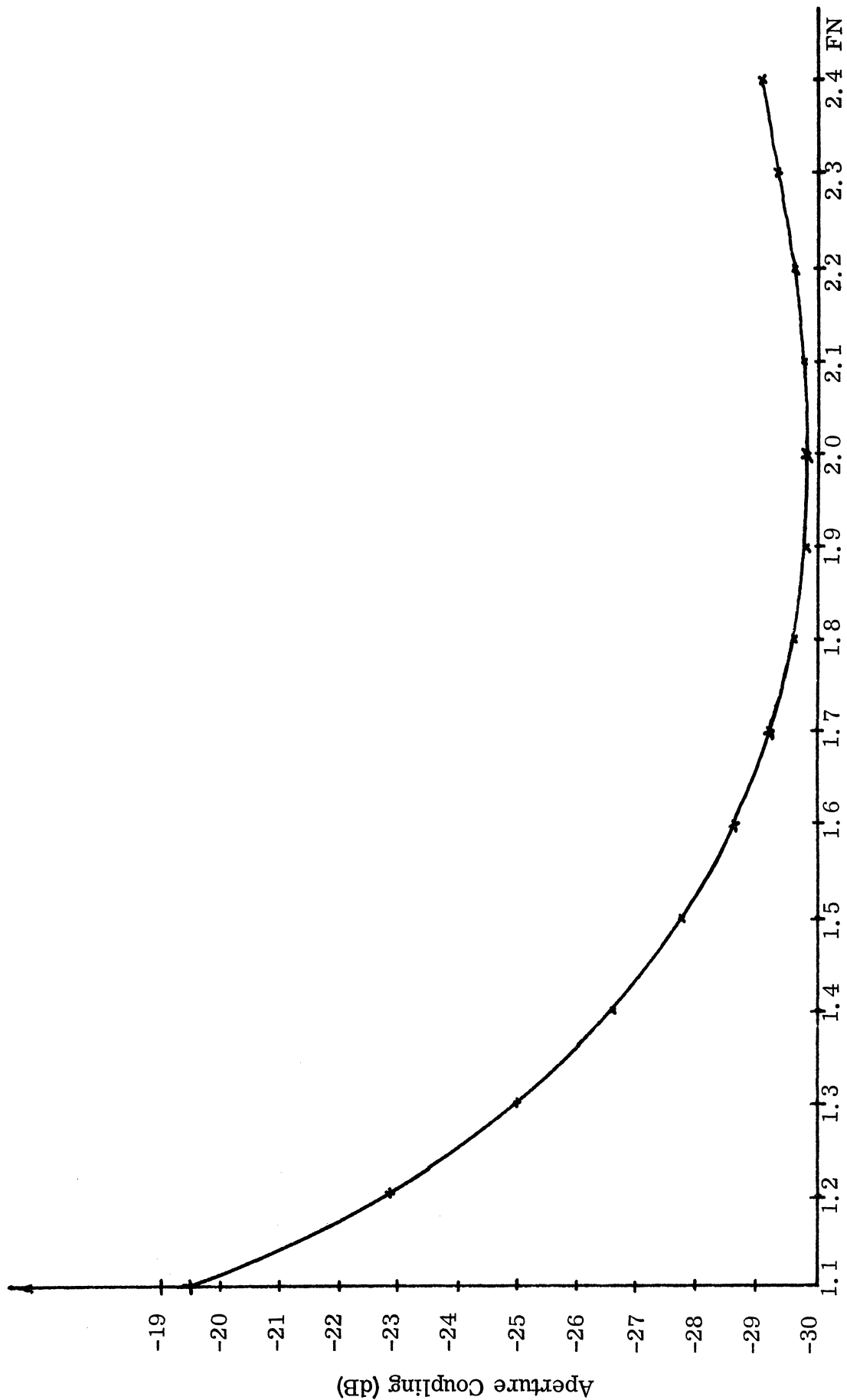


FIG. 3-10(g): APERTURE TO APERTURE E-PLANE COUPLING OF LOADED SLOTS
 $a=0.022286\text{m.}$, $b=0.01016\text{m.}$, $x_1=0.013\text{m.}$, $\mu_r=1$, $\epsilon_r=15$.

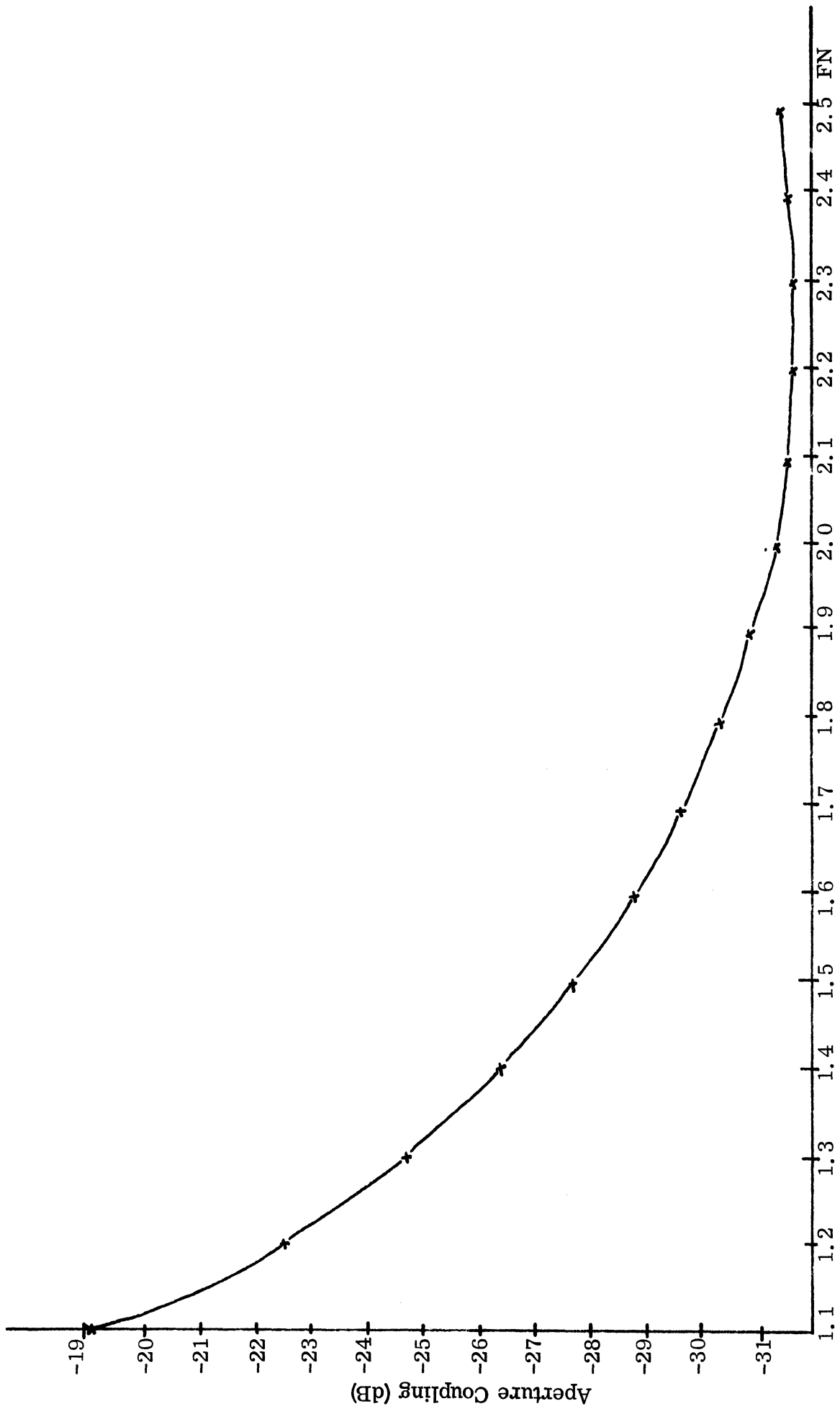


FIG. 3-10(h): APERTURE TO APERTURE E-PLANE COUPLING OF LOADED SLOTS

$a=0.02286m.$, $b=0.01016m.$, $x_1=0.013m.$, $\mu_r=1$, $\epsilon_r=20$.

The increment in spacing for calculations was taken to be smaller in the range from 0.1λ up to 2λ , namely every 0.1λ to show in more detail the effect of interaction between the slots which is more pronounced for closer spacings. From a spacing of 2λ up to 10λ it was varied in steps of 1λ . Also the modified program included the program of Section 3.2 as a subroutine which could be called upon to evaluate the aperture conductance and susceptance; also the aperture reflection coefficient can be obtained as shown in the examples of the computer output given in Appendix B.

3.4.2 Graphs

3.4.2(a): Figure 3-11 which is drawn on semi-logarithmic paper represents the coupling in dB versus spacing in wavelength. (see also Appendix B).

As has been mentioned before the effect of the interaction between the two slots is noticeable for closer spacings. For slots further apart in wavelength the differences due to interaction is very small. This curve agrees within a fraction of a dB with Fig. 4-4 of Lyon et al².

3.4.2(b): For the loaded case of aperture-to-aperture coupling it is shown in Fig. 3-12 that the approximation of 6 dB/octave of spacing is quite good. Notice in this case spacings can be smaller than 0.4λ as in Fig. 3-11; for this case the parameters of the guide are $a=0.02286\text{m.}$, $b=0.01016\text{m.}$, and it is filled with dielectric material with relative permittivity of 11.0. The operating frequency in this case is S-band; therefore it was possible to go down to $0.1\lambda_0$, where λ_0 is in the free-space wavelength (Fig. 3-12).

3.5 Evaluation of the Cavity Effect

Due to the loaded cavities which are backing both transmitter and receiver slots, as shown in Fig. 4-2 of Chapter IV, the resonance and anti-resonance points become very distinct. These waveguides can be considered as a five-sided cavity as was explained in Chapter II.

An approximate way for rapid calculations of the resonance and anti-resonance points can be made according to the analysis in Chapter II.

For resonance points:

$$l = n \frac{\lambda_g}{2} \quad (n = 1, 2, 3, \dots)$$

where l is as defined before (length of the cavity) and λ_g is the waveguide wavelength.

For anti-resonance:

$$l = n \frac{\lambda_g}{4}, \quad (n = 1, 2, 3, \dots)$$

A formula has been developed to predict the resonant frequency; likewise another one for anti-resonance could be developed.

For resonance:

$$l = n \frac{\lambda_g}{2},$$

but

$$\lambda_g = \frac{\lambda_0}{\sqrt{\mu_r \epsilon_r}} \frac{1}{\sqrt{1 - \left(\frac{f_c}{f}\right)^2}} = \frac{3 \times 10^{10}}{\sqrt{\mu_r \epsilon_r}} \frac{1}{\sqrt{f^2 - f_c^2}},$$

$$l = n \frac{3 \times 10^{10}}{2} \frac{1}{\sqrt{\mu_r \epsilon_r} \sqrt{f^2 - f_c^2}}.$$

Finally

$$f_{\text{res.}} = \sqrt{\left[\frac{0.15n}{l \sqrt{\mu_r \epsilon_r}} \right]^2 + f_c^2} \quad \text{GHz} \quad (n=1, 2, 3, \dots) \quad (3.9)$$

where l is in meters,

$$f_c = \frac{1}{2a\sqrt{\mu_r \epsilon_r}} = \frac{0.3}{2a\sqrt{\mu_r \epsilon_r}} = \frac{0.15}{a\sqrt{\mu_r \epsilon_r}} \quad \text{GHz}, \quad (3.10)$$

where a is in meters. Therefore

$$f_{\text{res.}} = \frac{0.15}{\sqrt{\mu_r \epsilon_r}} \sqrt{\frac{n^2}{l^2} + \frac{1}{a^2}}. \quad (3.11)$$

It is to be noted in the empty or unloaded cavity $\mu_r=1$ and $\epsilon_r=1$. Therefore Eq. (3. 11) becomes

$$f_{\text{res.}} = 0.15 \sqrt{\frac{n^2}{\ell^2} + \frac{1}{a^2}}, \quad (n = 1, 2, 3, \dots) \quad (3. 12)$$

By comparing (3. 11) and (3. 12) note that the resonance frequency is determined by the broadside length of the aperture 'a' and the depth of the cavity. It also depends on the parameters of the material loading.

Another way to find the resonance of the cavity and at the same time be able to predict the bandwidth is by means of Eq. (2. 79) in Chapter II which is:

$$Z(0) = Z_{1g} \tanh (\alpha_{1g} + j \beta_{1g}) \ell ,$$

or

$$Y(0) = \frac{1}{Z_{1g}} \coth (\alpha_{1g} + j \beta_{1g}) \ell ,$$

and

$$|Y^2(0)| = \frac{1}{|Z_{1g}|^2} \left[\frac{\cosh^2 \alpha_{1g} \ell \cos^2 \beta_{1g} \ell + \sinh^2 \alpha_{1g} \ell \sin^2 \beta_{1g} \ell}{\sinh^2 \alpha_{1g} \ell \cos^2 \beta_{1g} \ell + \cosh^2 \alpha_{1g} \ell \sin^2 \beta_{1g} \ell} \right] .$$

This last equation is proportional to the power received. A computer program has been written for this equation to evaluate $|Y(0)|^2$ versus frequency. The output of the computer is best presented by means of the plots shown in Figs. 3-13 to 3-16. These graphs were plotted directly by means of the University of Michigan Digital Plotting System. An example for calculating the resonant frequency corresponding to the half-wavelength method is given below.

Example 1

For $a = 0.02286\text{m.}$, $b=0.01016\text{m.}$, $\ell = 0.031\text{m.}$, $\epsilon_r = 7.0$, $\mu_r = 1.0$,

$$f_c = 2.48008 \text{ GHz.}$$

For n = 1

$$f_{1 \text{ res.}} = \frac{0.15}{\sqrt{\mu_r \epsilon_r}} \sqrt{\frac{n^2}{\ell^2} + \frac{1}{a^2}} = 3.08163 \text{ GHz.}$$

For n= 2

$$f_{2 \text{ res.}} = 4.41935 \text{ GHz.}$$

Example 2

For a=0,02286 m., b=0.01016m., $\ell=0.031\text{m.}$, $\mu_r = 1.0$, $\epsilon_r = 11.0$

$$f_c = 1.97842.$$

For n = 1

$$f_{1 \text{ res.}} = 2.4583 \text{ GHz.}$$

For n= 2

$$f_{2 \text{ res.}} = 3.5254 \text{ GHz.}$$

Now consider the perturbation formulas applying to this case. For the metal probe and $\mu_r=1$, $\epsilon_r= 11.0$,

diameter = 0.1143 cm. (metal probe)

projected length inside the guide = 0.47498 cm.

$$d_1 = 2.48792 \text{ cm}$$

$$d_2 = 0.60706 \text{ cm}$$

$$d = 3.09498 \text{ cm.}$$

Here d_1 , d_2 and d are as shown in Fig. 2-11 of Chapter II.

Then

$$\frac{\omega - \omega_0}{\omega_0} = + \frac{2V}{abd} \left[\cos^2 \frac{2\pi d_1}{d} - \frac{\pi^2}{k^2} \cos^2 \frac{\pi d_1}{d} \right].$$

Now take

$$f = 2.4583$$

then

$$k = k_0 \sqrt{\mu_r \epsilon_r} = \frac{2\pi \times f}{3 \times 10^{10}} \sqrt{\mu_r \epsilon_r} = 17.0674876.$$

Now

$$V = \frac{\pi (\text{dia})^2}{4} \times \text{length} = 0.0060943 \text{ cm}^3$$

and

$$\begin{aligned} \frac{2V}{abd} &= \frac{2 \times 0.0061}{2.286 \times 1.016 \times 3.10} \left[\cos^2(289.39) - \frac{\pi^2}{(17.07 \times 2.286)^2} \cos^2(144.69) \right] \\ &= 0.0017 \left[\sin^2(19.39) - 0.00645 \sin^2(54.69) \right] \\ &= 0.0017 \left[(0.33199)^2 - 0.00645 \times (0.816)^2 \right] \\ &= 0.00018 \quad (\text{this is very small}). \end{aligned}$$

For the material filled hole or cylinder around the probe consider it to be filled with polystyrene having a dielectric constant of 2.54 and at the range of frequencies considered.

$$\frac{\omega - \omega_0}{\omega_0} = - \frac{2V}{abd} \left[\frac{\Delta \epsilon}{\epsilon} \sin^2 \frac{\pi d_1}{d} \right]$$

$$\text{diameter of the cylinder} = 0.55118 \times 10^{-2} \text{ m.}$$

$$\text{length of the hole} = 1.016 \times 10^{-2} \text{ m.}$$

In the above $\Delta \epsilon$ is negative or positive corresponding to changing to a lower or higher dielectric constant respectively. The volume is easily found to be

$$V = \frac{\pi (\text{dia.})^2}{4} = 0.2423 \text{ cm}^3 .$$

Also

$$\frac{2V}{abd} = 0.0675.$$

Also

$$\frac{\Delta \epsilon}{\epsilon} = \frac{2.54 - 11}{11} = -0.7691 .$$

Therefore

$$\frac{\omega - \omega_0}{\omega_0} = -0.0675 \left[-0.7691 \times \cos^2(54.69) \right] = 0.0173435 .$$

The total perturbation = 0.0175 or 1.75 percent.

Therefore f_1 should be = 2.4583 (1+0.0175) = 2.501 GHz. For the other peak the material perturbation is the same but the probe perturbation changes because of the factor k in the formula. The metal probe perturbation at 3.5254 GHz is now found:

$$\frac{\omega - \omega_0}{\omega_0} = 0.0017 \times \left[(0.33199)^2 - \frac{9.8596 \times (0.816)^2}{(24.48)^2 \times 2.286} \right] = 0.0001792.$$

Then for 3.5254 GHz the total perturbations are 0.017522. This is not much different from that at 2.4583 GHz. Therefore,

$$f_2 = 3.5254 (1+0.017522) = 3.587 \text{ GHz.}$$

Notice that these values are very close to the experimental measurements (see Fig. 4-7 in Ch. IV). There is good agreement considering the errors in measuring the dimensions and the experimental errors of instrumentation. Also, there might be some variation due to a slight change in ϵ_r with a change of frequency.

Example 3

For $a = 0.02286\text{m.}$, $b = 0.01016\text{m.}$, $\ell = 0.031 \text{ m.}$, $\mu_r = 1.0$, $\epsilon_r = 15.0$

$$f_c = 1.6942 \text{ GHz (cutoff frequency) .}$$

Using Eq. (3.11) the resonance frequencies are:

For $n = 1$

$$f_{1 \text{ res.}} = 2.105 \text{ GHz .}$$

For $n = 2$

$$f_{2 \text{ res.}} = 3.01899 \text{ GHz .}$$

Example No. 4(a)

For $a = 0.02286 \text{ m.}$, $b = 0.01016 \text{ m.}$, $l = 0.1015 \text{ m.}$, $\mu_r = 1.0$, $\epsilon_r = 15.0$
the following corresponding resonant frequencies using Eq. (3.11) are :

$n = 1$	$f_1 = 1.7368$
$n = 2$	$f_2 = 1.8583$
$n = 3$	$f_3 = 2.0448$
$n = 4$	$f_4 = 2.2804$
$n = 5$	$f_5 = 2.5516$
$n = 6$	$f_6 = 2.8482$
$n = 7$	$f_7 = 3.1631$
$n = 8$	$f_8 = 3.4913$
$n = 9$	$f_9 = 3.8293$
$n = 10$	$f_{10} = 4.1750$

Example No. 4(b)

For $a = 0.02286 \text{ m.}$, $b = 0.01016 \text{ m.}$, $l = 0.1015 \text{ m.}$, $\mu_r = 1.0$, $\epsilon_r = 11.0$, the
resonance frequencies using (3.11) are

$n = 1$	$f_1 = 2.027$
$n = 2$	$f_2 = 2.169$
$n = 3$	$f_3 = 2.388$
$n = 4$	$f_4 = 2.663$
$n = 5$	$f_5 = 2.979$
$n = 6$	$f_6 = 3.325$
$n = 7$	$f_7 = 3.694$
$n = 8$	$f_8 = 4.077$

Example No. 4(c)

For $a = 0.02286 \text{ m.}$, $b = 0.01016 \text{ m.}$, $l = 0.1015 \text{ m.}$, $\mu_r = 1.0$, $\epsilon_r = 7.0$, the
resonance frequencies using (3.11) are:

$n = 1$	$f_1 = 2.54$
$n = 2$	$f_2 = 2.72$
$n = 3$	$f_3 = 2.99$
$n = 4$	$f_4 = 3.338$
$n = 5$	$f_5 = 3.735$

Note that these resonance frequencies agree with the digital plots shown.

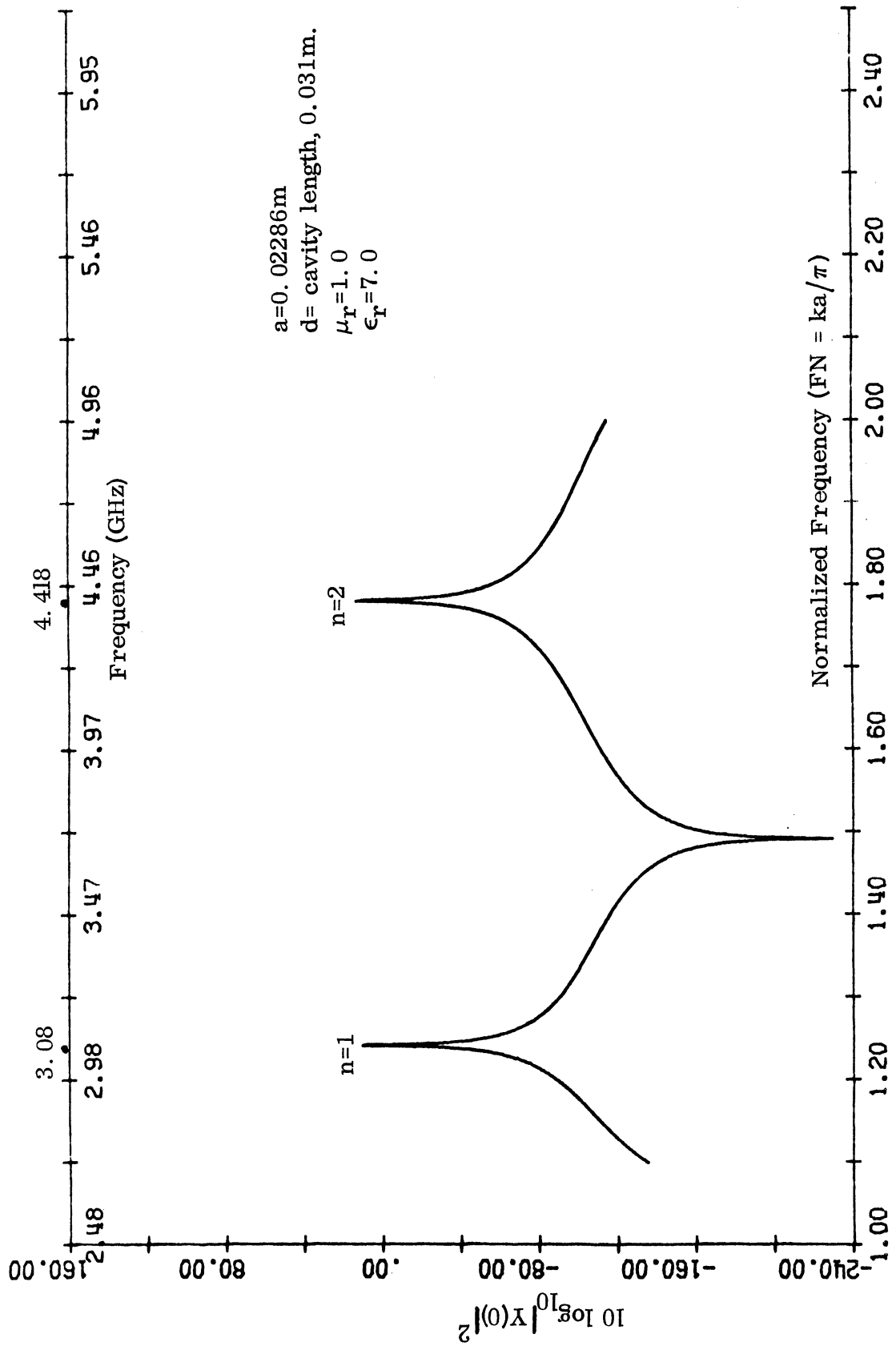


FIG. 3-13(a): RESONANCE OF THE CAVITY (Digital Plot).

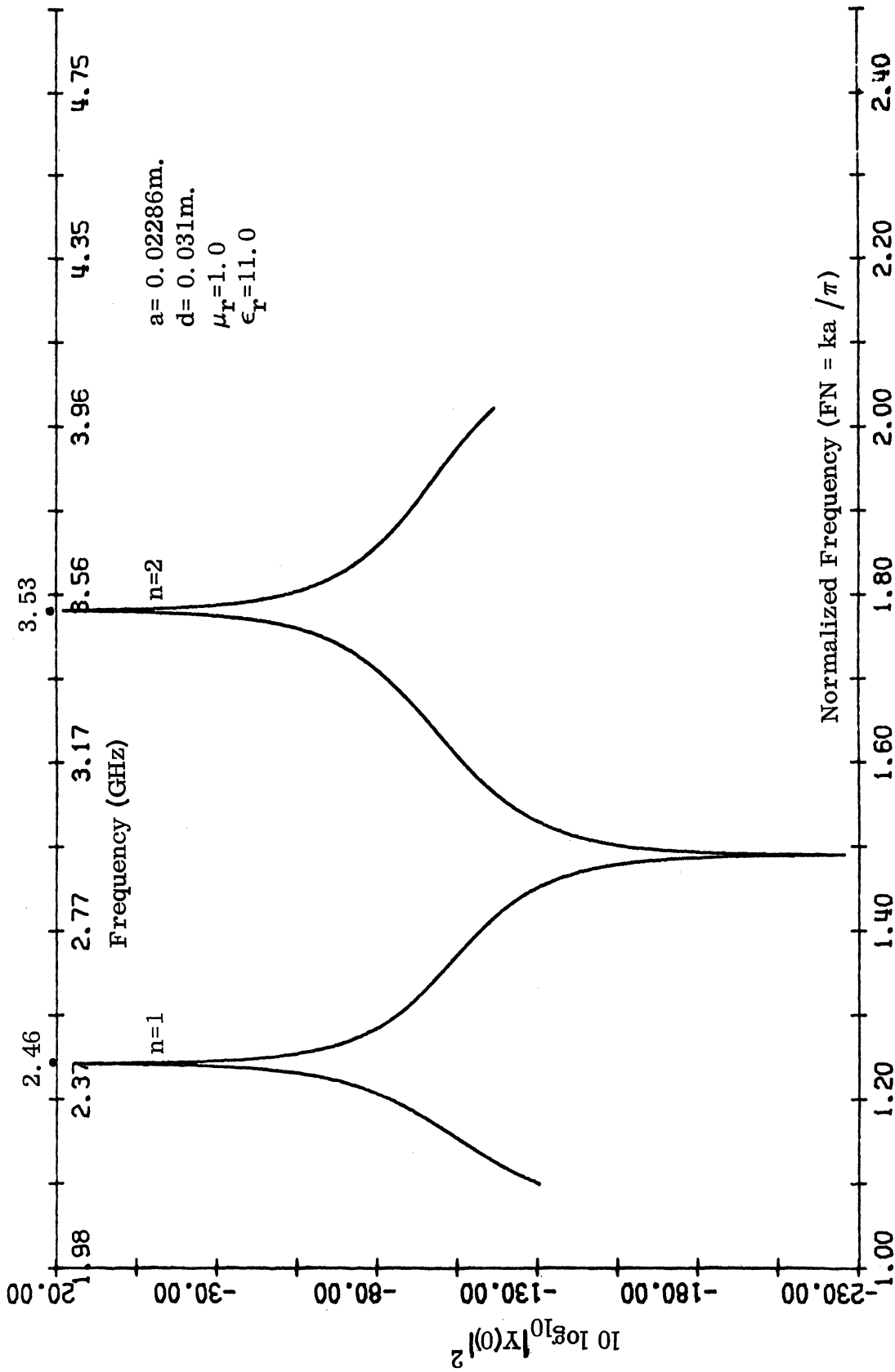


FIG 3-13(b): RESONANCE OF THE CAVITY (Digital Plot) .

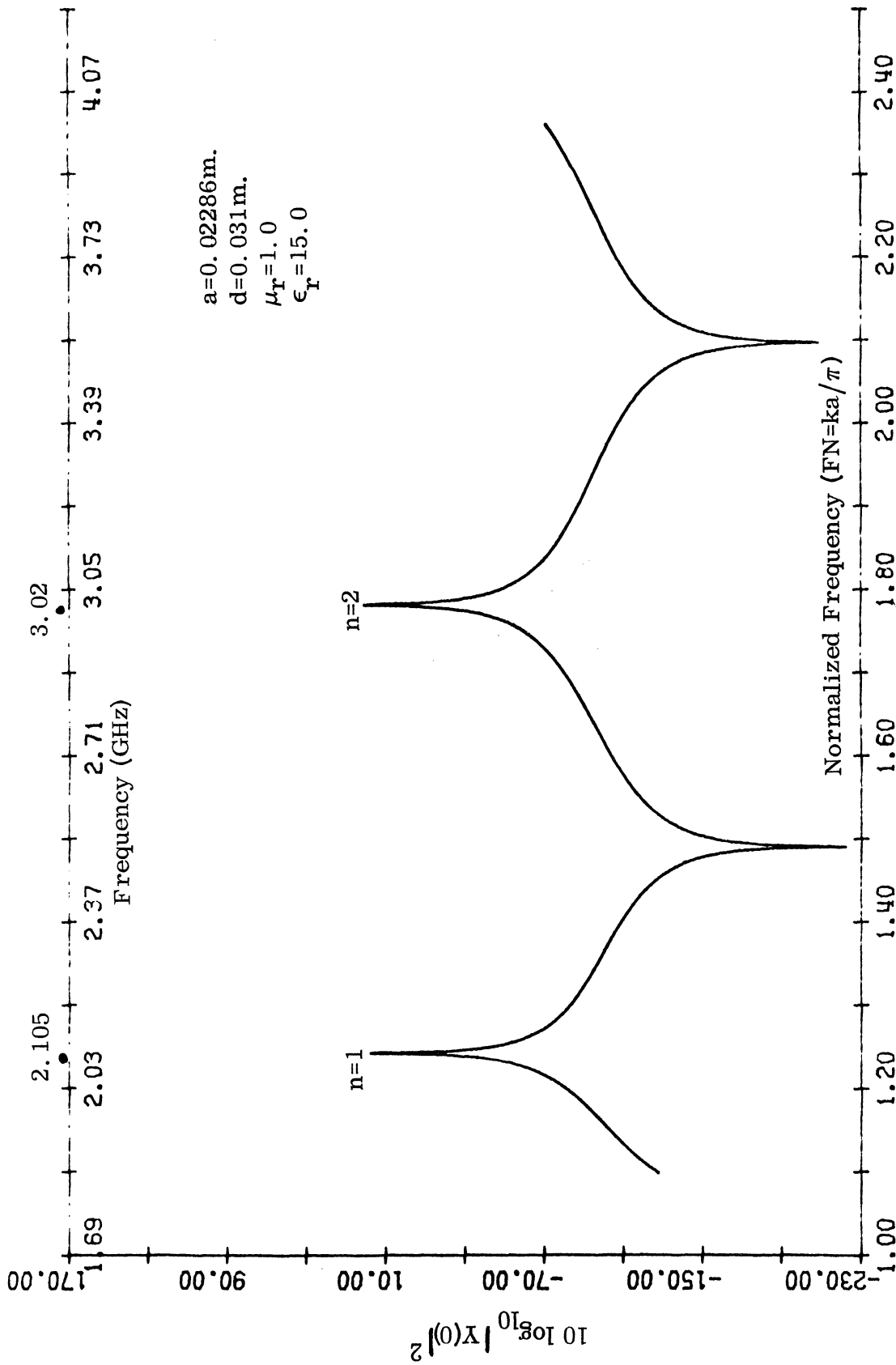


FIG. 3-13(c): RESONANCE OF THE CAVITY (Digital Plot).

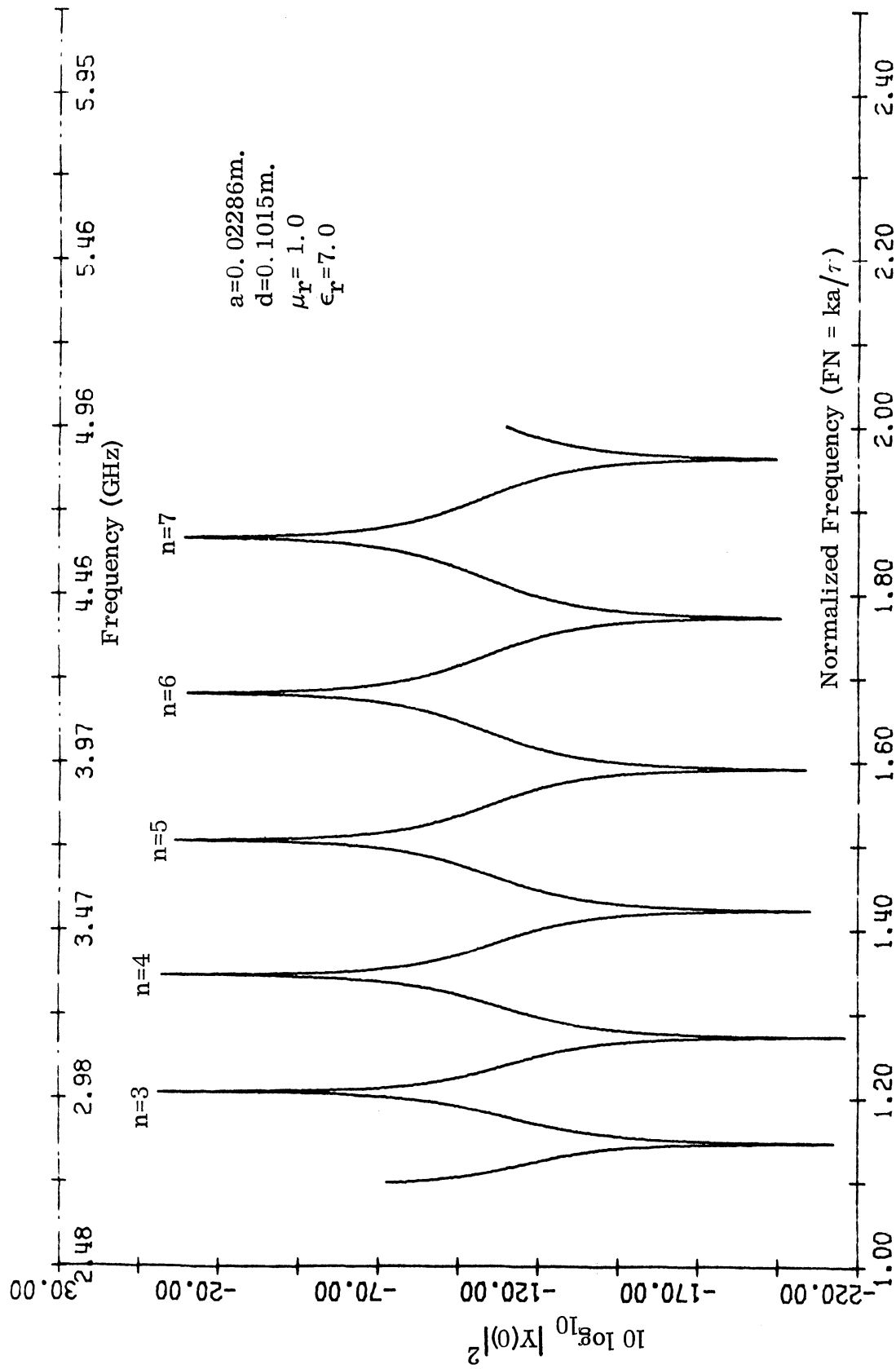


FIG 3-14(a): RESONANCE OF THE CAVITY (Digital Plot).

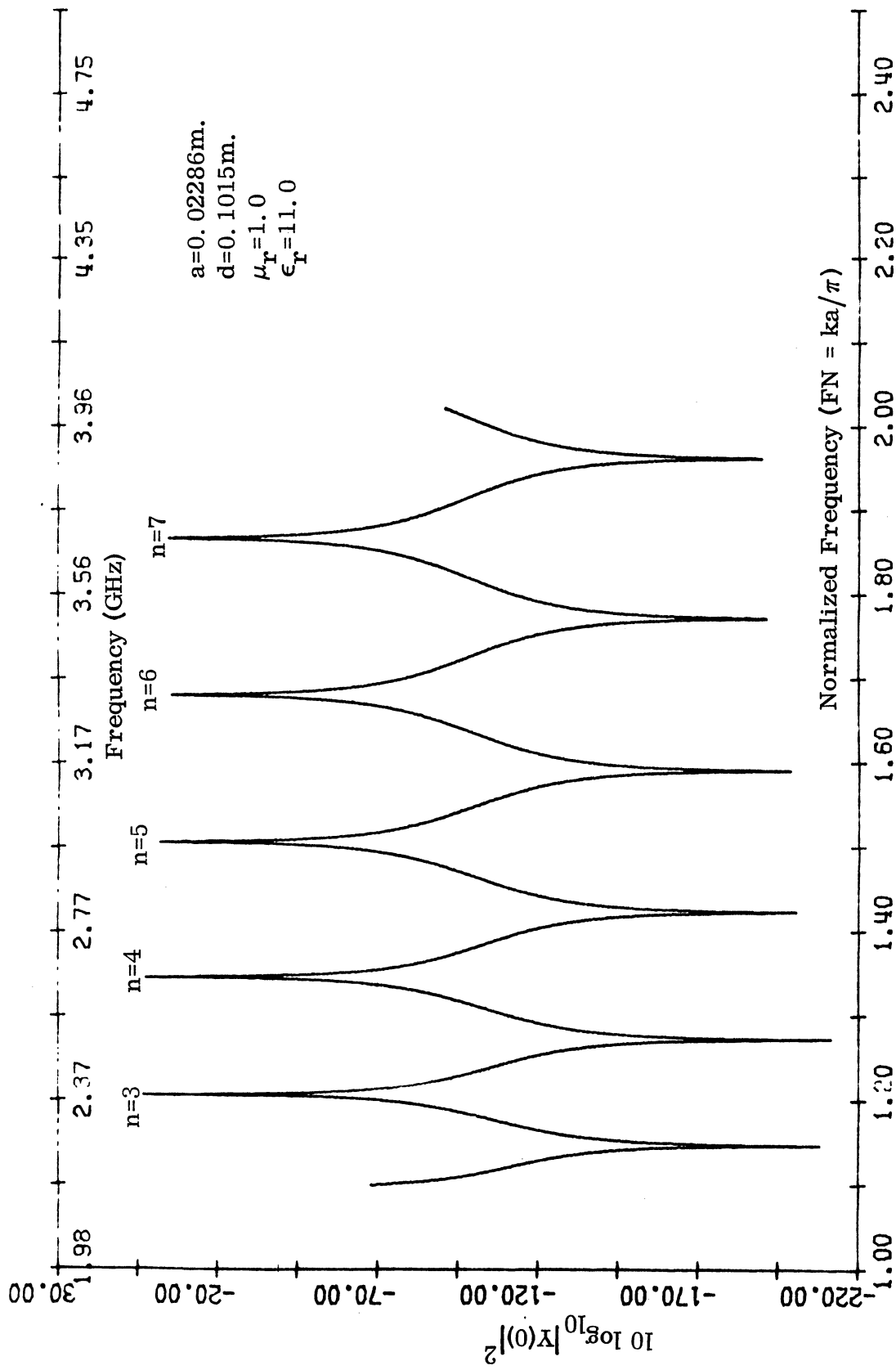


FIG. 3-14(b): RESONANCE OF THE CAVITY (Digital Plot).

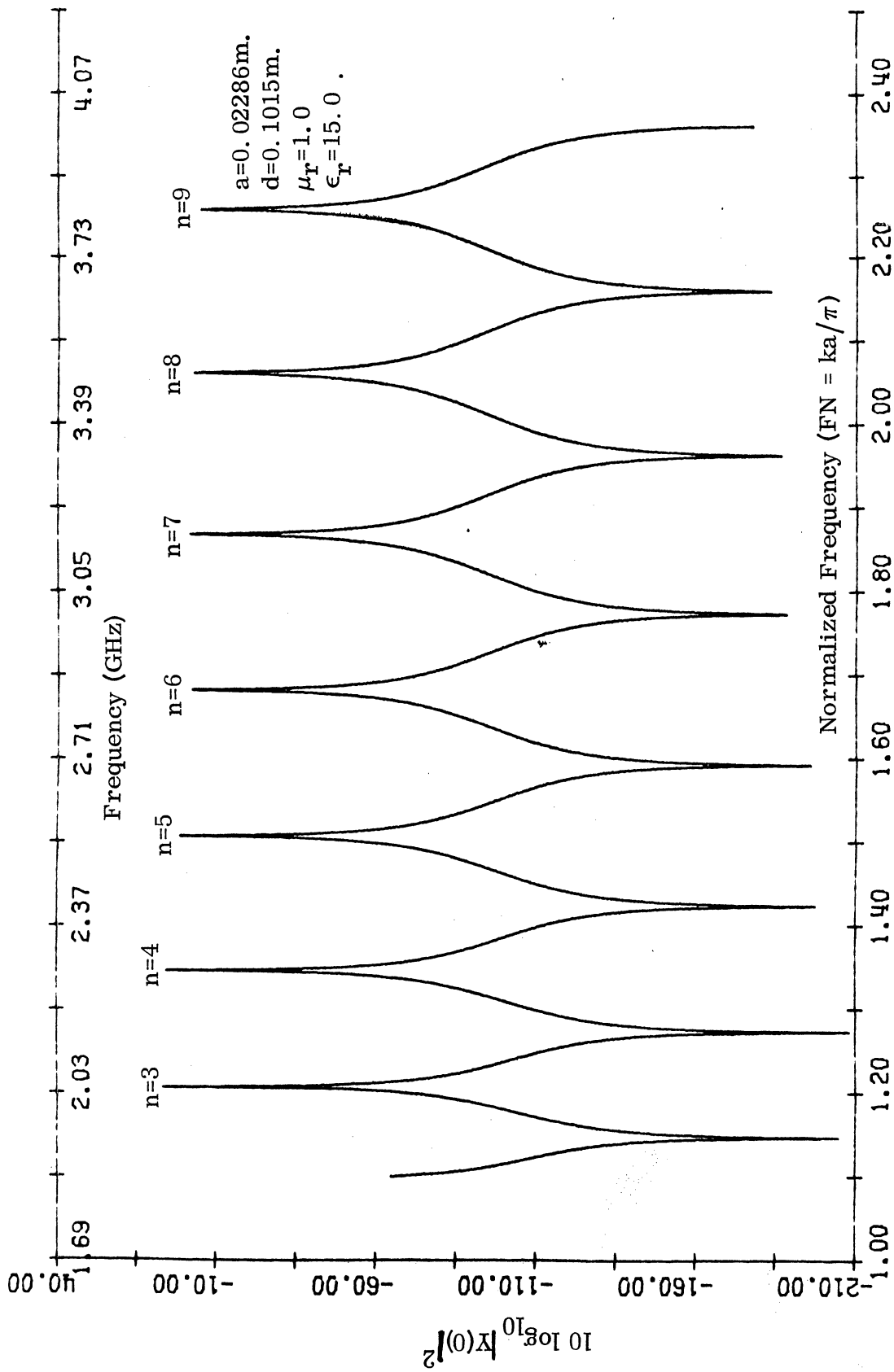


FIG. 3-14(c): RESONANCE OF THE CAVITY (Digital Plot).

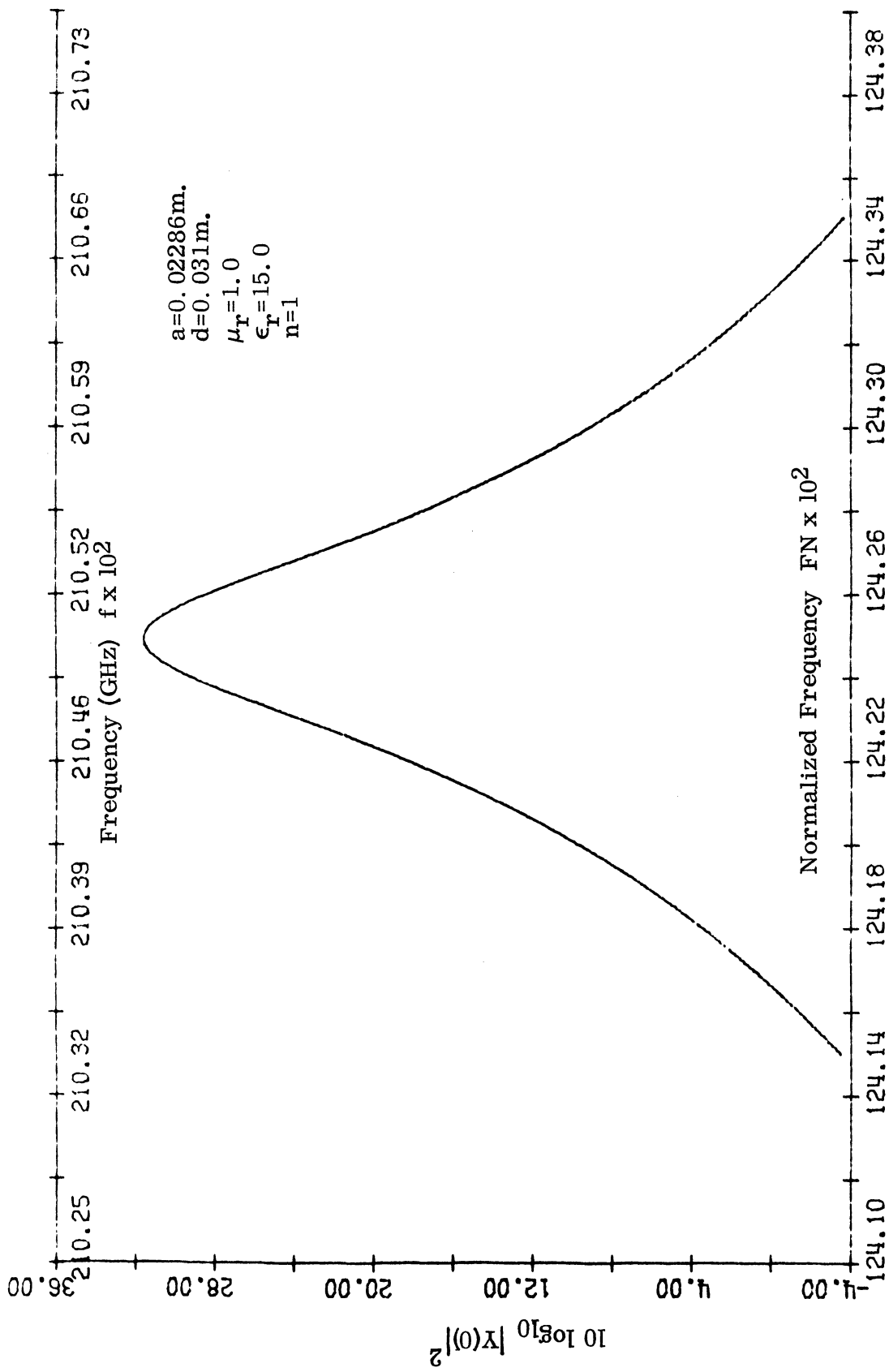


FIG. 3-15(a): AN EXPANDED DIGITAL PLOT FOR THE RESONANCE PEAKS.

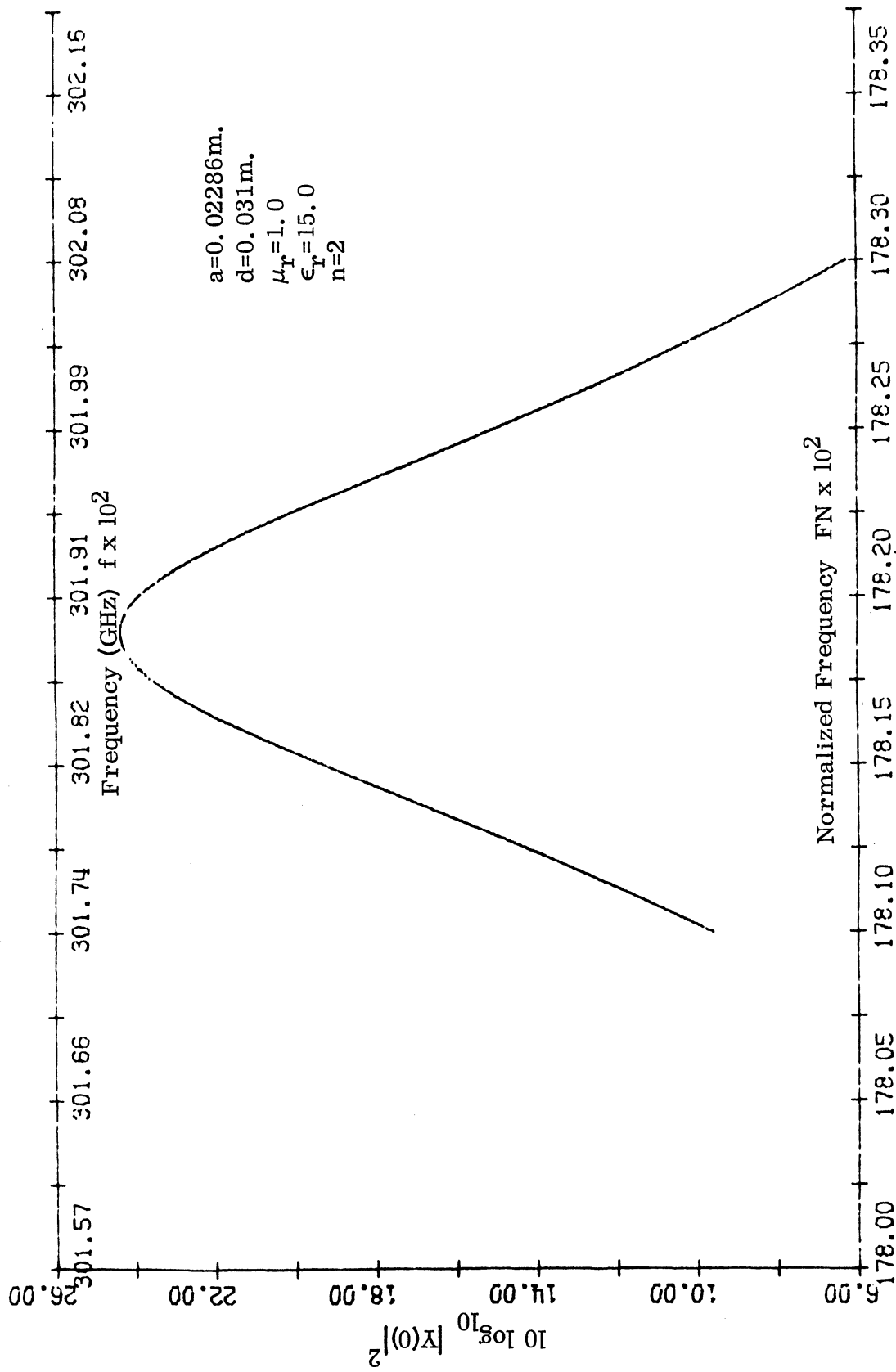


FIG. 3-15(b): AN EXPANDED DIGITAL PLOT FOR THE RESONANCE PEAKS.

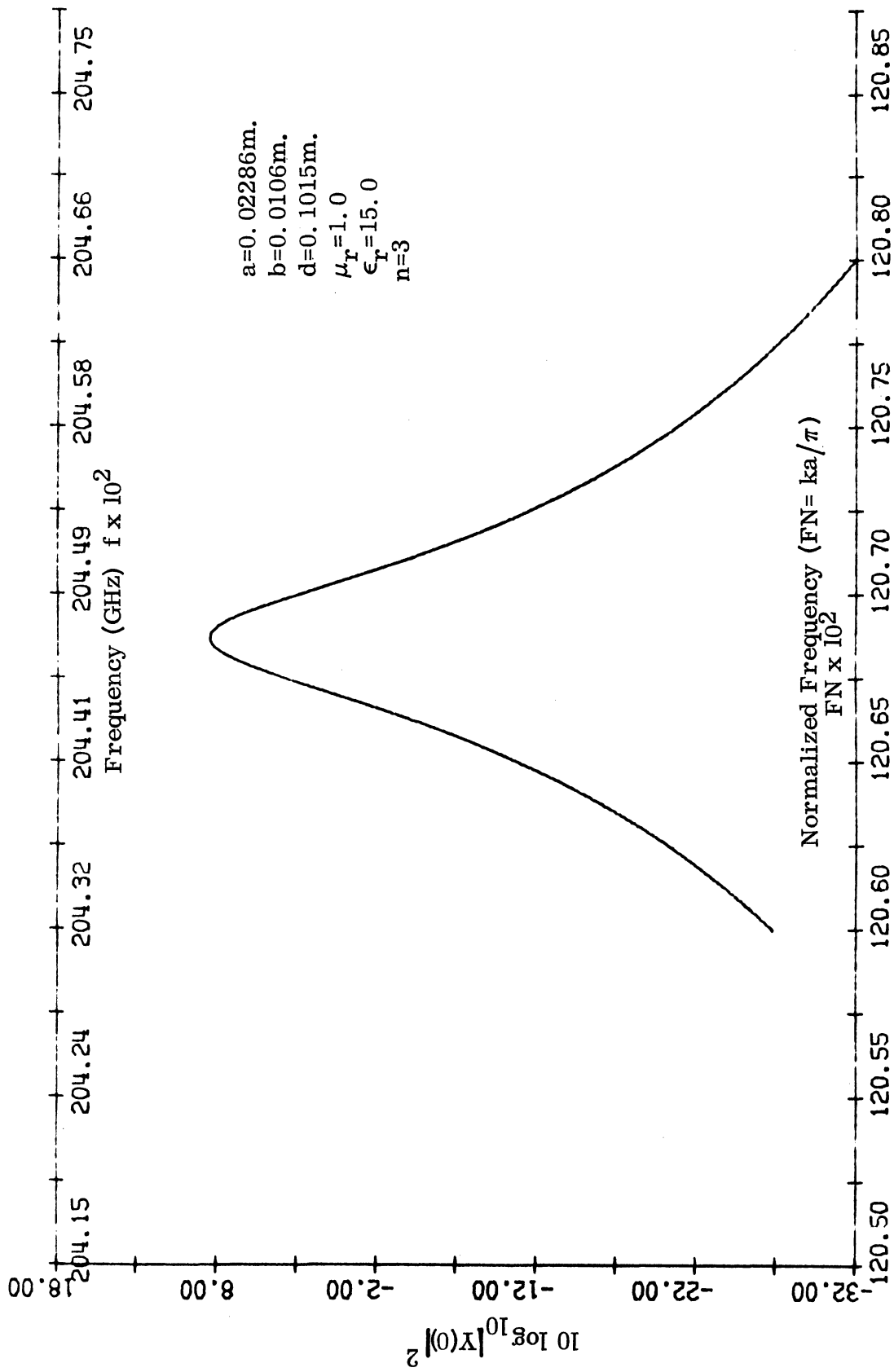


FIG. 3-16(a): AN EXPANDED DIGITAL PLOT FOR RESONANCE PEAK.

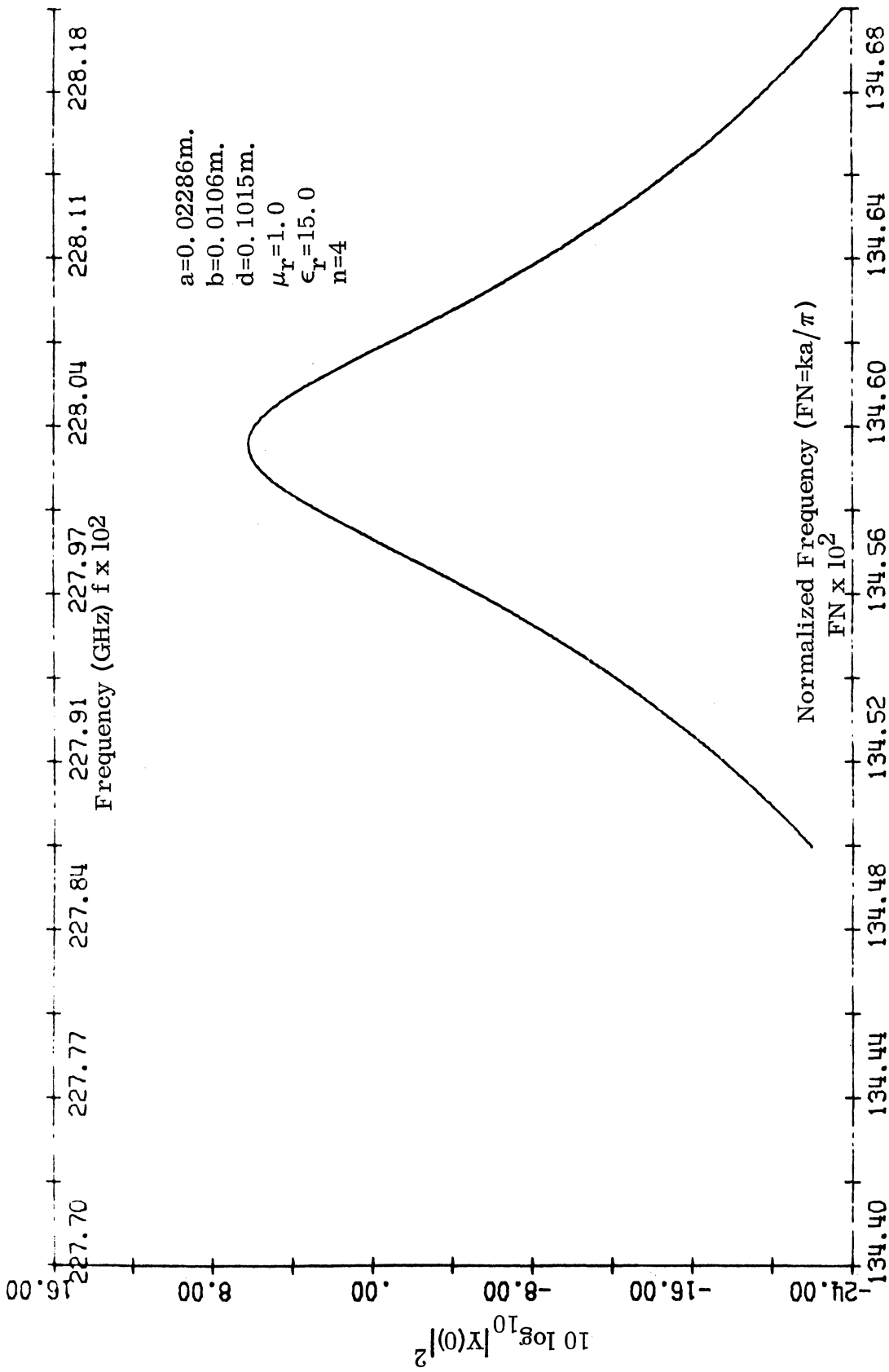


FIG. 3-16(b): AN EXPANDED DIGITAL PLOT FOR RESONANCE PEAK.

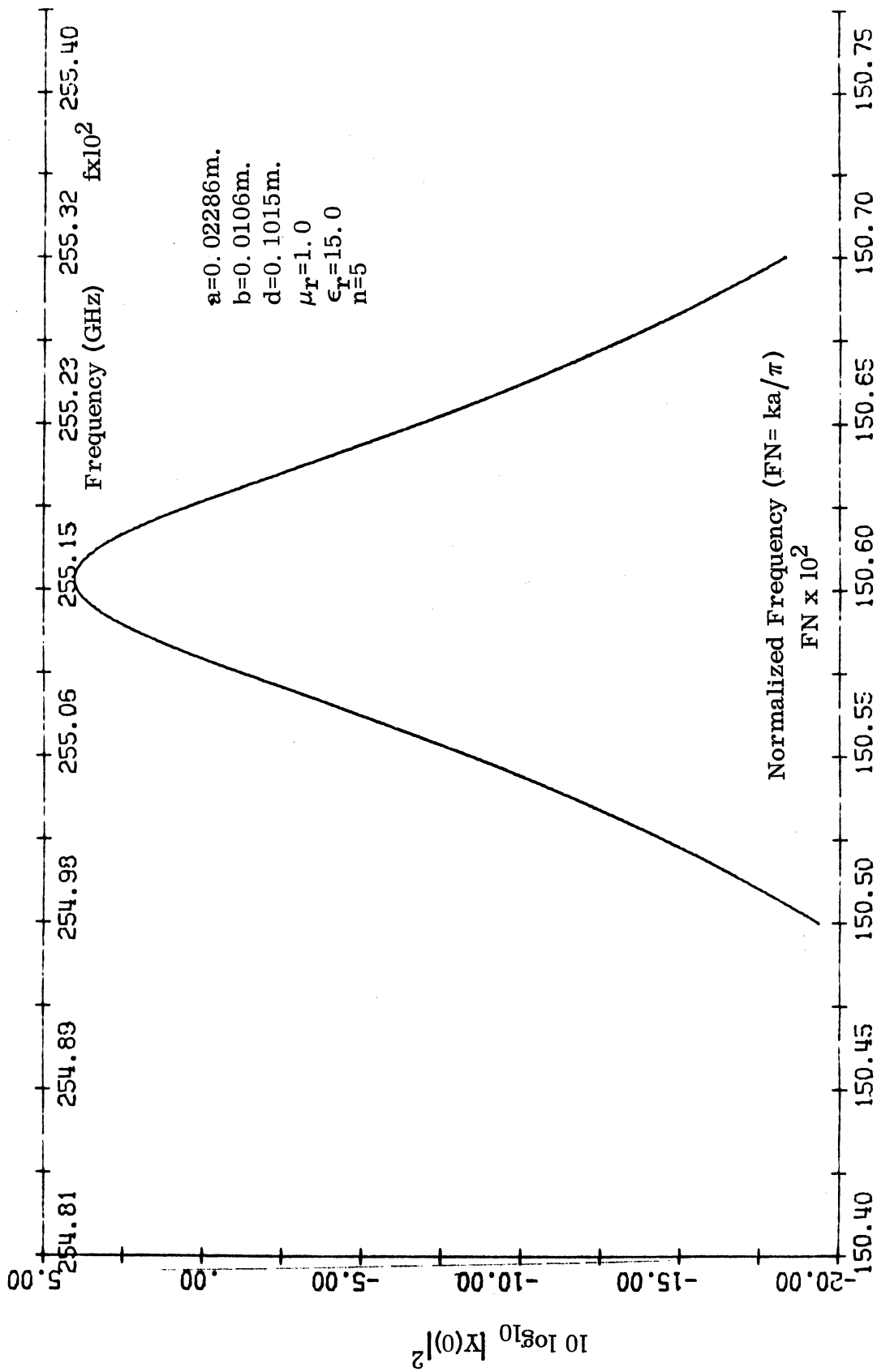


FIG. 3-16(c): AN EXPANDED DIGITAL PLOT FOR RESONANCE PEAK.

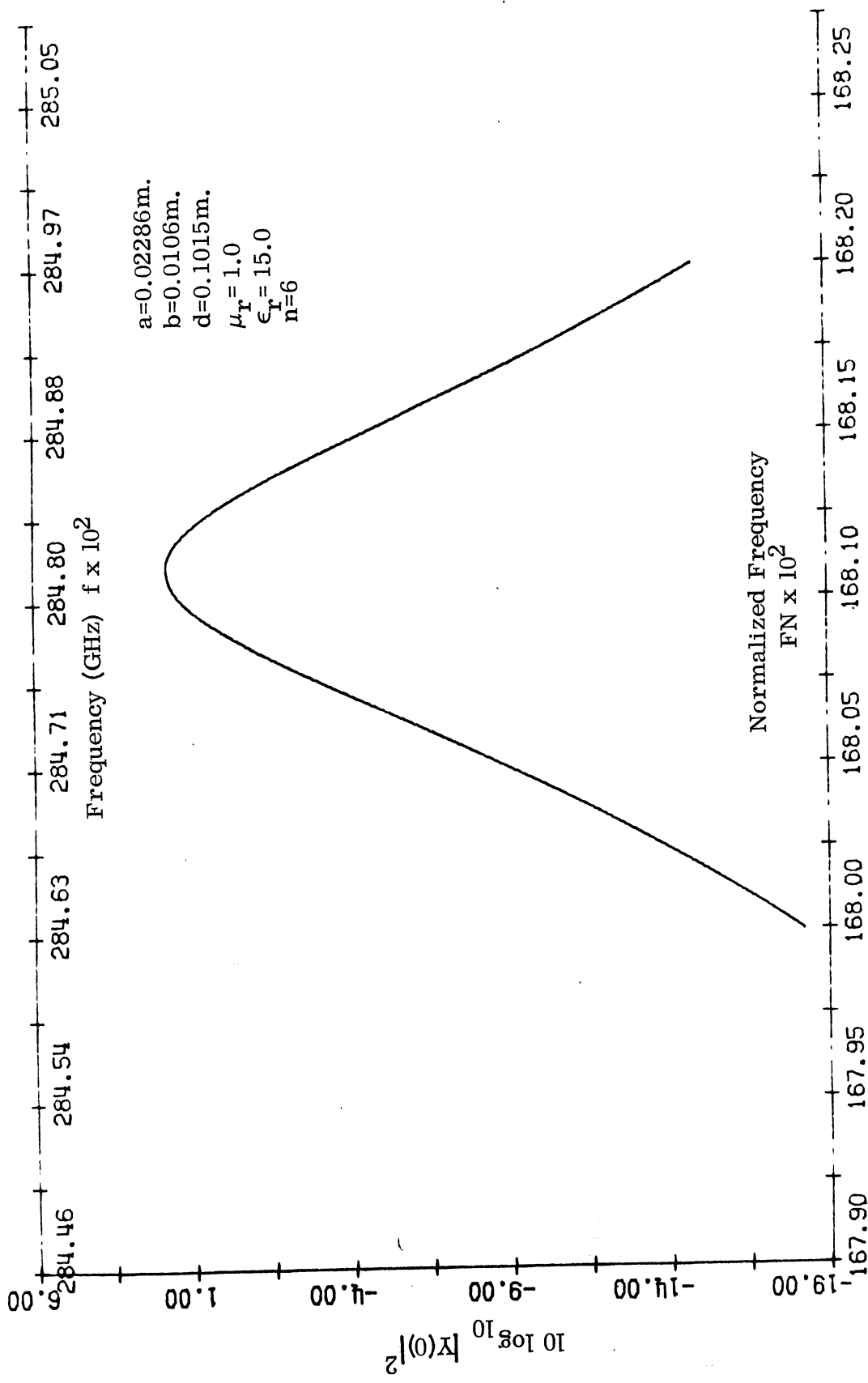


FIG. 3-16(d): AN EXPANDED DIGITAL PLOT FOR RESONANCE PEAK.

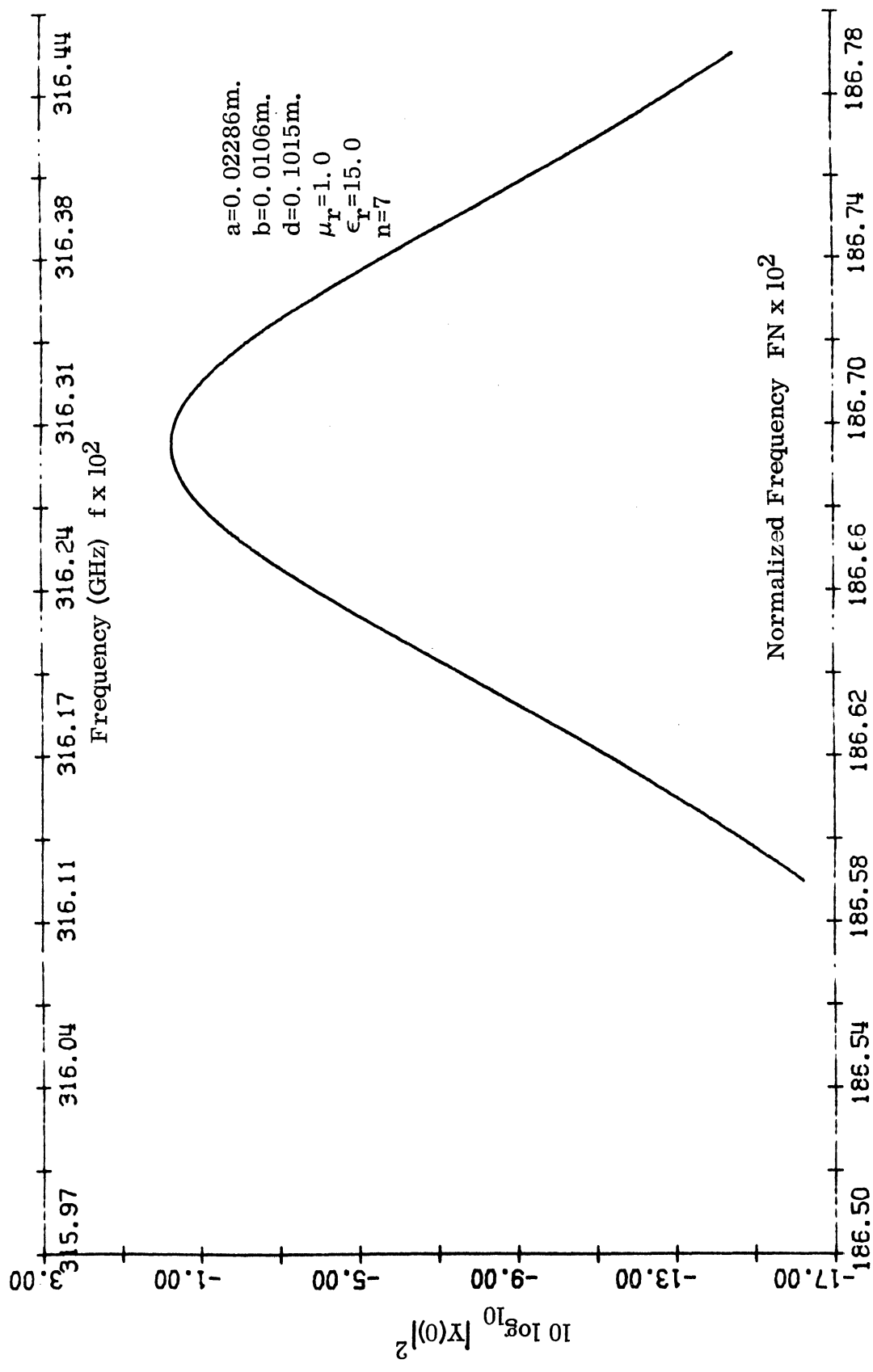


FIG. 3-16(e): AN EXPANDED DIGITAL PLOT FOR RESONANCE PEAK.

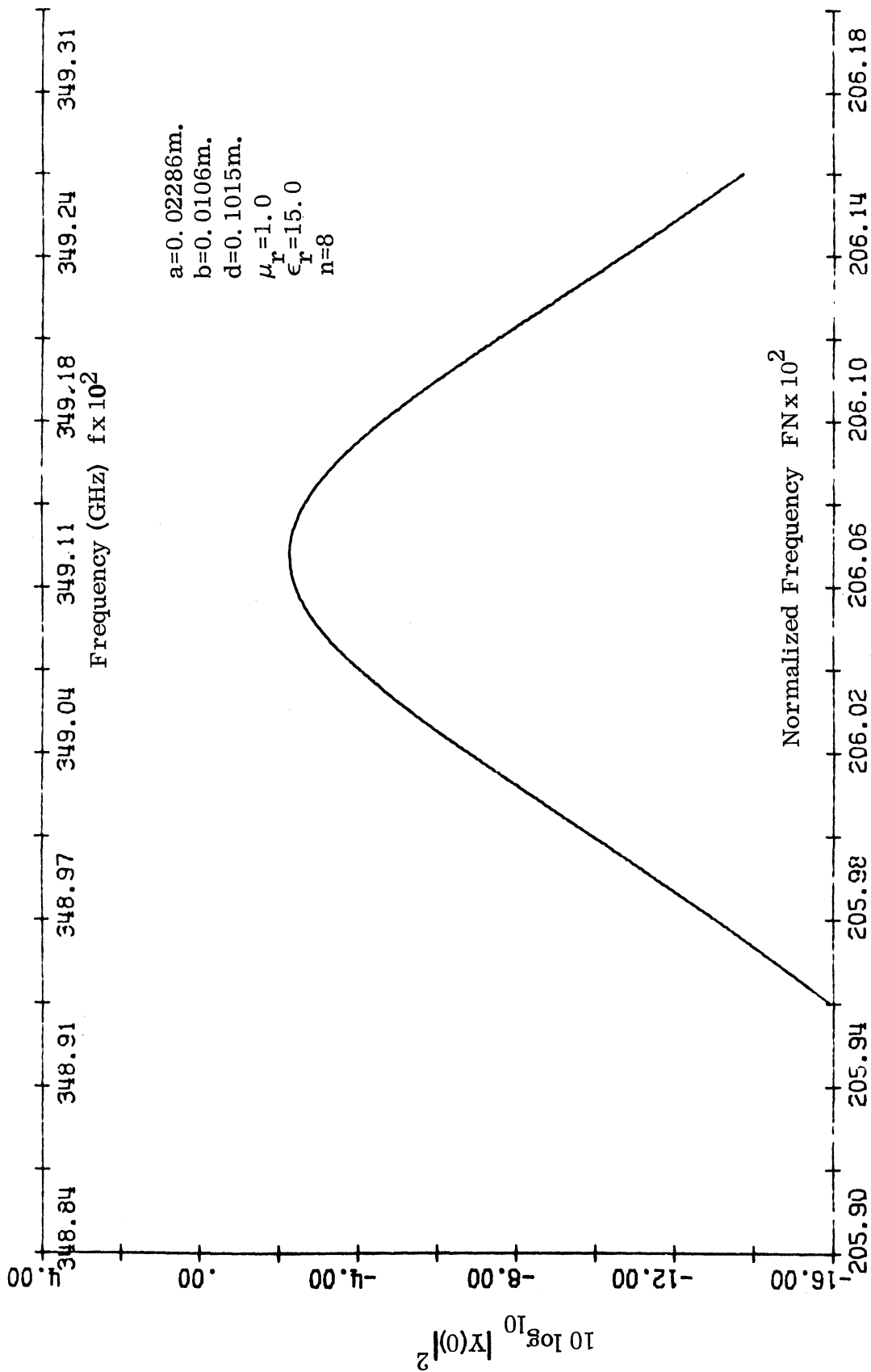


FIG. 3-16(f): AN EXPANDED DIGITAL PLOT FOR RESONANCE PEAK.

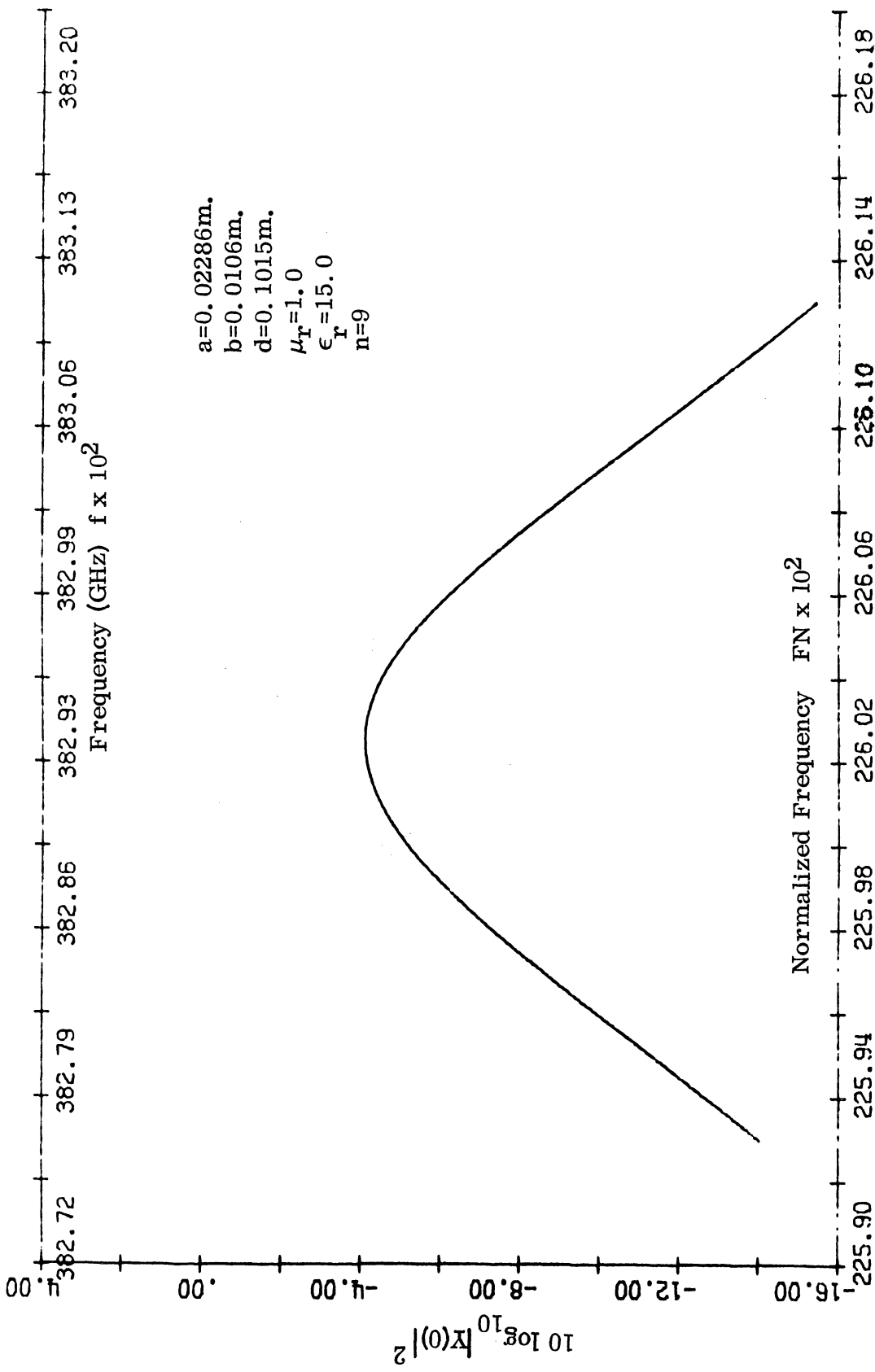


FIG. 3-16(g): AN EXPANDED DIGITAL PLOT FOR RESONANCE PEAK.

Example No. 5.

For $a = 5''$, $b = 2''$, $l = 3/2''$, $\mu_r = 6.63$ and $\epsilon_r = 12.6$,

$$f_c = 129.2246 \text{ MHz.}$$

Using Eq. (3. 11) the resonance frequencies are:

$n = 1$	$f_1 = 449.715114$	MHz
$n = 2$	$f_2 = 871.135869$	MHz
$n = 3$	$f_3 = 1.298692$	GHz

3.6 Evaluation of Coupling

From Sections 3.3 and 3.5 the coupling of two loaded guides opening into a perfectly conducting infinite ground plane can be obtained. From Eq. (2.99) in Chapter II which is:

$$|Y(0)|^2 = \frac{1}{|Z_{lg}|^2} \left[\frac{\cosh^2 \alpha_{lg}^l \cos^2 \beta_{lg}^l + \sinh^2 \alpha_{lg}^l \sin^2 \beta_{lg}^l}{\sinh^2 \alpha_{lg}^l \cos^2 \beta_{lg}^l + \cosh^2 \alpha_{lg}^l \sin^2 \beta_{lg}^l} \right],$$

the power received is proportional to this factor. Therefore by multiplication of this equation by an appropriate factor and adding to the coupling from aperture to aperture in dB the total coupling can be obtained. Also the resonance frequency and the theoretical bandwidth can be obtained. The effect on the resonance frequencies due to the material perturbation and metal probe perturbation might be taken into consideration as in Example No. 2

Chapter IV

EXPERIMENTAL INVESTIGATION

4.1 General Discussion

All the experimental work was performed in an anechoic chamber. The chamber dimensions were 50' x 30' x 15' , with an aluminum ground plane, 12' square by 1/8" thick mounted in the center of one of the 30' walls (see Fig. 4-1). The nine individual sections of the ground plane were joined by 2" wide aluminum tape to form an electrically continuous surface at microwave frequencies. The center section has a removable 2'x3' section for the test antennas. Within the 2'x3' part there was a removable circular disk of 14" diameter. Inside the disk there was a rectangular hole of dimensions 10" x 3" in which the slots could be mounted. Also, there was an additional fixture to make the X-band slots to fit in the mounting as shown in Fig. 4-2.

The ceiling and the floor were covered with B. F. Goodrich HV-4, vinyl-covered, four-inch hairflex microwave absorber. The rear 30' walls and the 50' walls are covered with VHP-18, pyramidal absorber. The center of the rear wall was covered with VHP-26 absorber. The chamber had been lined with interlocking aluminum foil sheets to provide a known uniform termination for the absorbing material and to shield the room from external signals.

The frequency range of the chamber is 500 MHz - 50 GHz and has a nominal reflection coefficient, for normal incidence, of -70 dB for X-band and higher frequencies, tapering off exponentially to -40 dB for lower frequencies.

The accuracy of coupling measurements was approximately within the range of ± 1 dB (i. e. , for the swept frequency use). For the case where the swept frequency generator was not used, both transmitter and receiver were tuned by means of a double-stub tuner, and the accuracy was a little less than the former (i. e. , within ± 2 dB).

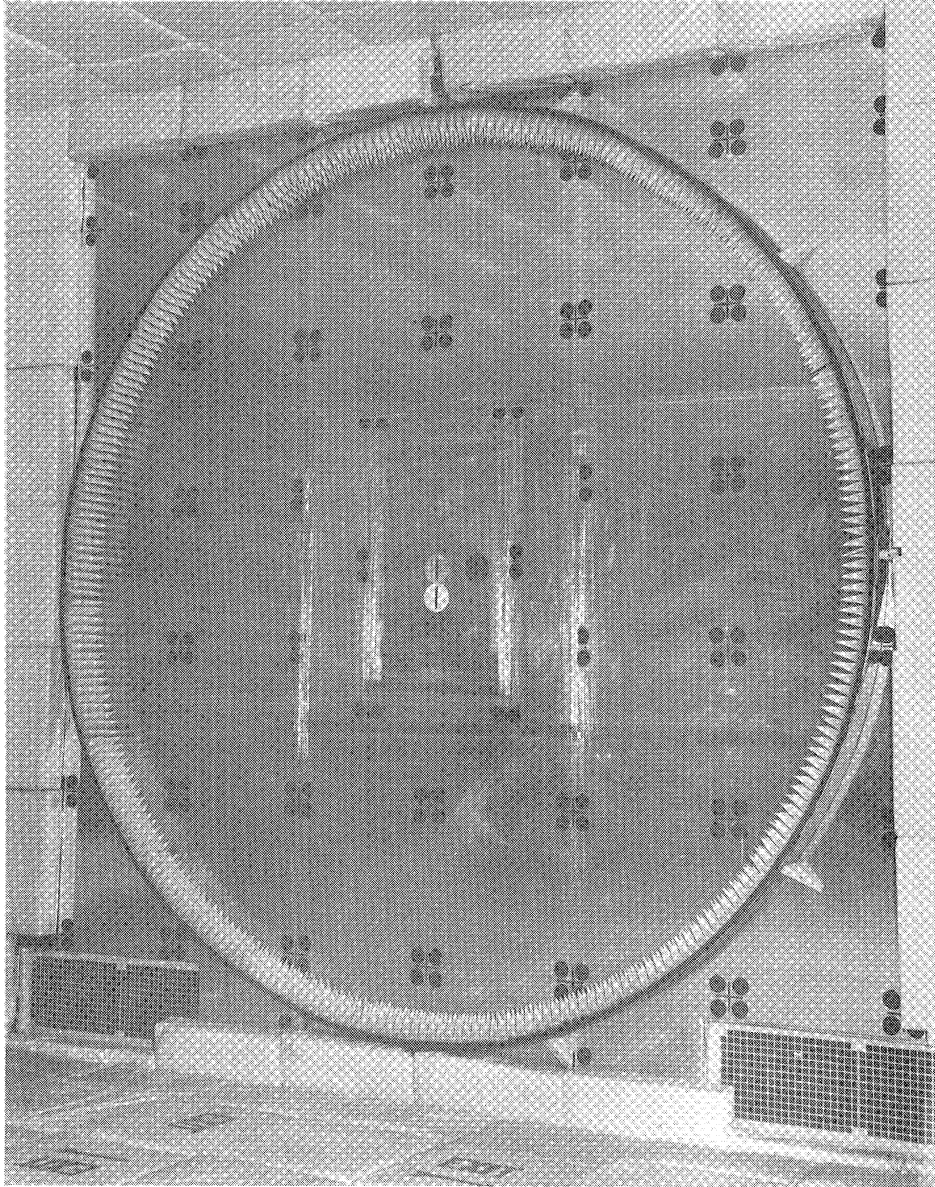


FIG. 4-1 : ANECHOIC CHAMBER GROUND PLANE.

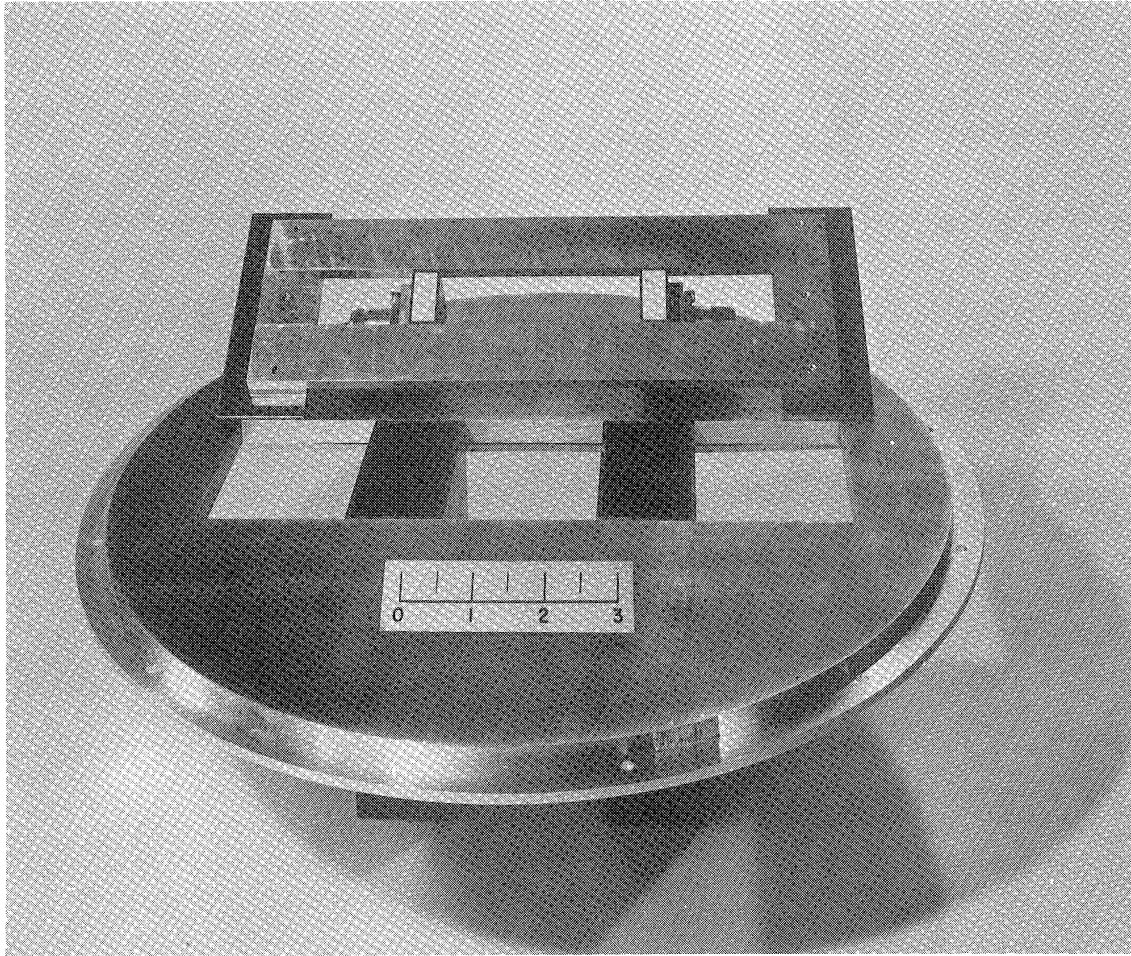


FIG. 4-2(a): TEST ANTENNA MOUNT.
(Comparison scale is in inches.)

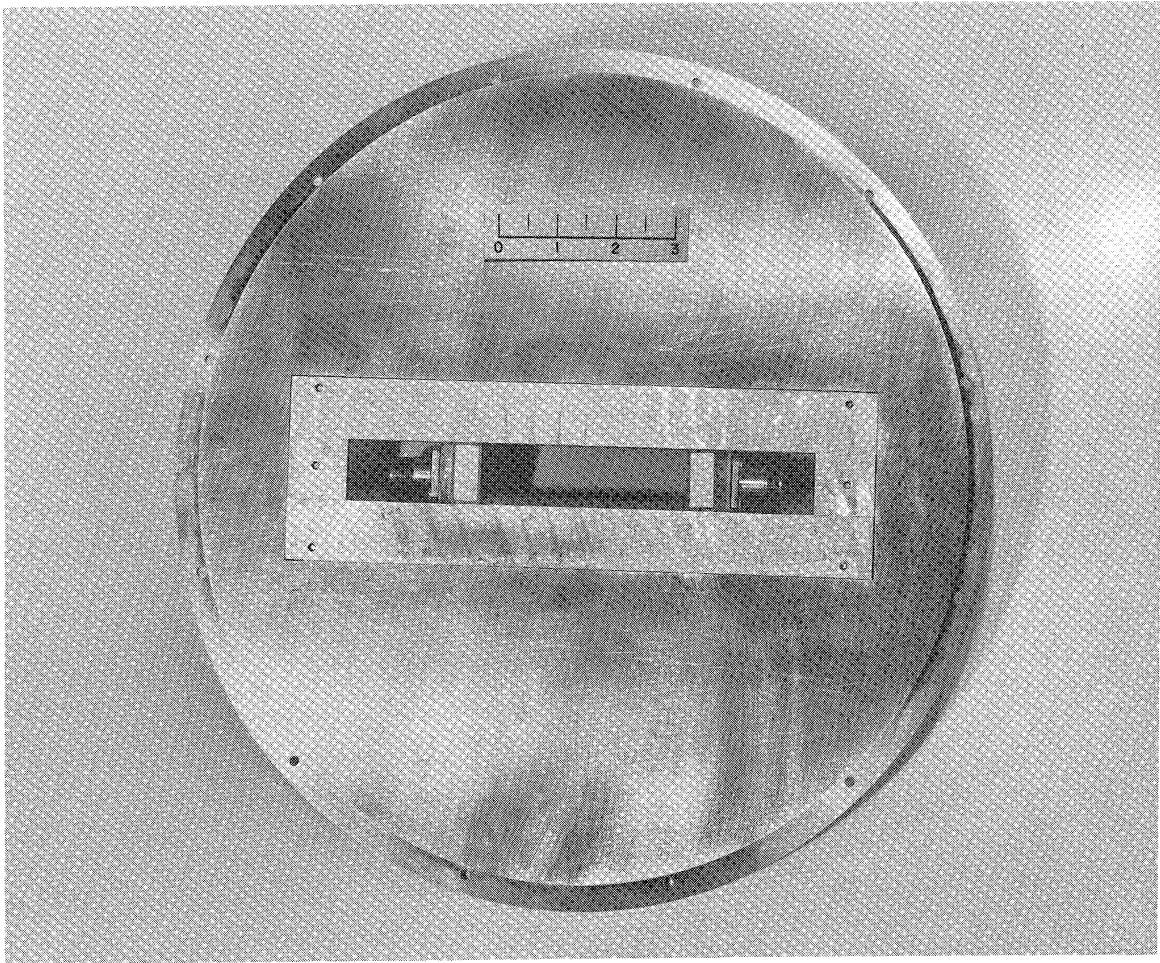


FIG. 4-2(b): ARRANGEMENTS FOR LOADED X-BAND WAVEGUIDES.
(Comparison scale is in inches.)

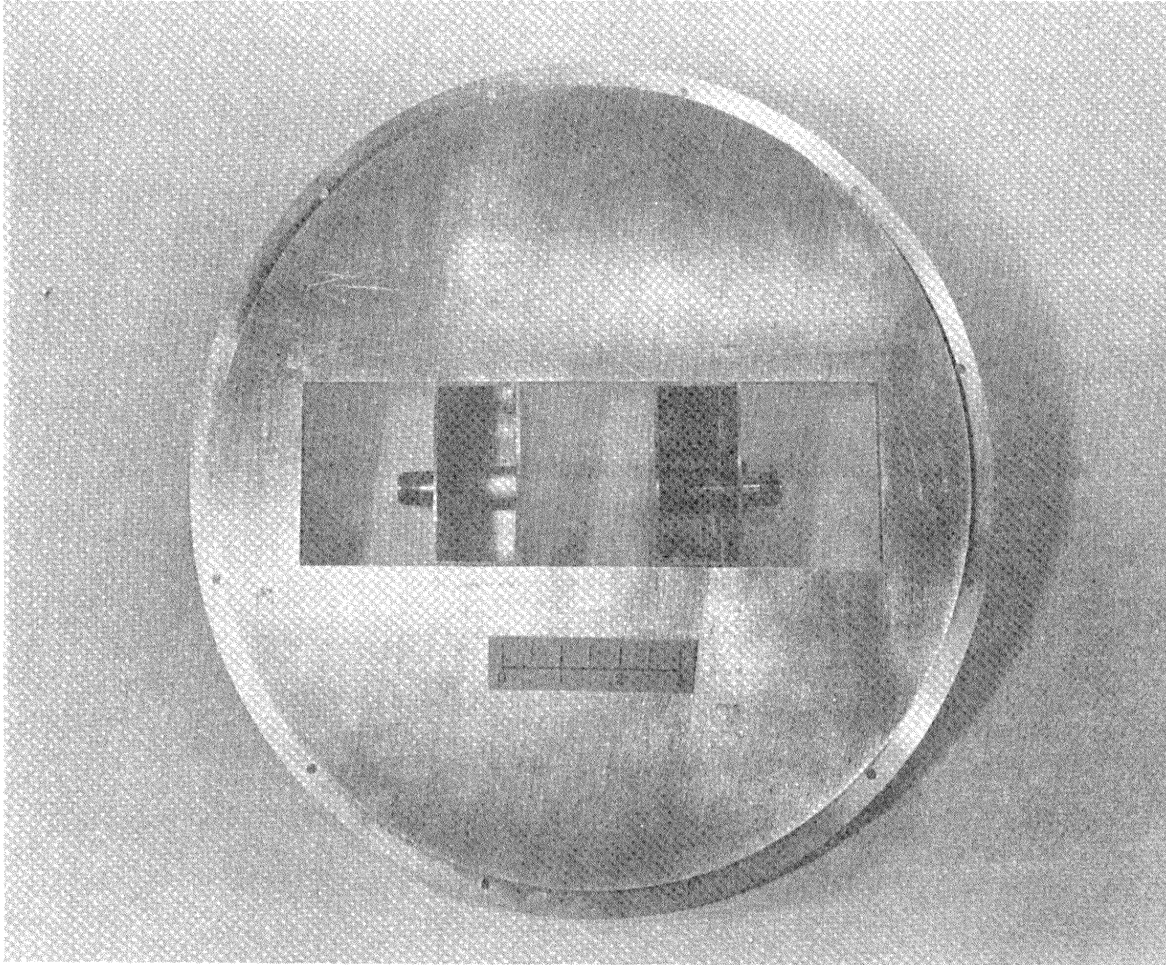


FIG. 4-2(c): ARRANGEMENTS FOR STANDARD S-BAND WAVEGUIDES.
(Comparison scale is in inches.)

4.2 Coupling Measurements

4.2.1 Swept Frequency

Most of the experiments in this section were made in the S-band frequency range, or, more specifically, the measurements were taken between 2.0 and 4.0 GHz. Also some experiments were carried out for swept frequencies in the X-band range of 8.2 to 12.4 GHz. For the X-band measurements, it was found that in feeding a loaded guide with X-band signal there is clear indication that there is more than the dominant mode propagating. This was observed from the shape of the radiation patterns. This was to be expected since the X-band range of frequencies is far above the cutoff frequency of the loaded guide.

At an early stage of the experimental work a dielectric powder was used to load the X-band waveguide. It was then realized that it was very sensitive to any movements. By moving the transmitting antenna from one position to another, it seemed that the granules of the dielectric filling moved around. For this reason it was difficult to get a repeatability in the graphs. A substitute to avoid this problem was a solid dielectric material which is machined to fit the size of the X-band waveguide. Emerson and Cuming's Stycast High K solid dielectric was used. The manufacturer gives a loss tangent for this material of 0.0008. Different values of the dielectric constant for the material were used such as $K' = 5, 7, 11$ and 15 . The material was machined to fit the cavity and also a hole was drilled for the probe of the feed as shown in Fig. 4-3(a). Two different waveguide lengths were used, $d=0.031\text{m}$ and $d=0.1015\text{m}$ as in Fig. 4-3(b) to demonstrate the effect of the cavity length on the resonant frequencies.

Also some measurements were performed for the cases of standard waveguides at Ku-, X- and S-band frequency ranges. It is interesting to note that the coupling obtained experimentally for these cases is within a fraction of one dB from the corresponding coupling obtained from the analytical formulations;

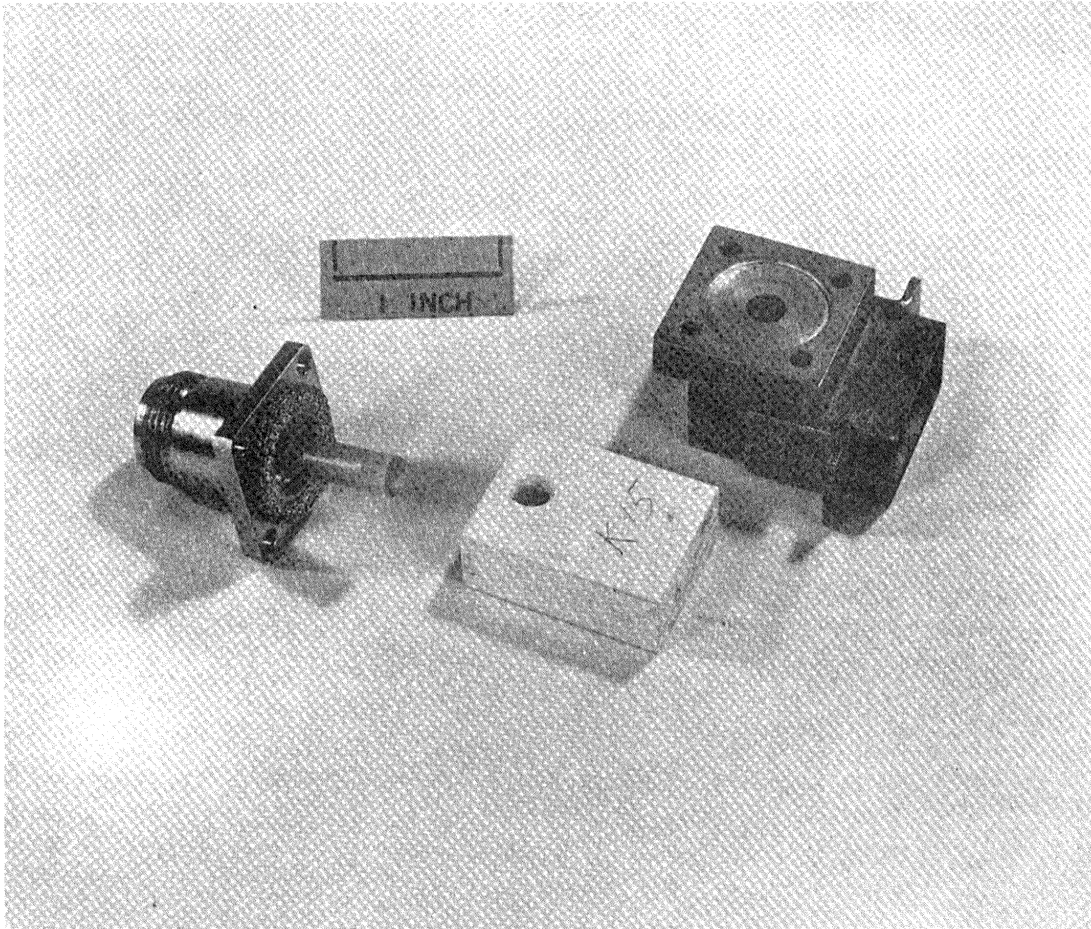


FIG. 4-3(a): THE RESONANCE CAVITY AND ITS DIELECTRIC FILLING PLUS THE COAXIAL TO WAVEGUIDE FEED.

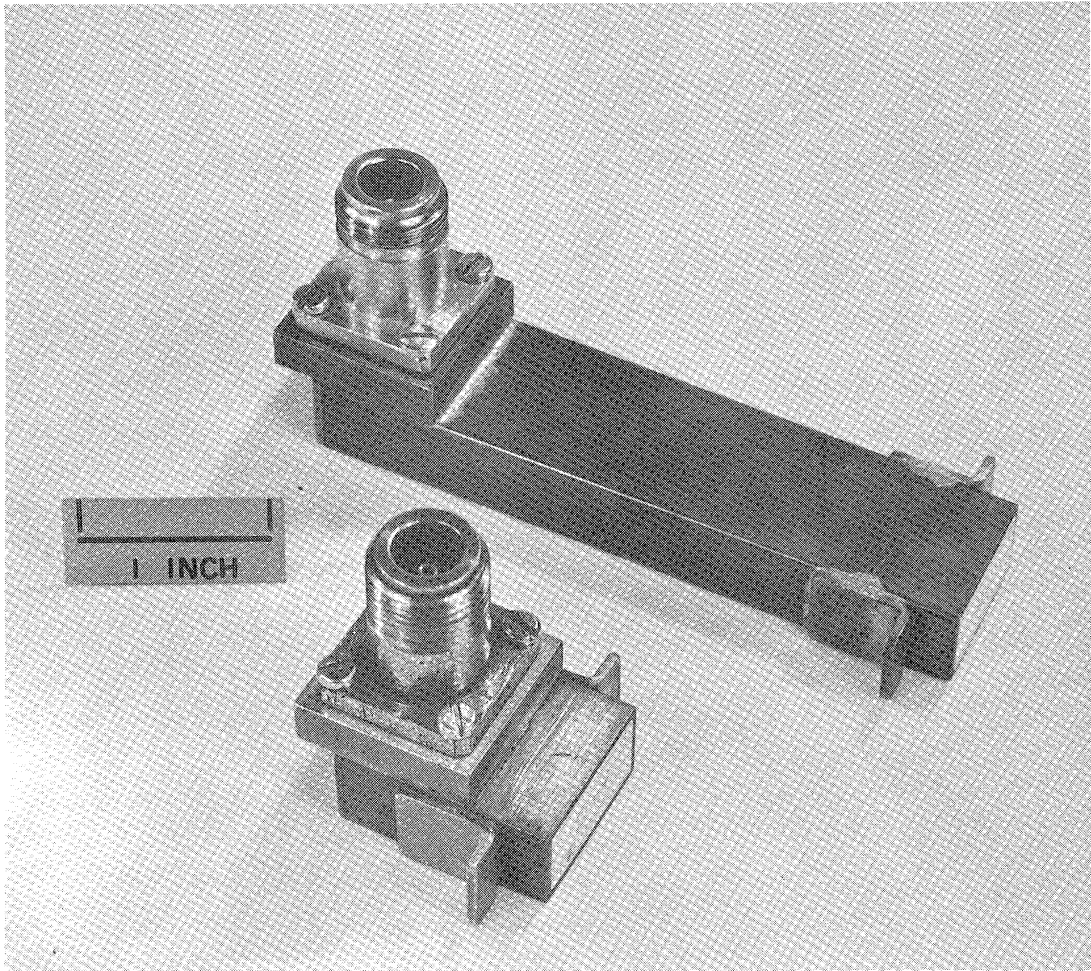


FIG.4-3(b): THE 0.031 m. AND THE 0.1015 m. DIELECTRIC LOADED CAVITIES.

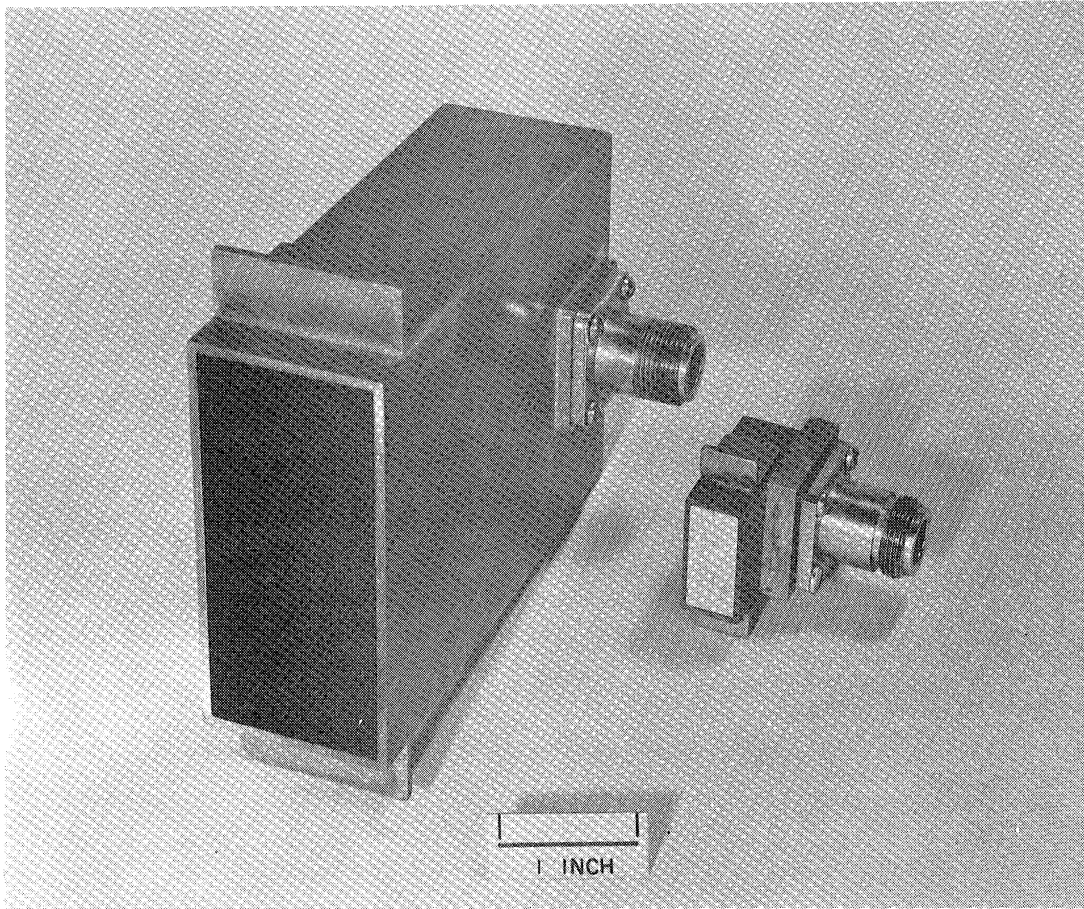


FIG. 4-3(c) COMPARISON BETWEEN LOADED AND UNLOADED CAVITY.

compare Figs. (4-4, 3-7), (4-5a, 3-8) and (4-5a, 3-9) .

Figure 4-4 is the coupling versus swept frequency between 2.00 GHz and 4.00 GHz for a pair of S-band waveguides spaced 0.075m apart, center-to-center. The upper curve of the graph is a measure of the power level from the transmitter obtained by connecting the two coaxial lines; in a way it is a measure of power level. The lower part is the coupling level with the two apertures flush mounted 0.075m apart and in the ground plane of the anechoic chamber. Notice that the coupling follows approximately the 6 dB/octave trend as frequency is varied. Also when the coupling was taken versus spacing for a fixed frequency it showed 6dB/octave of distance confirming the analytical results.

Figure 4-6 shows the coupling versus frequency for an X-band waveguide cavity of length 0.031m loaded with Stycast High K solid dielectric material machined to fit. In this particular case the material dielectric constant was 11.0. The level curve represents the level of the transmitted power through the coaxial lines from the transmitter to the receiver, as indicated in the experimental set-up shown in Fig. 4-14 , with a 25 dB attenuator added to the circuit. Note that the coupling resonant frequencies are approximately the same as those predicted in the analytical work. The small error may be due to the measurements of the guide length which might not be very exact. Also, errors in the measurement equipment may exist. It is believed that the split at the top of the resonance is due to the fact that the transmitter and receiver cavities do not have exactly the same length. Therefore, these two peaks represent the resonant frequency for each individual cavity. For that reason plus the occurrence of multiple reflections inside the cavities, the 3 dB or half-power bandwidth is wider than was expected theoretically.

Figures 4-7 and 4-8 are the coupling and gain respectively versus swept frequency for a cavity of loaded X-band waveguide with dielectric constant of 15.0 and the dimensions of the cavity 0.02286 x 0.01016 x 0.1015 meters. The gain curve was taken with the set-up for far-field pattern measurements as shown in Fig. 4-9. The standard antenna which was used on the boom was

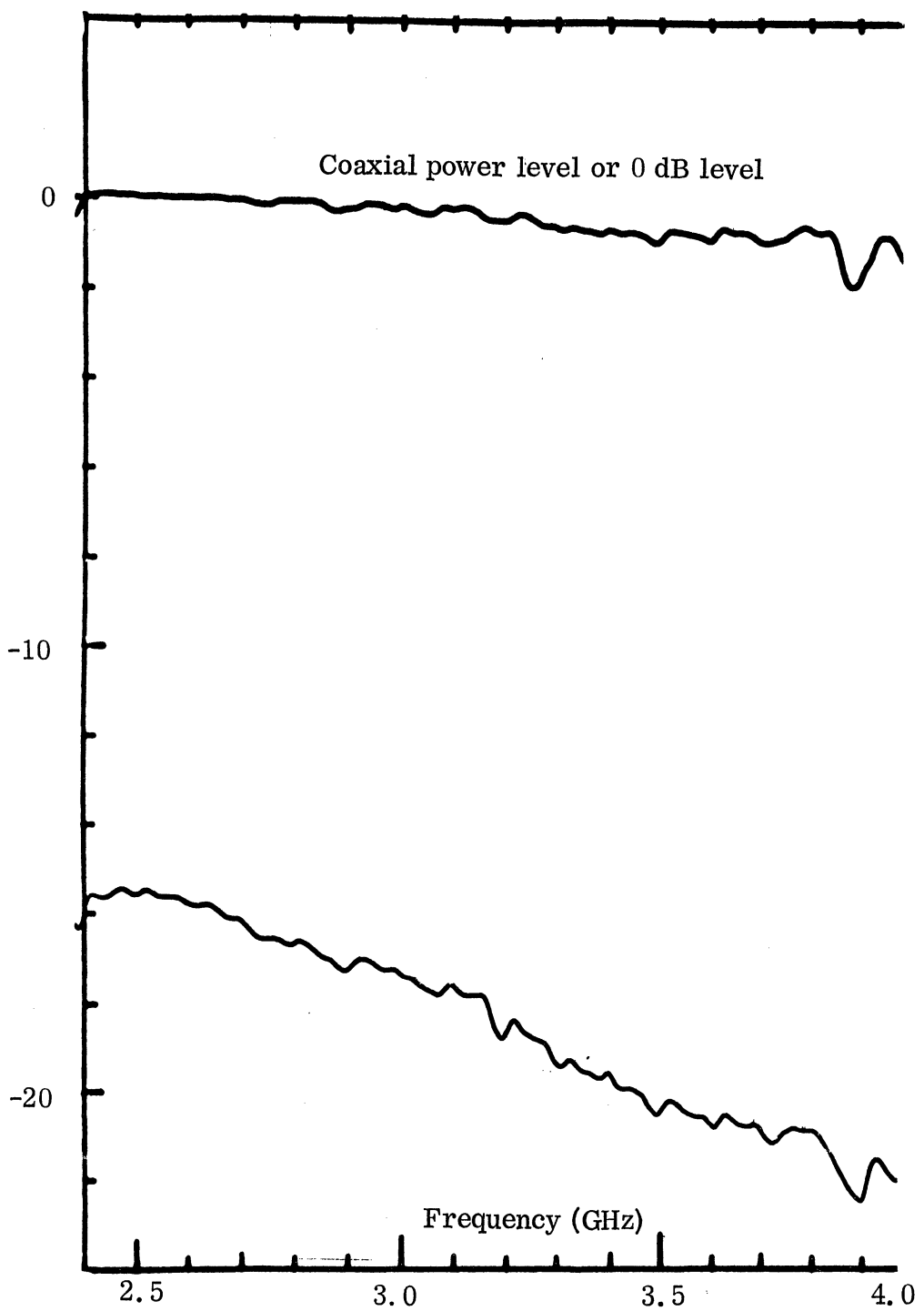
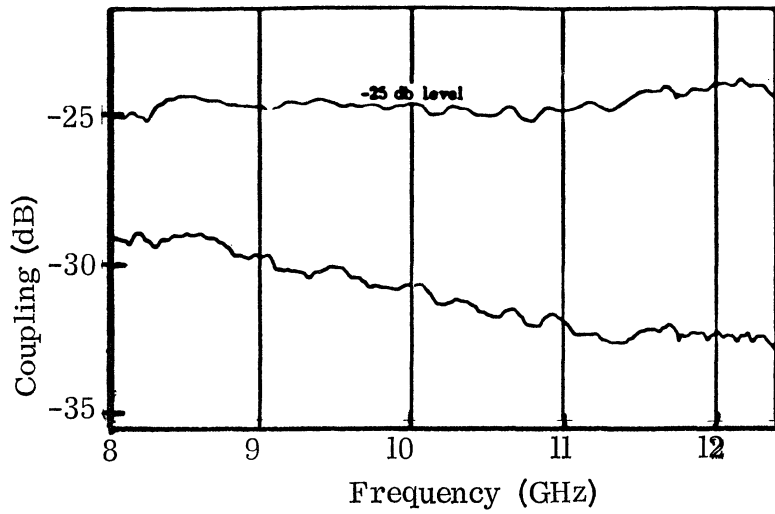
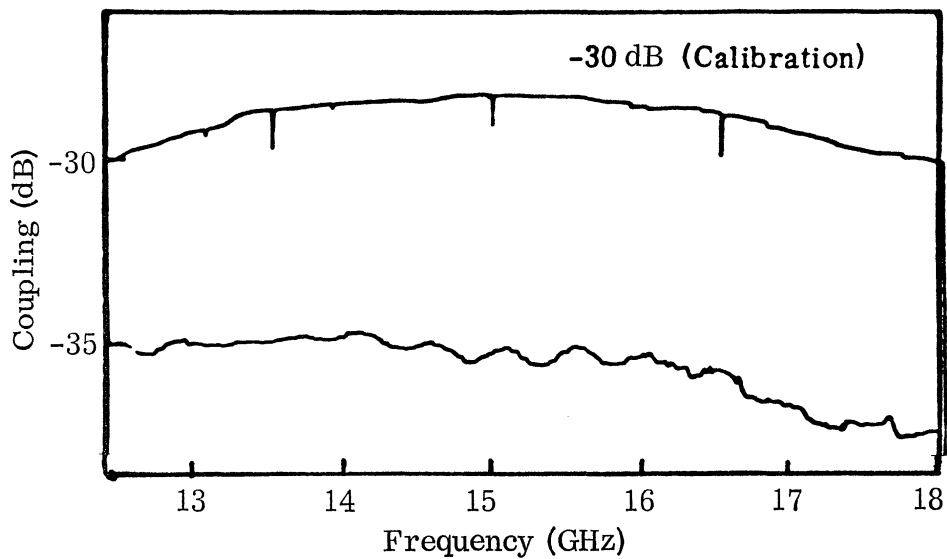


FIG. 4-4: STANDARD S-BAND WAVEGUIDE COUPLING VS FREQUENCY. $x_1=0.075m$.



(a)



(b)

FIG. 4-5: E-PLANE COUPLING VS FREQUENCY FOR TWO SLOTS SPACED 11.4 CM.

(a) Standard X-band Rectangular Waveguide.

(b) Standard Ku-band Rectangular Waveguide.

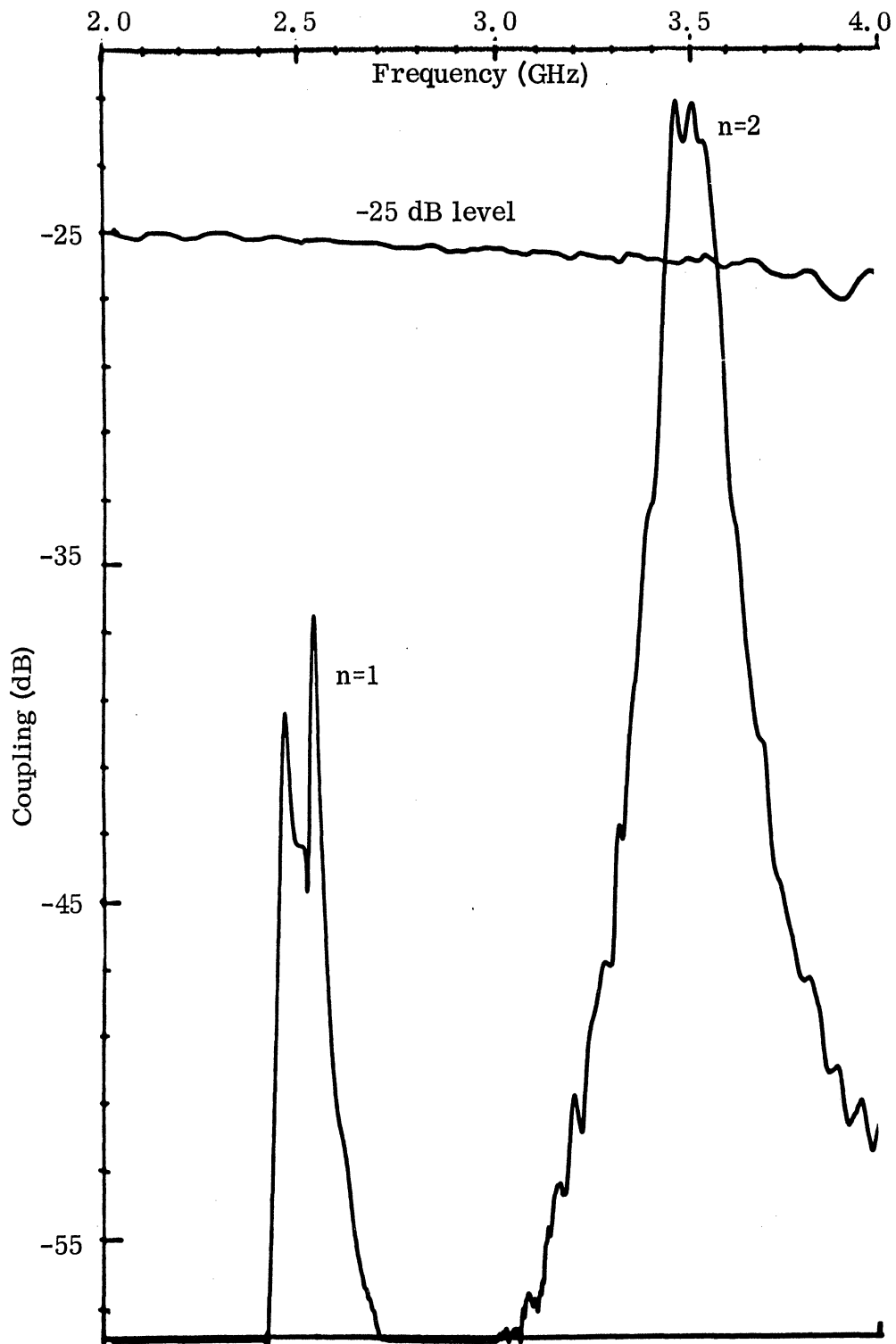


FIG. 4-6: COUPLING VS FREQUENCY FOR LOADED X-BAND WAVEGUIDES, $\mu_r=1.0$, $\epsilon_r=11.$, $d=0.031m.$, $x_1=0.03m.$, $a=0.02286m.$, $b=0.01016m.$

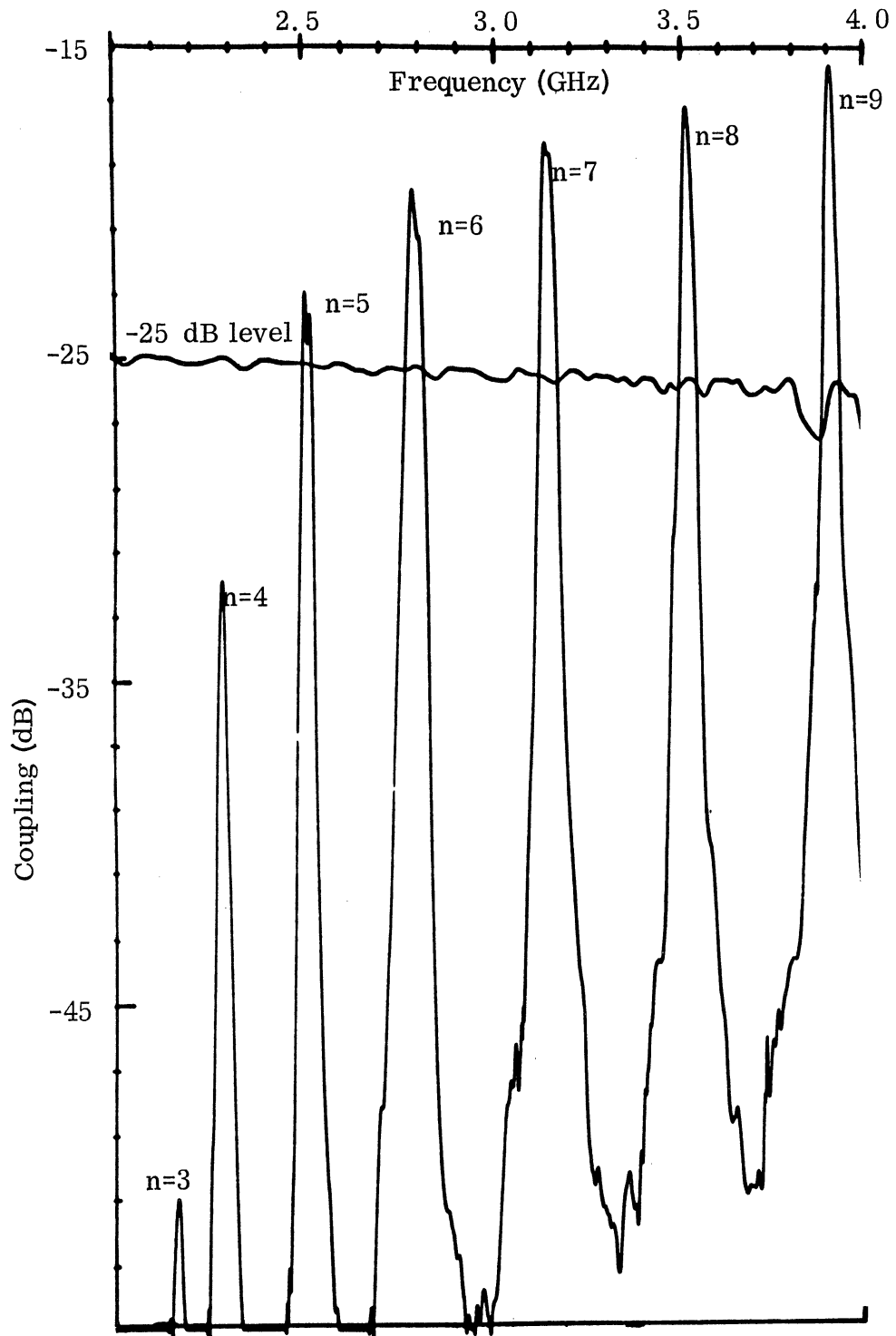


FIG 4-7: COUPLING VS FREQUENCY FOR LOADED X-BAND WAVEGUIDES, $\mu_r=1.0$, $\epsilon_r=15.0$, $d=0.1015m.$, $x_1=0.013m.$, $a=0.02286m.$, $b=0.01016m.$

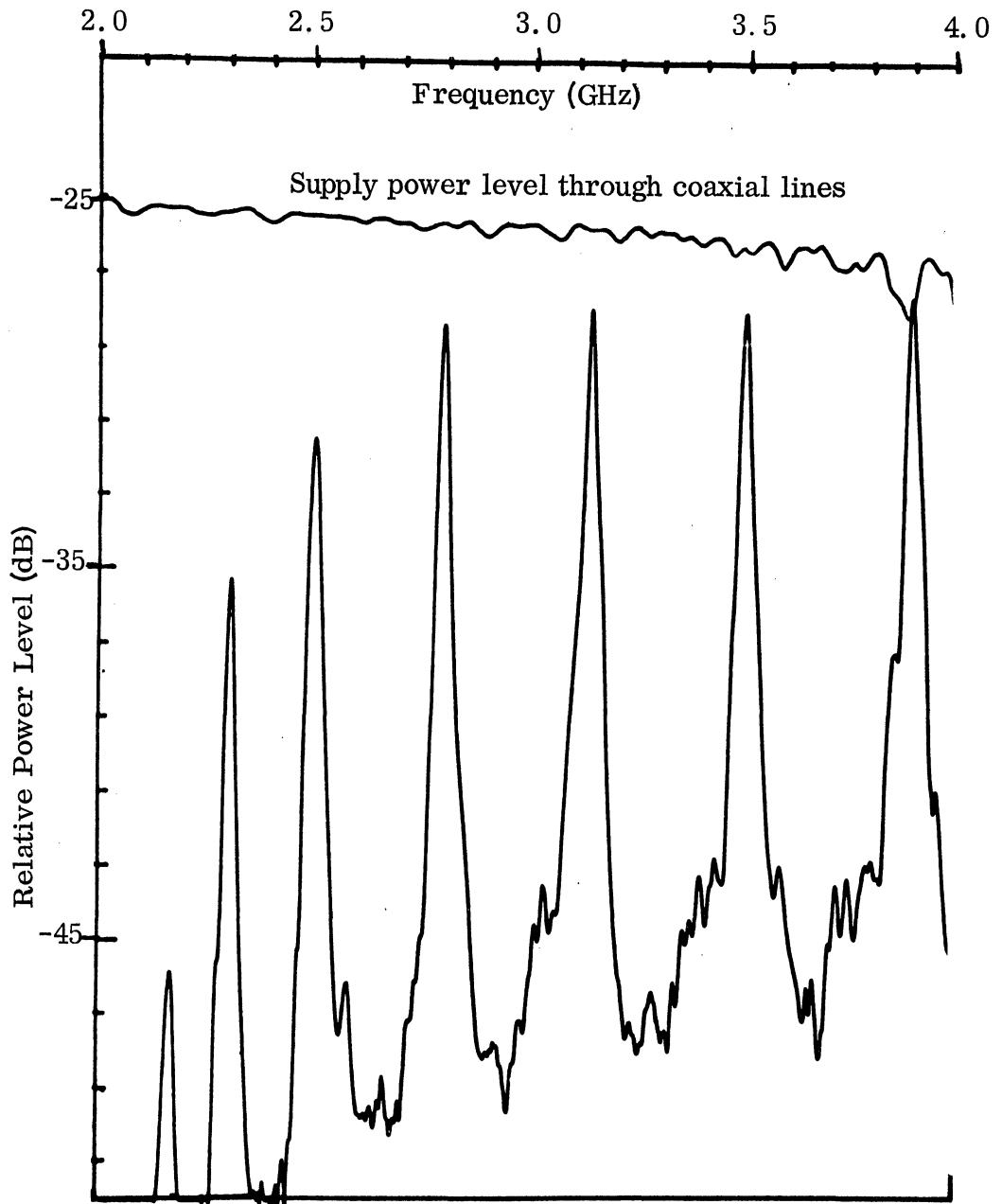


FIG. 4-8: GAIN VS FREQUENCY OF DIELECTRIC LOADED CAVITY,
 $\mu_r=1.0$, $\epsilon_r=15.0$, $d=0.1015$ m.

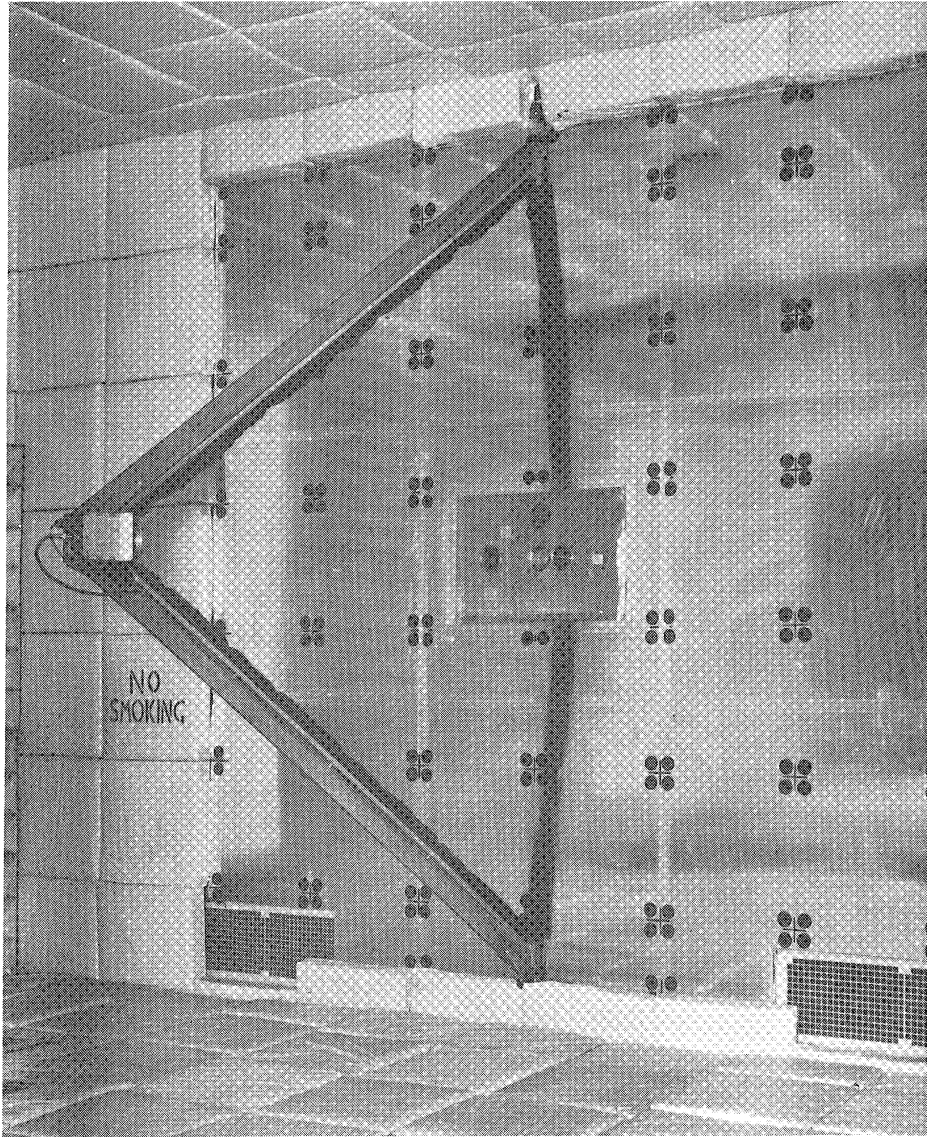


FIG. 4-9: ANECHOIC CHAMBER SET-UP FOR FAR-FIELD PATTERN MEASUREMENTS.

an AEL No. ARN101A (1.0-11.0 GHz) log-periodic type. The boom was fixed in its position and the frequency was swept between 2.00 - 4.00 GHz. Note that the coupling resonances approximately coincide with those resonances of the gain of the antenna. Also, the dynamic variation of the coupling without matching is about 35 dB and the peaks are lower as the frequency approaches the cut-off frequency which is due to the mismatch at the feed.

Similarly the coupling and gain graphs versus swept frequency were obtained for dielectric constants of 11.0 and 7.0 which are shown in Figs. 4-10 - 4-13.

4.2.2 Coupling Versus Frequency with Point by Point Tuning

There was no simple way to match the input port of the transmitting antenna and output port of the receiving antenna with swept frequency. A circuit had been constructed to take measurements while the frequency is varied point by point; a double stub tuner was used at both the transmitting and receiving ends as shown in Fig. 4-14. For each frequency the stubs were adjusted for maximum power received.

The experiments in this part were also conducted on the 0.1015m. and 0.031m. cavities. Also different values of dielectric constants were used as in the swept frequency. In Figs. 4-15 - 4-17 the zero dB power level represents the normalized coaxial power level. The line representing zero power level is not shown. It represents the transmitted power minus the power lost in the circuit from the transmitter to the receiver when the coaxial lines are connected as shown in Figure 4-14. The upper curve is the power level as in the coaxial case but it also includes the antennas with the two apertures connected together thus forming a cavity. The surface on the aperture was machined to be smooth enough such that the mating surfaces would not act as a discontinuity. Also the mating periphery was covered with foil tape such as to prevent power leakage and to form an electrically continuous surface between the guides. If this is done perfectly then the arrangement is like a cavity filled with dielectric material and there is an input at one end and output at the other end.

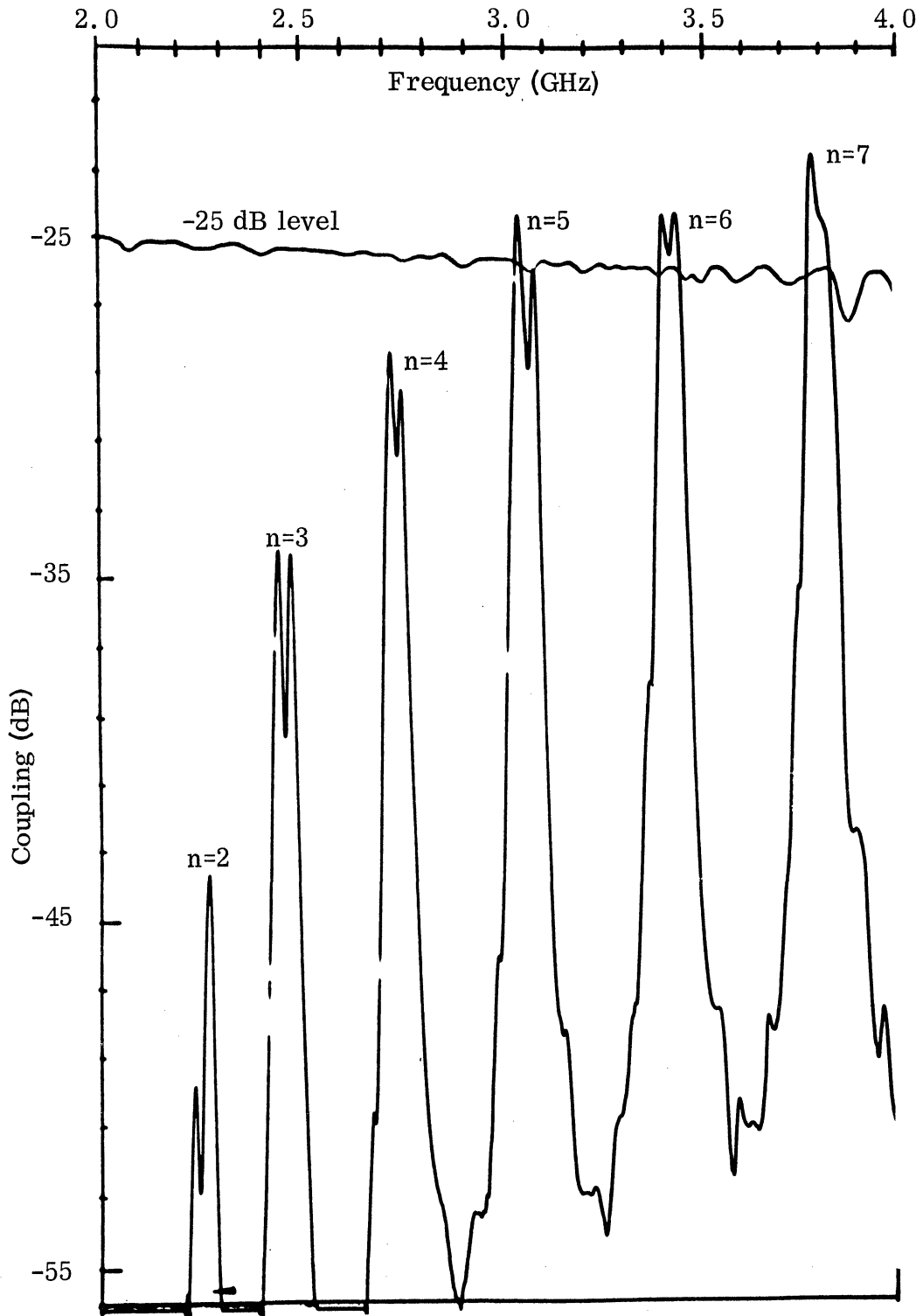


FIG. 4-10: COUPLING VS FREQUENCY FOR LOADED CAVITY,
 $\mu_r=1.0$, $\epsilon_r=11.0$, $d=0.1015\text{m.}$, $x_1=0.013\text{m.}$, $a=0.02286\text{m.}$,
 $b=0.01016\text{m.}$

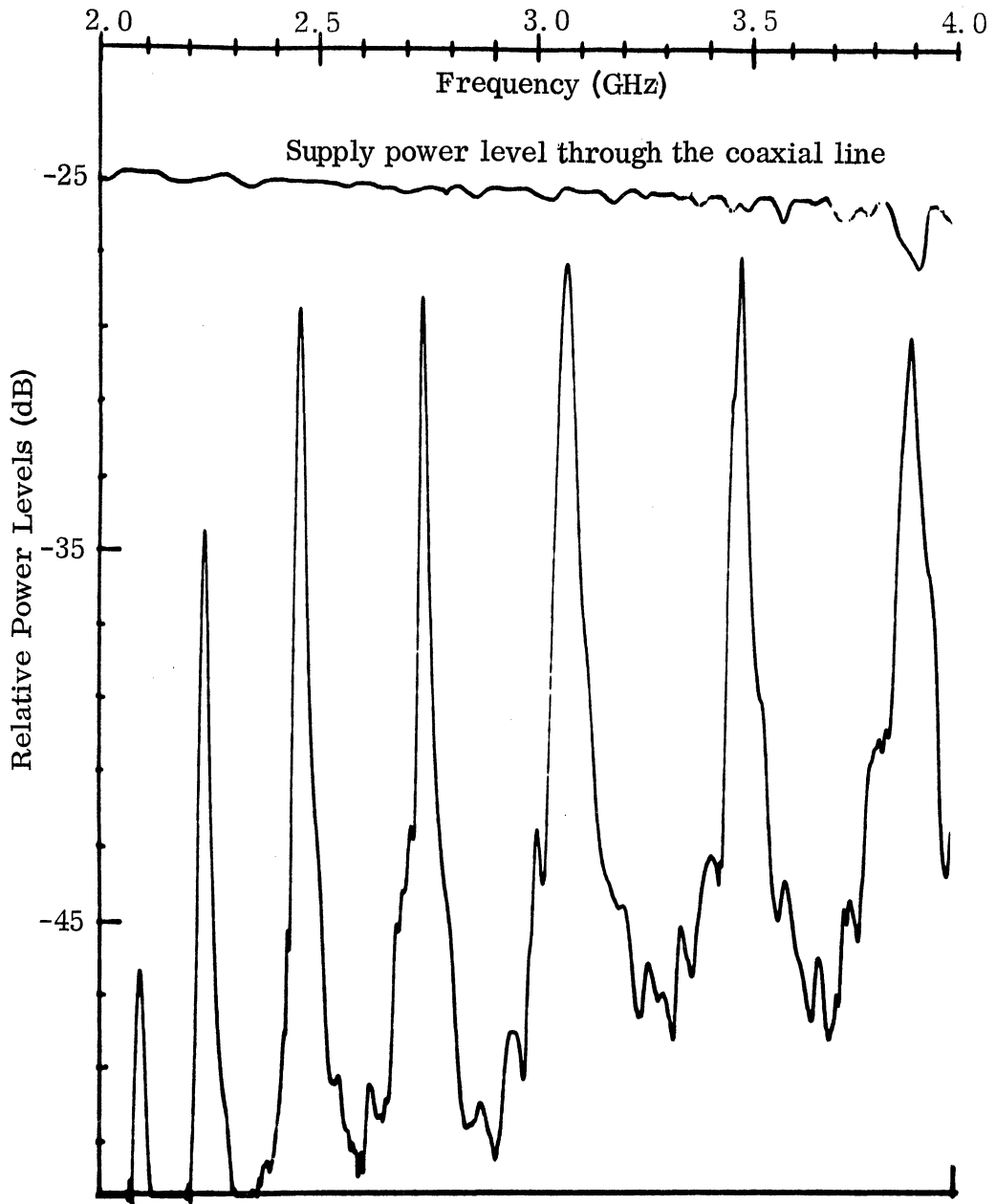


FIG. 4-11: GAIN VS FREQUENCY FOR LOADED CAVITY,
 $\mu_r=1.0$, $\epsilon_r=11.0$, $d=0.1015\text{m}$.

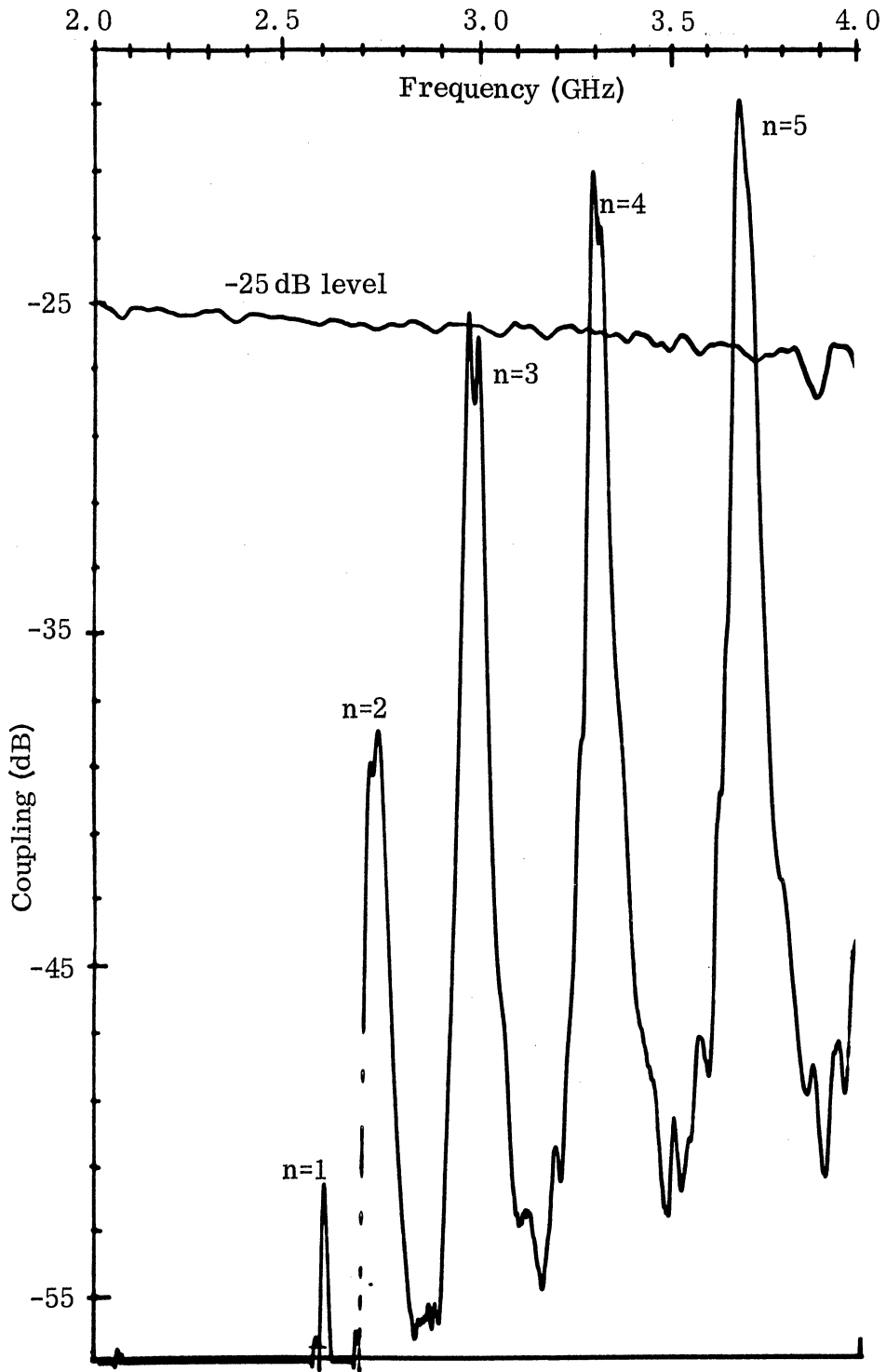


FIG. 4-12: COUPLING VS FREQUENCY FOR LOADED WAVEGUIDES,
 $\mu_r=1.0$, $\epsilon_r=7.0$, $d=0.1015\text{m.}$, $x_1=0.013\text{m.}$

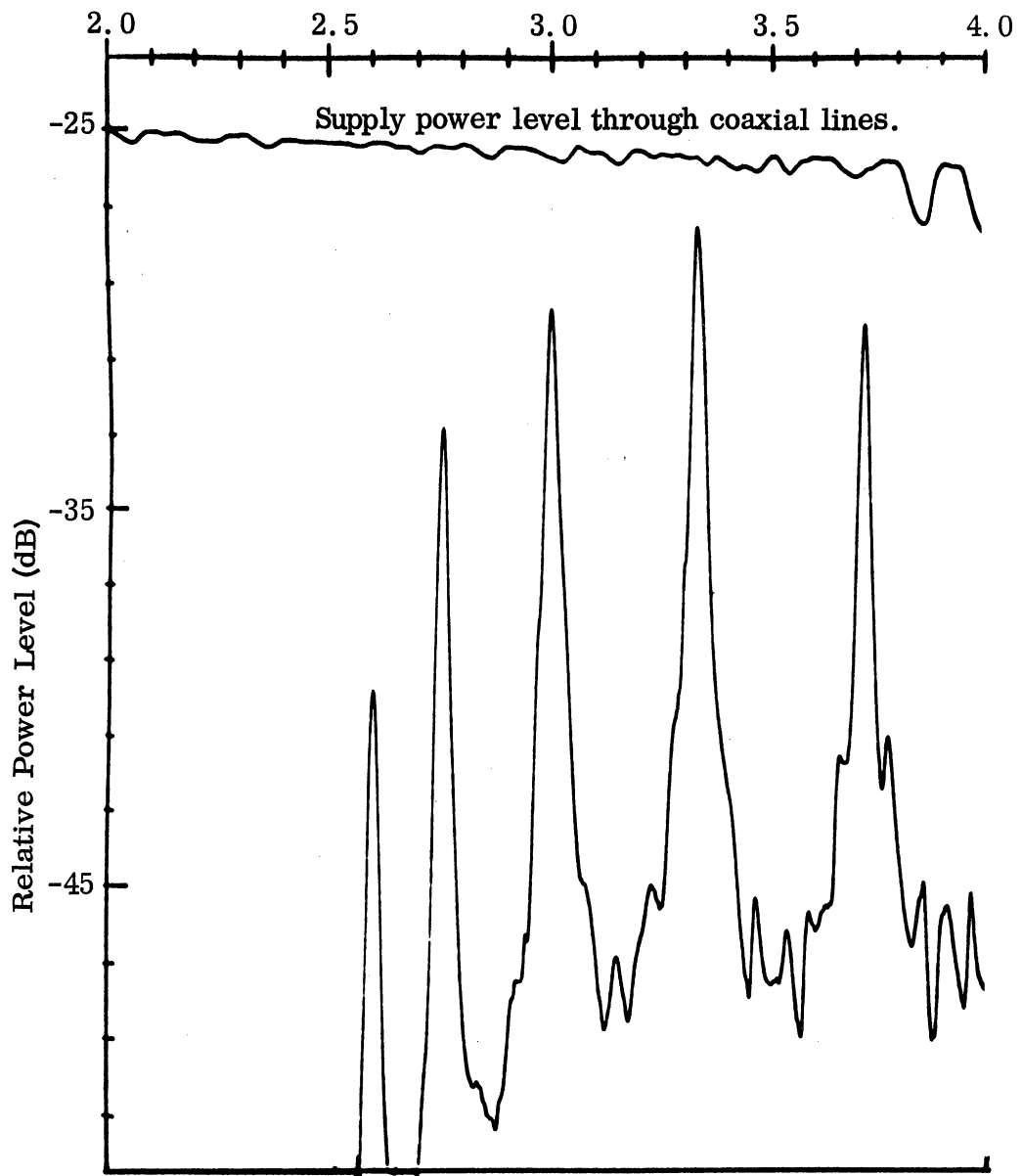


FIG. 4-13: GAIN VS FREQUENCY FOR LOADED CAVITY,
 $\mu_r=1.0$, $\epsilon_r=7.0$ and $d=0.1015\text{m}$.

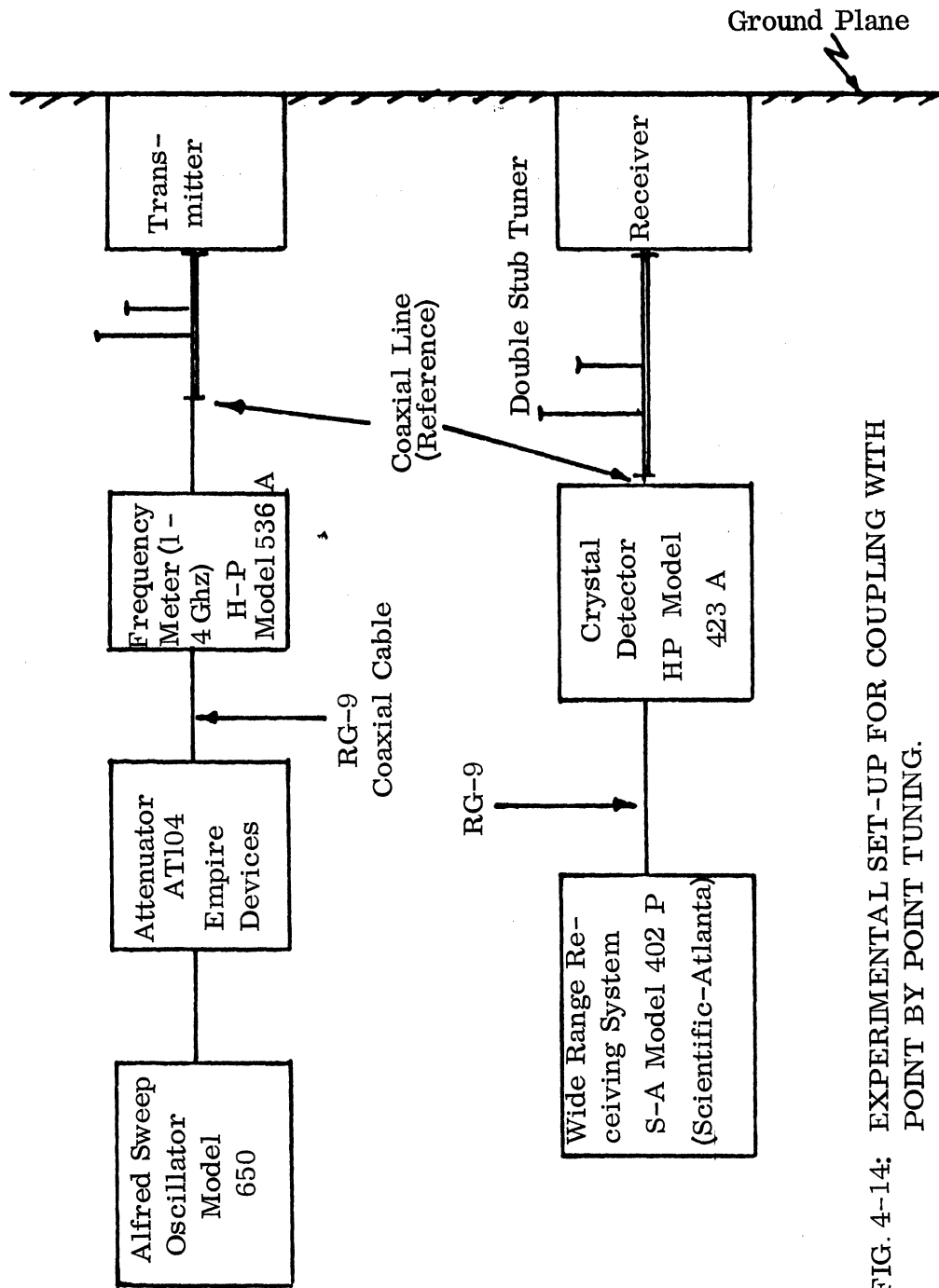


FIG. 4-14: EXPERIMENTAL SET-UP FOR COUPLING WITH POINT BY POINT TUNING.

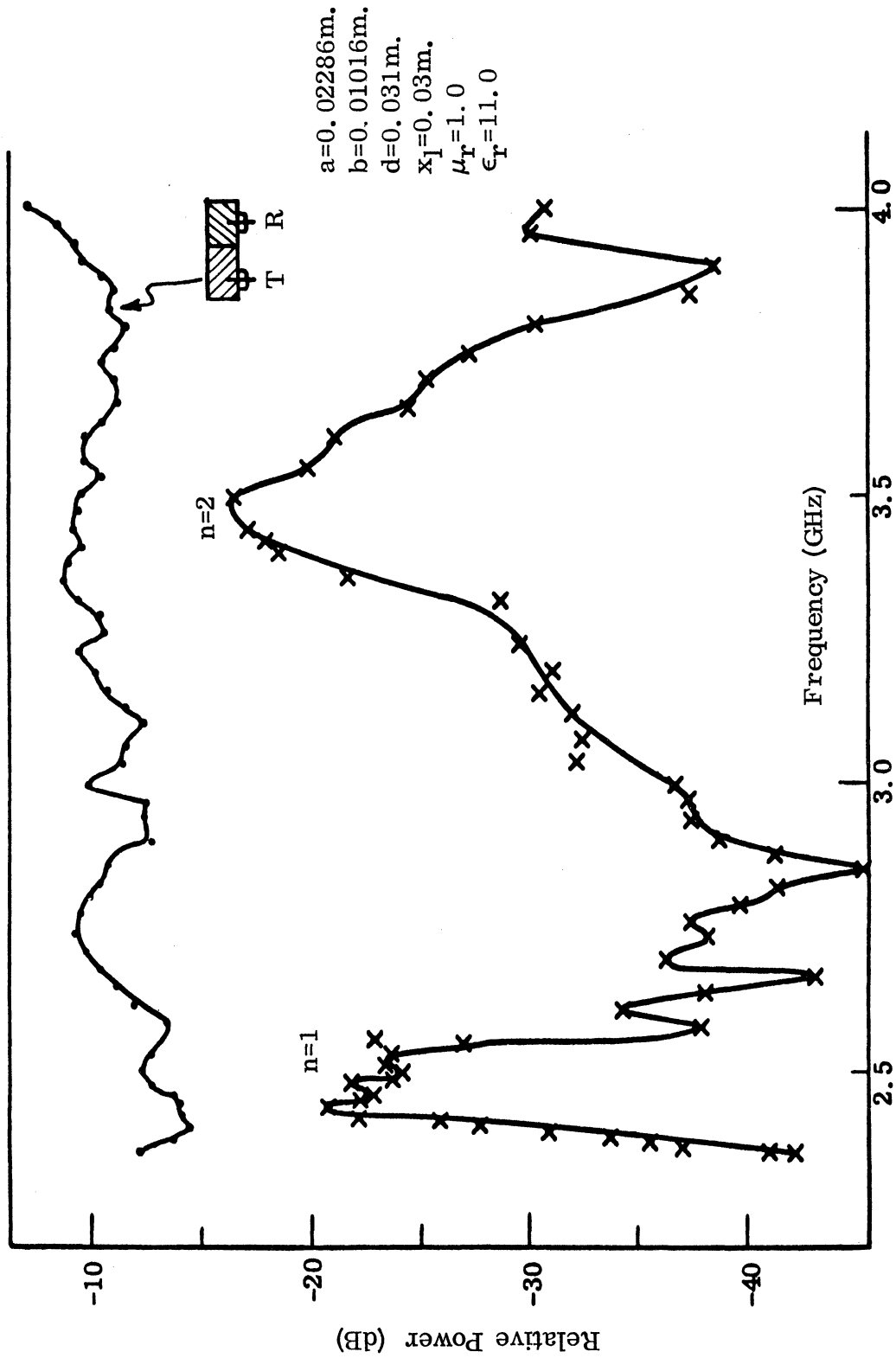


FIG. 4-15: COUPLING VS FREQUENCY WITH TUNING BOTH TRANSMITTER AND RECEIVER AT EACH POINT. (x) Coupling with $x_1=0.03\text{m.}$, (•) Power Level through Cavity formed from Transmitter and Receiver.

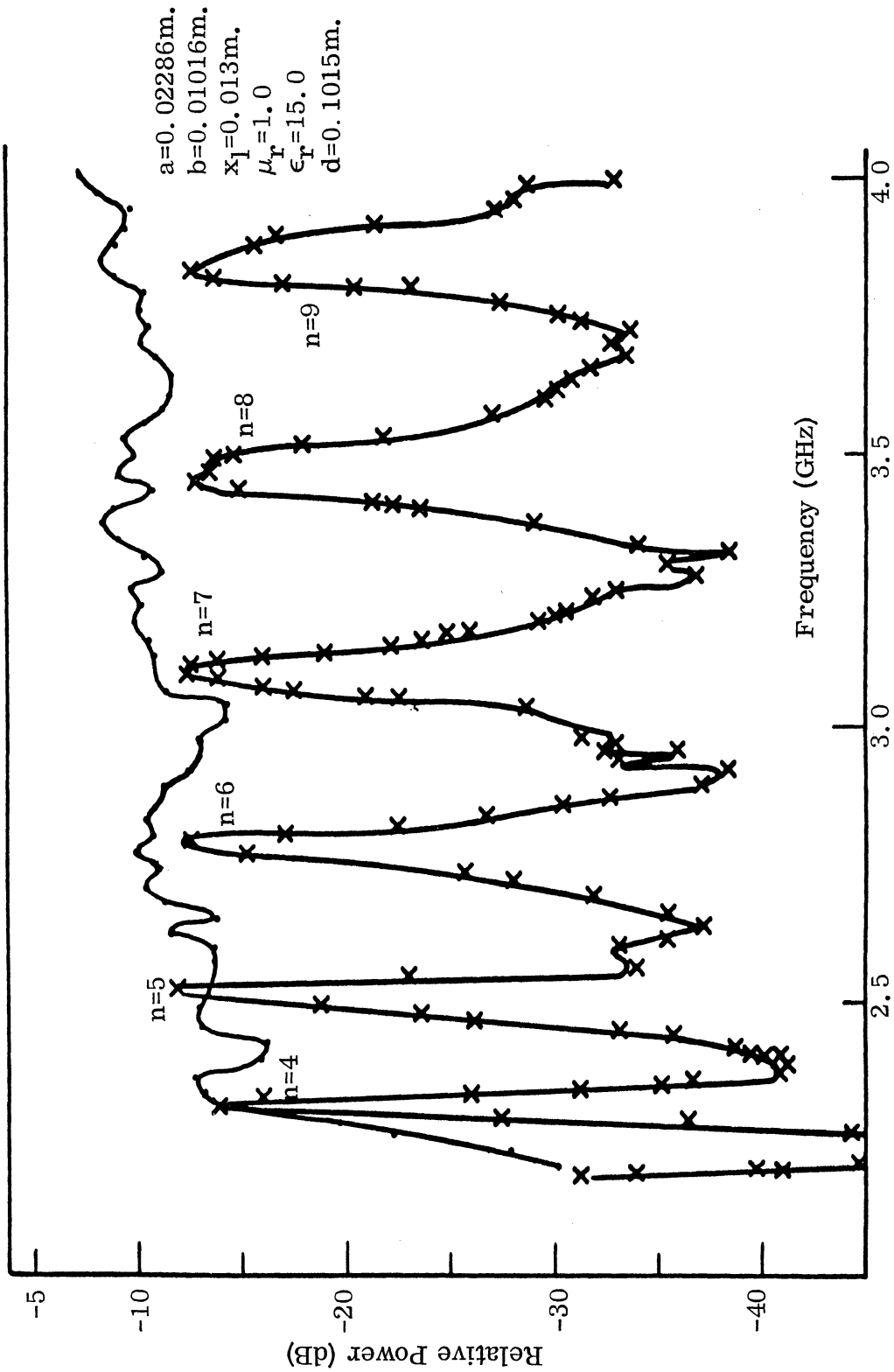


FIG. 4-16(a): COUPLING VS FREQUENCY POINT BY POINT. (x) Coupling with $x_1=0.013\text{m.}$,
 (•) Power Level through Cavity formed from Transmitter and Receiver.

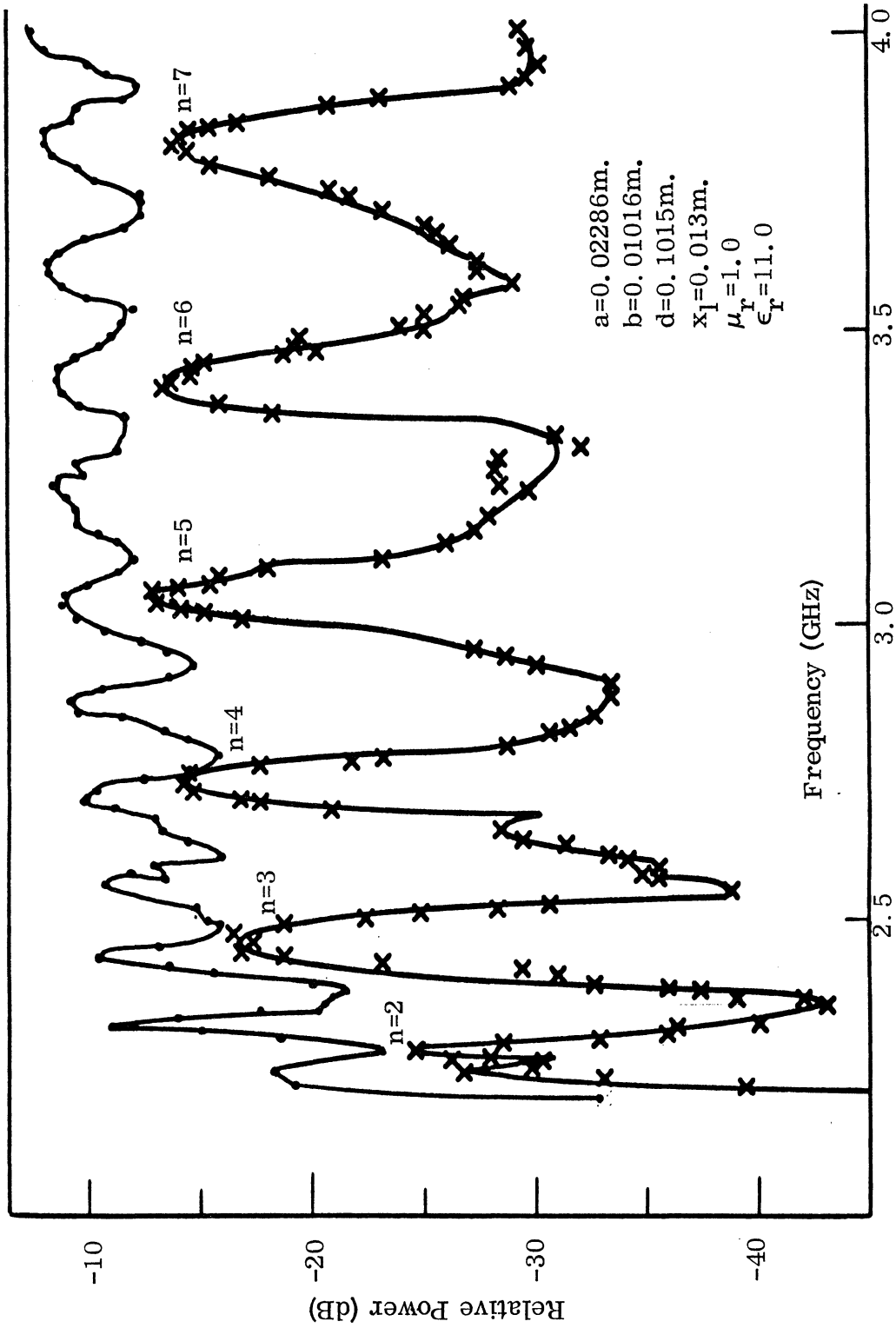


FIG. 4-16(b): COUPLING VS FREQUENCY POINT BY POINT. (x) Coupling vs Frequency with $x_1=0.013\text{m.}$, (•) Power Level through Transmitter and Receiver forming a Cavity.

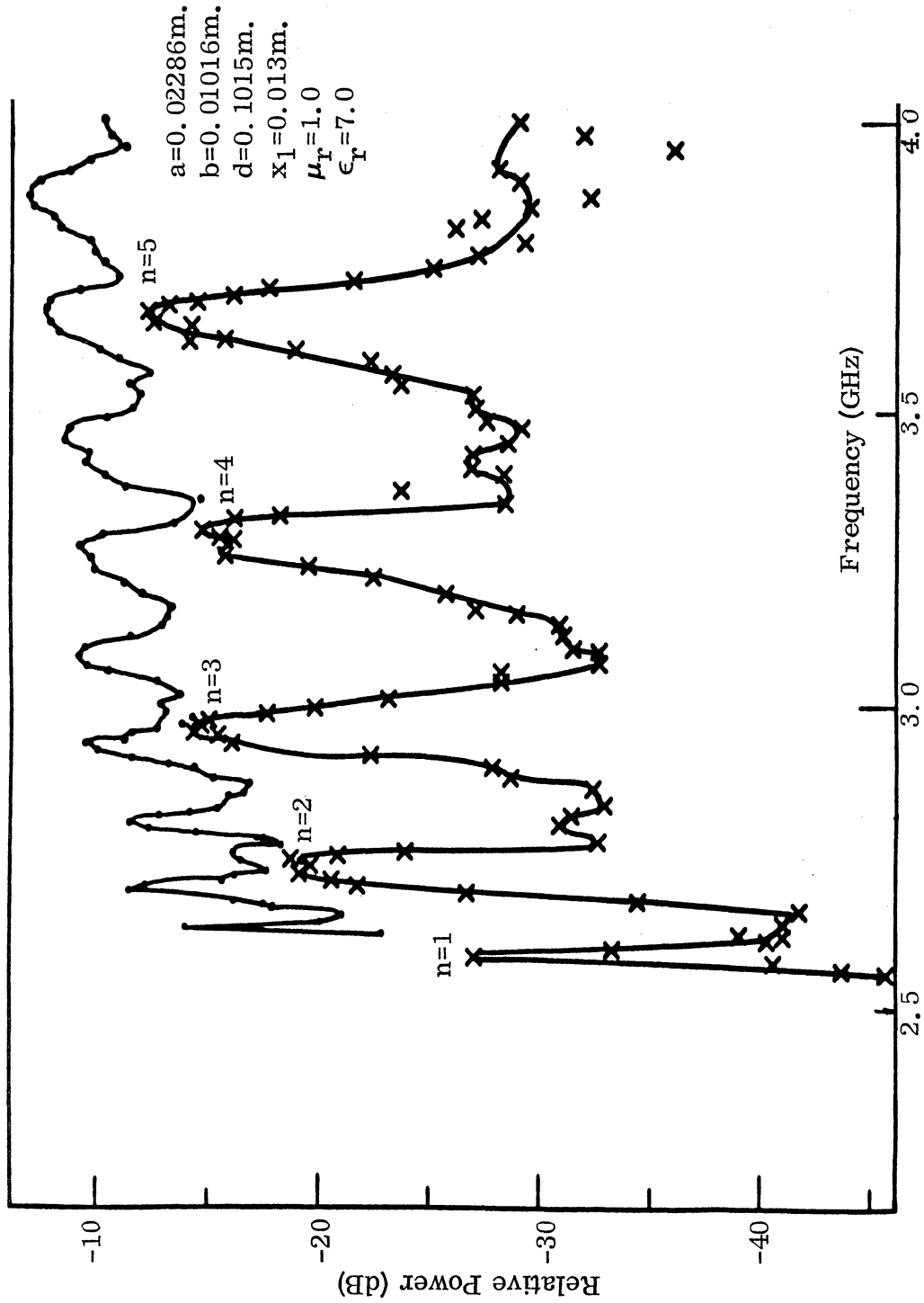


FIG. 4-16(c): COUPLING VS FREQUENCY POINT BY POINT. (x) Coupling with x_1 (spacing) = 0.013m., (•) Power Level through Transmitter and Receiver connected as a Cavity.

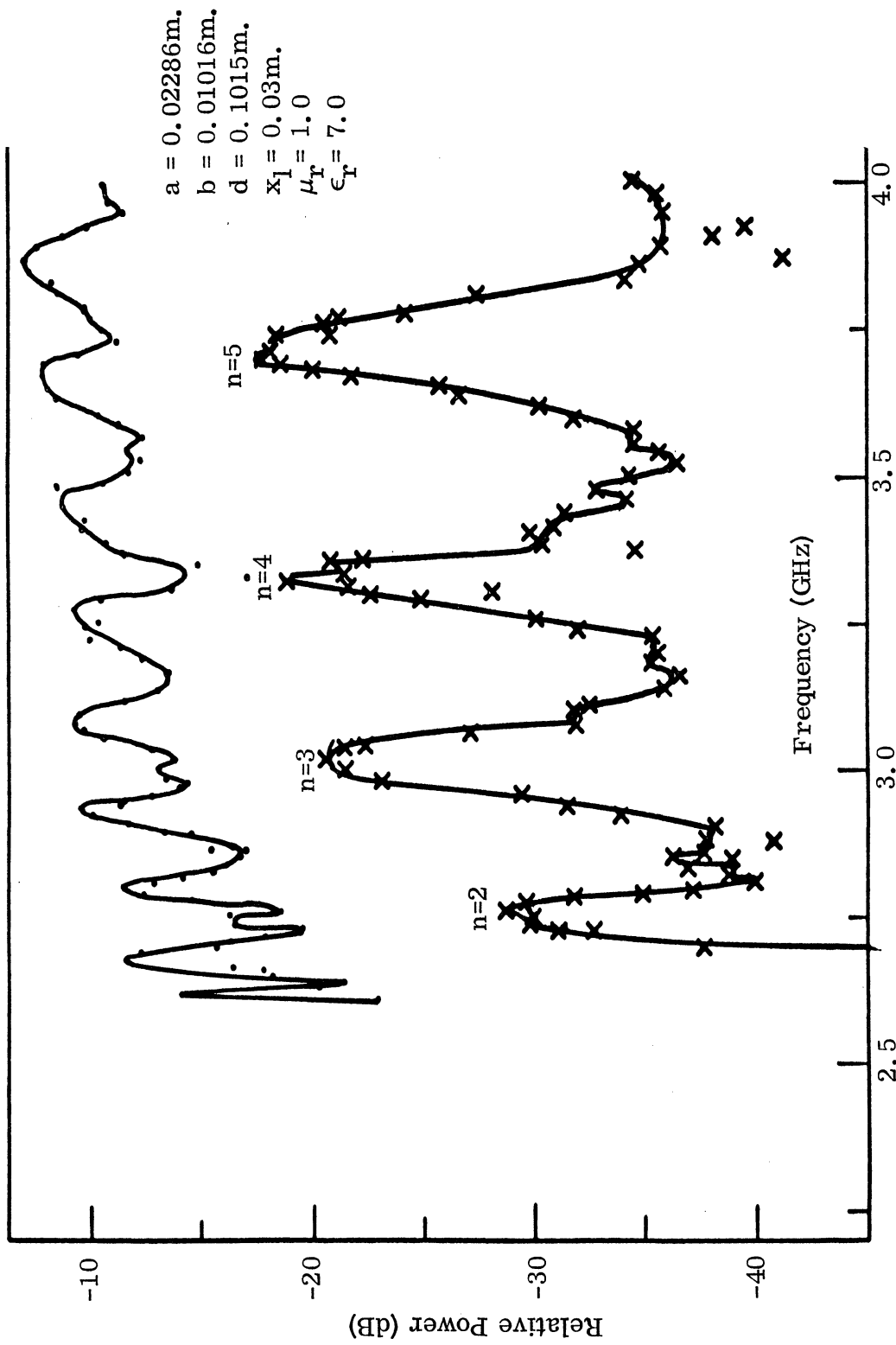


FIG. 4-17: COUPLING VS FREQUENCY POINT BY POINT. (x) Coupling vs Frequency with $x_1(\text{separation}) = 0.03\text{m.}$, (•) Power Level through Transmitter and Receiver connected as a Cavity.

Therefore the curve in comparison with the zero dB level represents the power lost in the transmitting and receiving cavities. It is to be noted that the level of the power lost shown by these curves is a little high because of the discontinuity at the mating surfaces in spite of all the precautions which were taken. The difference is probably within the range of 1 - 2 dB. The lower curves of the graphs represent the level of coupling for various separations, cavity lengths, and dielectric constants.

It should be observed that the differences between these graphs and the corresponding graphs with swept frequency are:

- i) the level of coupling is higher in the case of tuning,
- ii) the dynamic range of variations is less than before and it is around 20 dB,
- iii) the resonance points are about the same with or without tuning.

4.3 The Far-Field Patterns

The arrangement in Fig. 4-9 was used to measure the E-plane pattern which is with $\phi=0^\circ$; θ varies approximately from -90° to $+90^\circ$. The θ -plane is perpendicular to the plane of the aperture at $y = a/2$ and parallel to the x-axis (see Fig. 2-1). The reference antenna is AEL No. ARN101A (1 - 11 GHz) log-periodic and moves in a radius of 5'6".

The H-plane patterns were also measured. For this case $\phi=90^\circ$ and the reference antenna moves in a plane perpendicular to the aperture at $x = b/2$. The variation of θ is between -90° and $+90^\circ$.

Different values of frequencies were considered and both E- and H-plane patterns were drawn. A representative graph is shown in Figs. 4-18(a) and (b). There was no noticeable variation in the shape of the curves with different values of frequency in the S-band range except for the level of the gain. The variation of the gain with frequency was shown in Figs. 4-8, 4-11 and 4-13.

The differences between these patterns and those of a free-space S-band slot in a ground plane are:

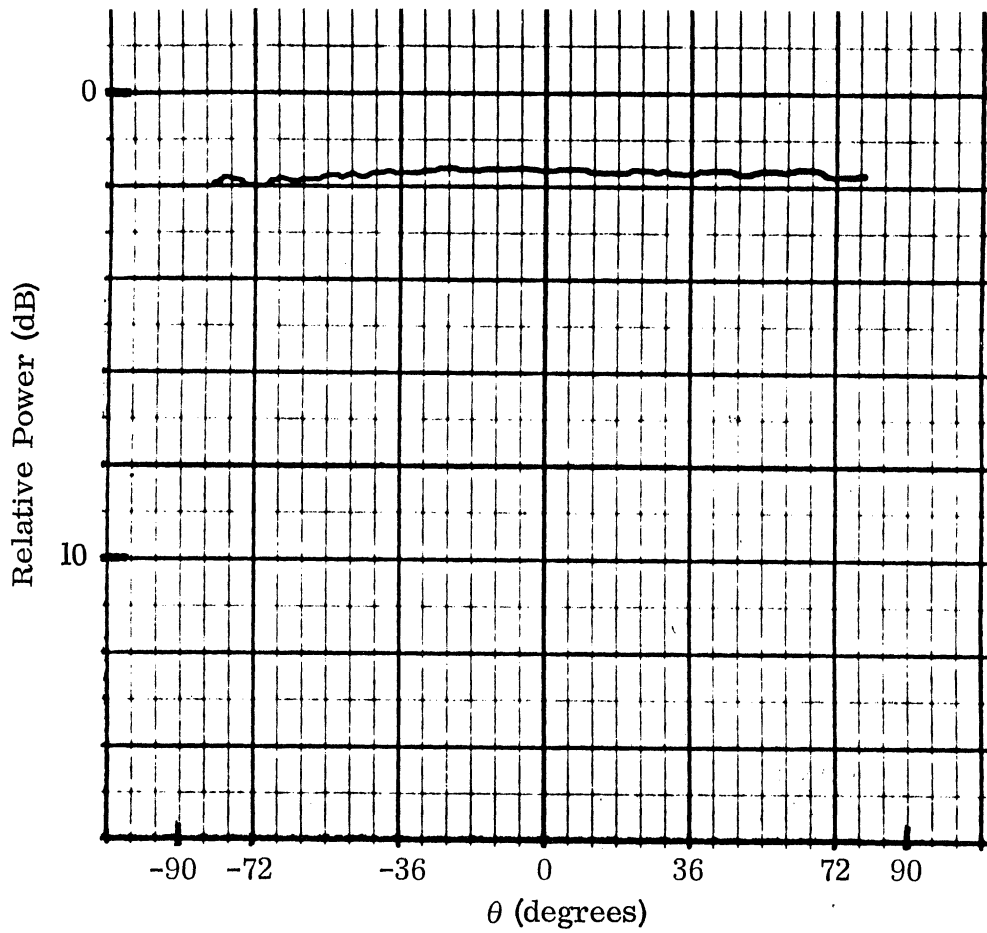


FIG. 4-18(a): E-PLANE RADIATION PATTERN OF A LOADED X-BAND WAVEGUIDE. $f=3.495$ GHz, $\epsilon_r=15.0$, $\mu_r=1.0$

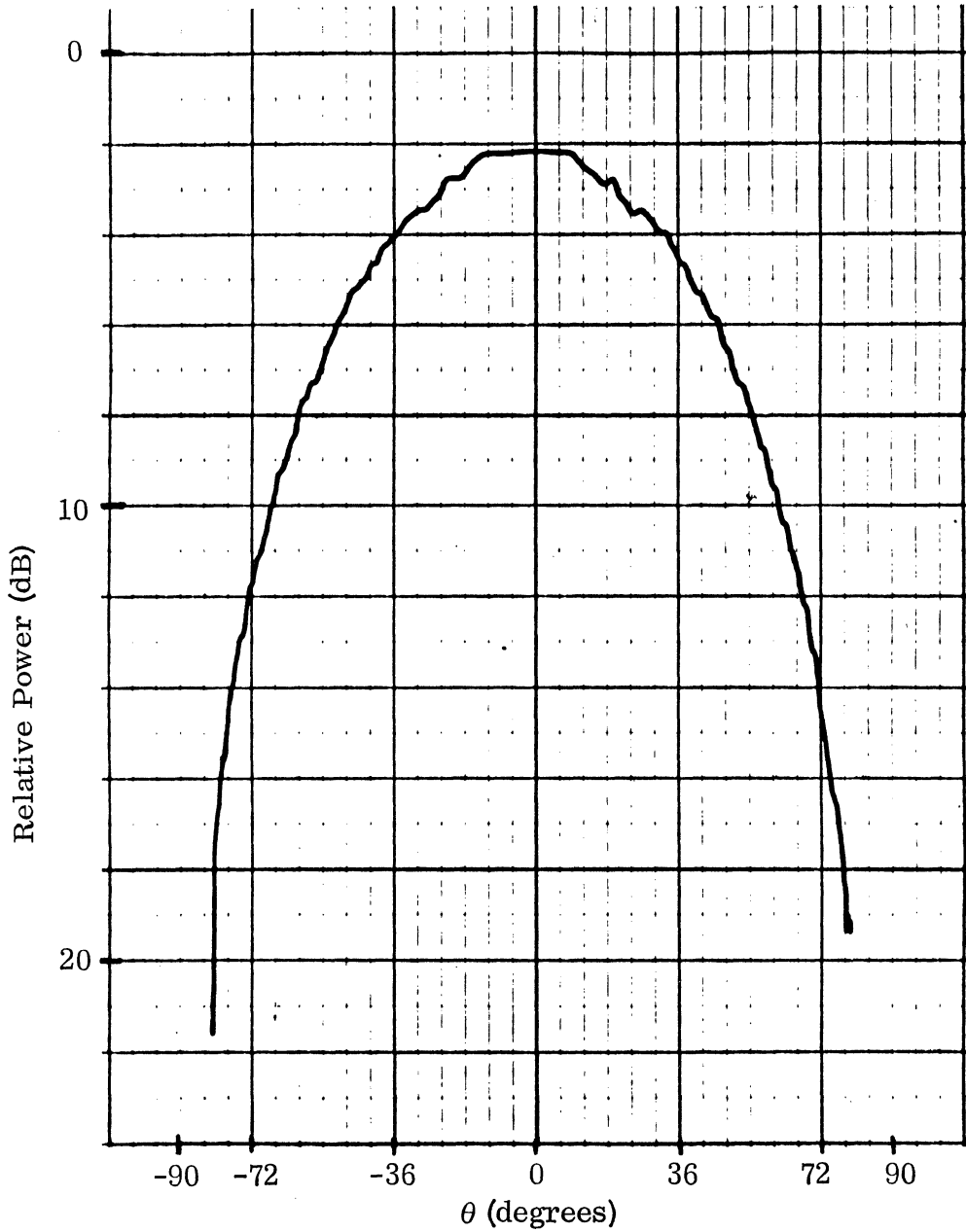


FIG. 4-18(b): H-PLANE RADIATION PATTERN OF A LOADED X-BAND WAVEGUIDE. $f=3.495$ GHz, $\epsilon_r=15.0$, $\mu_r=1.0$

- i) the E-plane pattern is almost a circular pattern, more so than for the corresponding unloaded case,
- ii) the H-plane pattern has the sidelobes somewhat higher in level than the corresponding unloaded case,
- iii) the gain is lower than in the unloaded case due to the losses in the dielectric and the mismatch at the aperture.

Chapter V

SUMMARY AND CONCLUSIONS

The preceding chapters describe a theoretical, numerical and experimental investigation of the coupling between slot antennas with the broadsides parallel; the slots were loaded or unloaded and placed in an infinite conducting ground plane. The two slots were backed with a material loaded cavity filled with homogeneous isotropic material. The investigation does not claim credit for development of new antennas since both loaded and unloaded slots have been introduced before in several papers and textbooks as mentioned in the Introduction. Instead use is made of existing antenna types and an investigation is made of the coupling for both cases. The results of the two cases are then compared. The investigation does not claim an advantage of loaded slots over unloaded ones or vice versa, since each has its own merits and drawbacks. Therefore it is up to the designer of the system, after taking into consideration the characteristics of each, to decide which would be the best choice for his system. For example, if a system has limited space and can tolerate the loss of some of the power it might be a worthwhile compromise to choose the loaded slots. As was seen in the investigation it was possible to use a standard X-band waveguide loaded with dielectric material for S-band frequency operation. It was also noted that the radiation patterns for this arrangement were rather similar to the ones obtained from the standard S-band slots.

A serious drawback of the dielectric loaded waveguides is the frequency sensitivity as shown in both coupling and gain curves versus frequency.

No experimental work has been done to obtain the coupling versus frequency for ferrite loaded slots but it is expected that the resonance phenomena would be less pronounced in this case. The coupling between the apertures with material loading did not follow the usual trend for the unloaded case which is a

drop of approximately 6 dB/octave of frequency. For the loaded slot case the behavior of the coupling between the apertures depended mainly on the parameter of the loading material. It was rather interesting to see that the coupling versus frequency was almost constant with frequency for low values of dielectric constant. For the higher dielectric constants the coupling changed more drastically. It varied from minimum to maximum as shown in Figs. 3-7 to 3-10 (Ch. III). The variation of coupling with spacing followed the 6 dB/octave of distance characteristic.

The phenomena of resonance was investigated and a method to predict the resonant frequencies and the half power bandwidth was obtained. A good agreement between experimental and theoretical results was obtained. It was noted that resonant frequencies occurred when the cavity length was such that $l = n (\lambda_g/2)$ where n is an integer.

It is interesting to note that if it is possible to maintain λ_g constant or approximately so corresponding to its value at the resonance peak, then it would be possible to have a wider bandwidth and reduce the frequency sensitivity. To look into the requirement to do so, consider Eq. (3.10) (Ch. III) which is:

$$f_c = \frac{0.15}{a \sqrt{\mu_r \epsilon_r}} \text{ GHz, where } a \text{ is in meters,}$$

also

$$\lambda_g = \frac{\lambda_0}{\sqrt{\mu_r \epsilon_r}} \frac{1}{\sqrt{1 - \left(\frac{f}{f_c}\right)^2}},$$

or

$$\lambda_g = \frac{0.3}{\sqrt{\mu_r \epsilon_r f^2 - \left(\frac{0.15}{a}\right)^2}} \text{ in meters,}$$

where f is in GHz and a is in meters.

Then for λ_g to be constant irrespective of f implies that

$$\mu_r \epsilon_r f^2 - \left(\frac{0.15}{a}\right)^2 = \text{constant.}$$

If the material loading is to be taken specifically to be dielectric or $\mu_r=1$ then

$$\epsilon_r \propto \frac{1}{f^2} .$$

This indicates that one way to have a wider bandwidth is by using a material with a dielectric constant inversely proportional to the square of the frequency over a certain band of frequency range. The existence or the physical realizability of such material needs further investigation.

Another outcome of the investigation was that, as mentioned in the previous chapters, the resonant frequencies depend on several factors which are; 1) the length of the cavity, 2) the broadside length of the slots, and 3) the material parameters. Therefore if two slots are spaced close to each other on a ground plane the mutual coupling can be controlled. For example, in order to decouple the two slots, the parameters affecting the resonance frequency could be chosen in such a way that the resonant frequency of one antenna coincides with the anti-resonant frequency of the other antenna. For this case each antenna is acting as a frequency filtering device to the power which is intercepted from the other antenna.

It is very interesting to note that the spacing of the resonance peaks is not uniform over the frequency scale. It is smaller nearest the cutoff frequency and becomes wider away from it. This was observed both experimentally (Fig. 4-7 and 4-16) and from digital plots of the resonance points (Fig. 3-14(a)→(c)). This can be explained by considering Eq. (3. 11) which is

$$f_{\text{res}} = \frac{0.15}{\sqrt{\mu_r \epsilon_r}} \sqrt{\frac{n^2}{l^2} + \frac{1}{a^2}} . \quad (3. 11)$$

Squaring both sides there results:

$$f_{\text{res}}^2 = \left(\frac{0.15}{\sqrt{\mu_r \epsilon_r}} \right)^2 \left[\frac{n^2}{l^2} + \frac{1}{a^2} \right] ,$$

or

$$\frac{f_{\text{res}}^2}{\left(\frac{0.15}{a\sqrt{\mu_r\epsilon_r}}\right)^2} - \frac{n^2}{\ell^2} = \frac{1}{a^2} ,$$

or

$$\frac{f_{\text{res}}^2}{\left(\frac{0.15}{a\sqrt{\mu_r\epsilon_r}}\right)^2} - \frac{n^2}{\left(\frac{\ell}{a}\right)^2} = 1 . \quad (5.1)$$

Equation (5.1) can be put in the form

$$\frac{f_{\text{res}}^2}{A_1^2} - \frac{n^2}{A_2^2} = 1 , \quad (5.2)$$

where

$$A_1 = \frac{0.15}{a\sqrt{\mu_r\epsilon_r}} , \quad (5.3)$$

$$A_2 = \ell/a , \quad (5.4)$$

with a and ℓ in meters. Equation (5.2) is a hyperbola as shown in Fig. 5-1. From the figure it can be seen that the resonance peaks are not uniformly spaced but become more nearly uniform at higher frequencies or at the asymptotic part of the curve. Also, from Eq. (3.10) (p. 75) it can be seen that A_1 represents the cutoff frequency for the specific parameters μ_r , ϵ_r , a of the loaded cavity.

5.1 Areas for Future Investigation

- 1) Experimental investigation of coupling for ferrite loaded slots.
- 2) Investigation or search for material to widen the bandwidth.
- 3) Study dielectric loaded slot array.
- 4) Study ferrite loaded slot array.
- 5) Design wide frequency band tuning arrangement for the feed.

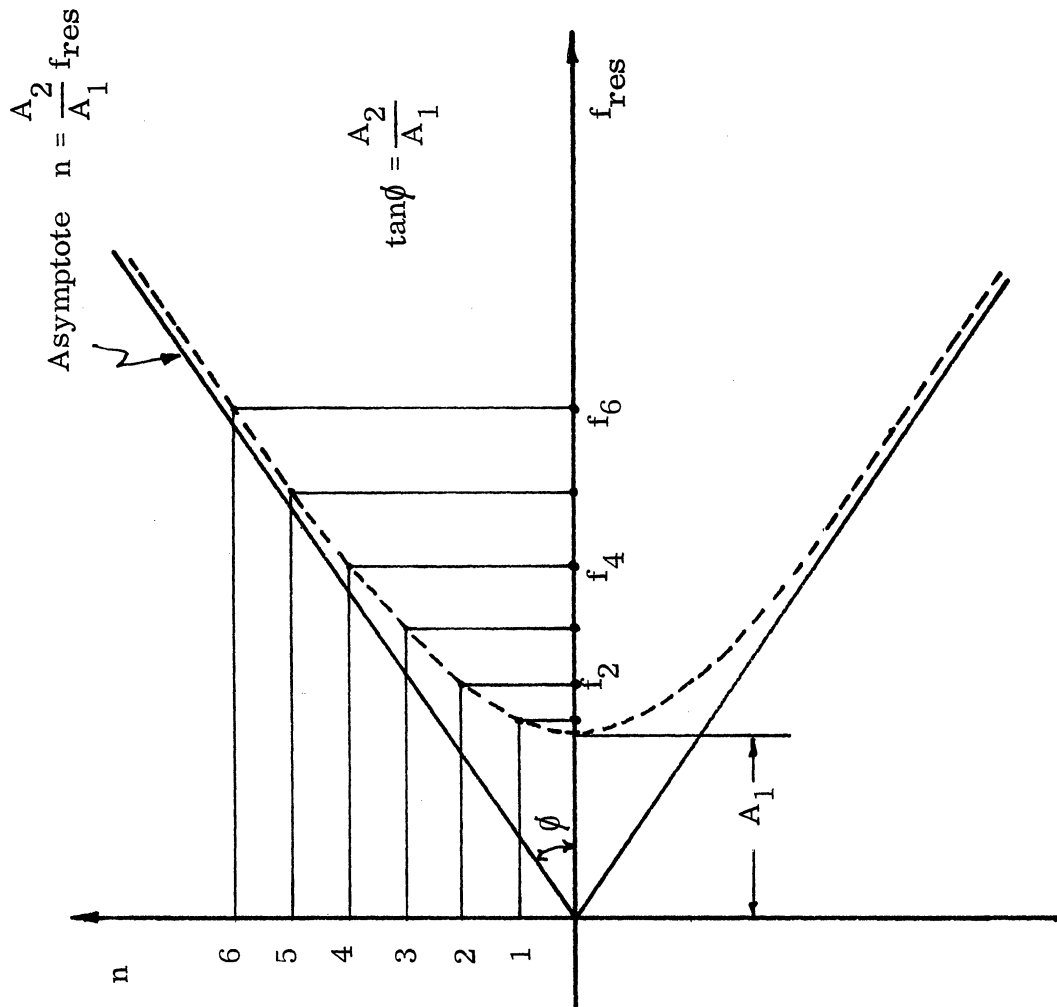


FIG. 5-1: EXPLANATION OF NON-UNIFORMITY OF SEPARATION OF THE RESONANCE PEAKS.

REFERENCES

1. Adams, A. T. (March 1964), "The Rectangular Cavity Slot Antenna with Homogeneous Isotropic Loading," The University of Michigan Cooley Electronics Laboratory Technical Report No. 147 (5549-7-T).
2. Lyon, J. A. M., R. M. Kalafus, Y-K Kwon, C. J. Digenis, M. A. H. Ibrahim and C-C Chen (April 1966), "Derivation of Aerospace Antenna Coupling-Factor Interference Prediction Techniques: Final Report," The University of Michigan Radiation Laboratory Technical Report 6633-1-F, AD 483051.
3. Ramo, S., J. R. Whinnery and T. Van Duzer (1965), Fields and Waves in Communication Electronics, John Wiley and Sons, New York.
4. Von Hippel, A. (1959), Dielectrics and Waves, John Wiley and Sons, New York.
5. Lewin, L. (1951), Advanced Theory of Waveguides, Iliffe and Sons, Ltd., London.
6. Levis, C. A. (August 1956), "Variational Calculations of Impedance Parameters of Coupled Antennas," The Ohio State University Report 667-16.
7. Kaplan, W. (1959), Advanced Calculus, Addison-Wesley Publishers.
8. Harrington, R. F. (1961), Time Harmonic Electromagnetic Fields, McGraw-Hill Book Company, New York.
9. -- (June 1968), "Techniques for Integrating Solid-State Circuitry into Antennas," The Ohio State University Electroscience Laboratory Report 2142-16.
10. Jennetti, A. G. (November 1965), "A 1 Gc Cavity-Backed Slot Antenna Field," The Ohio State University, Contract AF33(657)-10386.
11. Svoboda, D. E. (September 1966), "Correcting for the Pattern Distortion Effects of Mutual Coupling in Antenna Arrays," The Ohio State University Report 2142-6.
12. Richmond, J. H. (November 1961), "A Reaction Theorem and its Applications to Antenna Impedance Calculations," IRE Trans., AP-9, pp. 515-520.
13. Galejs, J. (February 1965), "Self and Mutual Admittances of Waveguides Radiating into Plasma Layers," Radio Science, 69D, pp. 179-189.
14. Mikenas, V. A. and P. E. Mayes (July 1967), "Analysis of a Log-periodic Cavity-slot Antenna Using Three Port Network," University of Illinois Technical Report AFAL-TR-67-109, Dept. of Electrical Engineering.
15. Rumsey, V. H. (June 1954), "Reaction Concept in Electromagnetic Theory," Physical Review, 94, No. 6, pp. 1483-1491.

16. Wu, C. P. (March 1969), "Numerical Solutions for the Coupling Between Waveguides in Finite Array, " Radio Science, 4, No. 3, pp. 245-254.
17. Archer, D. H. and G. S. Hardie (December 1963), "Investigation of Coupling Between Closely Spaced Antennas and Development of High Insulation Techniques, " Raytheon Space and Information Systems Division, Santa Barbara, California
18. Swift, C. T. and D. M. Hatcher (April 1968), "The Input Admittance of a Rectangular Aperture Antenna Loaded with a Dielectric Plug, " NASA Technical Note D-4430.
19. Cockrell, C. R. (October 1968), "Higher-order Mode Effects on the Aperture Admittance of a Rectangular Waveguide Covered with Dielectric and Plasma Slabs, " NASA Technical Note No. D-4774.
20. -- (November 1964), "Techniques for Integration of Active Elements into Antennas and Antenna Structure" Ohio State University Electrical Engineering Department Interim Engineering Report 1566-15.
21. -- (September 1967), "Techniques for Integrating Solid State Circuitry into Antennas, " The Ohio State University Department of Electrical Engineering Interim Technical Report 2142-12.

APPENDIX A

THE REDUCTION OF QUADRUPLE INTEGRALS TO DOUBLE INTEGRALS

For the numerical computations to reasonable in cost and programming for the computer calculations, it was necessary to reduce the quadruple integrals to double integrals. This was performed by means of coordinate transformations. It consisted of a rotation of axis, magnification and translations.

Consider the general coordinate transformation;

$$\mu_1 = \eta \cos \theta + y \sin \theta$$

$$\gamma_1 = -\eta \sin \theta + y \cos \theta$$

If we choose θ to be 45° , then

$$\mu_1 = \frac{1}{\sqrt{2}} (\eta + y)$$

$$\gamma_1 = \frac{1}{\sqrt{2}} (-\eta + y) \quad .$$

Take

$$\left. \begin{aligned} \mu_2 &= \sqrt{2} \mu_1 \\ \gamma_2 &= \sqrt{2} \gamma_1 \end{aligned} \right\} \text{(Magnification)}$$

Then

$$\mu_2 = (\eta + y)$$

$$\gamma_2 = (-\eta + y) \quad .$$

Performing translation along μ_2 such that the origin would be at the center of the rectangle as shown in Fig. 2-5 (Ch. II). Therefore

$$\mu = \mu_2 - a$$

or

$$\mu + a = \mu_2 = \eta + y \tag{A. 1}$$

Let

$$\gamma = \gamma_2$$

or

$$\gamma = y - \eta \quad . \quad (A. 2)$$

Due to the magnification

$$d\eta dy = \frac{1}{2} d\mu d\gamma \quad .$$

Therefore the integration:

$$\int_0^a \int_0^a f(y, \eta) d\eta dy = \frac{1}{2} \int_0^a \int_{-(a-\gamma)}^{(a-\gamma)} f(\mu, \gamma) d\mu d\gamma + \frac{1}{2} \int_{-a}^a \int_{-(a+\gamma)}^{(a+\gamma)} f(\mu, \gamma) d\mu d\gamma \quad (A. 3)$$

If $f(\mu, \gamma)$ is even in μ and γ then:

$$f(-\mu, \gamma) = f(\mu, -\gamma) = f(\mu, \gamma) \quad .$$

Therefore

$$\int_0^a \int_0^a f(y, \eta) d\eta dy = 2 \int_0^a \int_0^{a-\gamma} f(\mu, \gamma) d\mu d\gamma \quad .$$

Similarly

$$\int_0^b \int_0^b f(\xi, x') d\xi dx' = \frac{1}{2} \int_0^b \int_{-(b-\sigma)}^{(b-\sigma)} f(\sigma, \nu) d\nu d\sigma + \frac{1}{2} \int_{-b}^0 \int_{-(b-\sigma)}^{(b+\sigma)} f(\sigma, \nu) d\nu d\sigma \quad (A. 4)$$

also if $f(\sigma, \nu)$ is even in σ and ν then (A. 4) reduces to

$$\int_0^b \int_0^b f(\xi, z') d\xi dx' = 2 \int_0^b \int_0^{b-\sigma} f(\sigma, \nu) d\nu d\sigma \quad .$$

In general

$$\begin{aligned}
\int_0^b \int_0^a \int_0^a \int_0^b f(x', y, \eta, \xi) d\xi d\eta dy dx' &= \frac{1}{4} \int_0^a \int_0^b \int_{-(a-\gamma)}^{(a-\gamma)} \int_{-(b-\sigma)}^{(b-\sigma)} f(\gamma, \mu, \sigma, \nu) d\nu d\mu d\sigma d\gamma \\
&+ \frac{1}{4} \int_0^a \int_{-b}^0 \int_{-(a-\gamma)}^{(a-\gamma)} \int_{-(b+\sigma)}^{(b+\sigma)} f(\nu, \mu, \sigma, \gamma) d\nu d\mu d\sigma d\gamma \\
&+ \frac{1}{4} \int_{-a}^0 \int_0^b \int_{-(a+\gamma)}^{(a+\gamma)} \int_{-(b-\sigma)}^{(b-\sigma)} f(\nu, \mu, \sigma, \gamma) d\nu d\mu d\sigma d\gamma \\
&+ \frac{1}{4} \int_{-a}^0 \int_{-b}^0 \int_{-(a+\gamma)}^{(a+\gamma)} \int_{(b+\sigma)}^{(b+\sigma)} f(\nu, \mu, \sigma, \gamma) d\nu d\mu d\sigma d\gamma .
\end{aligned} \tag{A. 5}$$

In Chapter II $f(\gamma, \mu, \sigma, \nu)$ is an even function in γ, μ, ν . Therefore:

$$\begin{aligned}
\int_0^b \int_0^a \int_0^a \int_0^b f(x', y, \eta, \xi) d\xi d\eta dy dx' &= \int_0^a \int_0^b \int_0^{a-\gamma} \int_{-(b-\sigma)}^{(b-\sigma)} f(\gamma, \mu, \sigma, \nu) d\nu d\mu d\sigma d\gamma \\
&+ \int_0^a \int_{-b}^0 \int_0^{a-\gamma} \int_{-(b+\sigma)}^{(b+\sigma)} f(\gamma, \mu, \sigma, \nu) d\nu d\mu d\sigma d\gamma .
\end{aligned} \tag{A. 6}$$

APPENDIX B

EXAMPLES OF COMPUTER OUTPUT DATA ON COUPLING

B. 1 Coupling Versus Frequency

B. 1. 1

For an empty S-band waveguide for $x_1=0.0341m.$, $x_2=0.075m.$, $A = a$,
 $B = b$, $EPSR = \epsilon_r$, $FMUR = \mu_r$, $XI =$ separation center-to-center, $UC =$
coupling without interaction, and $UCI =$ coupling with interaction.

B. 1. 1a :

```
A = 0.7136000D-01  B = 0.3403600D-01  Q = 0.5000000D-01
EPSR = 1.000000    FMUR = 1.000000
NAI = 30  NBI = 30  NS = 30  NL = 50

FOR XI = 0.3410000D-01

FN          UC          UCI
           DB          DB
1.100     -10.33943     -9.987158
1.200     -12.28099     -12.13783
1.300     -13.16871     -13.13351
1.400     -13.71613     -13.76355
1.500     -14.13574     -14.25094
1.600     -14.51635     -14.68423
1.700     -14.90229     -15.10558
1.800     -15.31860     -15.53867
1.900     -15.78103     -15.99964
2.000     -16.30764     -16.50183
```

B. 1. 1b:

A = 0.7136000D-01 B = 0.3403600D-01 Q = 0.5000000D-01
EPSR = 1.000000 FMUR = 1.000000
NAI = 30 NRI = 30 NS = 30 NL = 50

FOR XI = 0.7500000D-01

FN	UC	UCI
	DB	DB
1.100	-15.11413	-15.12735
1.200	-17.16514	-17.07426
1.300	-18.12798	-18.00248
1.400	-18.72168	-18.60833
1.500	-19.16331	-19.09728
1.600	-19.54507	-19.54128
1.700	-19.91373	-19.96331
1.800	-20.29591	-20.37208
1.900	-20.70829	-20.77857
2.000	-21.16218	-21.20163

B. 1. 1c:

A = 0.7136000D-01 B = 0.3403600D-01 Q = 0.5000000D-01
EPSR = 1.000000 FMUR = 1.000000
NAI = 30 NRI = 30 NS = 30 NL = 50

FOR XI = 0.2075000

FN	UC	UCI
	DB	DB
1.100	-23.25791	-23.26242
1.200	-25.34572	-25.32054
1.300	-26.33617	-26.34358
1.400	-26.95072	-26.96499
1.500	-27.40811	-27.39611
1.600	-27.80182	-27.79544
1.700	-28.17953	-28.19244
1.800	-28.56864	-28.56822
1.900	-28.98639	-28.97585
2.000	-29.44464	-29.44963

B. 1. 2

For an empty X-band waveguide with spacing of $x_1=0.013\text{m.}$, $x_2=0.02286\text{m.}$,
0.114m.

B. 1. 2a:

A = 0.22860000D-01 B = 0.10160000D-01 Q = 0.50000000D-01
EPSR = 1.000000 FMUR = 1.000000
NAI = 30 NBI = 30 NS = 30 NL = 50

FOR X1 = 0.13000000D-01

FN	UC	UCI
	DB	DB
1.100	-11.67733	-11.75804
1.200	-13.60082	-13.74578
1.300	-14.45179	-14.64503
1.400	-14.94471	-15.17159
1.500	-15.29300	-15.53526
1.600	-15.58605	-15.82277
1.700	-15.86837	-16.07859
1.800	-16.16473	-16.33055
1.900	-16.49024	-16.59960
2.000	-16.85484	-16.90338

B. 1. 2b:

A = 0.22860000D-01 B = 0.10160000D-01 Q = 0.50000000D-01
EPSR = 1.000000 FMUR = 1.000000
NAI = 30 NBI = 30 NS = 30 NL = 50

FOR X1 = 0.22860000D-01

FN	UC	UCI
	DB	DB
1.100	-15.16875	-15.25937
1.200	-17.16429	-17.12500
1.300	-18.06707	-17.96615
1.400	-18.59560	-18.47585
1.500	-18.96640	-18.86764
1.600	-19.27116	-19.22250
1.700	-19.55607	-19.56723
1.800	-19.84716	-19.90658
1.900	-20.16037	-20.24134
2.000	-20.50626	-20.57800

B. 1. 2c:

A = 0.22860000-01 B = 0.10160000-01 Q = 0.50000000-01
EPSR = 1.000000 FMR = 1.000000
NAI = 30 NBI = 30 NS = 30 NL = 50

FOR XI = 0.1140000

FN	UC	UCI
	DB	DB
1.100	-28.21674	-28.20364
1.200	-30.25484	-30.26302
1.300	-31.18882	-31.18221
1.400	-31.74008	-31.74589
1.500	-32.12719	-32.12186
1.600	-32.44331	-32.44825
1.700	-32.73573	-32.73111
1.800	-33.03133	-33.03565
1.900	-33.34674	-33.34273
2.000	-33.69305	-33.69674

B. 1. 2d: Standard Ku-band waveguide coupling versus frequency output.

A = 0.15798800-01 B = 0.78994000-02 Q = 0.50000000-01
EPSR = 1.000000 FMR = 1.000000
NAI = 30 NBI = 30 NS = 30 NL = 50

FOR XI = 0.1140000

FN	UC	UCI
	DB	DB
1.200	-32.98682	-32.98475
1.300	-34.02749	-34.02482
1.400	-34.69629	-34.69853
1.500	-35.21258	-35.21388
1.600	-35.67041	-35.66819
1.700	-36.11813	-36.11780
1.800	-36.58381	-36.58572
1.900	-37.08549	-37.08514
2.000	-37.63593	-37.63455
2.100	-38.24509	-38.24580

B. 1. 3

For a standard X-band waveguide filled with dielectric material. These parameters are common for the three tables which follow: $a=0.02286m.$, $b=0.01016m.$, $\mu_r = 1.0$, separation center to center = $x_1=0.013m.$

B. 1. 3a: $\epsilon_r = 7.0$

FN	UC	UCI
	DB	DB
1.100	-19.92142	-19.96417
1.200	-22.74857	-22.75982
1.300	-24.04925	-24.04954
1.400	-24.62473	-24.61905
1.500	-24.78698	-24.77725
1.600	-24.70965	-24.69682
1.700	-24.49765	-24.48233
1.800	-24.21448	-24.19717
1.900	-23.89813	-23.87930
2.000	-23.57103	-23.55122
2.100	-23.24631	-23.22612
2.200	-22.93152	-22.91165

B 1. 3b: $\epsilon_r = 11.0$

FN	UC	UCI
	DB	DB
1.100	-19.83601	-19.91287
1.200	-23.20505	-23.23635
1.300	-25.18408	-25.20028
1.400	-26.47726	-26.48592
1.500	-27.30095	-27.30501
1.600	-27.76787	-27.76875
1.700	-27.96353	-27.96200
1.800	-27.96154	-27.95808
1.900	-27.82349	-27.81837
2.000	-27.59736	-27.59080
2.100	-27.31824	-27.31042
2.200	-27.01053	-27.00160

B. 1. 3c: $\epsilon_r = 15.0$

FN	UC	UCI
	DB	DB
1.100	-19.42214	-19.51548
1.200	-22.87672	-22.91717
1.300	-25.02914	-25.05214
1.400	-26.59214	-26.60652
1.500	-27.77097	-27.78025
1.600	-28.64666	-28.65255
1.700	-29.26152	-29.26498
1.800	-29.64876	-29.65036
1.900	-29.84291	-29.84302
2.000	-29.88097	-29.87981
2.100	-29.79956	-29.79730
2.200	-29.63168	-29.62845

B. 1. 3d:

A = 0.22860000-01 R = 0.10160000-01 Q = 0.50000000-01
EPSR = 20.00000 FMUR = 1.000000
NAI = 30 NBI = 30 NS = 30 NL = 50

FOR XI = 0.13000000-01

FN	UC	UCI
	DB	DB
1.100	-19.03111	-19.13669
1.200	-22.47551	-22.52264
1.300	-24.65389	-24.68171
1.400	-26.29247	-26.31078
1.500	-27.60813	-27.62084
1.600	-28.68750	-28.69654
1.700	-29.56957	-29.57504
1.800	-30.26899	-30.27354
1.900	-30.79920	-30.80227
2.000	-31.16974	-31.17161

B. 1. 3e:

A = 0.22860000D-01 B = 0.10160000D-01 Q = 0.50000000D-01
EPSR = 2.000000 FMUR = 1.000000
NAI = 30 NBI = 30 NS = 30 NL = 50

FOR XI = 0.13000000D-01

FN	UC	UCI
	DB	DB
1.100	-11.50556	-11.20670
1.200	-13.16504	-12.99226
1.300	-13.73232	-13.62388
1.400	-13.92855	-13.87707
1.500	-13.96825	-13.97640
1.600	-13.93971	-14.01147
1.700	-13.88555	-14.02285
1.800	-13.82837	-14.02949
1.900	-13.78094	-14.03980
2.000	-13.75081	-14.05700

B. 1. 3f:

A = 0.22860000D-01 B = 0.10160000D-01 Q = 0.50000000D-01
EPSR = 3.000000 FMUR = 1.000000
NAI = 30 NBI = 30 NS = 30 NL = 50

FOR XI = 0.13000000D-01

FN	UC	UCI
	DB	DB
1.100	-15.16019	-15.03304
1.200	-16.81772	-16.72254
1.300	-17.31772	-17.23417
1.400	-17.41552	-17.34109
1.500	-17.34165	-17.27812
1.600	-17.19165	-17.14257
1.700	-17.01123	-16.98092
1.800	-16.82412	-16.81700
1.900	-16.64328	-16.66336
2.000	-16.47602	-16.52637

B.1.3g:

A = 0.22860000-01 B = 0.10160000-01 Q = 0.50000000-01
EPSR = 4.000000 FMUR = 1.000000
NAI = 30 NBI = 30 NS = 30 NL = 50

FOR XI = 0.13000000-01

FN	UC	UCI
	DB	DB
1.100	-17.49192	-17.44991
1.200	-19.34451	-19.30167
1.300	-19.91738	-19.87284
1.400	-20.01899	-19.97312
1.500	-19.91176	-19.86559
1.600	-19.70868	-19.66379
1.700	-19.46463	-19.42311
1.800	-19.20811	-19.17239
1.900	-18.95446	-18.92724
2.000	-18.71212	-18.69618

B.1.3h:

A = 0.22860000-01 B = 0.10160000-01 Q = 0.50000000-01
EPSR = 5.000000 FMUR = 1.000000
NAI = 30 NBI = 30 NS = 30 NL = 50

FOR XI = 0.13000000-01

FN	UC	UCI
	DB	DB
1.100	-18.87111	-18.87219
1.200	-21.04860	-21.03350
1.300	-21.81286	-21.79115
1.400	-22.00886	-21.98292
1.500	-21.93478	-21.90581
1.600	-21.72867	-21.69765
1.700	-21.46081	-21.42880
1.800	-21.16862	-21.13683
1.900	-20.87251	-20.84238
2.000	-20.58375	-20.55689
2.100	-20.30854	-20.28670
2.200	-20.05019	-20.03519
2.300	-19.81039	-19.80400
2.400	-19.58983	-19.59373
2.500	-19.38866	-19.40432
2.600	-19.20671	-19.23530
2.700	-19.04364	-19.08595
2.800	-18.89901	-18.95541
2.900	-18.77234	-18.84271
3.000	-18.66316	-18.74688

B. 2 Coupling Versus Spacing

In the following these notations are common: $A = a$, $B = b$, $\text{EPSR} = \epsilon_r$,
 $\text{FMUR} = \mu_r$, $GB = N_1$ and N_2

where

$$N_1 = G/Y_0 \quad \text{and} \quad N_2 = B/Y_0$$

for the normalized frequency specified FN. Also,

$$R = N_3 \text{ and } N_4,$$

where N_3 is the real part of the reflection coefficient and N_4 is the imaginary part of the reflection coefficient. Also, L indicates the separation between the two slots center-to-center in wavelengths. X_1 indicates the equivalent in meters of L for the specific case at hand.

B.2.1

A = 0.22860000-01 H = 0.10160000-01 Q = 0.50000000-01
 EPSR = 1.000000 FMUR = 1.000000
 NAI = 30 NRI = 30 NS = 30 NL = 50

FOR FN = 1.403100

GB = 0.7829483 0.4157269 R = 0.63896190-01 -0.2480668

L	X1	UC	UCI
		DB	DB
0.4000000	0.13043290-01	-14.97216	-15.20092
0.5000000	0.16304120-01	-16.31901	-16.48411
0.6000000	0.19564940-01	-17.51634	-17.48162
0.7000000	0.22825760-01	-18.59381	-18.47401
0.8000000	0.26086580-01	-19.57092	-19.52553
0.9000000	0.29347410-01	-20.46249	-20.51396
1.0000000	0.32608230-01	-21.28048	-21.34061
1.1000000	0.35869050-01	-22.03482	-22.03359
1.2000000	0.39129880-01	-22.73379	-22.68967
1.3000000	0.42390700-01	-23.38432	-23.36022
1.4000000	0.45651520-01	-23.99224	-24.01144
1.5000000	0.48912350-01	-24.56245	-24.59180
1.6000000	0.52173170-01	-25.09914	-25.10116
1.7000000	0.55433990-01	-25.60584	-25.58383
1.8000000	0.58694810-01	-26.08560	-26.07137
1.9000000	0.61955640-01	-26.54105	-26.55060
2.0000000	0.65216460-01	-26.97445	-26.99154
2.1000000	0.68477280-01	-27.38779	-27.38984
3.1000000	0.1010855	-30.71521	-30.71659
4.1000000	0.1336937	-33.12343	-33.12435
5.1000000	0.1663020	-35.00959	-35.01024
6.1000000	0.1989102	-36.55952	-36.56000
7.1000000	0.2315184	-37.87489	-37.87525
8.1000000	0.2641267	-39.01733	-39.01762
9.1000000	0.2967349	-40.02702	-40.02725
10.1000000	0.3293431	-40.93158	-40.93178

B.2.2

The parameters are as in Section B.1.1.

A = 0.22860000-01 B = 0.10160000-01 Q = 0.50000000-01
 FPSR = 11.00000 FMUR = 1.000000
 NAI = 30 NBI = 30 NS = 30 NL = 50

FOR FN = 1.500000

GB = 0.30222470-01 -0.3090832 R = 0.7810194 0.5343343

L	X1	UC	UCI
		DB	DB
0.1000000	0.10109070-01	-23.17457	-23.20288
0.2000000	0.20218140-01	-31.24739	-31.24590
0.3000000	0.30327220-01	-33.75363	-33.75455
0.4000000	0.40436290-01	-35.71362	-35.71577
0.5000000	0.50545360-01	-37.37070	-37.37194
0.6000000	0.60654430-01	-38.79344	-38.79316
0.7000000	0.70763510-01	-40.03263	-40.03178
0.8000000	0.80872580-01	-41.12665	-41.12632
0.9000000	0.90981650-01	-42.10409	-42.10443
1.0000000	0.1010907	-42.98637	-42.98678
1.1000000	0.1111998	-43.78978	-43.78978
1.2000000	0.1213089	-44.52683	-44.52659
1.3000000	0.1314179	-45.20755	-45.20738
1.4000000	0.1415270	-45.83965	-45.83977
1.5000000	0.1516361	-46.42955	-46.42974
1.6000000	0.1617452	-46.98245	-46.98246
1.7000000	0.1718542	-47.50265	-47.50251
1.8000000	0.1819633	-47.99378	-47.99368
1.9000000	0.1920724	-48.45887	-48.45893
2.0000000	0.2021814	-48.90053	-48.90064
2.1000000	0.2122905	-49.32099	-49.32101
3.1000000	0.3133812	-52.68622	-52.68623
4.1000000	0.4144720	-55.10825	-55.10826
5.1000000	0.5155627	-57.00095	-57.00095
6.1000000	0.6166534	-58.55448	-58.55448
7.1000000	0.7177441	-59.87203	-59.87203
8.1000000	0.8188349	-61.01590	-61.01590
9.1000000	0.9199256	-62.02657	-62.02658
10.10000	1.021016	-62.93185	-62.93185

DOCUMENT CONTROL DATA - R & D

(Security classification of title, body of abstract and indexing annotation must be entered when the overall report is classified)

1. ORIGINATING ACTIVITY <i>(Corporate author)</i> The University of Michigan Radiation Laboratory, Dept. of Electrical Engineering, 201 Catherine Street, Ann Arbor, Michigan 48108		2a. REPORT SECURITY CLASSIFICATION UNCLASSIFIED	
		2b. GROUP -----	
3. REPORT TITLE 300 MHz Array Using Physically Small Slot Antenna Elements			
4. DESCRIPTIVE NOTES <i>(Type of report and inclusive dates)</i> Second Interim Report, Technical			
5. AUTHOR(S) <i>(First name, middle initial, last name)</i> Medhat A. H. Ibrahim and John A. M. Lyon			
6. REPORT DATE August 1969	7a. TOTAL NO. OF PAGES 172	7b. NO. OF REFS 27	
8a. CONTRACT OR GRANT NO. F33615-68-C-1381	9a. ORIGINATOR'S REPORT NUMBER(S) 1770-2-T		
b. PROJECT NO. 6278			
c. Task No. 627801	9b. OTHER REPORT NO(S) <i>(Any other numbers that may be assigned this report)</i> AFAL-TR-69-299		
d.			
10. DISTRIBUTION STATEMENT This document is subject to special export control and each transmittal to foreign governments or foreign nationals may be made only with prior approval of AFAL (AVWE), Wright-Patterson Air Force Base, Ohio, 45433			
11. SUPPLEMENTARY NOTES		12. SPONSORING MILITARY ACTIVITY Air Force Avionics Laboratory Air Force Systems Command Wright-Patterson Air Force Base, Ohio	
13. ABSTRACT <p>The coupling between two loaded rectangular waveguides opening in an infinite conducting ground plane has been investigated. The slots are equal in size and placed so as to have the broadsides parallel. The analysis is made in two steps: 1) the coupling between the apertures is derived, and 2) the effect of the backing cavities on the coupling is determined. The reaction concept, a form of the "variational technique" was used in the analysis. This method helped to simplify the mathematical work and provided very reasonable results.</p> <p>Substantial experimental work on the behavior of coupling versus frequency and coupling versus slot separation was performed. In order to simplify the experimental investigation the standard empty X-band waveguide (0.9"x0.4") was filled with dielectric loading of Emerson and Cuming Stycast Hi-K dielectric material. Materials having dielectric constants of 5, 7, 11 and 15 were used. Most of the measurements for the loaded case were in the S-band range of frequency (2.6 - 3.95 GHz). The choices of the S-band frequency range and the dielectric constant were made to permit use of the anechoic chamber in the first instance with reasonable accuracy and small waveguide in the second instance.</p> <p>An extensive comparison of coupling for the case of standard waveguides with and without loading has been made and explanations are given for the observed differences. An iteration procedure has been used to determine the effect of the electromagnetic interaction between the slots.</p> <p>Detailed computer programs were developed for the analytical expressions. Numerical results for many important cases were then obtained. Methods and results can readily be extended to other frequencies and other slot sizes.</p>			

14. KEY WORDS	LINK A		LINK B		LINK C	
	ROLE	WT	ROLE	WT	ROLE	WT
Antennas Antenna Arrays Electromagnetic Coupling Coupling Reduction Dielectric Loaded Antennas						

DISTRIBUTION LIST

<u>Nr Copies</u>	<u>Company</u>	<u>Nr Copies</u>	<u>Company</u>
1	Adams-Russell Company Inc Attn: Technical Library 280 Bear Hill Road Waltham MA 02154	1	Bell Aircraft Corporation Attn: Technical Library PO Box 1 Buffalo NY 14205
1	Aerospace Corporation Attn: Technical Library Box 95085 Los Angeles CA 90045	1	Bell Telephone Laboratories Inc Attn: Technical Library Whippany Road Whippany NJ 07981
1	Airborne Instruments Laboratories Inc Cutler-Hammer Division Attn: Technical Library Walt Whitman Road Melville LI NY 11746	1	Bendix Corporation Bendix Pacific Division Attn: Technical Library 11600 Sherman Way North Hollywood CA 91605
1	American Electronics Laboratories Inc Attn: Technical Library PO Box 552 Lansdale PA 19446	1	Bendix Corporation Radio Division Attn: Technical Library E Joppa Road Baltimore MD 21204
1	Andrew Alford Consulting Engineers Attn: Technical Library 299 Atlantic Avenue Boston MA 02110	1	Bendix Corporation Research Laboratories Division Attn: Technical Library 20800 10 1/2 Mile Road Southfield MI 48076
1	AVCO Corporation Research and Advanced Development Division Attn: Technical Library 201 Lowell Street Wilmington MA 01887	1	Boeing Company Attn: Technical Library 3801 South Oliver Wichita KS 67210
1	AVCO Corporation Electronics Division Attn: Technical Library 2630 Glendale-Milford Road Cincinnati OH 45241	1	Boeing Company Commercial Airplane Division PO Box 707 Renton WA 98055
		1	Boeing Company Aero Space Division Attn: Technical Library PO Box 3707 Seattle WA 98124

DISTRIBUTION LIST

<u>Nr Copies</u>	<u>Company</u>	<u>Nr Copies</u>	<u>Company</u>
1	Bunker-Ramo Corporation Defense Systems Division Attn: Technical Library 8433 Fallbrook Avenue Canoga Park CA 91304	1	Dorne & Margolin Inc Attn: Technical Library 2950 Veterans Memorial Highway Bohemia LI NY 11762
1	Chance Vought Aircraft Inc Attn: Technical Library PO Box 1500 Arlington TX 75222	1	Electronic Communications Inc Research Division Attn: Technical Library 1830 York Road Timonium MD 21093
1	Chu Associates Attn: Technical Library Box 387 Littleton MA 01460		
		1	Emerson Electric Company Electronics & Space Division Attn: Technical Library 8100 Florissant Avenue St Louis MO 63136
1	Collins Radio Company Attn: Technical Library 2100 North Alma Road Richardson TX 75207	1	General Dynamics/Electronics Division Attn: Technical Library PO Box 127, Mail Zone 715 San Diego CA 92112
1	Conductron Corporation Attn: Technical Library 343 South Main Street Ann Arbor MI 48104	1	General Dynamics/Fort Worth Attn: Technical Library PO Box 748, Mail Zone E-93 Fort Worth TX 76101
1	Dalmo Victor Company Attn: Technical Library 1515 Industrial Way Belmont CA 94002		

DISTRIBUTION LIST

<u>Nr Copies</u>	<u>Companies</u>	<u>Nr Copies</u>	<u>Companies</u>
1	General Electric Company Research and Development Center Attn: Technical Library 1 River Road Schenectady NY 12301	1	Hughes Aircraft Corporation Attn: Technical Library 1901 W Malvern Avenue Fullerton CA 92634
1	General Electric Company Electronics Laboratory Attn: Technical Library Electronics Park Syracuse NY 13201	1	Hughes Aircraft Corporation Attn: Technical Library Florence & Teale Streets Culver City CA 90232
1	General Electric Company Light Military Electronics Attn: Technical Library French Road Utica NY 13503	1	ITT/Avionics Division Attn: Technical Library 500 Washington Avenue Nutley NJ 07110
1	General Precision Inc Kearfott Division 1150 McBride Avenue Little Falls NJ 07424	1	Jasik Laboratories Attn: Dr. Henry Jasik 100 Shames Drive Westbury NY 11590
1	Goodyear Aircraft Corporation Arizona Division Attn: Technical Library PO Box 85 Litchfield Park AZ 85340		
1	Goodyear Corporation Attn: Technical Library 1210 Massilon Road Akron OH 44315	1	KMS Industries Inc PO Box 1778 Ann Arbor MI 48108
1	Grumman Aircraft Engineering Corporation Attn: Technical Library South Oyster Bay Road Bethpage NY 11714	1	Ling-Temco-Vought Corporation Military Electronic Division Attn: Technical Library 1200 Jupiter Street Garland TX 75040

DISTRIBUTION LIST

<u>Nr Copies</u>	<u>Companies</u>	<u>Nr Copies</u>	<u>Companies</u>
1	Litton Systems Inc Amecom Division Attn: Technical Library 1140 E W Highway Silver Spring MD 20910	1	Martin Marietta Company Attn: Technical Library PO Box 988 Baltimore MD 21203
1	Lockheed Aircraft Corp Electronic & Armaments System Office Attn: Technical Library PO Box 551 Burbank CA 91503	1	McDonnell Douglas Aircraft Corporation Attn: Technical Library Box 516 St Louis MO 63166
1	Lockheed Aircraft Corp Missiles and Space Division Attn: Technical Library PO Box 504 Sunnyvale CA 94088	1	McDonnell Douglas Aircraft Corporation Attn: Technical Library 3855 Lakewood Boulevard Long Beach CA 90801
1	Lockheed Aircraft Corp Lockheed-Georgia Division Attn: Technical Library South Cobb Drive Marietta GA 30060	1	McDonnell Douglas Aircraft Corporation Attn: Technical Library 3000 Ocean Park Blvd Santa Monica CA 90406
1	Lockheed Aircraft Corp Lockheed Electronics Company Attn: Technical Library US Highway 22 Plainfield NJ 07060	1	McDonnell Aircraft Company Attn: Technical Library 2000 North Memorial Drive Tulsa OK 74115
1	Martin Marietta Company Denver Division Attn: Technical Library PO Box 179 Denver CO 80201	1	Melpar Inc Attn: Technical Library 7700 Arlington Boulevard Falls Church VA 22046
1	Martin Marietta Company Orlando Division Attn: Technical Library PO Box 5837 Orlando FL 32805	1	Mitre Corporation Attn: Technical Library Middlesex Turnpike PO Box 508 Bedford MA 01730
		1	Motorola Inc Government Electronics Division Attn: Technical Library 8201 E McDowell Road Scottsdale AZ 85257

DISTRIBUTION LIST

<u>Nr Copies</u>	<u>Companies</u>	<u>Nr Copies</u>	<u>Companies</u>
1	North American Aviation Inc Autonetics Division Attn: Technical Library 3370 Miraloma Avenue Anaheim CA 92803	1	Radiation Inc Systems Division Attn: Technical Library Box 37 Melbourne FL 32901
1	North American Aviation Inc Attn: Technical Library International Airport Los Angeles CA 90009	1	Radiation Inc Attn: Technical Library 1755 Old Meadow Road McLean VA 22101
1	North American Aviation Inc Attn: Technical Library 4300 E Fifth Street Columbus OH 43216	1	Radio Corporation of America Missile & Surface Radar Division Attn: Technical Library Mail Stop 101-210 Moorestown NJ 08057
1	Northrop Aircraft Corp Norair Division Attn: Technical Library 3901 West Broadway Hawthorne CA 90250	1	Rantec Corporation Attn: Technical Library 23999 Ventura Blvd Calabasas CA 91302
1	Page Communications Engineers Inc Attn: Technical Library 3300 Whitehaven Street Wash DC 20007	1	Raytheon Corporation Attn: Technical Library Santa Barbara Operation PO Box 1542 Goleta CA 93017
1	Philco-Ford Corporation Aeronutronic Division Attn: Technical Library Ford Road Newport Beach CA 92663	1	Raytheon Corporation Missile Systems Division Attn: Technical Library Hartwell Street Bedford MA 01730
		1	Raytheon Corporation Equipment Division Attn: Technical Library 40 Second Street, PO Box 520 Waltham MA 02154

DISTRIBUTION LIST

<u>Nr Copies</u>	<u>Companies</u>	<u>Nr Copies</u>	<u>Companies</u>
1	Republic Aviation Division Fairchild Hiller Attn: Technical Library Department 61, Mezz 9 Farmingdale NY 11735	1	Sperry Rand Corporation Sperry Gyroscope Division Attn: Technical Division Mail Station V-119 Great Neck LI NY 11020
1	Ryan Aeronautical Company Attn: Technical Library 5650 Kearny Mesa Road PO Box 311 San Diego CA 92112	1	Sperry Rand Corporation Sperry Microwave Electronics Division Attn: Technical Library PO Box 1828 Clearwater FL 33517
1	Sanders Associates Inc Microwave Division Attn: Technical Library 95 Canal Street Nashua NH 03061	1	Stanford Research Institute Attn: Technical Library Ravenswood Avenue Menlo Park CA 94025
1	Scientific Atlanta Inc Attn: Technical Library PO Box 13654 Atlanta GA 30324	1	Sylvania Electronics - West Electronic Defense Laboratories Attn: Technical Library PO Box 205 Mountain View CA 94040
1	Sedco Attn: Technical Library 130 Schmitt Boulevard Farmingdale LI NY 11735	1	Sylvania Electronics Systems Attn: Technical Library 100 East First Avenue Waltham MA 02154
1	HRB Singer Corporation Attn: Technical Library Box 60, Science Park State College PA 16801	1	Teledyne Systems Corporation Attn: Technical Library 12525 South Daphne Avenue Hawthorne CA 90066
1	Southwest Research Institute Attn: Technical Library 8500 Culebra Road San Antonio TX 78206	1	Texas Instruments Inc Attn: Technical Library 13500 N Central Expressway Dallas TX 75222
1	Space Technology Laboratory Attn: Technical Library 1 Space Park Redondo Beach CA 90278		

DISTRIBUTION LIST

<u>Nr Copies</u>	<u>Companies</u>	<u>Nr Copies</u>	<u>Government Offices</u>
1	TRW Systems Thompson Ramo Wooldridge Inc Attn: Technical Library 1 Space Park Redondo Beach CA 90278	3	AFAL (AVWE - Mr. Horton) Wright-Patterson AFB OH 45433
		1	AFAL (AVWC - Mr. Whrig) Wright-Patterson AFB OH 45433
1	Westinghouse Electric Corp Aerospace Division Attn: Technical Library PO Box 746 Baltimore MD 21203	1	AFAL (AVTM - Mr. Greene) Wright-Patterson AFB OH 45433
		1	ASD (ASEP - Mr. Brooks) Wright-Patterson AFB OH 45433
1	Westinghouse Electric Corp Defense and Space Center Attn: Technical Library PO Box 1897 Baltimore MD 21203	1	FTD (TDCES - Mr. Wiegert) Wright-Patterson AFB OH 45433
		1	FTD (TDEE) Wright-Patterson AFB OH 45433
1	Wheeler Laboratory Attn: Technical Library Box 561 Smithtown NY 11787	1	ASD (SEACC - Mr. Stahler) Wright-Patterson AFB OH 45433
		1	ASD (SEAEM - Mr. Mulligan) Wright-Patterson AFB OH 45433
	<u>Government Offices</u>	1	ASD (ASNPD-30) Wright-Patterson AFB OH 45433
1	USAF (AFCSAI) Wash D C 20330	1	ASD (ASBED-20 - Mr. Stecher) Wright-Patterson AFB OH 45433
1	Hq AFSC (SCAP) Andrews AFB Wash D C 20331	1	AFSC (SCSE) Andrews AFB Wash DC 20331
1	EWASL Wright-Patterson AFB OH 45433	1	RADC (EMATA) Griffiss AFB NY 13442
		1	RADC (EMCRA) Griffiss AFB NY 13442
		1	RADC (EMCT) Griffiss AFB NY 13442
		1	AFCRL (CRD - Mr. C. J. Sletten) L G Hanscom Fld Bedford MA 01730

DISTRIBUTION LIST

<u>Nr Copies</u>	<u>Government Offices</u>	<u>Nr Copies</u>	<u>Government Offices</u>
1	AFETR (ETGCS) Patrick AFB FL 32925	1	Director Surveillance Department Evans Area
1	Hq USAF (AFRDD - Lt Col Lieber) Wash DC 20330		Attn: Technical Document Center Belmar NJ 08056
1	Hq USAF (AFXAI) Air Battle Analysis Center Deputy Director of Plans for War Plans Wash DC 20330	1	Commander US Naval Air Test Center Attn: WSST-54 Patuxent River MD 20670
1	Commanding Officer USARDVL (Attn: SIGRA/NAI) Fort Monmouth NJ 07703		
1	Commanding General US Army White Sands Missile Range Attn: Technical Library White Sands NM 88002	1	Director US Navy Electronics Laboratory Code 3220 Attn: Library San Diego CA 92152
1	Commanding Officer US Army Electronics R&D Activity Attn: SELWS-ED White Sands NM 88002		Commander US Naval Ordnance Test Station Code 4021 (Mr. J. A. Mosko) China Lake CA 93557
1	Department of the Army Ballistic Research Laboratory Attn: Technical Library Aberdeen Proving Ground MD 21005	1	Commander US Naval Ordnance Laboratory Attn: Mr. Dave Schriener Corona CA 91720
1	Commanding Officer Harry Diamond Laboratories Conn Avenue & Vann Ness Street, NW Attn: 240 Wash DC 20438	20	DDC Cameron Station Alexandria VA 22314
1	Chief, Bureau of Ships Attn: Code 312 Main Navy Building Wash DC 20360	1	AUL (3T-AUL-59-30) Maxwell AFB AL 36112
1	Director Naval Research Laboratory Attn: Code 5200 Wash DC 20390	1	NASA Goddard Space Flight Center Attn: Antenna Branch - Mr. Lantz Greenbelt MD 20771
1	Director Naval Research Laboratory Attn: Code 5200 Wash DC 20390	1	NASA PO Box 33 College Park MD 20740

DISTRIBUTION LIST

<u>Nr Copies</u>	<u>Universities</u>	<u>Nr Copies</u>	<u>Universities</u>
1	Cornell Aeronautical Laboratory Attn: Technical Library Buffalo NY 14221	1	Polytechnical Institute of Brooklyn Microwave Research Institute Attn: Technical Library 55 Johnson Street Brooklyn NY 11201
1	Georgia Institute of Technology Engineering Experiment Station Attn: Technical Library Atlanta GA 30331	1	Stanford Electronic Laboratory Attn: Technical Library Stanford CA 94305
1	Johns Hopkins University Applied Physics Laboratory 8621 Georgia Avenue Silver Spring MD 20910	1	Syracuse University Electrical Engineering Department Attn: Technical Library Syracuse NY 13210
1	Lincoln Laboratories MIT Attn: Technical Library Lexington MA 20653	1	University of Dayton Research Institute Attn: Technical Library 300 College Park Dayton OH 45409
1	New Mexico State University Head, Antenna Department Physical Science Department University Park NM 88070	1	University of Illinois Department of Electrical Engineering Attn: Technical Library Urbana IL 61803
1	North Carolina State of the University of North Carolina Attn: Technical Library PO Box 5275 Raleigh NC 27607	1	University of Michigan Radiation Laboratory Willow Run Attn: Technical Library 201 Catherine Street Ann Arbor MI 48104
1	Northeastern University Attn: Dodge Library Boston MA 02115	1	University of Southern California Electrical Engineering Department Attn: Technical Library University Park Los Angeles CA 90007
1	Ohio University Electrical Engineering Department Attn: Technical Library Athens OH 45701	1	University of Texas Electrical Engineering Research Laboratory Attn: Technical Library Route 4, Box 189 Austin TX 78756
1	Johns Hopkins University Carlyle Barton Laboratory Charles & 34th Streets Baltimore MD 22218	1	

